Philipps-Universität Marburg
Fachbereich Biologie
- Tierphysiologie -

Regulationsmechanismen während des Torpors und der zitterfreien Thermogenese: Neue Einblicke und der Einsatz von Magnetresonanztomographie

Dissertation

zur Erlangung des Doktorgrades
der Naturwissenschaften (Dr. rer. nat.)

vorgelegt von
Kirsten Grimpo
geboren in Wiesbaden

Marburg/Lahn 2014

Für meine Oma

Vom Fachbereich Biologie der Philipps-Universität Marburg als
Dissertation am _____ angenommen.
Erstgutachter: Prof. Dr. Gerhard Heldmaier
Zweitgutachter: Prof. Dr. Monika Hassel
Tag der mündlichen Prüfung am: _____

Inhaltsverzeichnis

I. Zusammenfassung

Säugetiere bevölkern nahezu jede Nische der Erde, weil sie ihre Körpertemperatur unabhängig von der Umgebungstemperatur regulieren können. Diese endotherme Lebensweise ist, besonders für Kleinsäuger, energetisch sehr kostspielig und lässt sich nur durch eine präzise Regulation der Energieausgaben verwirklichen. Regulationsmechanismen, die einer Absenkung des Stoffwechsels, um Energie zu sparen oder einer Stoffwechselsteigerung, um die Körpertemperatur bei Kälteexposition zu verteidigen, zugrunde liegen, sind komplex und in weiten Teilen unverstanden.

Messungen von Sauerstoffverbrauch und Körpertemperatur der arid lebenden Goldstachelmaus (*Acomys russatus*) ergaben, dass *A. russatus* eine 50%ige Futterreduktion bei hohen Umgebungstemperaturen (32°C und 35°C) energetisch kompensieren kann. Durch eine Reduktion ihres Ruhestoffwechsels um 30% im Vergleich zu *ad libitum* Bedingungen und täglich mehrstündige torpide Phasen, hielt sie ihr Körpergewicht trotz der verringerten Energiezufuhr nahezu konstant. Im Gegensatz zu Torpor bei Umgebungstemperaturen von 23°C und 27°C, blieb die Körpertemperatur dabei auf einem normothermen Level. Die rapide Absenkung des Metabolismus, ein Charakteristikum von Torpor, kann demnach entkoppelt von einer hypothermen Körpertemperatur stattfinden und ist somit entgegen der landläufigen Meinung nicht nur in kalten, sondern auch in anderen klimatischen Bedingungen eine effiziente Strategie der Energieeinsparung.

Als Auslöser für die regulierte Stoffwechselabsenkung im Torpor stehen die Mitochondrien in der Diskussion. Ein aktives Abschalten der Zellatmung könnte zu einer Stoffwechseldepression führen, wie sie bei Eintritt in den Torpor auftritt. Untersuchungen verschiedener Gewebe (z.B. Leber) von torpiden Stachelmäusen ergaben jedoch keine Verringerung der mitochondrialen Succinat-Respiration im Vergleich zu normometabolen Tieren. Auch das Membranpotential der isolierten Mitochondrien und die Effizienz der ATP-Synthase unterschieden sich nicht. Dies galt für torpide Stachelmäuse mit normothermer als auch hypothermer Körpertemperatur. Es weist darauf hin, dass die Absenkung der Stoffwechselrate im Torpor bei *A. russatus* nicht durch eine Inhibition der Zellatmung induziert wird.

Winterakklimatisierte Dsungarische Zwerghamster (*Phodopus sungorus*) dagegen zeigten im Torpor eine aktive Inhibition der Substratoxidation in den Lebermitochondrien. Die Atmungsraten der Mitochondrien korrelierten mit der Körpertemperatur der Hamster, die bei Umgebungstemperaturen von 15°C sehr tiefe Werte erreichte.

Diese Daten lassen die Schlussfolgerung zu, dass eine aktive Inhibition der mitochondrialen Respiration artspezifisch ist und eher eine Anpassung an niedrige Körpertemperaturen im torpiden Zustand als die Ursache des Torporeintritts an sich. Die Mechanismen, die zum Eintritt in den Torpor führen, bleiben somit unklar.

Um neue Wege für die Entschlüsselung der Regulationsmechanismen im Torpor zu eröffnen, wurde im nächsten Schritt ein kombinierter Messaufbau aus indirekter Kalorimetrie und Magnetresonanztomographie (MRT) entwickelt, der erlaubte torpide Zwerghamster bildgebend zu untersuchen. Die notwendige Hardware und Software wurde soweit optimiert, dass *P. sungorus* in einem 7 Tesla-Tomographen torpid wurde und erstmalig morphologische, angiographische und spektroskopische Aufnahmen an einem nicht-narkotisierten Tier im Torpor akquiriert werden konnten. Solch funktionelle Messungen mittels MRT bieten das Potential, neue Einblicke in die Abläufe des Torpors zu gewinnen.

Eine weitere Stärke der MRT ist ihr hervorragender Weichgewebekontrast, der es zuließ Gewebe von narkotisierten Tieren *in vivo* zu untersuchen. Selbst Unterschiede zwischen dem weißen Speicherfett und dem thermogenetisch aktiven braunem Fett ließen sich darstellen und mit gaschromatischen Messungen *ex vivo* validieren. Weißes Fettgewebe wies einen höheren Gehalt an ungesättigten Fettsäuren auf als braunes Fettgewebe. In der Winteranpassung nahm der Gehalt an ungesättigten Fettsäuren in beiden Geweben bei *P. sungorus* zu. Daraus lässt sich eine bedeutsame Funktion der Fettsäuren für die Vorbereitung auf Torpor und kalte Umgebungstemperaturen ableiten.

Im letzten Teil der Arbeit wurde die thermogenetische Funktion des braunen Fettgewebes tiefergehend untersucht. Braunes Fettgewebe spielt eine wichtige Rolle um den Körper aus hypothermen Phasen des Torpors wieder aufzuheizen und um eine normotherme Körpertemperatur bei Kälteexposition zu verteidigen. Hierfür generiert braunes Fett nach noradrenerger Stimulation mittels eines spezifischen Entkopplerproteins (UCP1) zitterfreie Wärme, indem die oxidative Phosphorylierung in den Mitochondrien von der Atmungskette entkoppelt wird. Bei langanhaltender Kälteexposition steigt die Fähigkeit zur zitterfreien Thermogeneses durch Erhöhung der respiratorischen Kapazität des Gewebes, und diese wird hauptsächlich auf UCP1-vermittelte Thermogenese zurückgeführt. *Knockout*-Mäuse, die kein UCP1 besitzen, zeigten dennoch eine Steigerung der zitterfreien Wärmebildung, was auf eine Kompensation der UCP1-vermittelten Thermogenese hinweist. Spektroskopische und bildgebende MRT-Messungen konnten bei UCP1-KO Mäusen wie bei Wildtypmäusen eine Umstrukturierung des braunen Fettgewebes bei Kälteanpassung visualisieren. Nach noradrenerger Stimulation konnte eine Erhöhung des Lipidmetabolismus nachgewiesen werden.

Der gesteigerte Lipidstoffwechsel führte bei beiden Genotypen zu einem immensen Export von Fettsäuren, dem wichtigsten Substrat der Thermogenese, aus dem braunen Fettgewebe. Die Daten sprechen für einen UCP1-unabhängigen Mechanismus zur adaptiven Thermogenese und eine wichtige Funktion des braunen Fettgewebes im Lipidstoffwechsel, die über die Oxidation von Fettsäuren für die UCP1-vermittelte Thermogenese hinausgeht.

Die Ergebnisse der vorliegenden Arbeit tragen zu einem weiterführenden Verständnis der Regulationen des Energiehaushalts kleiner Säugetiere bei. Sie decken Zusammenhänge zwischen der aktiven Stoffwechselabsenkung, der Körpertemperatur, der Umgebungstemperatur und der mitochondrialen Respirationsleistung auf. Sie beleuchten den Einsatz der MRT als innovative Methode für die Untersuchung physiologischer Fragestellungen und werfen ein neues Licht auf die Funktion des braunen Fettgewebes bei der UCP1-unabhängigen zitterfreien Thermogenese.

II. Summary

Mammals are able to regulate their body temperature independent of the ambient temperature and thus inhabit almost every ecological niche all over the world. This endothermic way of life is especially for small mammals energetically expensive and requires a balanced energy management. The mechanisms for metabolic reduction in order to save energy, i.e. torpor, or the increase of energy metabolism in order to defend body temperature against ambient temperatures are complex and barely understood.

Measuring oxygen consumption and body temperature of Golden spiny mice (*Acomys russatus*) revealed that these desert rodents were able to compensate a 50% food restriction when kept at ambient temperatures of 32°C or 35°C. The spiny mice defended their body weight against the reduced energy supply through a 30% reduction of resting metabolic rate compared to *ad libitum* conditions as well as by using daily torpor. During torpor at these ambient temperatures they maintained their body temperature at a normothermic level whereas they became hypothermic during torpor at ambient temperatures of 23°C or 27°C. This implies that the metabolic reduction during torpor can occur autonomously from a hypothermic body temperature. It demonstrates that torpor is an efficient strategy for saving energy in a variety of habitats and not just in cold environments as previously assumed.

Mitochondria are discussed to trigger the regulated metabolic depression in torpor, as it has been hypothesized that a shutdown of cell respiration could be responsible for the rapid reduction of metabolic rate during torpor entrance. For this reason mitochondrial succinate respiration of four tissues (e.g. liver) were investigated from torpid spiny mice but no differences were detected when compared to normometabolic individuals. There was no change in membrane potential or ATP-synthase efficiency of isolated mitochondria during torpor. These results were true for torpid *A. russatus* with normothermic and hypothermic body temperature and indicate that the decrease of metabolic rate during torpor in this species is not caused by a depression of mitochondrial respiration. In contrast, mitochondrial respiration of liver from winter-acclimated Djungarian hamsters (*Phodopus sungorus*) was significantly reduced during torpor due to an active inhibition of substrate oxidation. The respiration rates of liver mitochondria correlated with the body temperature of the hamsters, which reached very low values at an ambient temperature of 15°C. In conclusion the active inhibition of mitochondrial respiration seems to be species-specific and more an adaptation to a low body temperature in the torpid state rather than being the cause of torpid state per se.

Thus, the intrinsic mechanisms of entrance into torpor still remain unclear.

To further elucidate the mechanisms which underlie the regulation of torpor in the Djungarian hamster a combination of indirect calorimetry and magnetic resonance imaging (MRI) was developed. Hardware and software of the experimental setup were optimized so that *P. sungorus* became torpid inside the 7 Tesla scanner allowing for the first time successful acquirements of imaging, angiography and spectroscopy data in a non-anaesthetized animal. Such functional measurements via MRI promise new insights into the processes of torpor. Another advantage of MRI, its excellent soft tissue contrast, was used for characterization of adipose tissue of anaesthetized animals *in vivo*. Differences between the white adipose tissue that serves mainly as lipid storage and the thermogenically important brown adipose tissue were detected with MRI and data were validated with *ex vivo* gas-chromatographic measurements. White adipose tissue had a higher content of unsaturated fatty acid than brown fat. In both tissues the amount of unsaturated fatty acids increased following acclimation to short photoperiod, indicating a contribution of fatty acids to the preparation of torpor behavior and adaptation to cold.

The thermogenic function of brown adipose tissue was investigated more closely in the last part of the thesis. Brown adipose tissue is essential for small mammals to reheat from hypothermic states in torpor and to defend normothermic body temperature during cold exposure. For this purpose after noradrenergic stimulation brown adipose tissue generates heat by uncoupling the oxidative phosphorylation from the respiratory chain via uncoupling protein 1 (UCP1) activity.

Long term cold exposure results in an increased respiratory capacity of brown adipose tissue and this adaptive non-shivering thermogenesis is mainly attributed to UCP1 induced thermogenesis. However, UCP1-depleted mice increased their capacity of non-shivering thermogenesis after adaptation to cold, indicating a compensatory mechanism of UCP1-dependent thermogenesis. MRI visualized a remodeling of brown adipose tissue in UCP1-KO and wildtype mice following cold acclimation. By using magnetic resonance spectroscopy an advanced lipid metabolism after noradrenergic stimulation was detected that led to an export of fatty acids, the main substrate of non-shivering thermogenesis, from brown adipose tissue. The data suggest an UCP1-independent adjustment of brown adipose tissue to cold exposure and a contribution to lipid metabolism that exceeds the oxidation of fatty acids for UCP1-dependent thermogenesis.

The results of the present PhD-Thesis contribute to a better understanding of the energy metabolism in small mammals. They untangle the interactions between an active down-regulation of metabolism, body temperature, ambient temperature and mitochondrial respiration. They discuss the potential of MRI as an innovative method in order to answer physiological questions and stress the role of brown adipose tissue concerning UCP1-independent thermogenesis.

III. Abkürzungsverzeichnis

ADP	Adenosindiphosphat
ATP	Adenosintriphosphat
BAT	Braunes Fettgewebe (brown adipose tissue)
DEE	Täglicher Energieverbrauch (daily energy expenditure)
DEI	Täglicher Energieeinnahme (daily energy intake)
FCCP	Carbonylcyanid-4-trifluormethoxy-phenylhydrazon
FFS	Freie Fettsäuren
fMRI	funktionelle Magnetresonanztomographie
HSL	Hormonsensitive Lipase
MR	Magnetresonanz
MRS	Magnetresonanzspektroskopie
MRT	Magnetresonaztomographie
MHz	Megahertz
P_i	Inorganisches Phosphat
PCr	Phosphokreatin
RMR	Ruhestoffwechsel (resting metabolic rate)
SNR	Signal-zu-Rausch-Verhältnis (signal to noise ratio)
ROI	Ausgewählte Region (region of interest)
RQ	Respiratorischer Quotient
T	Tesla
TA	Aufwachvorgang aus dem Torpor (torpor arousal)
T_a	Umgebungstemperatur (ambient temperature)
T_b	Körpertemperatur (body temperature)
TE	Torporeintritt
TOF	Angiographie-Sequenz (time-of-Flight)
TP	Tiefer Torpor (torpor plateau)
TPMP	Triphenylmethylphosphonium
UCP1	Entkopplerprotein 1 (uncoupling protein 1)
VO_2	Sauerstoffverbrauch = Maß für Stoffwechselrate
WAT	Weißes Fettgewebe (white adipose tissue)

1 Einleitung

1.1 Kleine Körpergröße - Große Herausforderung

Nagetiere (Rodentia) bilden innerhalb der Säugetiere (Mammalia) die artenreichste Ordnung und sind auf sämtlichen Erdteilen (ausgenommen der Antarktis) beheimatet. Bis auf wenige Ausnahmen gehören sie zu den kleineren Vertretern der Säuger (Puschmann 2004). Um auch extreme Klimazonen bevölkern zu können, haben sie bemerkenswerte Anpassungsstrategien hinsichtlich ihres Energiehaushalts und ihrer Temperaturregulation entwickelt.

Ihre geringe Körpergröße bringt unter energetischen und thermoregulatorischen Gesichtspunkten besondere Herausforderungen mit sich. Der gewichtsspezifische Energieverbrauch verhält sich allometrisch zur Körpermasse und steigt bei zwischenartlichen Vergleichen mit Abnahme des Körpergewichts (Kleiber 1932; Hayssen and Lacy 1985; White and Seymour 2003). Je kleiner also das Tier, desto höher ist im Verhältnis sein Energieverbrauch. Zudem halten Nagetiere, wie alle endothermen Tiere, ihre warme Körpertemperatur über einen weiten Außentemperaturbereich aufrecht. Mit sinkender Körpergröße steigt der Wärmeverlust eines Tieres, da seine Oberfläche im Verhältnis zum Volumen zunimmt (Heldmaier 1971). Die Möglichkeiten isolierende Fettdepots und Fellschichten anzulegen, die den Wärmeverlust verringern, sind begrenzt. Eine ausreichende Kompensation des Wärmeverlusts lässt sich nur durch eine hohe Stoffwechselleistung realisieren, die permanent Wärme erzeugt. In der Thermoneutralzone reicht allein die Abwärme des basalen Stoffwechsels aus, um eine normotherme Körpertemperatur aufrecht zu erhalten (I.U.P.S. Commission for Thermal Physiology 2001). Die Thermoneutralzone einer Hausmaus (*Mus musculus*) beispielsweise liegt bei einer Umgebungstemperatur von 30-32°C, während die eines Pferdes von 5°C bis 25°C reicht (Hudson and Scott 1979; Morgan 1998). Unterschreitet die Umgebungstemperatur die Thermoneutralzone (Kälte-Exposition) setzen endogene Mechanismen der Wärmebildung ein, die zu einer Stoffwechselsteigerung führen. Man unterscheidet zwischen der zitterfreien Thermogenese und dem Kältezittern. Bei Nagern und anderen eutherischen Kleinsäugern findet das Gros der zitterfreien Thermogenese im braunen Fettgewebe statt und ist für die Regulation der Körpertemperatur von großer Bedeutung (Laury and Portet 1974; Foster and Frydman 1978). Erst wenn die Kapazität der zitterfreien Wärmebildung nicht ausreicht, um die Körpertemperatur aufrecht zu erhalten, sprechen die für das Kältezittern verantwortliche Thermorezeptoren im Rückenmark an und eine Kontraktion der Skelettmuskulatur setzt ein (Fuller et al. 1977; Banet et al. 1978). Bei dieser Art der Muskelbewegung wird keine mechanische Arbeit verrichtet, sondern chemische Energie in Wärme umgesetzt.

1.2 Heiß - Das kleine Braune

In Anpassung an ihre Umwelt weisen einige Nagerarten im Verhältnis zu ihrem Körpergewicht beträchtliche Mengen an braunem Fettgewebe auf. Die braunen Fettdepots sind stark innerviert und vaskularisiert. Die interscapularen, dorsal zervikalen, axillaren und substernalen Depots umgeben den Thorax und sorgen dafür, dass bei Bedarf erwärmtes Blut zum Herzen gelangt und dadurch im Körper umverteilt wird (Cannon and Nedergaard 2004; Heldmaier et al. 2013). Die Wärmegeneration des braunen Fettgewebes wird über das Entkopplerprotein 1 (uncoupling protein 1, UCP1) vermittelt, das spezifisch in der inneren Mitochondrienmembran brauner Adipozyten lokalisiert ist. Bei noradrenerger Stimulation des braunen Fettgewebes durch das sympathische Nervensystem wird UCP1 aktiviert und entkoppelt in den Mitochondrien die oxidative Phosphorylierung von der Atmungskette (Lafrance et al. 1980; Cannon and Nedergaard 2004). Freie Fettsäuren spielen bei diesem Prozess eine wichtige Rolle, da sie sowohl als Substrat für die Atmungskette als auch als Aktivator des UCP1 dienen (Carneheim et al. 1984; Fedorenko et al. 2012). Die im Protonengradienten gespeicherte Energie wird nicht mehr als chemische Energie in Form von ATP gebunden, sondern als Wärme frei (Abb. 1, Cannon and Nedergaard 2004). Entsprechend ihrer thermogenetischen Funktion zeichnen sich braune Adipozyten durch einen hohen Zytoplasmagehalt aus, sind reich an Mitochondrien und arm an ATP-Synthasen (Houstěk et al. 1995). Durch ihre multilokulären Lipidtröpfchen unterscheiden sie sich deutlich von weißen Adipozyten, die unilokuläre Lipidtröpfchen und wenig Zytoplasma aufweisen (Cinti 2005). Es ist nach wie vor umstritten, welchen Anteil die Wärmebildung im braunen Fett an der gesamten zitterfreien Thermogenese hat und ob eine Steigerung der Thermogeneseleistung bei Kälteexposition ausschließlich UCP1-vermittelt ist. Je nach Akklimatisationsgrad und abhängig von der Tierart entstehen vermeintliche 30% bis zu 70% der Wärmebildung im braunen Fettgewebe (Heldmaier and Buchberger 1985; Puchalski et al. 1987). Für diese adaptive Thermogenesekapazität ist eine Rekrutierung von braunem Fett, mit einem gesteigerten Mitochondriengehalt und einer erhöhten UCP1-Expression in den Adipozyten, von großer Bedeutung (Heldmaier 1974; Heldmaier et al. 1981; Klingenspor 2003). Interessanterweise sind auch Mäuse ohne funktionelles UCP1 (UCP1-KO) in der Lage kalte Umgebungstemperaturen zu tolerieren und dabei ihre normotherme Körpertemperatur zu verteidigen. Dies lässt auf weitere Mechanismen endogener Wärmebildung schließen, die ein Wegfallen der UCP1-abhängigen Thermogenese kompensieren können.

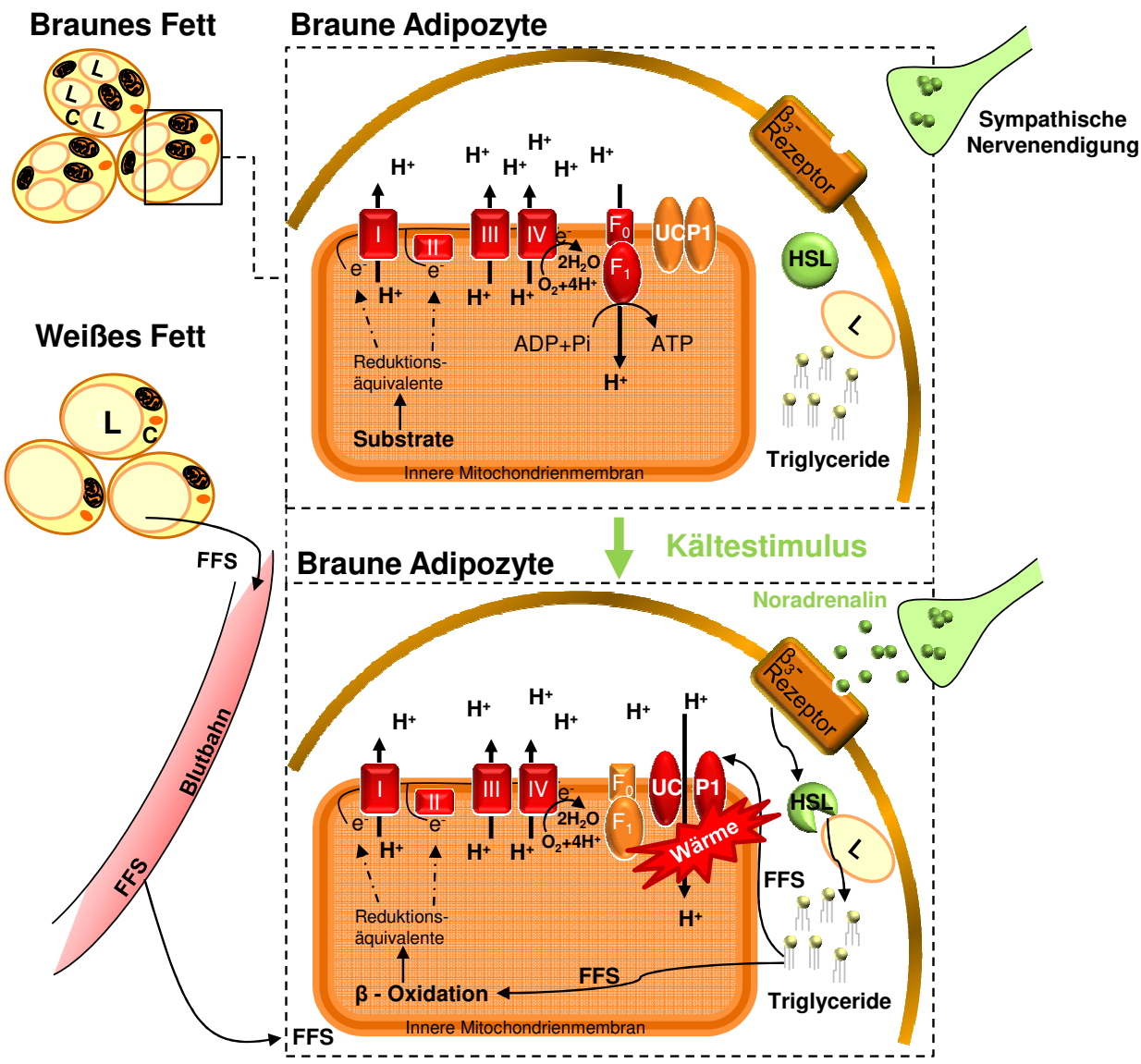

Abbildung 1 *Zitterfreie Thermogenese im braunen Fettgewebe nach noradrenerger Stimulation.* Kälteexposition induziert die Freigabe von Noradrenalin aus den Synapsen des sympathischen Nervensystems. Noradrenalin bindet an β-adrenerge Rezeptoren der braunen Adipozyten und setzt eine Kaskade in Gang, die zur Aktivierung von Lipasen (z.B. hormonsensitive Lipase, HSL) und damit zur Lipolyse freier Fettsäuren (FFS) aus den Lipidtröpfchen (L) führt. Im Gegensatz zum Ruhezustand werden nun nicht mehr hauptsächlich Substrate aus der Glykolyse, sondern FFS in den Mitochondrien oxidiert. Die Elektronen ihrer Reduktionsäquivalente wandern entlang der Atmungskette, an deren Ende sie Sauerstoff zu Wasser reduzieren. Auf diesem Weg werden Protonen aus der Matrix über die Atmungskomplexe in den Intermembranraum gepumpt, so dass ein Protonengradient über die innere Mitochondrienmembran entsteht. Aktivierung des Entkopplerproteins 1 (UCP1) durch FFS erlaubt einen Rückstrom der Protonen in die mitochondriale Matrix, die ATP-Synthese kommt zum Erliegen und die protonenmotorische Energie wird statt dessen als Wärme frei. Das weiße Fettgewebe liefert zusätzlichen Nachschub an FFS. Es unterscheidet sich durch einen geringeren Zytoplasmagehalt (C) mit wenigen Mitochondrien deutlich vom braunen Fettgewebe.

Bisherige Begründungen für die Kältetoleranz von UCP1-KO Mäusen beruhen auf einer antrainierten Steigerung des Kältezitterns oder auf einem erhöhten Energiedurchsatz im weißen Fettgewebe (Golozoubova et al. 2001; Ukropec et al. 2006; Meyer et al. 2010). Der Beitrag anderer Organe sowie ein UCP1-unabhängiger Beitrag des braunen Fettgewebes zur zitterfreien Thermogenese sind ebenfalls denkbar.

1.3 Torpor - Der aktive Energiesparmodus

Endogene Wärmebildung bei Kälteexposition, unabhängig welcher Ressource, bedeutet einen erhöhten Energieumsatz. Die entstehenden thermoregulatorischen Kosten sind bei kleinen Tieren besonders hoch (Scholander et al. 1950) und ein erhöhter Energiestoffwechsel birgt besonders dann Probleme, wenn die Energiezufuhr durch saisonale Schwankungen limitiert ist. Im Freiland führen ein reduziertes Nahrungsangebot, verminderte Wasserverfügbarkeit oder niedrige Umgebungstemperaturen dazu, dass Tiere mit einer negativen Energiebilanz konfrontiert werden und auf interne Energiereserven zurückgreifen müssen. Torpor ist eine physiologische Anpassungsstrategie von diversen Säugerarten, aber auch von Vögeln (Heldmaier et al. 2004; Melvin and Andrews 2009; Geiser 2013), um den Energiebedarf abzusenken. Während eines Torporbouts verringert sich der Sauerstoffverbrauch des Tieres auf ein Minimum der normometabolen Werte und seine Körpertemperatur sinkt auf wenige °C über Umgebungstemperatur. So können die thermoregulatorischen Kosten einer konstant hohen Körpertemperatur eliminiert werden. Die durch Torpor erreichte Energieeinsparung beträgt zwischen 30% und 90% (Ruf and Heldmaier 1992; Körtner and Geiser 2009).

Die Bereitschaft in den Torpor einzutreten kann interspezifisch und habitatabhängig stark variieren. Dies lässt sich an folgenden drei Beispielen verdeutlichen (Abb. 2). Der Dsungarische Zwerghamster (*Phodopus sungorus*) ist in den Steppen Kasachstans und Sibiriens heimisch und zeigt einen ausgeprägten saisonalen Dimorphismus. Mit abnehmender Tageslichtlänge (< 13 h) färbt sich das Fell des Hamsters von grau-braun zu weiß. Er verliert Körpergewicht und seine Körperzusammensetzung ändert sich (Hoffmann 1982; Wade and Bartness 1984; Klingenspor et al. 2000). Nur während dieser Winteranpassung zeigt *P. sungorus* spontanen Torpor, dann jedoch selbst bei thermoneutraler Umgebungstemperatur (23°C) und *ad libitum* Futterangebot (Heldmaier and Steinlechner 1981; Kirsch et al. 1991).

Für die arid lebende Goldstachelmaus (*Acomys russatus*) sind Futter- und Wasserverfügbarkeit dagegen ein wichtigerer Torporstimulus als die Photoperiode (Levy et al. 2011a).

Im Labor zeigt *A. russatus* Torpor bei moderat kalten Umgebungstemperaturen (27°C) unter Futterreduktion, während Torporbouts unter *ad libitum* Bedingungen bisher noch nicht beschrieben wurden (Ehrhardt et al. 2005; Gutman et al. 2006).

Bei der Hausmaus (*Mus musculus*) lässt sich Torpor durch eine Kombination aus Futterreduktion und Absenkung der Umgebungstemperatur von thermoneutralen 30°C auf 18°C induzieren (Swoap and Gutilla 2009; Oelkrug et al. 2011). Bei allen drei Beispielen dauert die torpide Phase kürzer als 24 Stunden an (hauptsächlich in der circadianen Ruhephase der Tiere) und man spricht von täglichem Torpor oder Tagesschlaflethargie (Abb. 2). Im Winterschlaf dagegen kann ein einzelner Torporbout Tage bis Wochen andauern (Arnold et al. 1989).

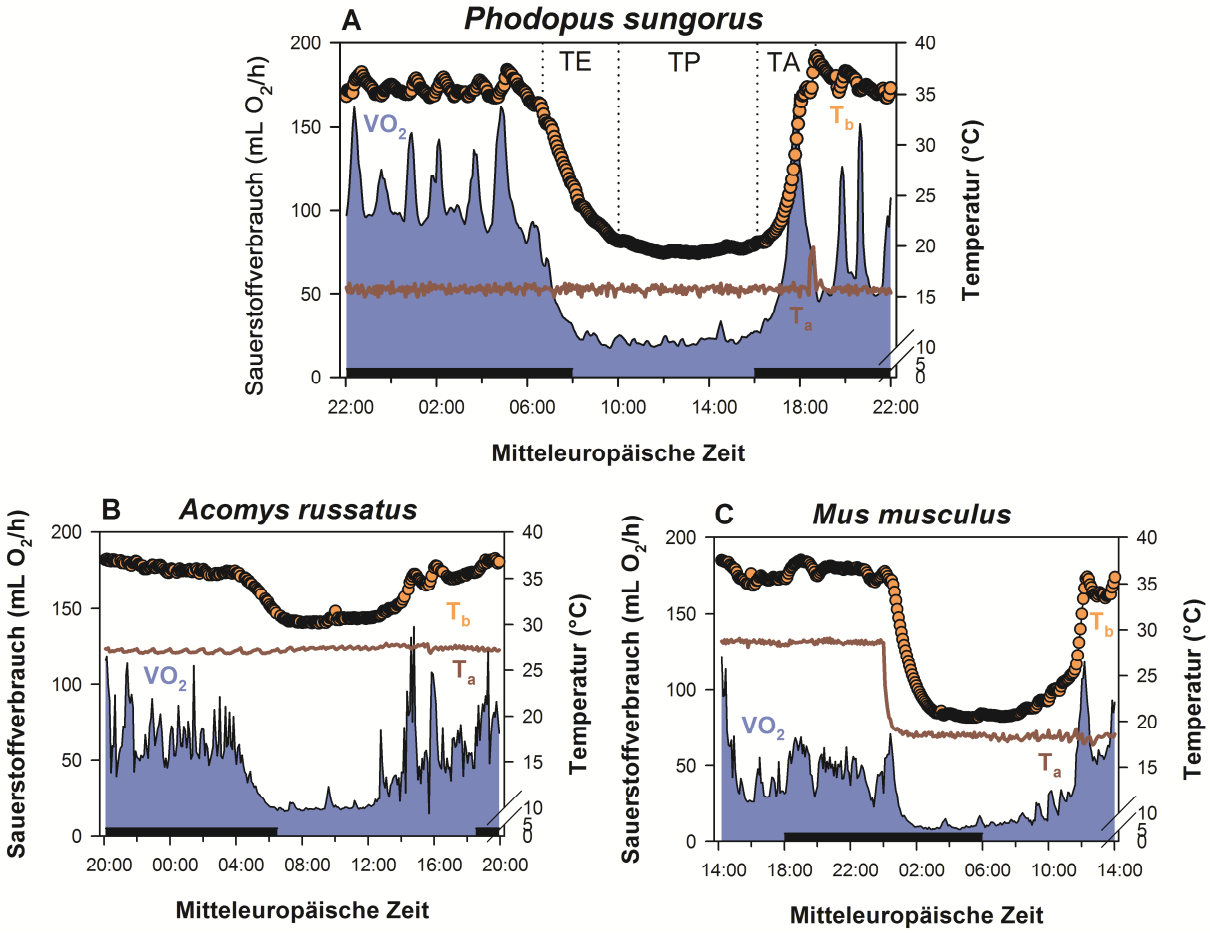

Abbildung 2 *Messungen des Sauerstoffverbrauchs (VO_2) und der Körpertemperatur (T_b) verschiedener Nagerspezies bei unterschiedlichen Umgebungstemperaturen (T_a).* Alle drei Tiere beginnen am Ende der Dunkelphase (schwarzer Balken) einen mehrstündigen Torporbout (Torporeintritt (TE), Torporplateau (TP), Torporarousal (TA)). *P. sungorus* erhielt Futter *ad libitum*, während *A. russatus* 50% futterreduziert war und *M. musculus* das Futter vor Beginn der Messung entzogen wurde. (unveröffentlichte Daten der AG Heldmaier)

Trotz unterschiedlicher Umweltbedingungen läuft der Eintritt in den Torpor charakteristisch ab. Zuerst sinken Sauerstoffverbrauch, Atem- und Herzschlagrate massiv ab, bevor die Körpertemperatur fällt (Heldmaier and Ruf 1992; Elvert and Heldmaier 2005). Es stellt sich die Frage, welche externen oder internen Faktoren einen Torporbout regulieren. Da der Stoffwechsel vor der Körpertemperatur sinkt, spricht dies für eine aktive Depression des Metabolismus und nicht für einen passiven Effekt der abgesenkten Körpertemperatur als Ursache für den hypometabolen Zustand.

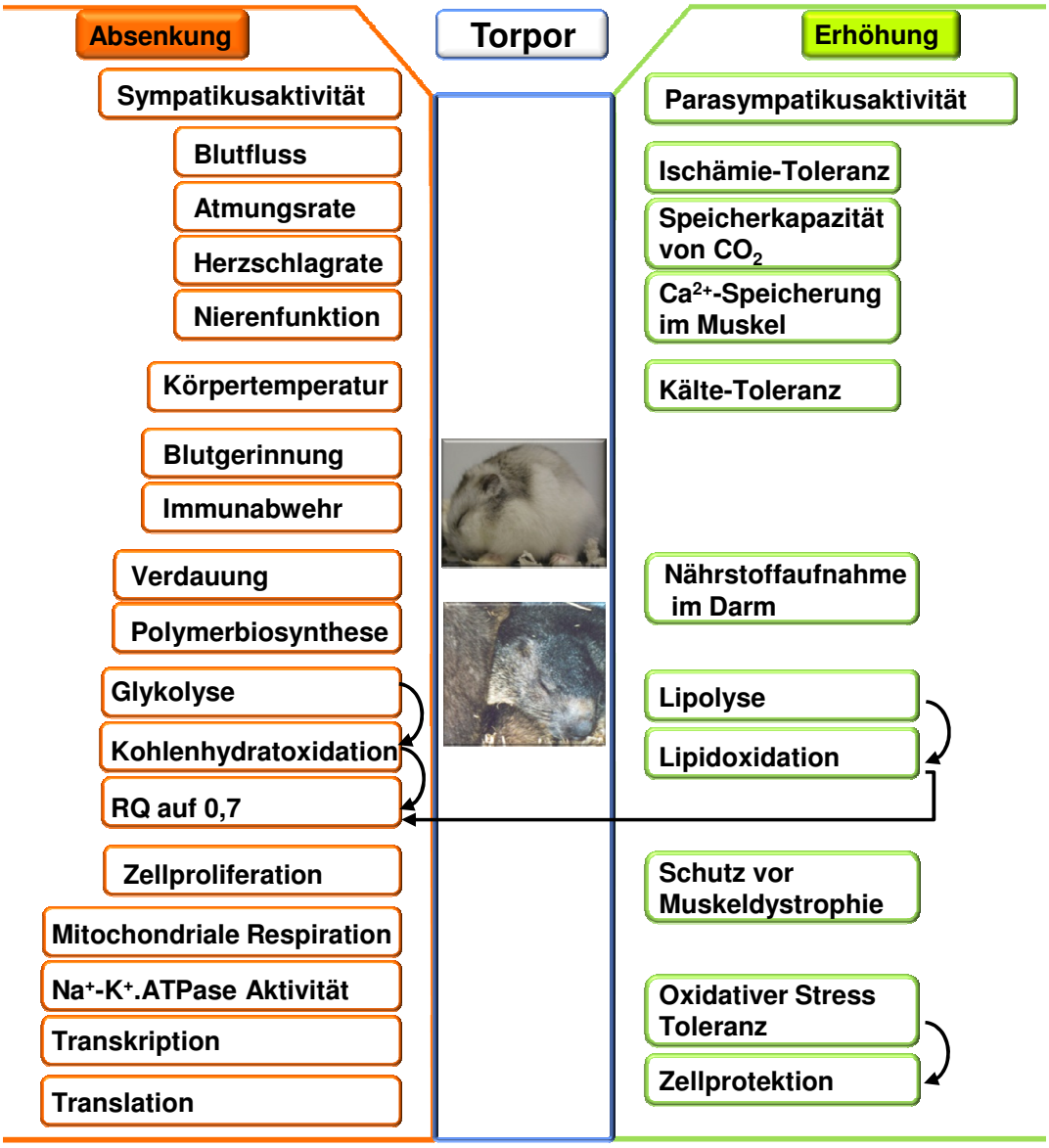

Abbildung 3 *Überblick der physiologischen, zellulären und molekularen Änderungen im Torpor.* Die Angaben beziehen sich auf torpide Tiere im Vergleich zu ihrem normothermen Zustand und stammen hauptsächlich aus Untersuchungen an winterschlafenden Arten.

Es konnte zudem gezeigt werden, dass die Thermosensitivität auch im tiefen Torpor erhalten bleibt und die Körpertemperatur weiterhin, auf ihrem abgesenkten Level, durch aktive Änderungen in der Stoffwechselrate reguliert wird (Heldmaier and Steinlechner 1981; Ortmann and Heldmaier 2000; Buck and Barnes 2000). Es ist leicht vorstellbar, dass intrinsische Änderungen stattfinden müssen, damit der Organismus extrem niedrige Temperaturen, verlangsamte Stoffwechselvorgänge, Minderdurchblutung aller Organe und auftretenden Zellstress während eines Torporbouts tolerieren kann, ohne Schäden davonzutragen (van Breukelen et al. 2010; Talaei et al. 2011). Welche Faktoren den aktiven Eintritt in den torpiden Zustand auslösen und welche molekularen Signalwege zusammenspielen, um ihn aufrechtzuerhalten und "auszuhalten", ist indes nur lückenhaft erforscht und verstanden (Abb. 3) (Carey et al. 2003; Heldmaier et al. 2004; Drew et al. 2007; Melvin and Andrews 2009).

Darüber hinaus ist unklar inwieweit eine niedrige Körpertemperatur im Torpor notwendig ist und ob thermodynamische Effekte eine Absenkung der Stoffwechselrate bei Torporeintritt unterstützen. Einerseits wird eine hypotherme Körpertemperatur in der Regel als Charakteristikum von Torpor angeführt. Selbst Tiere, die für ihren „Sommertorpor" bekannt sind, bevorzugen kühle Bauten oder die kühleren Stunden des Tages für den Torporeintritt (Barclay et al. 2001; Liu and Karasov 2011; Turner et al. 2012). Andererseits konnten bei einigen Arten wie z.B. torpiden Lemuren und Siebenschläfern trotz verhältnismäßig hohen Körper- und Umgebungstemperaturen niedrige Stoffwechselraten beobachtet werden (Dausmann et al. 2005; Elvert and Heldmaier 2005). Es bleibt daher fraglich, ob Torpor auch bei Umgebungstemperaturen auftreten kann, die ein Absinken der Körpertemperatur gänzlich unterbinden.

Weiterhin ist nicht verstanden, ob die hypometabole Stoffwechselrate hauptsächlich durch eine verringerte Verfügbarkeit an Energie (ATP) oder durch eine Inhibition energieverbrauchender Prozesse erlangt wird. Hauptbildungsort von ATP ist die oxidative Phosphorylierung in den Mitochondrien, die mehr als 90% des Sauerstoffverbrauchs eines normothermen Säugetieres in Anspruch nimmt (Rolfe and Brown 1997). Es wird diskutiert, ob eine verringerte Zellatmung als Ursache für die metabolische Inhibition im Torpor anzunehmen ist und welche molekularen Mechanismen zu einer Absenkung der mitochondrialen Atmung beitragen können (Staples and Brown 2008).

Ersten Studien zufolge könnte eine aktiv reduzierte Atmungsrate der Lebermitochondrien einen wichtigen Beitrag beim Eintritt in den Torpor leisten, wenn die Körpertemperatur des Tieres noch hoch ist (Brown et al. 2007).

1.4 Magnetresonanztomographie - Schau mal rein

Viele Fragen hinsichtlich der Regulation des Energiemetabolismus im Torpor und der zitterfreien Thermogenese sind noch unbeantwortet. Gleichzeitig wächst das Interesse auf diesem Gebiet. Torpor und braunes Fettgewebe haben in den letzten Jahren für die translationale Forschung an Bedeutung gewonnen (Bouma et al. 2012; Jinka and Duffy 2013), besonders seit aktives braunes Fett vor wenigen Jahren auch im Menschen nachgewiesen wurde (Lichtenbelt et al. 2009; Virtanen et al. 2009; Cypess and Kahn 2010; Gunawardana 2012). Um neue Blickwinkel auf dieses Gebiet zu erlangen, bieten sich bildgebende Methoden an.

Magnetresonanztomographen mit hohen Magnetfeldstärken (> 7 Tesla) eignen sich heutzutage für wissenschaftliche Untersuchungen von Kleintieren. Wegen des hervorragenden Weichgewebekontrasts wird die Magnetresonanztomographie (MRT) verbreitet in der Diagnostik pathologischer oder phänotypischer Veränderungen eingesetzt (Lyons 2005; Nieman et al. 2005; Waerzeggers et al. 2010). Überdies sind spektroskopische Untersuchungen möglich (Serkova et al. 2009). Mit Protonenspektroskopie lassen sich Fettsäurezusammensetzung und Fettgehalt von Organen bestimmen oder Neurotransmitter und Stoffwechselmetabolite darstellen. Phosphorspektren zeigen energiereiche Phosphate und sind hilfreich, um Änderungen im Energiemetabolismus oder dem intrazellulären pH-Wert verschiedener Gewebe zu detektieren (Willenborg et al. 2011; Agrawal et al. 2011; Kemp and Brindle 2012). Die Datenerhebung mittels MRT ist eine non-invasive Methode, die *in vivo* stattfindet. Ein großer Vorteil, um dynamische Prozesse in der tierexperimentellen Forschung verfolgen zu können.

In der Regel ist eine Narkotisierung der Versuchstiere während der Messung notwendig. Auf den Spuren der aktiven metabolischen Depression im Torpor ist dies jedoch kontraindiziert, da Anästhetika eine metabolische Inhibition verursachen und Hypothermie hervorrufen. MRT-Studien an Winterschläfern sind bisher selten und eine Weiterentwicklung des MRT-Potentials auf diesem Forschungsgebiet ist ein Teil der vorliegenden Arbeit (Bock et al. 2002; Henry et al. 2007; Hu et al. 2011).

Weniger kritisch sind Fragestellungen, die die morphologische Charakterisierung des braunen Fettes oder dessen thermoregulatorische Aktivierung betreffen. Neuste Messsequenzen erlauben eine Differenzierung und Quantifizierung von braunem und weißem Fettgewebe bei Mäusen und Ratten *in vivo* (Hu et al. 2010; Peng et al. 2013; Smith et al. 2013; Holstila et al. 2013). MRT spezifische Parameter, die den Bildkontrast beeinflussen, ändern sich in thermogenetisch aktivem braunem Fettgewebe (Hu et al. 2012).

Neben seiner ausgezeichneten Gewebedarstellung bietet MRT somit ein hohes Potential für die Visualisierung dynamischer Stoffwechselprozesse während der Thermoregulation und Kälteanpassung (Sbarbati et al. 2006; Khanna and Branca 2012).

1.5 Zielsetzung

Die vorliegende Promotionsarbeit befasst sich mit stoffwechselphysiologischen Prozessen, die einerseits die aktive Absenkung des Energiestoffwechsels bei *A. russatus* und *P. sungorus* anderseits die gezielte Stoffwechselsteigerung während der Thermogenese bei UCP1-KO Mäusen betreffen.

Der erste Teil dieser Arbeit stellt die Untersuchung der Stoffwechselreduktion bei Nahrungsmangel und während des täglichen Torpors in den Vordergrund.

- Welche metabolischen Anpassungen sind bei der arid lebenden Goldstachelmaus unter Futterreduktion zu beobachten? Ist Torporeintritt auch bei Umgebungstemperaturen möglich, die ein Absinken der Körpertemperatur auf hypotherme Werte unterbinden?
- Kann eine Inhibition der mitochondrialen Respiration als Auslöser für die metabolische Depression im torpiden Zustand angesehen werden?

Der zweite Teil dieser Arbeit fokussiert auf den Einsatz der Magnetresonanztomographie. Es soll ein Setup entwickelt werden, das die kontinuierliche Überwachung des metabolischen Zustands parallel zur Kleintierbildgebung ermöglicht und erlaubt, torpide Zwerghamster bildgebend zu untersuchen.

- Ist es möglich, dass nicht-narkotisierte, freibewegliche Zwerghamster in dem selbst-entwickelten Versuchsaufbau torpid werden? Tolerieren torpide Hamster das MRT-Scanning?

Zudem soll die Magnetresonanz (MR) für Bildgebung und Spektroskopie (MRS) genutzt werden, um braunes Fett *in vivo* zu charakterisieren und neue Einblicke in die Abläufe während der zitterfreien Thermogenese zu gewinnen.

- Lässt sich metabolisch aktives und inaktives Fettgewebe differenzieren? Welchen Einfluss hat die Photoperiode auf die Fettsäurezusammensetzung des weißen und braunen Fettgewebes von *P. sungorus*?
- Inwieweit lassen sich dynamische Prozesse im braunen Fettgewebe während der zitterfreien Thermogenese visualisieren und welchen Einfluss hat UCP1 dabei?

2 Methoden

2.1 Versuchstiere

Es wurden drei Spezies aus der Ordnung der Rodentia herangezogen. Alle Tiere stammten aus der institutseigenen Zucht der Philipps-Universität Marburg. Entsprechend der jeweiligen Fragestellung wurden die Tiere unter verschiedenen Photoperioden, Fütterungsbedingungen und Temperaturregimen gehalten.

2.1.1 Goldstachelmaus (*Acomys russatus*)

In ihrem natürlichen Habitat, der Judäischen Wüste Israels, toleriert *A. russatus* extrem hohe Umgebungstemperaturen und ein saisonal limitiertes Nahrungs- und Wasserangebot. In den Sommermonaten herrschen selbst in ihrem Unterschlupf Temperaturen von 32°C bis über 40°C (Lee et al. 1998; Elvert et al. 1999). Ein Absinken der Körpertemperatur auf hypotherme Werte ist unter diesen Bedingungen nicht möglich.

Um die Anpassungsstrategien von *A. russatus* an Futterreduktion und das Auftreten von Torpor über eine weite Umgebungstemperaturspanne zu studieren, wurden Körpergewicht, Stoffwechselrate und Körpertemperatur der Stachelmäuse protokolliert. Zunächst unter *ad libitum* Fütterung bei einer Umgebungstemperatur von 27°C (24 h lang) sowie bei 23°C, 32°C oder 35°C (weitere 24 h). Darauf folgend erhielten die Stachelmäuse nur noch 50% des *ad libitum* Futterverbrauchs und wurden eine Woche lang bei konstanten 27°C und weitere zwei Wochen bei 23°C, 32°C oder 35°C gehalten. Am Ende der dreiwöchigen Futterreduktion wurde die mitochondriale Bioenergetik der torpiden und normometabolen Stachelmäuse untersucht und mit *ad libitum* gefütterten Individuen verglichen.

2.1.2 Dsungarischer Zwerghamster (*Phodopus sungorus*)

Kurztagakklimatisierte (LD 8:16) Zwerghamster zeigen eine hohe Bereitschaft für spontanen, täglichen Torpor. Um den Einfluss der mitochondrialen Bioenergetik auf Torpor zu entschlüsseln, wurde die Respirationsleistung isolierter Mitochondrien von torpiden und normothermen sowie gefasteten (18 h) Zwerghamstern gemessen. Als Indikator für den metabolen Zustand wurde in diesem Versuch die Körpertemperatur der Tiere registriert.

Bei einer Umgebungstemperatur von 15°C sind die Torporbouts von *P. sungorus* besonders lang und tief (Ruf et al. 1993). Deshalb wurde *P. sungorus* für die Pilotstudie gewählt, Untersuchungen an einem nicht-narkotisierten, frei beweglichen Versuchstier im Kleintiertomographen durchzuführen.

Die Hamster wurden bei 15°C in einer Stoffwechselküvette im Magnetresonanztomographen platziert. Mittels indirekter Kalorimetrie wurde ihre Stoffwechselrate kontinuierlich gemessen, so dass die Bildgebung bei Erreichen des torpiden Zustands gestartet werden konnte. Ebenfalls mit MRT, jedoch unter Narkose, wurde die Gewebezusammensetzung von braunem und weißem Fettgewebe der Hamster bildgebend und spektroskopisch untersucht. Hierbei wurden kurztagakklimatisierte Zwerghamster (23°C und 5°C) und solche aus dem Langtag (LD 16:8, 23°C) verglichen. Die präparierten Gewebe wurden im Anschluss an die MRT mittels Gaschromatographie analysiert, um die erhobenen Daten zu validieren.

2.1.3 UCP1-knockout Maus (*Mus musculus*) 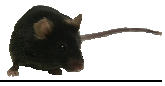

Im Vergleich zu Wildtypmäusen (C57BL/6J) besitzen UCP1-*knockout* (UCP1-KO) Mäuse kein funktionelles UCP1, da im *ucp1* Gen mittels homologer Rekombination das zweite Exon sowie Teile des dritten Exons durch eine Neomycin-Resistenzkassette ersetzt wurden. Dies führt zur Deletion einer wichtigen Transmembran-Domäne und somit zum Funktionsverlust des Proteins (Enerbäck et al. 1997). Um die Funktionalität von braunem Fett ohne UCP1 und die Fähigkeit zur UCP1-unabhängigen Thermogenese zu untersuchen, wurden UCP1-KO Mäuse und ihre wildtypischen Wurfgeschwister sukzessive für drei Wochen an 30°C, drei Wochen an 18°C und zwei Wochen an 5°C Umgebungstemperatur akklimatisiert und miteinander verglichen. Mit MR-Bildgebung wurde die Zusammensetzung des braunen Fettgewebes in jeder Temperaturstufe dargestellt. Die dynamische Reaktion nach Stimulation des braunen Fettgewebes durch Noradrenalin-Injektion wurde mit Wasserstoff- und Phosphorspektroskopie *in vivo* verfolgt. Über indirekte Kalorimetrie wurde zudem an wachen Mäusen die Steigerung des Energieumsatzes nach noradrenerger Stimulation im Vergleich zum Ruhestoffwechsel gemessen und die Kapazität der zitterfreien Thermogenese berechnet. Alle Messungen wurden unter annähernd thermoneutralen Bedingungen durchgeführt, um die metabolische Antwort auf Noradrenalin unter gleichen Voraussetzungen zu erhalten.

2.2 Methoden für die Datenerhebung

Für die Datenerhebung wurden die im Folgenden aufgelisteten Methoden eingesetzt. Auf die Grundlagen der indirekten Kalorimetrie, der Respirationsmessung isolierter Mitochondrien und der Magnetresonanztomographie wird in diesem Kontext vertiefend eingegangen. Weitere Informationen zu allen angewendeten Methoden und der statistischen Auswertung der erhobenen Daten sind im Material und Methodenteil der einzelnen Manuskripte (Kapitel 6) zu finden. Die in Kapitel 3 angegeben Ergebniswerte zeigen Mittelwerte (± Standardfehler).

Tierexperimentelle Arbeiten

- Akklimatisierung an verschiedene Photoperioden und Umgebungstemperaturen
- Dokumentation von Körpergewicht und Futteraufnahme
- Telemetrie der Körperkerntemperatur nach Implantation temperatursensitiver Sender
- Überwachung von Atemfrequenz, Herzschlagrate (mittels Elektrokardiogramm) und rektaler Körpertemperatur
- Indirekte Kalorimetrie zur Bestimmung von Ruhestoffwechsel, minimaler Stoffwechselrate, täglichem Energieverbrauch und zur Überwachung von Torporverhalten
- Bestimmung der zitterfreien Thermogenesekapazität nach noradrenerger Stimulation mittels indirekter Kalorimetrie
- Induktion von Torporverhalten durch Futterreduktion
- Inhalations- und Injektionsnarkose für Laparotomie und MRT-Untersuchungen
- Tötung zur Organentnahme (Leber, Niere, Herz und Skelettmuskel, epididymales weißes Fett, interscapulares und dorsal zervikales braunes Fett)

Alle durchgeführten Tierversuche wurden nach dem Deutschen Tierschutzgesetz beantragt und genehmigt.

Arbeiten zur mitochondrialen Bioenergetik

- Isolation von Mitochondrien aus Leber-, Nieren-, Skelettmuskel- und Herzgewebe mittels differentieller Zentrifugation
- Proteinquantifizierung mittels Biuret
- Messung des mitochondrialen Sauerstoffverbrauchs und Membranpotentials mit Clark-Elektrode und $TPMP^+$ sensitiver Elektrode
- Ermittlung des ADP/O-Verhältnisses, als Maß für die Effizienz der ATP-Synthase

- Messung der Wasserstoffperoxidproduktionsrate der Atmungskette als Maß für die Produktion reaktiver Sauerstoffverbindungen mittels Amplex Red Nachweis

Molekulare und analytische Verfahren

- Genotypisierung der UCP1-KO und wildtypischen Mäuse mittels Polymerease-Kettenreaktion
- Nachweis von UCP1 im braunen Fett mittels Western Blot Analyse
- Gaschromatographische Analyse von Fettsäuren
- Lipidisolation aus braunem und weißem Fettgewebe durch Chloroform-Methanol Extraktion
- Fettsäureisolation durch Transesterifikation der Triglyzeride

Entwicklung

- Entwicklung einer Stoffwechselküvette zur parallelen Anwendung von indirekter Kalorimetrie und MR-Bildgebung am nicht-narkotisierten Tier
- Etablierung eines Messaufbaus für indirekte Kalorimetrie mit einer Vorrichtung zur Temperaturregulierung der entsprechenden Stoffwechselküvette

*Magnetresonanztomo*graphie

- Planen und Einstellen von MRT-Messprotokollen
- Morphologische Bildgebung (T1 und T2 gewichtete Sequenzen)
- Relaxometriemessungen im braunen und weißen Fettgewebe (Ermittlung der T1- und T2-Zeiten)
- Spektroskopie (^{31}P und ^{1}H) im braunen und weißen Fettgewebe
- Angiographie der Sulzerschen Vene
- Volumetrische Vermessung des braunen Fettgewebes
- Nachverarbeitung der ^{31}P und ^{1}H Spektren durch Erstellen von Ergebnisprotokollen

2.2.1 Indirekte Kalorimetrie

Die Berechnung des Energieumsatzes eines Lebewesens aus seinem Sauerstoffverbrauch und seiner Kohlendioxidproduktion wird als indirekte Kalorimetrie bezeichnet. Pro Liter verbrauchtem Sauerstoff werden etwa 20 kJ Energie bereitgestellt (Ferrannini 1988). Der Sauerstoffverbrauch (VO_2) lässt sich mittels Gasanalyse aus der Differenz des Sauerstoffgehaltes von Einatemluft und Ausatemluft ermitteln, wodurch indirekt die Stoffwechselrate bzw. der Energieverbrauch eines Organismus bestimmt werden kann. Das Verhältnis zwischen Kohlendioxidproduktion und VO_2 wird als respiratorischer Quotient (RQ) bezeichnet und lässt Rückschlüsse auf das verstoffwechselte Substrat zu. So liegt der RQ bei 1,0 wenn ausschließlich Kohlenhydrate oxidiert werden und bei 0,7 wenn der Körper Fett verbrennt (Gnaiger 1983).

Die kalorimetrischen Messungen wurden in einem offenen respiratorischen System durchgeführt. Dazu wurden die Tiere in Messküvetten gehalten, die permanent mit Frischluft durchströmt wurden. Die Luft wurde mit einer konstanten Flussrate aus der Küvette abgesaugt, getrocknet und in die Gasanalysatoren geleitet.

In verschiedenen Versuchsteilen wurde der Energieumsatz der Tiere kontinuierlich einige Stunden bis mehrere Tage dokumentiert. Für die Messungen, die nicht mit MRT gekoppelt waren, wurden die Tiere in einem Klimaschrank mit regulierten Temperatur- und Lichtbedingungen gehalten. In diesem System konnten bis zu fünf Tiere parallel kalorimetrisch untersucht werden. Aus der Multiplikation von Flussrate und Änderungen im Gasgehalt (ΔO_2 in Vol%) wurde der VO_2 pro Zeiteinheit (ml O_2/h) berechnet.

Für die parallele Anwendung von MRT und indirekter Kalorimetrie eines Einzeltieres wurde eine Messanlage installiert, die den speziellen Anforderungen der MR-Bildgebung entsprach. Die Entwicklung spezieller Küvetten und Vorrichtungen erlaubte, die Atemluft sowohl von narkotisierten als auch nicht-narkotisierten Tieren direkt aus dem Tomographen zu registrieren. Die Regulation der Küvettentemperatur wurde unter Verwendung eines Wärmetauschers ermöglicht. Die Datensoftware der indirekten Kalorimetrie wurde angepasst und verbessert (flexibleres Messintervall, Berechnung des VO_2 mit Haldane-Transformation (Wagner and Horvath 1973)).

2.2.2 Mitochondriale Bioenergetik

Die Mitochondrien der Hamster und Stachelmäuse wurden aus Leber, Niere, Herz und Skelettmuskel isoliert. Für die Messung der mitochondrialen Respiration wurde eine temperaturregulierte, luftdichte Inkuionskammer verwendet, die am Boden mit einer Platin/Silber-Elektrode ausgestattet ist. Die Elektroden wurden mit Kaliumchlorid überschichtet und mit einer Teflonmembran abgedeckt, bevor der Messpuffer in die Inkubationskammer gegeben wurde. In diesem wurden die isolierten Mitochondrien suspendiert. Die Messung der Sauerstoffkonzentration in der Mitochondriensuspension basiert auf einer Redoxreaktion zwischen der polarisierten Platinelektrode und der Silberelektrode. Der messbare Stromfluss zwischen den Elektroden verhält sich dabei proportional zum Sauerstoffpartialdruck der Messlösung. Der Sauerstoffausgangsgehalt (nmolO/ml) des Messpuffers in der Kammer wurde in Abhängigkeit von der Inkubationstemperatur berechnet (Reynafarje et al. 1985). Als Inkubationstemperatur wurde in etwa die normotherme Körpertemperatur der Tiere gewählt und betrug für Hamstermitochondrien 37°C und für Stachelmausmitochondrien 34°C.

Es wurden vier mitochondriale Respirationszustände unterschieden:

State 2: Nach Zugabe von Rotenon, um Komplex I der Atmungskette zu inhibieren, wird die mitochondriale Atmung durch Zugabe von Succinat als Substrat gezielt über Komplex II initiiert.

State 3, phosphorylierende Atmung: Die Zugabe von ADP erhöht den Sauerstoffverbrauch der Mitochondrien, da der Protonengradient durch die ATP-Synthase abgebaut wird.

State 4, nicht-phosphorylierende oder Leck-Atmung: Nach Zugabe von Oligomycin, einem Inhibitor der ATP-Synthase, oder nach dem gänzlichen Verbrauch von ADP verringert sich die Atmungsrate. Die verbleibende Respiration ist auf dem geringen Rückstrom der Protonen über das basale Protonenleck der inneren Mitochondrienmembran begründet.

In den Lebermitochondrien wurde neben der State 4 Atmung mit einer $TPMP^+$ sensitiven Elektrode zusätzlich das mitochondriale Membranpotential gemessen, um Anhaltspunkte zu den Kopplungseigenschaften der Mitochondrienmembran zu erhalten.

FCCP, maximale Atmung: Durch Zugabe des künstlichen Entkopplers FCCP (Carbonylcyanid-4-trifluormethoxy-phenylhydrazon) wird die oxidative Phosphorylierung von der Atmungskette entkoppelt und die maximale Atmungskapazität der Mitochondrien gemessen.

2.2.3 Magnetresonanztomographie (MRT)

Die Tiere wurden in einem MRT-System speziell für Kleintiere untersucht. Zu den Hauptkomponenten zählen ein supraleitender Magnet, der ein statisches Magnetfeld (7 Tesla) erzeugt, sowie Shimspulen für den Ausgleich von Feldinhomogenitäten und Gradientenspulen zur periodischen Erzeugung von Magnetfeldgradienten (290 mT/m). Sende- und Empfangsspulen sorgen für die Einstrahlung von Hochfrequenzimpulsen und empfangen das Signal für die Bilderzeugung. Die Steuerung und Signalverarbeitung erfolgt über ein komplexes Gradienten-, Hochfrequenz- und Computersystem.

Die MRT basiert auf dem Kernspin von Atomen mit ungerader Massenzahl, die als rotierende elektrische Ladung ein eigenes magnetisches Moment aufweisen. Im Kleintierscanners richten sich die Spins längs zum starken Magnetfeld aus und präzedieren je nach Kern mit einer unterschiedlichen Larmorfrequenz. Durch Anregung der Spins mit einem Hochfrequenzpuls aus der Sendespule, kippen die Kernspins aus ihrer Längsmagnetisierung in eine Transversalmagnetisierung und induzieren in der Empfangsspule ein Signal. Durch den Einsatz periodisch geschalteter Magnetfeldgradienten können die Signale der Atome räumlich zugeordnet und zu Schnittbildern verarbeitet werden. Aufgrund ihrer natürlichen Häufigkeit in jedem Organismus und ihrer relativen Empfindlichkeit werden in der Regel Wasserstoffatome für die MRT herangezogen. Abhängig von ihrer Umgebung verhalten sich die Protonen im Magnetfeld anders, so dass das erzeugte Signal in jedem Gewebe unterschiedlich ausfällt. Drei gewebespezifische Parameter (Protonendichte, T1-Zeit und T2-Zeit) bilden die Grundlage dafür, dass der Gewebekontrast im Bild entsteht und sich verschiedene Gewebe mittels MRT differenzieren lassen.

Nicht nur die äußere Umgebung, sondern auch die direkte chemische Nachbarschaft eines Kerns beeinflusst sein Signal. So verhalten sich die Protonen einer Methylengruppe im Magnetfeld anders als die einer Methylgruppe. Mit Hilfe der Magnetresonanzspektroskopie (MRS) können so Molekülbausteine oder Moleküle in einem Gewebe aufgeschlüsselt werden. Bei dieser Methode wird das Signal nicht in ein Bild umgewandelt, sondern die relative chemische Verschiebung der Kerne zueinander in einem Spektrum dargestellt (de Graaf, 2007). Die MRS nutzt neben Protonen (^{1}H-Spektroskopie) auch andere Kerne wie z.B. Phosphor (^{31}P-Spektroskopie) als Signalgeber. Da jeder Kern im Magnetfeld mit einer spezifischen Larmorfrequenz präzediert, wird bei 7 T für die Anregung von Phosphor eine Phosphorspule mit einer Frequenz von 121,62 MHz und für Wasserstoff eine Wasserstoffspule mit einer Frequenz von 300,40 MHz benötigt.

Die Messsequenzen für die gewünschte Bildgenerierung (Orientierung und Kontrast der Schnittbilder) und die Spektren wurden entsprechend der Fragestellung entwickelt und optimiert. Braunes und weißes Fettgewebe wurde *in vivo* gescannt, um Parameter wie T1- und T2-Zeiten, Volumen oder morphologisches Erscheinungsbild zu bestimmen. Mit Protonenspektroskopie wurden Rückschlüsse auf den Lipidgehalt und die Lipidzusammensetzung gezogen. Verschiedene energiereiche Phosphate wurden mit Phosphorspektroskopie ermittelt.

3 Ergebnisse und Diskussion

3.1 Torpor statt Siesta: Warme Außentemperaturen kommen futterreduzierten Stachelmäusen gerade recht

(zu Kapitel 6.2; Grimpo et al. 2013)

Im Gegensatz zu anderen arid lebenden Nagetieren legt die Stachelmaus keine unterirdischen Bauten mit Futtervorräten an (Shkolnik 1966; Kronfeld-Schor and Dayan 1999). Stattdessen lagert sie bei ausreichend vorhandenem Nahrungsangebot Energiereserven in Form von Fettdepots ein (Shafrir and Adler 1983; Gutman et al. 2008). Die Oxidation von Körperfett dient als Energie- und metabolische Wasserquelle (Schmidt-Nielsen and Schmidt-Nielsen 1951). Das Ausgangsgewicht der *ad libitum* gefütterten Stachelmäuse im Versuch betrug 50-72 g und lag somit über dem Durchschnittsgewicht wildlebender Tiere (Elvert et al. 1999; Levy et al. 2011a). Während der ersten Woche Futterreduktion verloren alle Stachelmäuse deutlich an Körpergewicht. Bei moderaten Haltungstemperaturen kann *A. russatus*, früheren Studien zufolge, einem initialen Gewichtsverlust entgegensteuern und das Körpergewicht auf einem niedrigeren Level längerfristig halten (Merkt and Taylor 1994; Gutman et al. 2007). Dies war in der gegenwärtigen Untersuchung ebenfalls der Fall, wenn die Umgebungstemperatur von 27°C auf 32°C oder 35°C erhöht wurde. Bei einer Absenkung der Temperatur von 27°C auf 23°C dagegen, sank das Körpergewicht der Stachelmäuse stetig weiter. Doch selbst mit fortwährender Kälteexposition war der Gewichtsverlust (ca. 20%) am Ende der Futterreduktion vergleichsweise geringer als bei futterreduzierten Mäusen oder Gerbils (Merkt and Taylor 1994; Gutman et al. 2006).

Dieser geringe Körpergewichtsverlust bei allen untersuchten Umgebungstemperaturen lässt sich nur dadurch begründen, dass *A. russatus* ihre Energieausgaben drastisch einschränken kann. Tatsächlich reduzierten fast alle Stachelmäuse im Vergleich zur *ad libitum* Fütterung ihren täglichen Energieverbrauch (DEE) signifikant. Bei einer Umgebungstemperatur von 32°C bzw. 35°C soweit, dass trotz 50%iger Futterreduktion eine Stagnation der Körpergewichtsabnahme verzeichnet werden konnte.

Durch eine differenzierte Betrachtung der Stoffwechselraten ließ sich nachvollziehen, dass es sich bei der Absenkung des täglichen Energieverbrauchs um eine mehrstufige Anpassungsleistung von *A. russatus* handelt.

Die Thermoneutralzone der Stachelmaus (32-34°C) ist, wie bei anderen arid und semiarid lebenden Nagetieren, verhältnismäßig hoch (Haim and Borut 1981; Haim 1987).

Gleichzeitig weisen wüstenlebende Nagetiere einen sehr niedrigen Grundumsatz auf, wodurch der transepidermale Wasserverlust herabgesetzt wird (McNab and Morrison 1963; Haim and Izhaki 1993; Rubal et al. 1995). Der Ruhestoffwechsel der Stachelmäuse (40,9 ± 2,9 mlO_2/h) lag bei *ad libitum* Fütterung 40% unter dem Wert, den man für ein Nagetier dieser Gewichtsklasse annehmen würde (berechnet nach (Hayssen and Lacy 1985; Lovegrove 2003)). In der circadianen Ruhephase (Schlafphase) sank die Stoffwechselrate der Stachelmäuse um weitere 25% und minimale Stoffwechselwerte von 30,9 ± 1,8 mlO_2/h wurden gemessen. Bemerkenswerterweise war *A. russatus* während der Futterreduktion in der Lage ihre bereits extrem niedrigen Stoffwechselraten noch weiter abzusenken. So betrug der Ruhestoffwechsel nun 30,9 ± 2,2 mlO_2/h und die minimale Stoffwechselrate nur noch 19,1 ± 0,8 mlO_2/h (Abb. 4). Diese minimale Stoffwechselrate ließ sich bei den meisten Tieren als Torpor identifizieren, indem die Werte mit der individuellen torpiden Stoffwechselrate bei 27°C Umgebungstemperatur verglichen wurden.

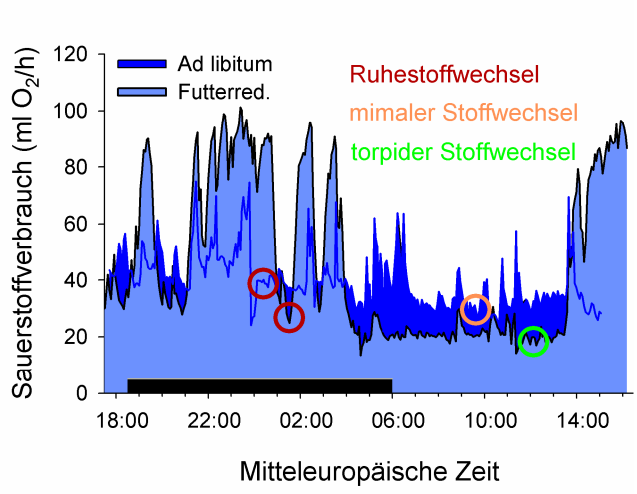

Abbildung 4 *Bestimmung verschiedener Stoffwechselraten von A. russatus bei 32°C Umgebungstemperatur.*
Die Ruhestoffwechselrate in der Aktivitätsphase (schwarzer Balken) und die minimale Stoffwechselrate in der Ruhephase bei *ad libitum* Fütterung (Graph im Hintergrund) und unter 50% Futterreduktion (vorderer Graph) wurden bestimmt. Die minimale Stoffwechselrate unter Futterreduktion entspricht in diesem Beispiel einer torpiden Stoffwechselrate.

Bei 23°C oder 27°C konnte das Auftreten von Torpor problemlos ermittelt werden, da neben der Stoffwechselreduktion auch die hypotherme Körpertemperatur als Indikator diente. Hier zeigten die Stachelmäuse während der Futterreduktion ebenfalls lange Torporepisoden, jedoch keine Reduktion der Ruhestoffwechselrate. Ältere Studien beschreiben bei Umgebungstemperaturen unterhalb der Thermoneutralzone entweder eine Absenkung des Ruhestoffwechsels oder das Auftreten von Torpor bei *A. russatus* als Antwort auf Futterreduktion (Merkt and Taylor 1994; Ehrhardt et al. 2005; Gutman et al. 2006; Gutman et al. 2007). Die Kombination beider Mechanismen wie sie in Thermoneutralität offensichtlich auftritt wurde bisher noch nicht dokumentiert.

Eine Differenzierung von Ruhestoffwechsel und torpidem Stoffwechsel in der Thermoneutralzone ist diffizil, da die Körpertemperatur nur geringfügig absinkt und eben nicht, wie bei niedrigen Umgebungstemperaturen, eindeutig hypotherme Werte annimmt. In den letzten Jahren wurden einige Berechnungsmodelle für Schwellenwerte entwickelt, um das Auftreten und die Länge von Torporereignissen anhand der Körpertemperatur auch in warmen Lebensräumen zu bestimmen (Barclay et al. 2001; Willis 2007; McKechnie et al. 2007). Basierend darauf wurde das Auftreten von täglichem Torpor bei *A. russatus* während der Sommermonate im Freiland beschrieben (Levy et al. 2011a). Unsere Datensätze zeigten jedoch, dass die Körpertemperatur besonders bei hohen Temperaturen zeitlich hinter der Stoffwechselrate zurückblieb oder die berechneten Schwellenwerte nicht unterschritt und somit eine Körpertemperatur basierte Auswertung zu Fehlinterpretationen des Torporverhaltens führt. Durch Messung der Stoffwechselrate hingegen ließen sich bis auf eine Ausnahme bei allen Individuen torpide Phasen bei 32°C und 35°C Umgebungstemperatur identifizieren. Dabei senkten die futterreduzierten Stachelmäuse ihre minimale Stoffwechselrate bei 32°C um 38% und bei 35°C um 25% im Vergleich zu ihrer Ruhestoffwechselrate ab. Ihre Körpertemperatur betrug 34,6 ± 0,2°C bzw. 36,9 ± 0,1°C und lag somit bis zu 10°C über der Körpertemperatur von Stachelmäusen, die bei 23°C torpid wurden (26,4 ± 0,6°C).

Die minimale Stoffwechselrate korrelierte mit der Körpertemperatur im tiefen Torpor. So wiesen torpide Stachelmäuse bei 23°C Umgebungstemperatur eine niedrigere Stoffwechselrate auf (13,6 ml O_2/h) als Tiere bei 35°C (18,9 ml O_2/h), weil sich biochemische Abläufe mit sinkender Temperatur verlangsamen (Q_{10}-Effekt (Malan 1993)). Die Relation zwischen Stoffwechselrate im Torpor und Körpertemperatur konnte mit einer exponentiellen Gleichung beschrieben werden ($MR_{torp} = 4.0554e^{(0.0447Tb)}$) und resultierte in einem Q_{10}-Wert von 1,7. Anhand dieser Gleichung wurden „torpide“ Stoffwechselraten für genau die Körpertemperatur ermittelt, die *A. russatus* während ihres Ruhestoffwechsels aufwies. Bei den 32°C akklimatisierten Tieren lag sie 36% niedriger als die Ruhestoffwechselrate während der Futterreduktion und sogar 51% niedriger im Vergleich zum Ruhestoffwechsel während der *ad libitum* Fütterung. Diese Ergebnisse verdeutlichen, dass täglicher Torpor bei konstant hoher Umgebungs- und normothermer Körpertemperatur bei *A. russatus* nicht nur möglich sondern äußerst effizient ist.

Ähnliche Hochrechnungen einer temperaturunabhängigen Depression der Stoffwechselrate von Winterschläfern in warmen Habitaten wie Schlafbeutlern (32%), Siebenschläfern (54%) und madagassischen Dickschwanz-Makis (28%) liegen in einer ähnlichen Größenordnung (Song et al. 1997; Heldmaier and Elvert 2004; Dausmann et al. 2009).

Im Torpor bei niedrigen Umgebungstemperaturen (23°C) wird diese temperaturunabhängige, aktive Stoffwechseldepression vom passiven Effekt der abgesenkten Körpertemperatur synergistisch begleitet, so dass besonders geringe Stoffwechselraten verzeichnet werden konnten.

Bei einigen Stachelmäusen konnten nur kurze und wenige torpide Phasen als Folge der Futterreduktion beobachtet werden. Zusätzlich zeigten diese Individuen statt einer Absenkung, eine Zunahme des DEE. Dies ist möglicherweise auf ein übersteigertes Explorationsverhalten zurückzuführen. Gutman et al. (2007) beschreiben sogenannte „non-resistant“ Stachelmäuse, die bei Futterentzug hyperaktives Verhalten und gar keinen Torpor zeigen. Als Ursache für dieses Verhalten ziehen sie einen verringerten Plasmaleptin-Spiegel der nicht-resistenten Tiere in Betracht. Tatsächlich hemmt die Applikation von Leptin fasteninduzierte Hyperaktivität bei Ratten (Exner et al. 2000). Die Kombination von Hyperaktivität und Torpor wurde bei *A. russatus* und anderen kleinen Nagern früher schon beobachtet (Ruf et al. 1991; Williams et al. 2002; Ehrhardt et al. 2005) und unterstreicht die Plastizität ihres Verhaltens auf Futterrestriktion. In diesen Fällen wurden die erhöhten Aktivitätskosten durch Torpor bedingte Energieeinsparungen wieder ausgeglichen, so dass keine Steigerung des DEE folgte. Die Ursache für einen Umschwung von Torporverhalten zu exzessiver Hyperaktivität mit der Folge einer negativen Energiebilanz ist noch unklar (Abb. 5). Es bleibt abzuwarten ob das Unterschreiten eines gewissen Körperfettgehaltes und entsprechend niedrige Leptinspiegel als Auslöser für die Hyperaktivität in Frage kommen.

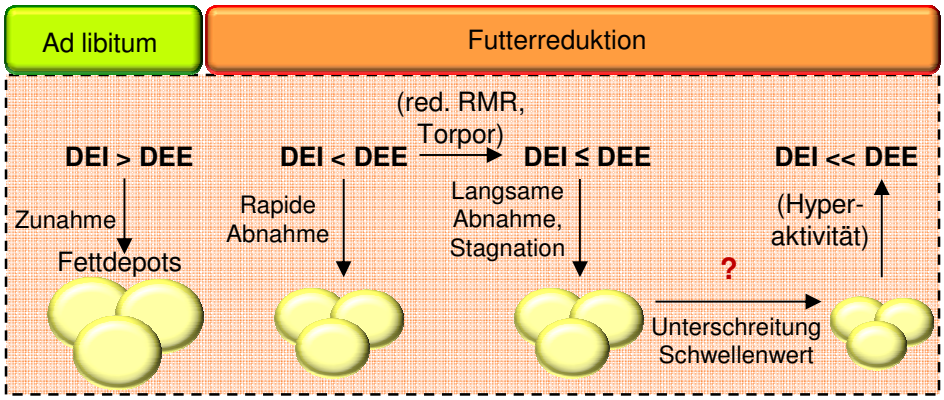

Abbildung 5 *Übersichtsschema der Anpassungsvorgänge von A. russatus an ein verändertes Nahrungsangebot durch langfristige Futterreduktion.* Die initiale Gewichtsabnahme bei Futterreduktion induziert eine Absenkung des Energiestoffwechsels, die einem weiteren Gewichtsverlust entgegenwirkt. Die Ursache für einen Wechsel von Energieeinsparmechanismen zu hyperaktivem Verhalten ist unklar. Als hypothetische Annahme kommen ein stark verringerter Körperfettgehalt und Änderungen im Plasmaleptin-Spiegel in Frage. DEI: Tägliche Energiezufuhr; DEE: Täglicher Energieverbrauch; red. RMR: reduzierter Ruhestoffwechsel

Ein hohes Körpergewicht und die Verabreichung von Leptin jedenfalls vermindern die Torporbereitschaft von *A. russatus* (Ehrhardt et al. 2005; Gutman et al. 2008).

Das Auftreten von Torpor bei *ad libitum* gefütterten Stachelmäusen unter Laborbedingungen wurde in dieser Studie erstmalig beobachtet. Es hebt hervor wie flexibel das Torporverhalten von *A. russatus* ist. Die Torporbouts traten primär bei Kälteexposition (23°C und 27°C) auf. Ein präventiver Gebrauch von Torpor, um thermoregulatorische Kosten zu reduzieren und Energiereserven zu schonen oder Torpor als Meideverhalten vor Fressfeinden wurde bei anderen Tierarten bereits mehrfach beschrieben (Geiser and Baudinette 1987; Bieber and Ruf 2009; Munn et al. 2010). Im Freiland konnte Torpor bei *A. russatus* ebenfalls trotz ausreichendem Nahrungsangebot vereinzelt beobachtet werden und die Koexistenz mit einer anderen Stachelmausart (*A. cahirinus*) führt zu einer gesteigerten Torporhäufigkeit (Levy et al. 2011a; Levy et al. 2011b).

Die ausführliche metabolische Kartierung von *A. russatus* unter Futterreduktion und *ad libitum* Bedingungen bei verschiedenen Umgebungstemperaturen in dieser Studie unterstreicht, dass die minimale Stoffwechselrate eines Organismus keine feste Größe ist, sondern entsprechend der energetischen Anforderungen kontrolliert reguliert werden kann. Der Einsatz von täglichem Torpor zur Schonung der internen Energiereserven ist auch bei sehr hohen Temperaturen eine wirkungsvolle Strategie und im Tierreich möglicherweise verbreiteter als bislang angenommen. Um Torpor bei Hitze zuverlässig erkennen und charakterisieren zu können, ist die Messung der Stoffwechselrate unabdingbar. Es ist ungewiss welche Mechanismen Torpor auslösen. Eine Absenkung des Sauerstoffverbrauchs in den Mitochondrien könnte zu einer rapiden Stoffwechseldepression führen, wie sie im Topor der Fall ist.

3.2 Die Zellatmung wird nicht abgeschaltet um Torpor bei *A. russatus* zu induzieren

(zu Kapitel 6.3; Grimpo und Kutschke et al. 2014)

Es wird vermutete, dass den Mitochondrien als primären Sauerstoffkonsumenten des Organismus, eine Schlüsselrolle bei der Regulation des Torporeintritts zukommt. So zeigen einige Winterschläfer und Dsungarische Zwerghamster im torpiden Zustand eine aktive Inhibition der mitochondrialen Atmung (Staples and Brown 2008). Um zu prüfen, ob dies auch im Torpor von futterreduzierten Stachelmäusen zutrifft, wurde die mitochondriale Bioenergetik von 32°C akklimatisierten Tieren untersucht. Anders als bei torpiden Zwerghamstern, deren phosphorylierende Atmung in den Lebermitochondrien um 30% reduziert ist (Brown et al. 2007), wiesen die Mitochondrien der torpiden Stachelmäuse in keinem der vier untersuchten Respirationszustände eine Änderung auf. Es unterschieden sich weder die State 2, die phosphorylierende (State 3) und die nicht-phosphorylierende (State 4) Atmungsrate noch die maximale Atmungskapazität von Mitochondrien aus Leber, Herz, Skelettmuskel und Niere zwischen normothermen und torpiden Stachelmäusen. Eine gleichbleibende State 4 Atmung kann unter Umständen auftreten, wenn sich das basale Protonenleck und das Membranpotential von Mitochondrien simultan ändern (Keipert and Jastroch 2014). Dies war bei *A. russatus* nicht der Fall, wie Messungen des Protonenlecks an isolierten Lebermitochondrien zeigten. Somit liegt hier ein weiterer Unterschied zu *P. sungorus*, dessen Membrandurchlässigkeit im Torpor erhöht ist (Brown et al. 2007). Vergleiche des ATP/O-Verhältnisses von Leber- und Nierenmitochondrien der normothermen und torpiden Stachelmäuse ergaben keine Unterschiede in der Effizienz der ATP-Synthase. Um Effekte der Futterreduktion auf die mitochondrialen Atmungseigenschaften auszuschließen (Hagopian et al. 2005) wurden *ad libitum* gefütterte mit futterreduzierten Stachelmäusen verglichen. Es ergaben sich keine Unterschiede in den mitochondrialen Atmungsraten der vier untersuchten Gewebe, dem Membranpotential der Leber oder im ATP/O-Verhältnis von Leber- und Nierenmitochondrien.

Die ermittelten Ergebnisse sind besonders hervorzuheben, weil die thermoneutral gehaltenen *A. russatus* im Torpor eine normotherme Körpertemperatur hatten. Bisher wurde den Mitochondrien eine regulierende Rolle für den Torporeintritt zugeschrieben, wenn die Körpertemperatur der Tiere noch normotherm ist (Brown et al. 2007; Brown and Staples 2010).

Brown et al. schlussfolgerten dies aus der Beobachtung, dass ein Unterschied in der phosphorylierenden Atmung der Lebermitochondrien zwischen normothermen und torpiden Hamstern nur zu finden ist, wenn die Mitochondrien bei einer hohen Inkubationstemperatur (37°C) gemessen werden, nicht aber bei 15°C.

Die Stachelmäuse zeigten jedoch keine Depression der mitochondrialen Respirationsrate, obwohl sie im Torpor eine konstant hohe Körpertemperatur aufwiesen. Dieser Befund stellt die Bedeutung einer mitochondrialen Inhibition bei hohen Körpertemperaturen für den Torporeintritt, wie sie bisher angenommen wurde, in Frage.

Kaltakklimatisierte Stachelmäuse, die bei einer Umgebungstemperatur von 23°C nicht nur ihre Stoffwechselrate, sondern auch ihre Körpertemperatur im Torpor signifikant verringerten, zeigten ebenfalls keine Absenkung der mitochondrialen Atmungsraten in den vier untersuchten Geweben. In Niere und Skelettmuskel torpider Stachelmäuse war die phosphorylierende Atmung im Vergleich zu normothermen Individuen sogar etwas erhöht. Das ATP/O Verhältnis der Leber- und Nierenmitochondrien blieb unverändert.

Die Gesamtheit der Ergebnisse weist darauf hin, dass die reduzierte Absenkung der Stoffwechselrate im Torpor bei *A. russatus* nicht durch eine aktive Inhibition der mitochondrialen Respiration induziert wird. Bei *P. sungorus* dagegen könnte eine aktive Hemmung der Substratoxidation in den Lebermitochondrien bis zu 23% der metabolischen Reduktion im Torpor erklären (Brown et al. 2007).

Offen bleibt, welche molekularen Mechanismen bei futterreduzierten *A. russatus* zu der beobachteten Stoffwechseldepression führen. Eine regulierte Verringerung energieverbrauchender Vorgänge wie der Proteinbiosynthese sowie die Hemmung ATP-liefernder Prozesse wie der Glykolyse sind vorstellbar und wurden bereits bei winterschlafenden Arten und torpiden Zwerghamstern nachgewiesen (Berriel Diaz et al. 2004; Andrews 2007; Storey and Storey 2010).

Futterreduzierte Stachelmäuse senkten ihre Energieausgaben bei thermoneutraler Haltung im Vergleich zu *ad libitum* Bedingungen nicht nur durch Torpor ab, sondern reduzierten ihren gesamten Grundstoffwechsel. Nach dreiwöchiger Futterreduktion waren die Organgewichte der Leber, Niere und des Herzmuskels im Vergleich zu *ad libitum* gefütterten Kontrolltieren verringert. Da die metabolische Aktivität aller Organe zum Grundstoffwechsel beiträgt, erklärt eine Abnahme der Organgewichte anteilig den reduzierten Energieverbrauch (Ferraris et al. 2001). Eine Korrelation zwischen Stoffwechselrate oder Körpertemperatur und mitochondrialer Respiration der präparierten Organe, wie bei gefasteten und gefütterten Mäusen beschrieben (Brown and Staples 2010), konnte indes bei *A. russatus* nicht ermittelt werden.

3.3 Abgekühlt: Lebermitochondrien reduzieren ihre Atmung in Anpassung an Hypothermie im Torpor

(zu Kapitel 6.4; Kutschke und Grimpo et al. 2013)

Im Gegensatz zur arid lebenden Stachelmaus sind Dsungarische Zwerghamster und winterschlafende Ziesel im Winter mit sehr kalten Umgebungstemperaturen konfrontiert. Sie weisen im Torpor sehr niedrige Körpertemperaturen auf, das Arktische Ziesel bis zu -3°C (Barnes 1989). Eine verringerte mitochondriale Atmung im Torpor wurde bei diesen Tierarten bereits mehrfach beobachtet (Fedotcheva et al. 1985; Martin et al. 1999; Barger et al. 2003; Muleme et al. 2006; Brown et al. 2007). Im Vergleich der mitochondrialen Respiration von torpiden und normothermen Zwerghamstern konnten in einem ersten Schritt die Beobachtungen von Brown et al. (2007) bestätigt werden. Bei einer Inkubationstemperatur von 37°C war die phosphorylierende Atmung (State 3) der isolierten Lebermitochondrien aus torpiden Individuen signifikant reduziert. Zudem waren die State 2 und die nicht-phosphoylierende Atmung (State 4) sowie tendenziell die maximale Respirationskapazität verringert.

Es sind verschiedene Angriffspunkte denkbar, die zu einer Änderung der mitochondrialen Respiration führen konnten; die Substratoxidation, die Phosphorylierung oder das basale Protonenleck (Hafner et al. 1990). Weil alle Atmungszustände verringert waren und gleichzeitig bei Messungen des Protonenlecks keine Änderung der Membrandurchlässigkeit festgestellt wurde, konnte in unserer Studie auf eine Inhibition der Succinatoxidation geschlossen werden. Dieser Befund steht in Übereinstimmung mit Brown et al. (2007), die eine Inhibition der Atmungskomplexe I und II als Ursache für die verringerten Atmungsraten der Lebermitochondrien vermuten. Welche Moleküle die intrinsische Inhibition bewirken kann bisher nur spekuliert werden. Jedenfalls blieb sie während der Mitochondrienisolation aus dem Gewebe erhalten. Untersuchungen an Zieseln weisen darauf hin, dass eine Hemmung der Succinatdehydrogenase (Komplex II der Atmungskette) im Winterschlaf durch Oxalacetat hervorgerufen werden kann (Fedotcheva et al. 1985; Armstrong and Staples 2010).

Durch weitere Untersuchungen wurden die Ergebnisse von Brown et al. (2007) ergänzt, um die physiologischen Ursachen für die aktive Inhibition der Mitochondrien zu identifizieren. Alle Hamster unserer Studie waren nachweislich in der Lage torpid zu werden und hatten ein ähnliches Körpergewicht. Mögliche Effekte der Torporfähigkeit oder des Körpergewichts als Impuls für die abweichende mitochondriale Oxidationsleistung zwischen torpiden und normothermen Tieren kamen folglich nicht in Frage (Polymeropoulos et al. 2012).

Ein Vergleich zwischen *ad libitum* gefütterten und gefasteten Hamstern zeigte zudem keine Unterschiede in der mitochondrialen Bioenergetik von Leber und Niere.

Somit bestand kein Anlass die beobachteten Änderungen im Torpor auf eine verringerte Nährstoffzufuhr zurückführen.

Interessanterweise korrelierten die State 3 und State 4 Atmung der Lebermitochondrien mit der Körpertemperatur der Hamster zum Zeitpunkt der Tötung. Bei normothermen Mäusen wurde ein vergleichbarer Zusammenhang zwischen mitochondrialer Atmungsrate und Körpertemperatur beschrieben (Brown and Staples 2010). Diese Temperaturabhängigkeit spricht dafür, dass die Inhibition der mitochondrialen Leberrespiration eine aktive Anpassung an die hypotherme Körpertemperatur im Torpor ist und weniger mit dem torpiden Zustand per se zusammenhängt. Dies würde auch erklären, warum eine mitochondriale Depression bei Tierarten zu finden ist, die an kalte Umgebungstemperaturen angepasst sind (Fedotcheva et al. 1985; Martin et al. 1999; Barger et al. 2003; Muleme et al. 2006; Brown et al. 2007), aber nicht bei *A. russatus*, die auf hypometabole Zustände in Wärme spezialisiert ist.

Bei *P. sungorus* scheinen nur die Mitochondrien der Leber betroffen zu sein, denn in anderen stoffwechselaktiven Geweben (Skelettmuskel, Herz oder Niere) wurden keine Änderungen der mitochondrialen Respirationsleistung festgestellt.

Das Ausmaß der aktiven Inhibition als Reaktion auf hypotherme Temperaturen scheint nicht nur gewebespezifisch sondern auch artspezifisch unterschiedlich zu sein. So ist die State 3 Respiration von Lebermitochondrien zweier Zieselarten im Winterschlaf bis zu 75% reduziert (Barger et al. 2003; Muleme et al. 2006), während sie bei einer dritten Art nur um etwa 30% absinkt (Martin et al. 1999). Bei einigen Arten ist nur die State 3 Respiration betroffen, bei anderen wiederum die phosphorylierende und die nicht-phosphorylierende Atmung (Martin et al. 1999; Barger et al. 2003; Muleme et al. 2006). Die Änderung der Respirationsrate beruht nicht immer auf einer reduzierten Aktivität bestimmter Atmungskomplexe, sondern kann auch durch verringerten Elektronentransfer über die Atmungskette, Änderungen in der Membranfluidität oder der Membrandurchlässigkeit begründet sein (Staples and Brown 2008).

In Anbetracht aller Befunde ist die aktive Inhibition der Substratoxidation, wie sie bei *P. sungorus* in den Lebermitochondrien auftritt, nur eine mögliche Stellschraube der mitochondrialen Bioenergetik als Antwort auf eine hypotherme Körpertemperatur und Torpor. Es bleibt spannend das komplexe Zusammenspiel zwischen Energiehaushalt, Zellatmung und Körpertemperatur weiter zu entwirren.

3.4 Ohne Narkose und trotz Lärm: *In vivo* Bildgebung von torpiden Zwerghamstern lässt sich verwirklichen

(zu Kapitel 6.5; Grimpo et al. In Vorbereitung)

Mit MRT sind prinzipiell verschiedenste morphologische und funktionelle *in vivo* Messungen, bis hin zur Ermittlung des ATP Flux in den Mitochondrien, an narkotisierten Tieren möglich (Amara et al. 2008; Lee and Marcinek 2009). Messungen am wachen Tier sind selten und setzen häufig ein aufwendiges Training der Tieren voraus (Martin et al. 2013). Der Aufbau einer indirekten Kalorimetrie-Messanlage am 7 T Magnetresonanztomographen und die Entwicklung einer Stoffwechselküvette mit integrierter Protonenspule ist eine apparative Neuentwicklung. Sie erlaubte es, die Stoffwechselrate nicht-narkotisierter Hamster zu überwachen, während sie im Tomographen untersucht wurden. Das Setup konnte soweit optimiert werden, dass die Hamster im Tomographen torpid wurden und den torpiden Zustand für die Dauer der MRT-Messung aufrechterhielten. Dazu trugen sowohl eine Schallisolierung aus Akustikschaum um die Küvette als auch ein extern geschalteter Kühlkreislauf zur Regulation der Küvettentemperatur bei. Da eine Wasserkühlung die Bildgebung stören würde, wurde mit Hilfe eines Wärmetauschers 15°C kalte Luft eingeleitet. In der gekühlten Küvette wurden 10 von 13 getesteten Hamstern torpid. An insgesamt 30 Versuchstagen wurden 13 Torporbouts registriert. Diese Torporquote von etwa 50% ist vergleichbar mit Hamstern in einer Standardhaltung (Ruf et al. 1993). Während 10 der 13 Torporbouts konnten MRT-Messungen durchgeführt werden, ohne dass die Hamster aus dem Torpor erwachten. Die an der Küvette montierte Volumenspule erlaubte die Akquisition hochauflösender Ganzkörperbilder, sowie die Bildgebung einzelner Organe (z.B. Gehirn) in allen drei Schnittebenen. Die zusammengekauerte Körperhaltung im Torpor zentrierte die Organe auf die Körpermitte, so dass z.B. das Herz dicht von den braunen Fettdepots umgeben war (siehe Anhang). Eine schnelle Umverteilung der im braunen Fett generierten Wärme während der Aufwachphase aus dem Torpor wird somit gewährleistet. Erste angiographische Darstellungen der großen Blutgefäße konnten ohne Kontrastmittel visualisiert werden. Es gelangen protonenspektroskopische Messungen im braunen Fettgewebe. Im akquirierten Lipidspektrum ließ sich nicht nur die Fett- von der Wasserfraktion unterscheiden. Durch die hohe Auflösung konnten auch Signale von kleinen Molekülkomponenten mit geringem Signalpotential (z.B. CH=CH Bindungen) im Spektrum dargestellt werden. Es ist also erstmalig gelungen, torpide Hamster ohne Narkose mit MRT bildgebend und spektroskopisch zu untersuchen. Um zukünftig Datensätze zu erheben, die mehr über die funktionellen Vorgänge im Torpor aussagen, sind weitere Optimierungen der Hard- und Software nötig.

Ein verbessertes Signal- zu Rauschverhältnis sowie ein höheres örtliches Auflösungsvermögen können durch Änderungen in den Messsequenzen oder höhere Sensitivität der Spule erreicht werden. So würde eine verfeinerte Darstellung des Blutgefäßsystems die Voraussetzung schaffen, Blutflussmessungen innerhalb der Organe und Gewebe durchzuführen. Der Einsatz von langanhaltenden Kontrastmitteln zur Signalverstärkung wäre ebenfalls denkbar. Die Spektroskopie würde davon profitieren, wenn die Spule dichter am Hamster platziert wäre. Je besser das Signal ist, desto mehr Peaks können in den Spektren differenziert werden. Änderungen im Laktatspiegel oder verschiedene Neurotransmitter könnten dann detektiert werden (Graaf 2007). Die Entwicklung einer doppeltgetunten Oberflächenspule für Protonen und Phosphor, die sowohl Bildgebung als auch die Spektroskopie energiereicher Phosphate zuließe, wäre hilfreich, um mehr über die Energiehomöostase verschiedener Gewebe im Torpor zu erfahren. Funktionelle Messungen, wie Spektroskopie oder die Quantifizierung des Blutflusses erfordern Messsequenzen mit einer längeren Akquisitionszeit als die einfache Bildgebung. Dies macht sie anfällig gegenüber Bewegungsartefakten. Da Zwerghamster auch im Torpor mobil sind, erschwert dies die Durchführung zeitaufwendiger Messsequenzen. Die Bewegungen der Hamster konnten durch mehr Nistmaterial in der Küvette sowie die Erhöhung des Sitzbrettrandes bereits erfolgreich verringert werden. Eine technische Weiterentwicklung ist nun die Voraussetzung, um hochqualitative *in-vivo* Ergebnisse während des Torpors zu erhalten und das Potential der MRT ausschöpfen zu können (Abb. 6).

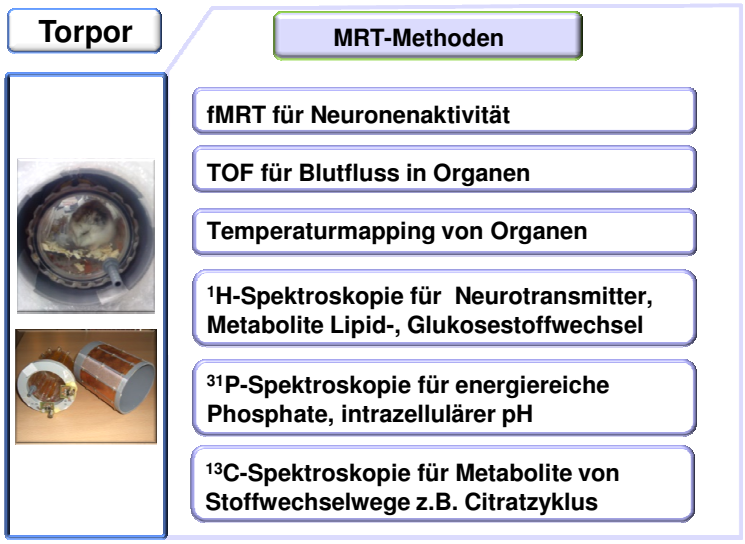

Abbildung 6 *Funktionelle Messmethoden mit Magnetresonanztomographie (MRT)*
Durch eine Optimierung des Versuchssetups wären verschiedene Messungen mit MRT vorstellbar, die Rückschlüsse und neue Anhaltspunkte über die Regelmechanismen im Torpor geben könnten. fMRT: funktionelles MRT, TOF: Time of Flight Sequenz

3.5 Fett ist nicht gleich Fett: Eine Differenzierung von thermogenetisch aktivem und inaktivem Fettgewebe *in vivo* ist möglich

(zu Kapitel 6.5; Grimpo et al. In Vorbereitung)

Die Steigerung der Thermogenesekapazität in Folge einer kürzeren Photoperiode oder länger anhaltender Kälteexposition beruht hauptsächlich auf einer Umstrukturierung des braunen Fettgewebes. In *ex vivo* Untersuchungen wurde vielfach gezeigt, dass kleinlumigere Lipidtröpfchen, sowie ein erhöhter Zytoplasma-, Mitochondrien- und UCP1-Gehalt der braunen Adipozyten hierbei den Ausschlag geben (Heldmaier 1974; Klingenspor 2003; Li et al. 2014). Zudem ist die Aktivierung des braunen Fettgewebes von einer stärkeren Durchblutung begleitet (Baba et al. 2007).

Die Änderungen der Gewebezusammensetzung spiegelten sich in der Bildgebung mittels MRT wider. Eine T1-gewichtete Darstellungen des braunen Fettgewebes ergab bei kurztagakklimatisierten Hamstern verglichen mit langtagakklimatisierten Individuen ein hypointenses Signal. Zusätzliche Kälteexposition (Haltung bei 5°C) verringerte das Signal noch weiter. Zudem wies das braune Fettgewebe der kurztagakklimatisierten Hamster eine längere T1-Zeit und eine kürzere T2-Zeit auf. Das verringerte Signal und die MRT-spezifischen Parameter sind eindeutige Indikatoren für eine Verringerung des Fettgehaltes und eine Erhöhung des Wassergehaltes im Gewebe. Wie bei den Hamstern konnte auch in C57BL/6J Mäusen eine vergleichbare thermogenetische Aktivierung des braunen Fettgewebes *in vivo* beobachtet werden. Die Mäuse waren stufenweise von thermoneutraler Umgebungstemperatur (30°C) an Kälte (18°C und 5°C) akklimatisiert worden. Bei zunehmender Kälteexposition nahm das Signal im interscapularen braunen Fettdepots von medial nach proximal ab. Spektroskopische Untersuchungen bestätigten anhand des $(CH_2)_n$-Peaks einen geringeren Lipidgehalt im Kernbereich des braunen Fettdepots bei den kaltakklimatisierten Mäusen. Eine Abnahme des Fett-Signal Anteils im interscapularen braunen Fett von kälteexponierten Mäusen wird auch durch eine neuere Studie belegt (Smith et al. 2013). Nicht nur eine längerfristige Kälteanpassung, sondern auch eine akute pharmakologisch induzierte Aktivierung der zitterfreien Thermogenese, spiegelt sich in einer Abnahme des MR-Signals von braunem Fettgewebe wider (Sbarbati et al. 2006; Khanna and Branca 2012). Die Ergebnisse zeigen, dass die Aktivierung des braunen Fettgewebes im MRT visualisiert werden kann.

Eine größere Herausforderung stellt die Quantifizierung der aktiven braunen Fettdepots dar, da hierfür eine deutliche Abgrenzung zu weißem Fettgewebe erforderlich ist. Zwar ist der mit MRT ermittelte Fett-Signal Anteil im braunen Fett geringer als im weißen Fett und basierend auf diesem Unterschied ist eine Quantifizierung der verschiedenen Fettdepots prinzipiell möglich

(Hu et al. 2010; Hu et al. 2012; Peng et al. 2013). Dennoch wird die Differenzierung bei sehr kleinen Depots oder wenn braunes und weißes Fett gemischt vorliegen knifflig. Ideal wäre eine Messsequenz mit der das braune Fettgewebe im MRT-Bild dargestellt werden könnte während das Signal des weißen Fettgewebes unterdrückt würde. Dazu müssten sich die gewebespezifischen Relaxationszeiten (T1, T2) ausreichend unterscheiden, denn auf ihnen beruht die Einstellung des Bild-Kontrastes.

Die Untersuchung der Signalstärke und der Relaxationszeiten (T1- oder T2- Zeit) des epididymalen weißen Speicherfettes von *P. sungorus* ergab keine Veränderung nach Kurztagakklimatisierung. Das epididymale Fettgewebe weist in kurzer Photoperiode zwar eine erhöhte Lipidmobilisation und Noradrenalinsensitivität auf (Klingenspor et al. 1996b; Bowers et al. 2005), aber offensichtlich keine morphologischen Änderungen, die die MR-Parameter beeinflussen. Im Vergleich zu braunem Fettgewebe war die T2-Zeit des weißen Fettgewebes tatsächlich in allen Akklimatisationsstufen signifikant höher. Allerdings unterschieden sich die T1-Zeiten nicht voneinander. Somit ließ sich eine alleinige Unterdrückung des weißen Fettgewebes im Bild nicht realisieren. Die ermittelten Zeiten werden allerdings zukünftig zu einem optimierten Gewebekontrast in der Kleintierbildgebung im Ultrahochfeld beitragen können. Bisherige Literaturwerte beziehen sich in der Regel auf Untersuchungen am Menschen mit niedrigeren Feldstärken und besonders die T1-Zeit wird von der Magnetfeldstärke beeinflusst (Schick 2005). Die im Hamster ermittelten T1-Zeiten (440-480 ms) und T2-Zeiten (120-140 ms) für das weißes Fettgewebe lagen vermutlich deshalb über den Literaturwerten (T1: 260-380 ms, T2: 68-80 ms; de Bazelaire et al. 2004; Köchli et al. 2009). Für braunes Fettgewebe ließen sich keine Referenzwerte finden.

Für eine Analyse von Auswirkungen der Photoperiode auf die Fettsäurezusammensetzung verschiedener Gewebe bei *P. sungorus*, diente die MR-Spektroskopie. Die mittlere Kettenlänge der Fettsäuren im interscapularen braunen und epididymalen weißen Fett unterschied sich nicht, wohl aber der Sättigungsgrad der Fettsäuren. Die Spektroskopie ergab Hinweise auf ein höheres Vorkommen von Doppelbindungen im weißen Fettgewebe. Sowohl der Anteil ungesättigter Fettsäuren insgesamt als auch der Anteil der mehrfach ungesättigten Fettsäuren lag im weißen Fett über dem des braunen Fettgewebes. Diese Beobachtung deckt sich mit Untersuchungen an Mäusen und an isoliertem Gewebe von Ratten (Zancanaro et al. 1994; Strobel et al. 2008; Mosconi et al. 2011; Hamilton et al. 2011).

Die ^{1}H-MRS Ergebnisse konnten *post mortem* mittels gaschromatographischer Analyse des Fettgewebes validiert werden. Die Ergebnisse beider Methoden bezüglich Kettenlänge und Sättigung der Fettsäuren korrelierten miteinander.

Die Variabilität der *ex vivo* Daten fiel jedoch geringer aus als die *in vivo* Ergebnisse, so dass Unterschiede, die in den spektroskopischen Daten marginal waren mit Gaschromatographie als signifikant bestätigt werden konnten. Ein Photoperiodeneffekt war bei den mehrfach ungesättigten Fettsäuren zu beobachten. Ihr Anteil nahm bei Kurztaganpassung im weißen Fett und laut gaschromatographischer Analyse auch im braunen Fett signifikant zu. Eine kürzlich erschienene Studie, die das braune Fettgewebe von Hamstern aus kurzer und langer Photoperiode verglich, fand keine Unterschiede im Sättigungsgrad der Gewebe, obwohl sich in Folge der Kurztagakklimatisierung das Vorkommen einiger Fettsäuren erheblich verschob (Geiser et al. 2013). So nahm, wie in meiner Analyse, die Stearinsäure im Kurztag signifikant zu und die Palmitoleinsäure ab. Hier stieg jedoch die Konzentration der Linolensäure deutlich, während diese bei Geiser et al. unverändert blieb. Eine Ursache für diese Diskrepanz liegt möglicherweise in der Fütterung der Tiere begründet, die Diäten unterschiedlicher Hersteller (Altromin vs. Ssniff) erhielten. So kann das Futter die Fettsäurezusammensetzung des Gewebes erheblich beeinflussen (Frank 1992; Florant et al. 1993). Die Verfügbarkeit von ungesättigten Fettsäuren in der Nahrung wirkt sich dabei positiv auf das Torporverhalten im Winterschlaf aus (Geiser and Kenagy 1987; Florant 1998). Ziesel verzehren vor der Winterschlafsaison gezielt eine Kost mit hohem Anteil an mehrfach ungesättigten Fettsäuren (Frank 1994; Frank et al. 1998). Die Autoren vermuten, dass ungesättigte und langkettige Fettsäuren die Fluidität der Zellmembran steigern und somit tiefere Körpertemperaturen im Torpor zulassen. Einen Zusammenhang zwischen der veränderten Fettsäurezusammensetzung als Antwort auf die kurze Photoperiode, in der *P. sungorus* täglichen Torpor zeigt, liegt nahe (Geiser et al. 2013) und tritt meinen Daten zufolge nicht nur im thermogenetisch wichtigen braunen Fett, sondern auch im weißen Speicherfett auf. Kürzlich durchgeführte Studien an Mäuse legen nahe, dass mehrfach ungesättigte Fettsäuren die respiratorische Kapazität der beiden Fettgewebe erhöhen und somit den Energiehaushalt positiv beeinflussen (Flachs et al. 2011; Flachs et al. 2013).

3.6 Noch heißer: Durch erhöhte Lipidmobilisation leistet das braune Fettgewebe einen UCP1-unabhängigen Beitrag zur zitterfreien Thermogenese

(zu Kapitel 6.6; Grimpo et al. 2014)

Ein wichtiger Mechanismus, um bei Kälteexposition eine normotherme Körpertemperatur aufrechtzuerhalten, ist die zitterfreie Thermogenese. Wo die Wärme im Organismus gebildet wird und ob sie ausschließlich UCP1-abhängig ist, wird kontrovers diskutiert. Unbestritten ist, dass Mäuse mit funktionellem braunem Fett ihre Fähigkeit zur zitterfreien Thermogenese adaptiv steigern können. Dies ließ sich bei Mäusen aus unterschiedlichen Akklimatisierungsstufen gut beobachten. Unter gleichen Messbedingungen (26°C) steigerten 5°C akklimatisierte Individuen in Folge einer noradrenergen Injektion ihren Energieumsatz im Vergleich zu denen aus thermoneutraler Haltung um ein Vierfaches.

Bemerkenswerterweise zeigten auch UCP1-KO Mäuse aus der 5°C Haltung nach noradrenerger Stimulation eine signifikant höhere maximale Stoffwechselrate und eine dreimal höhere Thermogenesekapazität als 30°C akklimatisierte UCP1-KO Mäuse. Meyer et al. (2010) und Mineo et al. (2012) beschreiben ebenfalls eine Steigerung der Wärmeproduktion bei Mäusen ohne UCP1 in Folge einer Kälteexposition.

Kaltakklimatisierte Wildtypen erreichten eine deutlich höhere maximale Stoffwechselrate und Thermogenesekapazität als ihre UCP1-KO Geschwister, was bestätigt, dass funktionelles braunes Fettgewebe für einen Großteil der adaptiven Wärmebildung verantwortlich ist. Andererseits wird deutlich, dass Mäuse auch die UCP1-unabhängige Thermogeneseleistung adaptiv steigern können. Wie genau ist allerdings noch ungeklärt. Kaltakklimatisierte Mäuse ohne UCP1 zeigen eine beige Verfärbung des weißen Fettgewebes (Auftreten von multilokulären Adipozyten, die denen des braunen Fetts ähneln) (Ukropec et al. 2006). Es weist eine erhöhte Genexpression sowie Mitochondriendichte und eine verbesserte respiratorische Aktivität auf. Ein UCP1-unabhängiger Beitrag zur zitterfreien Wärmebildung durch seine erhöhte metabolische Aktivität wäre als Kompensationsmechanismus für das thermogenetisch inaktive braune Fett durchaus denkbar (Ukropec et al. 2006; Meyer et al. 2010). Auch der Herzmuskel ist ein Kandidat für UCP1-unabhängige Wärmebildung. Die Untersuchung der Wildtyp- und UCP1-KO Mäuse offenbarte nach noradrenerger Stimulation eine Steigerung der Herzschlagrate und aus früheren Studien ist bekannt, dass während der zitterfreien Thermogenese der ventrikuläre Blutfluss zunimmt (Puchalski et al. 1987). Hinweise auf eine adaptive Thermogeneseleistung der Skelettmuskulatur bestehen ebenfalls (Simonsen et al. 1992; Bal et al. 2012). Eine UCP1-unabhängige Änderung in der Gewebezusammensetzung des interscapularen braunen Fettgewebes nach initialer Kälteexposition konnte mittels MRT beobachtet werden.

Wie bereits für C57BL/6J Mäuse und Zwerghamster beschrieben, nahm das MRT-Signal des braunen Fettgewebes bei den UCP1-KO Mäusen in Folge der Kälteakklimatisation (18°C und 5°C) ab. Verglichen mit Wildtypen blieb das Erscheinungsbild bei 5°C jedoch heterogener. Es ließ sich ein thermogenetisch aktiver Kernbereich von einem fetthaltigeren Randbereich abgrenzen. Dementsprechend war der mitochondrienreiche und zytoplasmahaltige Part im interscapularen Fettgewebe der UCP1-KO Mäuse bei 5°C Akklimatisierung kleiner als bei den Wildtypen. Inwieweit eine komplette Umstrukturierung des Gewebes zeitverzögert stattfindet oder durch das Fehlen von UCP1 gänzlich beeinträchtigt ist, bleibt offen. Der Fettgehalt im Kernbereich des braunen Fettdepots unterschied sich zwischen den Genotypen nicht. Er lag bei warm (30°C) gehaltenen Mäusen signifikant höher als bei denen der kalten Temperaturstufen.

Mit Hilfe der Protonenspektroskopie konnten dynamische Veränderungen im braunen Fettgewebe während noradrenerger Stimulation verfolgt werden. Der Lipidgehalt im interscapularen Depot nahm nach Noradrenalin-Injektion bei beiden Genotypen rapide ab, wobei die thermogenetische Antwort der Wildtypen schneller und stärker ausgeprägt war. Bei einer Akklimatisationstemperatur von 5°C lag ihre Lipidabnahme 16,5 min nach Injektion signifikant höher als bei den UCP1-KO Mäusen. Die verringerte Lipidabnahme der UCP1-KO Mäuse hängt möglicherweise direkt mit der eingeschränkten Umstrukturierung des Fettdepots zusammen. Die Akklimatisationstemperatur selbst beeinflusste die Menge an abgebautem Lipid nicht. Sie betrug über den Zeitraum von 16,5 min bei Wildtypen zwischen 9 und 12 mg, bei den UCP1-KO Mäusen zwischen 5 und 8 mg. Ein gleichbleibendes Sättigungsverhältnis des braunen Fettgewebes ließ darauf schließen, dass weder ungesättigte noch gesättigte Fettsäuren bevorzugt abgebaut wurden.

Die Menge an abgebauten Lipiden lag um ein Vielfaches über der Lipidmenge, die im braunen Fettgewebe tatsächlich oxidiert wurde. Dies war sowohl bei Wildtyp- als auch bei UCP1-KO Mäusen der Fall und spricht für einen Export von freien Fettsäuren aus dem braunen Fettgewebe. *In vitro* Untersuchungen zeigen, dass mit Noradrenalin stimuliert braune Adipozyten durch Lipolyse über ihren eigenen Bedarf hinaus Fettsäuren freisetzen und diese aus dem Gewebe entlassen (Nedergaard and Lindberg 1979; Kuusela et al. 1986). Messungen des Plasmalipidlevels nach Noradrenalin-Gabe oder Kälteexposition bestätigen die Exporteigenschaft des braunen Fettgewebes bei Mäusen und anderen kleinen Nagern *in vivo* (Brooks et al. 1983; Heldmaier and Seidl 1985; Ma and Foster 1986; Laury et al. 1987).

Die Fettsäuremobilisation der UCP1-KO Mäuse ließ darauf schließen, dass der Export von Fettsäuren eine natürliche, UCP1 unabhängige Eigenschaft des braunen Fettgewebes ist. Vögel besitzen kein UCP1 und ihr Fettgewebe ist thermogenetisch nicht aktiv (Saarela et al. 1989).

Dennoch weist es multilokuläre Adipozyten auf, lässt sich durch Faktoren, die bei der Differenzierung von braunen Fettzellen eine Rolle spielen, aktivieren und fungiert mutmaßlich als wichtiger Fettsäurelieferant für andere Gewebe wie der Muskulatur (Saarela et al. 1989; Mezentseva et al. 2008). Mäuse mit ektopischer Expression von UCP1 oder einem verminderten Energiemetabolismus im Muskel, zeigen eine Zunahme von beigen Fettzellen in ihrem weißen Fettgewebe (Kim et al. 2013; Keipert et al. 2013). Diese beigen Adipozyten weisen ein ähnliches Expressionsmuster auf wie braune Adipozyten, enthalten UCP1 und sind nachweislich thermogenetisch aktiv (Shabalina et al. 2013). Keipert et al. (2013) vermuten als Ursache für ihr Auftreten jedoch weniger eine thermogenetische Funktion, sondern einen verbesserten Energiesupport der Muskulatur durch Substratlieferung aus den beigen Adipozyten. Der von uns beobachtete Export von Fettsäuren nach noradrenerger Stimulation könnte ein Hinweis für die Funktion des braunes Fettgewebes als Fettsäurelieferant an andere Gewebe wie Herz, Skelettmuskulatur oder weißes Fett sein. Ohnehin ist eine enge Kooperation zwischen braunem und weißem Fettgewebe Voraussetzung für eine andauernde zitterfreie Thermogenese. Bei langanhaltender Kälteexposition kann die Thermogeneseleistung des braunen Fettgewebes nur durch fortwährenden Nachschub an Substrat für die Atmungskette aus dem weißen Fettgewebe aufrecht erhalten werden (Picard et al. 2002). Noradrenerge Stimulation aktiviert nicht nur das braune Fett, sondern auch die Lipolyse und Wiederveresterung von Fettsäuren in weißen Adipozyten (Garofalo et al. 1996; Lafontan and Langin 2009). Das braune Fettgewebe exprimiert verschiedene Fettsäurebindeproteine. Nach Noradrenalingabe wird deren Vorkommen als Reaktion auf die erhöhte Fettsäureverfügbarkeit deutlich erhöht (Daikoku et al. 1997). Braunes Fett ist demnach trotz seiner Fähigkeit zur *de novo* Lipogenese, Lipolyse und Wiederveresterung von Fettsäuren nicht nur auf eigene Reserven angewiesen, sondern auch ein Hauptkonsument von Fettsäuren aus dem Blut (Hagberg et al. 2010; Bartelt et al. 2011; Townsend and Tseng 2014). Der fortwährende Import und Export von Fettsäuren sowie ablaufende Substratzyklen des Lipidstoffwechsels unterstreichen die metabolische Aktivität und Interaktion von braunem und weißem Fett. Diese hohe metabolische Aktivität sollte als Quelle von zitterfreier Wärmebildung in Betracht gezogen werden. Die vorliegende und andere Studien zeigen, dass UCP1 keine Voraussetzung für die Lipidmobilisation oder die Veränderung der Adipozytenstruktur im Fettgewebe ist (Ukropec et al. 2006; Flachs et al. 2013).

Um die gleichzeitige Stimulation von Lipidkatabolismus und -anabolismus aufrecht zu erhalten, wird ausreichend Energie in Form von ATP benötigt. Die Ergebnisse der Phosphorspektroskopie zeigten, dass diese Voraussetzung selbst im braunen Fettgewebe der Wildtypen, die während der zitterfreien Thermogenese die oxidative Phosphorylierung entkoppeln, gewährleistet ist.

Es war keine Verschiebung im ADP/ATP Verhältnis festzustellen, die auf eine ATP-Schuld des braunen Fettgewebes während der induzierten Thermogenese hingewiesen hätte. Während der thermogenetischen Aktivität ist neben dem Lipidmetabolismus auch der Glukosemetabolismus des braunen Fettgewebes sehr aktiv. Gesteigerte Enzymaktivität und erhöhte Laktatlevel bei kaltakklimatisierten Nagern weisen darauf hin, dass eine ausreichende Versorgung mit ATP über die Glykolyse gewährleistet wird (Ma and Foster 1986; Heldmaier et al. 1989; Himms-Hagen 1990).

Die erhobenen Ergebnisse machen deutlich, dass zitterfreie Thermogenese bei Mäusen nicht ausschließlich über UCP1-vermittelte Wärmebildung im braunen Fettgewebe bestritten wird, sondern anderen Geweben ein berechtigter Beitrag zugeschrieben wird. Zudem scheint braunes Fettgewebe eine wichtige Rolle im Lipidstoffwechsel zu spielen, die UCP1-unabhängig ist und möglicherweise sogar ursprünglicher als seine UCP1-vermittelte thermogenetische Funktion.

4 Fazit und Ausblick

Im Rahmen der Promotionsarbeit konnten die komplexen Antworten des endothermen Energiestoffwechsels auf sich verändernde Umweltbedingungen ein Stück weiter entschlüsselt werden. Die gewonnenen Erkenntnisse tragen zu einem besseren Verständnis der Regulationsmechanismen im täglichen Torpors und der durch Thermogenese verursachten Stoffwechselsteigerungen bei und lassen die eingangs aufgeworfenen Fragen wie folgt beantworten:

- Die Goldstachelmaus passt ihren Metabolismus äußerst flexibel an verschiedene Gegebenheiten an und begegnet auf diese Weise den wechselnden Herausforderungen ihres ariden Lebensraums. Bei Umgebungstemperaturen von ≥ 32°C kann sie eine 50%ige Reduktion des *ad libitum* Futterverbrauchs durch energetische Einsparungen vollends kompensieren. Dies erreicht sie durch eine Verringerung des Ruhestoffwechsels und täglich mehrstündige Torporepisoden bei durchweg normothermer Körpertemperatur. Ein eindeutiger Beleg dafür, dass die aktive Stoffwechselreduktion bei Torporeintritt und die Aufrechterhaltung dieses hypometabolen Zustandes gänzlich entkoppelt von einer hypothermen Körpertemperatur stattfinden können.
- Mitochondrien torpider Stachelmäuse weisen keine Veränderungen ihrer Bioenergetik auf. Des Weiteren korreliert die mitochondriale Respiration der Leber von Dsungarischen Zwerghamstern mit der Körpertemperatur. Zusammengenommen spricht dies gegen eine Inhibition der mitochondrialen Respiration als Torporauslöser und vielmehr für eine aktive Drosselung der Substratoxidation als Anpassungsleistung der Mitochondrien an niedrige Körpertemperaturen im tiefen Torpor, wie sie bei *P. sungorus* und anderen Winterschläfern auftreten.
- Der neu etablierte Messaufbau aus kombinierter indirekter Kalorimetrie und MR-Bildgebung wird von *P. sungorus* toleriert und macht es erstmalig möglich torpide Hamster bildgebend zu untersuchen. Technische Weiterentwicklungen des Versuchssetups und Verfeinerungen der Messsequenzen müssen zukünftig stattfinden, um das volle Potential der MRT im Forschungsfeld „Torpor“ anwenden zu können.
- Metabolisch inaktive und aktive Fettgewebe können mittels MRT *in vivo* differenziert und analysiert werden. So unterscheiden sich nicht nur T2-Zeiten, Lipidgehalt und Fettsäurezusammensetzung von weißem und braunem Fettgewebe. Auch die Umstrukturierung des braunen Fettgewebes in Folge von Kälteexposition oder einer kürzeren Photoperiode lassen sich visualisieren.

Weißes Fett besitzt einen höheren Anteil ungesättigter Fettsäuren als braunes Fett. Dieser Anteil erhöht sich allein durch den saisonalen Stimulus einer kurzen Photoperiode und zwar im braunen und weißen Fettgewebe.

- Die Funktion des braunen Fettgewebes geht über seine Fähigkeit der UCP1-vermittelten Thermogenese hinaus. Nach noradrenerger Stimulation erfolgt ein UCP1-unabhängiger Fettsäureexport aus dem braunen Fettgewebe, der mittels MRS gemessen werden kann. Gleichzeitig fungiert braunes Fett als Konsument von Plasmafettsäuren und reguliert auf diese Weise den Gehalt der Blutfette. Dieser zyklische Lipidstoffwechsel findet in enger Kooperation mit anderen Geweben statt, die vermutlich einen Teil zur UCP1-unabhängigen Thermogenese beitragen. So nimmt das braune Fettgewebe durch seinen hohen Substratstoffwechsel auch bei der UCP1-unabhängigen, adaptiven Thermogeneseleistung, wie sie bei UCP1-KO Mäusen zu beobachten ist, eine Schlüsselrolle ein.

Die Methode der Magnetresonanztomographie hat sich für die Bearbeitung physiologischer Fragestellungen, wie der *in vivo* Charakterisierung von Fettgewebe, bewährt. Im Gegensatz zum PET/CT (Positronen-Emissions-Tomographie in Kombination mit Computertomographie), dem bisherigen Goldstandard zur Quantifizierung von aktivem braunem Fettgewebe, kommt sie ohne ionisierende Strahlung oder den Einsatz von radioaktiven Markern aus und ist somit weniger belastend. Dasselbe Versuchstier kann unter verschiedenen Akklimatisationsbedingungen wiederholt gemessen werden. Dies steigert nicht nur die Validität der biologischen Daten, sondern verringert nach der Validierungsphase auch die benötigte Versuchstierzahl. Die Magnetresonanztomographie ist ein vielversprechendes Tool, um die zeitlichen Abläufe im natürlichen Torpor zukünftig *in vivo* zu verfolgen und die Mechanismen der aktiven Stoffwechselabsenkung besser zu verstehen. Mit dem neu etablierten Messaufbau ist hierfür der erste Schritt getan. Die funktionellen Messungen des Lipid- und Energiestoffwechsels im braunen Fettgewebe während der zitterfreien Thermogenese eröffnen neue Blickwinkel.

Ein fundiertes Verständnis beider Themengebiete ist auch durch ihre potentielle Bedeutung für den menschlichen Organismus von besonderem Interesse. Die gezielte Induktion eines hypometabolen und normothermen Zustands könnte die Schädigungen bei Trauma- oder Infarktpatienten reduzieren und die Lebensdauer von Transplantationsorganen verlängern. Sogar eine sechsmonatige Weltraumreise zum Mars wäre im torpiden Sparmodus denkbar, da auf diese Weise physiologische Strapazen und Risiken einer solchen Mission deutlich reduziert würden.

Eine Erhöhung des Energiestoffwechsels durch die Aktivierung des braunen Fettgewebes auf der anderen Seite, verspricht therapeutische Ansatzpunkte für die Bekämpfung von Übergewicht und deren Begleitsymptome wie Herz-Kreislauferkrankungen und Diabetes (van der Lans et al. 2013). Auch wenn die thermogenetische Leistung des braunen Fettgewebes im menschlichen Organismus wohl eher eine untergeordnete Rolle einnimmt, so ist seine Rolle im Lipidmetabolismus von außerordentlichem Interesse.

Die Methode der MRT erfordert für jede Fragestellung eine Anpassung der Hard- und Software und setzt aufgrund ihrer technischen Komplexität eine Zusammenarbeit verschiedener Fachdisziplinen (Ingenieurtechnik, Physik, Biologie) voraus. Sie ist teuer, artefaktanfällig und in einigen Bereichen bisher weniger Aussagekräftig als entsprechende *ex vivo* Untersuchungen. Dennoch bietet sie ein hohes Potential dynamische Prozesse *in vivo* zu verfolgen und ist eine wertvolle non-invasive Methode, um im Sinne des Tierschutzgedanken eine Verbesserung des Versuchstierwohls und eine Verringerung der benötigten Versuchstierzahl zu erreichen.

5 Literatur

Agrawal a, Bainbridge A, Powis S, et al. (2011) *31-Phosphorus magnetic resonance spectroscopy for dynamic assessment of adenosine triphosphate levels in pancreas preserved by the two-layer method.* Transplant Proc 43:1801–1809.

Amara CE, Marcinek DJ, Shankland EG, et al. (2008) *Mitochondrial function in vivo: spectroscopy provides window on cellular energetics.* Methods 46:312–318.

Andrews MT (2007) *Advances in molecular biology of hibernation in mammals.* Bioessays 29:431–440.

Armstrong C, Staples JF (2010) *The role of succinate dehydrogenase and oxaloacetate in metabolic suppression during hibernation and arousal*. J Comp Physiol B 180:775–783.

Arnold W, Heldmaier G, Ortmann S, et al. (1991) *Ambient temperatures in hibernacula a n d their energetic consequences for alpine marmots (marmota marmota)*. J therm Biol 16:223–226.

Baba S, Engles JM, Huso DL, et al. (2007) *Comparison of uptake of multiple clinical radiotracers into brown adipose tissue under cold-stimulated and nonstimulated conditions.* J Nucl Med 48:1715–1723.

Bal NC, Maurya SK, Sopariwala DH, et al. (2012) *Sarcolipin is a newly identified regulator of muscle-based thermogenesis in mammals.* Nat Med 18:1575–1579.

Banet M, Hensel H, Liebermann H (1978) *The central control of shivering and non-shivering thermogenesis in the rat.* J Physiol 283:569–584.

Barclay RMR, Lausen CL, Hollis L (2001) *What's hot and what's not: defining torpor in free-ranging birds and mammals.* Can J Zool 79:1885–1890.

Barger JL, Brand MD, Barnes BM, Boyer BB (2003) *Tissue-specific depression of mitochondrial proton leak and substrate oxidation in hibernating arctic ground squirrels.* Am J Physiol Regul Integr Comp Physiol 284:1306–1313.

Barnes BM (1989) *Freeze avoidance in a mammal: body temperatures below 0 degree C in an Arctic hibernator.* Science 244:1593–1595.

Bartelt A, Bruns OT, Reimer R, et al. (2011) *Brown adipose tissue activity controls triglyceride clearance.* Nat Med 17:200–205.

De Bazelaire CMJ, Duhamel GD, Rofsky NM, Alsop DC (2004) *MR imaging relaxation times of abdominal and pelvic tissues measured in vivo at 3.0 T: preliminary results.* Radiology 230:652–659.

Berriel Diaz M, Lange M, Heldmaier G, Klingenspor M (2004) *Depression of transcription and translation during daily torpor in the Djungarian hamster (Phodopus sungorus)*. J Comp Physiol B 174:495–502.

Bieber C, Ruf T (2009) *Summer dormancy in edible dormice (Glis glis) without energetic constraints.* Naturwissenschaften 96:165–171.

Bock C, Strijkstra AM, Pörtner H-O (2002) *MRI and 31P NMR studies of brain metabolism in European ground squirrels during hibernation and arousal.* Proc. ISMRM 10th Sci. Meet. 1217, Honolulu, USA

Bouma HR, Verhaag EM, Otis JP, et al. (2012) *Induction of torpor: mimicking natural metabolic suppression for biomedical applications.* J Cell Physiol 227:1285–1290.

Bowers RR, Gettys TW, Prpic V, et al. (2005) *Short photoperiod exposure increases adipocyte sensitivity to noradrenergic stimulation in Siberian hamsters.* Am J Physiol Regul Integr Comp Physiol 288:1354–1360.

Van Breukelen F, Krumschnabel G, Podrabsky JE (2010) *Vertebrate cell death in energy-limited conditions and how to avoid it: what we might learn from mammalian hibernators and other stress-tolerant vertebrates*. Apoptosis 15:386–399.

Brooks BJ, Arch JR, Newsholme EA (1983) *Effect of some hormones on the rate of the triacylglycerol/fatty-acid substrate cycle in adipose tissue of the mouse in vivo*. Biosci Rep 3:263–267.

Brown JCL, Gerson AR, Staples JF (2007) *Mitochondrial metabolism during daily torpor in the dwarf Siberian hamster : role of active regulated changes and passive thermal effects*. Am J Physiol Regul Integr Comp Physiol 293:1833–1845.

Brown JCL, Staples JF (2010) *Mitochondrial metabolism during fasting-induced daily torpor in mice*. Biochim Biophys Acta 1797:476–486.

Buck CL, Barnes BM (2000) *Effects of ambient temperature on metabolic rate, respiratory quotient, and torpor in an arctic hibernator.* Am J Physiol Regul Integr Comp Physiol 279:R255–262.

Cannon B, Nedergaard J (2004) *Brown Adipose Tissue : Function and Physiological Significance.* Physiol Rev 84:277–359.

Carey H V, Andrews MT, Martin SL (2003) *Mammalian hibernation: cellular and molecular responses to depressed metabolism and low temperature.* Physiol Rev 83:1153–1181.

Carneheim C, Nedergaard J, Cannon B (1984) *Beta-adrenergic stimulation of lipoprotein lipase in rat brown adipose tissue during acclimation to cold.* Am J Physiol - Endocrinol Metab 246:327–333.

Cinti S (2005) *The adipose organ*. Prostaglandins Leukot Essent Fatty Acids 73:9–15.

Cypess AM, Kahn CR (2010) *Brown fat as a therapy for obesity and diabetes.* Curr Opin Endocrinol Diabetes Obes 17:143–149.

Daikoku T, Shinohara Y, Shima A, et al. (1997) *Dramatic enhancement of the specific expression of the heart-type fatty acid binding protein in rat brown adipose tissue by cold exposure*. FEBS Lett 410:383–386.

Dausmann KH, Glos J, Ganzhorn JU, Heldmaier G (2005) *Hibernation in the tropics: lessons from a primate.* J Comp Physiol B 175:147–55.

Dausmann KH, Glos J, Heldmaier G (2009) *Energetics of tropical hibernation*. J Comp Physiol B 179:345–357.

Drew KL, Buck CL, Barnes BM, et al. (2007) *Central nervous system regulation of mammalian hibernation: implications for metabolic suppression and ischemia tolerance*. J Neurochem 102:1713–1726.

Ehrhardt N, Heldmaier G, Exner C (2005) *Adaptive mechanisms during food restriction in Acomys russatus: the use of torpor for desert survival.* J Comp Physiol B 175:193–200.

Elvert R, Heldmaier G (2005) *Cardiorespiratory and metabolic reactions during entrance into torpor in dormice, Glis glis.* J Exp Biol 208:1373–1383.

Elvert R, Kronfeld N, Dayan T, et al. (1999) *Telemetric field studies of body temperature and activity rhythms of Acomys russatus and A . cahirinus in the Judean Desert of Israel.* Oecologia 119:484–492.

Enerbäck S, Jacobsson A, Simpson EM, et al. (1997) *Mice lacking mitochondrial uncoupling protein are cold-sensitive but not obese.* Nature 387:90–94.

Exner C, Hebebrand J, Remschmidt H, et al. (2000) *Leptin suppresses semi-starvation induced hyperactivity in rats: implications for anorexia nervosa.* Mol Psychiatry 5:476–481.

Fedorenko A, Lishko P V, Kirichok Y (2012) *Mechanism of fatty-acid-dependent UCP1 uncoupling in brown fat mitochondria.* Cell 151:400–413.

Fedotcheva NJ, Sharyshev AA, Mironova GD, Kondrashova MN (1985) *Inhibition of succinate oxidation and K+ transport in mitochondria during hibernation.* Comp Biochem Physiol B 82:191–195.

Ferrannini E (1988) *The theoretical bases of indirect calorimetry: A review*. Metabolism 37:287–301.

Ferraris RP, Cao QX, Prabhakaram S (2001) *Chronic but not acute energy restriction increases intestinal nutrient transport in mice*. J Nutr 131:779–786.

Flachs P, Rossmeisl M, Kuda O, Kopecky J (2013) *Stimulation of mitochondrial oxidative capacity in white fat independent of UCP1: A key to lean phenotype.* Biochim Biophys Acta 1831:986–1003.

Flachs P, Rühl R, Hensler M, et al. (2011) *Synergistic induction of lipid catabolism and anti-inflammatory lipids in white fat of dietary obese mice in response to calorie restriction and n-3 fatty acids*. Diabetologia 54:2626–2638.

Florant GL (1998) *Lipid Metabolism in Hibernators: The Importance of Essential Fatty Acids.* Integr Comp Biol 38:331–340.

Florant GL, Hester L, Ameenuddin S, Rintoul DA (1993) *The effect of a low essential fatty acid diet on hibernation in marmots.* Am J Physiol 264:747–753.

Foster DO, Frydman ML (1978) *Brown adipose tissue: the dominant site of nonshivering thermogenesis in the rat.* Experientia Suppl 32:147–151.

Frank CL (1992) *The Influence of Dietary Fatty Acids on Hibernation by Golden-Mantled Ground Squirrels (Spermophilus lateralis)*. Physiol Zool 65:906–920.

Frank CL (1994) *Polyunsaturate content and diet selection by ground squirrels (Spermophil us la teralis).* Ecology 75:458–463.

Frank CL, Dierenfeld ES, Storey KB (1998) *The Relationship Between Lipid Peroxidation, Hibernation, and Food Selection in Mammals*. AMER ZOOL 38:341–349.

Fuller CA, Horowitz JM, Horwitz BA (1977) *Spinal cord thermosensitivity and sorting of neural signals in cold-exposed rats*. J Appl Physiol 42:154–158.

Garofalo MA, Kettelhut IC, Roselino JE, Migliorini RH (1996) *Effect of acute cold exposure on norepinephrine turnover rates in rat white adipose tissue.* J Auton Nerv Syst 60:206–208.

Geiser F (2013) *Hibernation.* Curr Biol 23:188–193.

Geiser F, Baudinette R V. (1987) *Seasonality of torpor and thermoregulation in three dasyurid marsupials.* J Comp Physiol B 157:335–344.

Geiser F, Kenagy GJ (1987) *Polyunsaturated lipid diet lengthens torpor and reduces body temperature in a hibernator.* Am J Physiol 252:897–901.

Geiser F, Klingenspor M, McAllan BM (2013) *A Functional Nexus between Photoperiod Acclimation, Torpor Expression and Somatic Fatty Acid Composition in a Heterothermic Mammal*. PLoS One 8:e63803.

Gnaiger E (1983) *Calculation of Energetic and Biochemical Equivalents of Respiratory Oxygen Consumption*. In: Gnaiger E, Forstner H (eds) Polarogr. Oxyg. Sensors. Springer Berlin Heidelberg, Berlin, Heidelberg, pp 337–345

Golozoubova V, Hohtola E, Matthias A, et al. (2001) *Only UCP1 can mediate adaptive nonshivering thermogenesis in the cold.* FASEB J 15:2048–2050.

Graaf RA De (2007) *In Vivo NMR Spectroscopy: Principles and Techniques* – 2nd Edition. John Wiley & Sons, West Sussex, 1–592.

Gunawardana SC (2012) *Therapeutic value of brown adipose tissue: Correcting metabolic disease through generating healthy fat*. Adipocyte 1:250–255.

Gutman R, Choshniak I, Kronfeld-Schor N (2006) *Defending body mass during food restriction in Acomys russatus: a desert rodent that does not store food.* Am J Physiol 290:881–891.

Gutman R, Hacmon-Keren R, Choshniak I, Kronfeld-Schor N (2008) *Effect of food availability and leptin on the physiology and hypothalamic gene expression of the golden spiny mouse: a desert rodent that does not hoard food.* Am J Physiol 295:2015–2023.

Gutman R, Yosha D, Choshniak I, Kronfeld-Schor N (2007) *Two strategies for coping with food shortage in desert golden spiny mice.* Physiol Behav 90:95–102.

Hafner RP, Brown GC, Brand MD (1990) A*nalysis of the control of respiration rate, phosphorylation rate, proton leak rate and protonmotive force in isolated mitochondria using the "top-down" approach of metabolic control theory*. Eur J Biochem 188:313–319.

Hagberg CE, Falkevall A, Wang X, et al. (2010) *Vascular endothelial growth factor B controls endothelial fatty acid uptake*. Nature 464:917–921.

Hagopian K, Harper M-E, Ram JJ, et al. (2005) *Long-term calorie restriction reduces proton leak and hydrogen peroxide production in liver mitochondria*. Am J Physiol Endocrinol Metab 288:674–84.

Haim A (1987) *Thermoregulation and metabolism of Wagner's gerbil (Gerbillus dasyurus): a rock dwelling rodent adapted to arid and mesic environments*. J therm Biol 12:45–48.

Haim A, Borut A (1981) *Heat Production and Dissipation in Golden Spiny Mice , Acomys russatus from Two Extreme Habitats.* J Comp Physiol B 142:445–450.

Haim A, Izhaki I (1993) T*he ecological significance of resting metabolic rate a n d non-shivering thermogenesis for rodents*. J therm Biol 18:71–81.

Hamilton G, Smith DL, Bydder M, et al. (2011) *MR properties of brown and white adipose tissues. J Magn Reson imaging* 34:468–473.

Hayssen V, Lacy RC (1985) *Basal metabolic rates in mammals: taxonomic differences in the allometry of BMR and body mass.* Comp Biochem Physiol A 81:741–754.

Heldmaier G (1971) *Nonshivering Thermogenesis and Body Size in Mammals.* Z vergl Physiol 73:222–248.

Heldmaier G (1974) *Temperature Adaptation and Brown Adipose Tissue in Hairless and Albino Mice*. J comp Physiol 92:281–292.

Heldmaier G, Buchberger A (1985) *Sources of heat during nonshivering thermogenesis in Djungarian hamsters: a dominant role of brown adipose tissue during cold adaptation*. J Comp Physiol B 156:237–245.

Heldmaier G, Elvert R (2004) *How to enter torpor: Thermodynamic and physiological mechanisms of metablic depression.* In: Barnes BM, Carey H V (eds) Life in the cold: evolution, mechanisms, adaptation, and application. 12th ed. University of Alaska, pp 185–198

Heldmaier G, Klaus S, Wiesinger H, et al. (1989) *Cold acclimation and thermogenesis*. In: Malan A, Canguilhem B (eds) Living Cold II. Inserm, London Paris, pp 347–358

Heldmaier G, Neuweiler G, Rössler W (2013) *Vergleichende Tierphysiologie*. 2. Aufl. Springer Spektrum, Heidelberg 1-1178

Heldmaier G, Ortmann S, Elvert R (2004) *Natural hypometabolism during hibernation and daily torpor in mammals*. Respir Physiol Neurobiol 141:317–329.

Heldmaier G, Ruf T (1992) *Body temperature and metabolic rate during natural hypothermia in endotherms*. J Comp Physiol B 162:696–706.

Heldmaier G, Seidl K (1985) *Plasma free fatty acid levels during cold-induced and noradrenaline-induced nonshivering thermogenesis in the Djungarian hamster*. J Comp Physiol B 155:679–84.

Heldmaier G, Steinlechner S (1981) *Seasonal pattern and energetics of short daily torpor in the Djungarian hamster, Phodopus sungorus.* Oecologia 48:265–270.

Heldmaier G, Steinlechner S, Rafael J, Vsiansky P (1981) *Photoperiodic Control and Effects of Melatonin on Nonshivering Thermogenesis and Brown Adipose Tissue*. Science 212:917–919.

Henry P-G, Russeth KP, Tkac I, et al. (2007) *Brain energy metabolism and neurotransmission at near-freezing temperatures: in vivo $^{(1)}$H MRS study of a hibernating mammal.* J Neurochem 101:1505–1515.

Himms-Hagen J (1990) *Brown adipose tissue thermogenesis: interdisciplinary studies*. FASEB J 4:2890–2898.

Hoffmann K (1982) *The Critical Photoperiod in the Djungarian Hamster Phodopus sungorus.* In: Aschoff J, Daan S, Groos GA (eds) Vertebrate Circadian Systems. Springer Berlin Heidelberg, Berlin, Heidelberg, pp 297–304

Holstila M, Virtanen K a, Grönroos TJ, et al. (2013) *Measurement of brown adipose tissue mass using a novel dual-echo magnetic resonance Imaging Approach: A validation study*. Metabolism 62:1189–1198.

Houstěk J, Andersson U, Tvrdík P, et al. (1995) *The Expression of Subunit c Correlates with and Thus May Limit the Biosynthesis of the Mitochondrial F(0)F(1)-ATPase in Brown Adipose Tissue*. J Biol Chem 270:7689–7694.

Hu HH, Hines CDG, Smith DL, Reeder SB (2012) *Variations in T(2)* and fat content of murine brown and white adipose tissues by chemical-shift MRI*. Magn Reson Imaging 30:323–329.

Hu HH, Smith DL, Nayak KS, et al. (2010) *Identification of brown adipose tissue in mice with fat-water IDEAL-MRI.* J Magn Reson imaging 31:1195–1202.

Hu K, Meng Y, Lei H, Zhang S (2011) *Differential changes of regional cerebral blood flow in two bat species during induced hypothermia measured by perfusion-weighted magnetic resonance imaging*. J Comp Physiol B 181:117–123.

Hudson J, Scott I (1979) *Daily torpor in the laboratory mouse, Mus musculus var. albino*. Physiol. Zool. 205-218

I.U.P.S. Commission for Thermal Physiology (2001) *Glossary of terms for thermal physiology*. Jpn J Physiol, 51:245–280.

Jinka TR, Duffy LK (2013) *Ethical considerations in hibernation research*. Lab Anim (NY) 42:248–252.

Keipert S, Jastroch M (2014) *Brite/beige fat and UCP1 - is it thermogenesis?* Biochim. Biophys. Acta doi: 10.1016/j.bbabio.2014.02.008

Keipert S, Ost M, Johann K, et al. (2013) *Skeletal muscle mitochondrial uncoupling drives endocrine cross-talk through induction of FGF21 as a myokine.* Am. J. Physiol. Endocrinol. Metab.

Kemp GJ, Brindle KM (2012) *What do magnetic resonance-based measurements of Pi→ATP flux tell us about skeletal muscle metabolism?* Diabetes 61:1927–1934.

Khanna A, Branca RT (2012) *Detecting brown adipose tissue activity with BOLD MRI in mice*. Magn Reson Med 68:1285–1290.

Kim KH, Jeong YT, Oh H, et al. (2013) *Autophagy deficiency leads to protection from obesity and insulin resistance by inducing Fgf21 as a mitokine.* Nat Med 19:83–92.

Kirsch R, Ouarour A, Pevet P (1991) *Daily torpor in the Djungarian hamster (Phodopus sungorus): photoperiodic regulation, characteristics and circadian organization.* J Comp Physiol A 168:121–128.

Kleiber M (1932) *Body size and metabolic rate*. Hilgardia 6:318–353.

Klingenspor M (2003) *Cold-induced recruitment of brown adipose tissue thermogenesis*. Exp Physiol 88:141–148.

Klingenspor M, Ebbinghaus C, Hülshorst G, et al. (1996) *Multiple regulatory steps are involved in the control of lipoprotein lipase activity in brown adipose tissue*. J Lipid Res 37:1685–1695.

Klingenspor M, Niggemann H, Heldmaier G (2000) *Modulation of leptin sensitivity by short photoperiod acclimation in the Djungarian hamster, Phodopus sungorus*. J Comp Physiol B 170:37–43.

Köchli VD, Marincek B, Mri W, et al. (2009) *Wie funktioniert MRI?*, 6. Auflage. Springer Medizin Verlag, Heidelberg pp 1–172.

Körtner G, Geiser F (2009) *The key to winter survival: daily torpor in a small arid-zone marsupial.* Naturwissenschaften 96:525–30.

Kuusela P, Nedergaard J, Cannon B (1986) *Beta-adrenergic stimulation of fatty acid release from brown fat cells differentiated in monolayer culture*. Life Sci 38:589–599.

Lafontan M, Langin D (2009) *Lipolysis and lipid mobilization in human adipose tissue*. Prog Lipid Res 48:275–297.

Lafrance L, Lagacé G, Routhier D (1980) *Free fatty acid turnover and oxygen consumption. Effects of noradrenaline in nonfasted and nonanesthetized cold-adapted rats*. Can J Physiol Pharmacol 58:797–804.

Van der Lans AAJJ, Hoeks J, Brans B, et al. (2013) *Cold acclimation recruits human brown fat and increases nonshivering thermogenesis*. J Clin Invest 123:3395–403.

Laury, Chapey, Portet (1987) *Involvement of the sympathetic nervous system in lipolytic activity in brown adipose tissue of cold acclimated rats*. Comp Biochem Physiol A Comp Physiol 87:197–203.

Laury MC, Portet R (1974) *Effects of the partial removal of the brown fat and of theophylline on the calorigenic response to noradrenaline in the rat adapted to cold.* Rev Can Biol 33:15–25.

Lee D, Marcinek D (2009) *Noninvasive in vivo small animal MRI and MRS: basic experimental procedures*. J Vis Exp 32:1–5.

Lee T, Watkins J, Cash C (1998) *Acomys russatus*. Mamm species 590:1–4.

Levy O, Dayan T, Kronfeld-Schor N (2011a) *Adaptive thermoregulation in golden spiny mice: the influence of season and food availability on body temperature*. Physiol Biochem Zool 84:175–184.

Levy O, Dayan T, Kronfeld-Schor N (2011b) I*nterspecific competition and torpor in golden spiny mice: two sides of the energy-acquisition coin.* Integr Comp Biol 51:441–448.

Li Y, Lasar D, Fromme T, Klingenspor M (2014) *White , brite , and brown adipocytes : the evolution and function of a heater organ in mammals* Can J Zool 12:1–12.

Lichtenbelt WDVM, Vanhommerig JW, Smulders NM, et al. (2009) *Cold-Activated Brown Adipose Tissue in Healthy Men*. N Engl J Med 260:1500–1508.

Liu J-N, Karasov WH (2011) *Hibernation in warm hibernacula by free-ranging Formosan leaf-nosed bats, Hipposideros terasensis, in subtropical Taiwan*. J Comp Physiol B 181:125–135.

Lovegrove BG (2003) *The influence of climate on the basal metabolic rate of small mammals: a slow-fast metabolic continuum*. J Comp Physiol B 173:87–112.

Lyons SK (2005) *Advances in imaging mouse tumour models in vivo*. J Pathol 205:194–205.

Ma SWY, Foster DO (1986) *Uptake of glucose and release of fatty acids and glycerol by rat brown adipose tissue in vivo.* Can J Physiol Pharmacol 64:609–614.

Malan A (1993) *Temperature regulation, enzyme kinetics, and metabolic depression in mammalian hibernation*. In: Carey C, Florant GL, Wunder BA, Horwitz B (eds) Life in the cold: ecological, physiological, and molecular mechanisms. Westview Press, Bolder, pp 241–251

Martin CJ, Kennerley AJ, Berwick J, et al. (2013) *Functional MRI in conscious rats using a chronically implanted surface coil*. J Magn Reson Imaging 38:739–744.

Martin SL, Maniero GD, Carey C, Hand SC (1999) *Reversible depression of oxygen consumption in isolated liver mitochondria during hibernation.* Physiol Biochem Zool 72:255–264.

McKechnie AE, Ashdown RAM, Christian MB, Brigham RM (2007) *Torpor in an African caprimulgid, the freckled nightjar Caprimulgus tristigma*. J Avian Biol 38:261–266.

McNab B, Morrison P (1963) *Body temperature and metabolism in subspecies of Peromyscus from arid and mesic environments*. Ecol Monogr 33:63–82.

Melvin RG, Andrews MT (2009) *Torpor induction in mammals: recent discoveries fueling new ideas*. Trends Endocrinol Metab 20:490–498.

Merkt JR, Taylor CR (1994) *"Metabolic switch" for desert survival*. Proc Natl Acad Sci 91:12313–12316.

Meyer CW, Willershäuser M, Jastroch M, et al. (2010) *Adaptive thermogenesis and thermal conductance in wild-type and UCP1-KO mice.* Am J Physiol Regul Integr Comp Physiol 299:1396–1406.

Mezentseva N V, Kumaratilake JS, Newman S a (2008) *The brown adipocyte differentiation pathway in birds: an evolutionary road not taken*. BMC Biol 6:17.

Morgan K (1998) *Thermoneutral zone and critical temperatures of horses*. J therm Biol 23:59–61.

Mosconi E, Fontanella M, Sima DM, et al. (2011) *Investigation of adipose tissues in Zucker rats using in vivo and ex vivo magnetic resonance spectroscopy*. J Lipid Res 52:330–336.

Muleme HM, Walpole AC, Staples JF (2006) *Mitochondrial metabolism in hibernation: metabolic suppression, temperature effects, and substrate preferences.* Physiol Biochem Zool 79:474–83.

Munn AJ, Kern P, McAllan BM (2010) *Coping with chaos: unpredictable food supplies intensify torpor use in an arid-zone marsupial, the fat-tailed dunnart (Sminthopsis crassicaudata)*. Naturwissenschaften 97:601–605.

Nedergaard J, Lindberg O (1979) *Norepinephrine-stimulated fatty- acid release and oxygen consumption in isolated hamster brown- fat cells. Influence of buffers, albumin, insulin and mitochondrial inhibitors.* Eur J Biochem 15:139–145.

Nieman BJ, Bock NA, Bishop J, et al. (2005) *Magnetic resonance imaging for detection and analysis of mouse phenotypes.* NMR Biomed 18:447–468.

Oelkrug R, Heldmaier G, Meyer CW (2011) *Torpor patterns, arousal rates, and temporal organization of torpor entry in wildtype and UCP1-ablated mice.* J Comp Physiol B 181:137–45.

Ortmann S, Heldmaier G (2000) *Regulation of body temperature and energy requirements of hibernating alpine marmots (Marmota marmota).* Am J Physiol Regul Integr Comp Physiol 278:R698–704.

Peng X-G, Ju S, Fang F, et al. (2013) *Comparison of brown and white adipose tissue fat fractions in ob, seipin, and Fsp27 gene knockout mice by chemical shift-selective imaging and $^{(1)}$H-MR spectroscopy*. Am J Physiol Endocrinol Metab 304:160–167.

Picard F, Géhin M, Annicotte J-S, et al. (2002) *SRC-1 and TIF2 control energy balance between white and brown adipose tissues.* Cell 111:931–941.

Polymeropoulos ET, Heldmaier G, Frappell PB, et al. (2012) *Phylogenetic differences of mammalian basal metabolic rate are not explained by mitochondrial basal proton leak*. Proceedings Biol Sci 279:185–193.

Puchalski W, Böckler H, Heldmaier G, Langefeld M (1987) *Organ blood flow and brown adipose tissue oxygen consumption during noradrenaline-induced nonshivering thermogenesis in the Djungarian hamste*r. J Exp Zool 242:263–271.

Puschmann W (2004) *Zootierhaltung: Säugetiere*, 4. Aufl. Harri Deutsch, Frankfurt a. M. 1- 878.

Reynafarje B, Costa LE, Lehninger AL (1985) *O_2 solubility in aqueous media determined by a kinetic method*. Anal Biochem 145:406–418.

Rolfe DF, Brown GC (1997) *Cellular energy utilization and molecular origin of standard metabolic rate in mammals.* Physiol Rev 77:731–758.

Rubal A, Haim A, Choshniaks I (1995) *Resting metabolic rates and daily energy intake in desert and non-desert murid rodents.* Comp Biochem Physiol 112:511–515.

Ruf T, Heldmaier G (1992) *The impact of daily torpor on energy requirements in the Djungarian hamster, Phodopus sungorus.* Physiol Zool 65:994–1010.

Ruf T, Klingenspor M, Preis H, Heldmaier G (1991) *Daily torpor in the Djungarian hamster (Phodopus sungorus): interactions with food intake , activity , and social behaviour*. J Comp Physiol 160:609–615.

Ruf T, Stieglitz A, Steinlechner S, et al. (1993) *Cold exposure and food restriction facilitate physiological responses to short photoperiod in Djungarian hamsters (Phodopus sungorus).* J Exp Zool 267:104–112.

Saarela S, Hissa R, Pyörnilä A, et al. (1989) *Do birds possess brown adipose tissue?* Comp Biochem Physiol Part A Physiol 92:219–228.

Sbarbati A, Cavallini I, Marzola P, et al. (2006) *Contrast-enhanced MRI of brown adipose tissue after pharmacological stimulation*. Magn Reson Med 55:715–718.

Schick F (2005) *Whole-body MRI at high field: technical limits and clinical potential.* Eur Radiol 15:946–959.

Schmidt-Nielsen B, Schmidt-Nielsen K (1951) *A complete account of the water metabolism in kangaroo rats and an experimental verification*. J Cell Comp Physiol 38:165–181.

Scholander PF, Hock R, Walters V, et al. (1950) *Heat regulation in some arctic and tropical mammals and birds.* Biol Bull 99:237–258.

Serkova NJ, Hasebroock KM, Kraft SL (2009) *Magnetic Resonance Spectroscopy of Living Tissues*. In: Tainsky MA (ed) Tumor Biomarker Discovery. Humana Press, Totowa, NJ, pp 315–327

Shabalina IG, Petrovic N, de Jong JMA, et al. (2013) *UCP1 in Brite/Beige Adipose Tissue Mitochondria Is Functionally Thermogenic*. Cell Rep 5:1196–1203.

Shkolnik A (1966) *Studies in the comparative biology of Israeli's two species of spiny mice (genus acomys).* Doctoral dissertation, Hebrew University (Jerusalem).

Simonsen L, Bülow J, Madsen J, Christensen NJ (1992) *Thermogenic response to epinephrine in the forearm and abdominal subcutaneous adipose tissue*. Am J Physiol 263:E850–855.

Smith DL, Yang Y, Hu HH, et al. (2013) *Measurement of interscapular brown adipose tissue of mice in differentially housed temperatures by chemical-shift-encoded water-fat MRI*. J Magn Reson Imaging 38:1425–1433.

Song X, Körtner G, Geiser F, et al. (1997) T*hermal relations of metabolic rate reduction in a hibernating marsupial Thermal relations of metabolic rate reduction in a hibernating marsupial*. Am J Physiol 273:2097–2104.

Staples JF, Brown JCL (2008) *Mitochondrial metabolism in hibernation and daily torpor: a review*. J Comp Physiol B, 178:811–827.

Storey KB, Storey JM (2010) *Metabolic rate depression: the biochemistry of mammalian hibernation*. Adv Clin Chem 52:77–108.

Strobel K, van den Hoff J, Pietzsch J (2008) *Localized proton magnetic resonance spectroscopy of lipids in adipose tissue at high spatial resolution in mice in vivo*. J Lipid Res 49:473–480.

Swoap SJ, Gutilla MJ (2009) *Cardiovascular changes during daily torpor in the laboratory mouse.* Am J Physiol Regul Integr Comp Physiol 297:R769–74.

Talaei F, Hylkema MN, Bouma HR, et al. (2011) *Reversible remodeling of lung tissue during hibernation in the Syrian hamster.* J Exp Biol 214:1276–1282.

Townsend KL, Tseng Y-H (2014) *Brown fat fuel utilization and thermogenesis. Trends Endocrinol Metab*. doi: 10.1016/j.tem.2013.12.004

Turner JM, Körtner G, Warnecke L, Geiser F (2012) *Summer and winter torpor use by a free-ranging marsupial.* Comp Biochem Physiol A 162:274–80.

Ukropec J, Anunciado RP, Ravussin Y, et al. (2006) *UCP1-independent thermogenesis in white adipose tissue of cold-acclimated Ucp1$^{-/-}$ mice*. J Biol Chem 281:31894–31908.

Virtanen KA, Lidell ME, Orava J, et al. (2009) *Functional brown adipose tissue in healthy adults*. N Engl J Med 360:1518–1525.

Wade GN, Bartness TJ (1984) *Effects of photoperiod and gonadectomy on food intake, body weight, and body composition in Siberian hamsters*. Am J Physiol 246:26–30.

Waerzeggers Y, Monfared P, Viel T, et al. (2010) M*ouse models in neurological disorders: applications of non-invasive imaging*. Biochim Biophys Acta 1802:819–839.

Wagner J, Horvath S (1973) *Validation of open-circuit method for the determination of oxygen consumption*. J App 34:859–863.

White CR, Seymour RS (2003) *Mammalian basal metabolic rate is proportional to body mass 2 / 3*. PNAS 100:3–6.

Willenborg B, Schmoller A, Caspary J, et al. (2011) *Memantine prevents hypoglycemia-induced decrements of the cerebral energy status in healthy subjects*. J Clin Endocrinol Metab 96:E384–388.

Williams TD, Chambers JB, Henderson RP, et al. (2002) *Cardiovascular responses to caloric restriction and thermoneutrality in C57BL/6J mice.* Am J Physiol Regul Integr Comp Physiol 282:1459–1467.

Willis CKR (2007) *An energy-based body temperature threshold between torpor and normothermia for small mammals.* Physiol Biochem Zool 80:643–51.

Zancanaro C, Nano R, Marchioro C, et al. (1994) *Magnetic resonance spectroscopy investigations of brown adipose tissue and isolated brown adipocytes*. J Lipid Res 35:2191–2199.

6 Publikationen und Manuskripte

6.1 Erklärung: Eigene Beiträge zu den veröffentlichten Teilen der Arbeit

§8, Absatz 3 der Promotionsordnung der Philipps-Universität Marburg (Fassung vom 12.4.2000) sieht vor, dass für die Teile der Dissertation, die aus gemeinsamer Forschungsarbeit hervorgegangen sind, „die individuellen Leistungen des Doktoranden deutlich abgrenzbar und bewertbar sein“ müssen. Im Folgenden sind die eigenen Beiträge zu den entsprechenden Kapiteln 6.2 - 6.6 detailliert aufgeführt.

Zu Kapitel 6.2

That’s hot: golden spiny mice display torpor even at high ambient temperatures

- Planung und Vorbereitung der Experimente in Zusammenarbeit mit Dr. Cornelia Exner
- Durchführung von 95% aller Messungen, die restlichen 5% (Stoffwechselmessungen der Kontrolltiere) wurden von Karen Legler durchgeführt
- Auswertung und statistische Analyse sämtlicher Daten
- Anfertigung aller Abbildungen
- Verfassen des Manuskripts in Zusammenarbeit mit Prof. Gerhard Heldmaier

Dieses Kapitel wurde in der vorliegenden Form im **Journal of Comparative Physiology B** veröffentlicht: Grimpo K**,** Legler K, Heldmaier G, Exner C (2013) *That's hot: golden spiny mice display torpor even at high ambient temperatures.* J Comp Physiol B 184: 567-581.

Zu Kapitel 6.3

Metabolic depression during warm torpor in the Golden spiny mouse (*Acomys russatus*) does not affect mitochondrial respiration and hydrogen peroxide release

- Durchführung aller Stoffwechsel- und Körpertemperaturmessungen
- Präparation aller Gewebe für die mitochondrialen Messungen
- Durchführung der Isolierung und anschließende Atmungsmessungen von Leber- und Nierenmitochondrien mittels Clark-Elektrode
- Auswertung und statistische Analyse sämtlicher Daten
- Anfertigung aller Abbildungen
- Verfassen des Manuskripts in Zusammenarbeit mit Dr. Martin Jastroch

Dieses Kapitel wurde in der vorliegenden Form in **Comparative Biochemistry and Physiology, Part A** veröffentlicht: Grimpo K, Kutschke M, Kastl A, Exner C, Heldmaier G, Jastroch M (2014) *Metabolic depression during warm torpor in the Golden spiny mouse (Acomys russatus) does not affect respiration and hydrogen peroxide release in isolated mitochondria*. Comp Biochem Physiol A 167: 7-14.

Zu Kapitel 6.4

Depression of mitochondrial respiration during daily torpor of the Djungarian hamster, *Phodopus sungorus*, is specific for liver and correlates with body temperature

- Anfertigung aller Abbildungen
- Verfassen des Manuskripts in Zusammenarbeit mit Dr. Martin Jastroch
- Auswertung und statistische Analyse der Daten (20%) in Zusammenarbeit mit Maria Kutschke und Dr. Martin Jastroch (80%)

Dieses Kapitel wurde in der vorliegenden Form in **Comparative Biochemistry and Physiology, Part A** veröffentlicht: Kutschke M, Grimpo K, Kastl A, Schneider S, Exner C, Heldmaier G, Exner C, Jastroch (2013) *Depression of mitochondrial respiration during daily torpor of the Djungarian hamster, Phodopus sungorus, is specific for liver and correlates with body temperature.* Comp Biochem Physiol A 164: 584-589

Zu Kapitel 6.5

A new perspective for the investigation of torpid Djungarian hamsters (*Phodopus sungorus*) and photoperiod changes in adipose tissue composition using magnetic resonance

- Entwicklung der MRT-Stoffwechselküvette in Zusammenarbeit mit Maximilian Völker und der Feinmechanikwerkstatt des Fachbereichs Biologie
- Modifikation der MR-Sequenzen und Erstellung der Messprotokolls in Zusammenarbeit mit Maximilian Völker
- Durchführung aller Experimente
- Auswertung und statistische Analyse sämtlicher Daten
- Anfertigung der Abbildungen und des Textes des vorläufigen Manuskripts

Dieses Kapitel befindet sich derzeit in Vorbereitung und soll zeitnah bei **Journal of Magnetic Resonance** eingereicht werden. Grimpo K, Völker MN, Frank CK, Heverhagen JT, Heldmaier G (in Vorbereitung) *A new perspective for the investigation of torpid Djungarian hamsters (Phodopus sungorus) and photoperiod changes in adipose tissue composition using magnetic resonance spectroscopy.*

Zu Kapitel 6.6

Brown adipose tissue dynamics in wild-type and UCP1-knockout mice*: in vivo* insights with magnetic resonance

- Modifikation der MR-Sequenzen und Erstellung der Messprotokolls in Zusammenarbeit mit Maximilian Völker
- Durchführung von 70% der Messungen, die restlichen Messungen wurden unter meiner Betreuung von Nina Heppe durchgeführt.
- Auswertung und statistische Analyse sämtlicher Daten, teilweise in Zusammenarbeit mit Nina Heppe
- Anfertigung aller Abbildungen
- Verfassen des Manuskripts in Zusammenarbeit mit Prof. Gerhard Heldmaier

Dieses Kapitel wurde in der vorliegenden Form im **Journal of Lipid Research** veröffentlicht: Grimpo K, Voelker MN, Heppe EN, Braun S, Heverhagen JT, Heldmaier G. (2014) *Brown adipose tissue dynamics in wild-type and UCP1-knockout mice: in vivo insights with magnetic resonance.* J Lipid Res. 55: 398-409

6.2 Grimpo et al. 2013

That's hot: golden spiny mice display torpor even at high ambient temperatures

J Comp Physiol B
DOI 10.1007/s00360-012-0721-4

ORIGINAL PAPER

That's hot: golden spiny mice display torpor even at high ambient temperatures

Kirsten Grimpo · Karen Legler · Gerhard Heldmaier · Cornelia Exner

Received: 20 June 2012 / Revised: 13 November 2012 / Accepted: 13 November 2012

Abstract Golden spiny mice (*Acomys russatus*) living in the Judean desert are exposed to extended periods of food and water shortage. We investigated their thermal and metabolic response to three weeks of 50 % food reduction at ambient temperatures of 23, 27, 32 and 35 °C by long term records of metabolic rate and body temperature in the laboratory. At all ambient temperatures, *A. russatus* responded to starvation by a reduction of daily energy expenditure. At 32 and 35 °C, this metabolic adjustment fully compensated the reduced food availability and they maintained their energy balance at a slightly reduced body mass. At lower ambient temperatures, they could not fully compensate for the reduced food availability and kept a negative energy balance. The reduction of daily energy expenditure was largely achieved by the occurrence of daily torpor. Torpor even occurred at high ambient temperatures of 32 and 35 °C during which metabolic depression was not associated with a marked decrease of body temperature. The results show that the occurrence of daily torpor is not necessarily linked to cold exposure and the development of a pronounced hypothermia, but may even occur as depression of metabolic rate in a hot environment.

Keywords *Acomys russatus* · Body temperature · Daily torpor · Food restriction · Thermal load · Metabolic rate

Communicated by H.V. Carey.

K. Grimpo (✉) · K. Legler · G. Heldmaier · C. Exner
Department of Animal Physiology, Faculty of Biology, Philipps-Universität Marburg, Karl-von-Frisch-Straße 8, 35043 Marburg, Germany
e-mail: kirsten.grimpo@biologie.uni-marburg.de

Published online: 02 December 2012

Abbreviations

T_a	Ambient temperature
T_b	Body temperature
BMR	Basal metabolic rate
DEE	Daily energy expenditure
DEI	Daily energy intake
T_{bmin}	Minimal body temperature
MR	Metabolic rate, measured as oxygen consumption
MR_{min}	Minimal metabolic rate (during resting phase)
RMR	Resting metabolic rate (during active phase)
VO_2	Volume of consumed oxygen

Introduction

Golden Spiny mice, *Acomys russatus,* live in hot and arid environments of the great Syrio-African Rift Valley. *A. russatus* from the Judean desert near the Dead Sea (Ein Gedi, 31°28′N, 35°23′E, 100 ± 350 m below sea level) is exposed to air temperatures above 40 °C during summer months and ambient temperatures below 10 °C during winter (Elvert et al. 1999; Shargal et al. 2000; Kronfeld-Schor et al. 2001a; Levy et al. 2012). They hide in rock crevices and do not store food but can tolerate extended periods of food and water shortage utilising their endogenous energy stores. Starvation tolerance using endogenous energy stores is considered as an important prerequisite for desert survival (Shkolnik and Borut 1969; Haim and Borut 1976; Merkt and Taylor 1994; Gutman et al. 2006). In captivity, *A. russatus* has the remarkable ability to accumulate large amounts of body fat within a short period of time when food is available ad libitum, almost doubling body mass (Shafrir and Adler 1983).

A. russatus display a diurnal or crepuscular activity pattern in field. During the hottest hours of the day they rest in rock crevices where ambient temperatures are about 35 °C, but they are still active in the morning and during the afternoon (Shkolnik 1971; Elvert et al. 1999). *A. russatus* often coexists with the congeneric species *A. cahirinus* in the same habitat, and the latter has a nocturnal activity pattern (Kronfeld-Schor and Dayan 1999, Kronfeld-Schor et al. 2001a). When *A. cahirinus* is removed from the area, *A. russatus* develops additional nocturnal activity (Gutman and Dayan 2005). In the laboratory, *A. russatus* normally displays a nocturnal activity pattern (Kronfeld-Schor et al. 2001b). At present it is unclear which mechanisms are responsible for the different activity patterns of *A. russatus* in the field and in the laboratory, but it has been suggested that odour signals of the competing species may contribute to the diurnal activity pattern of *A. russatus* in the field (Haim and Rozenfeld 1993; Fluxman and Haim 1993; Friedman et al. 1997; Kronfeld-Schor et al. 2001b).

Daily torpor is a powerful mechanism for energy conservation and may reduce daily energy expenses by about 30–60 % and in single cases up to 90 % (Ruf and Heldmaier 1992; Körtner and Geiser 2009). This behaviour was found in an increasing number of small mammals (Schmid et al. 2000; Mzilikazi and Lovegrove 2004; Heldmaier and Elvert 2004; Oelkrug et al. 2012). Several species of mice show torpor in response to food limitation, and this was also observed in *A. russatus* (Morhardt and Hudson 1966; Oelkrug et al. 2011; Ehrhardt et al. 2005; Gutman et al. 2006). *A. russatus* exposed to temperatures below thermoneutrality (<32 °C) in the laboratory showed daily torpor under food restriction during the resting phase and an increased level of locomotion during the active phase (Ehrhardt et al. 2005). Gutman et al. (2006, 2007) observed so called "resistant" *A. russatus*, which decreased energy expenditure by entering torpor and reduced activity. They defended their body weight for 39 days in contrast to a small group of "non-resistant animals" that showed starvation-induced hyperactivity resulting in a permanent weight loss. Recently, it was discovered that free ranging *A. russatus* can also become torpid (Levy et al. 2011a). They were kept in large enclosures near the Dead Sea and torpor occurred spontaneously with natural food availability but was reduced when additional food was offered in the enclosures. Under natural food availability, the time spent torpid was more distinct during summer than during winter. The competition with *A. cahirinus* increases the use of torpor in *A. russatus* during winter, leading to a longer time spent torpid per day than during summer (Levy et al. 2011b).

During the hot and dry season in summer when green vegetation is limited, *A. russatus* feeds mainly on arthropods (Kronfeld-Schor and Dayan 1999). In July, ambient temperatures rise above 40 °C during daytime and decrease to 32 °C at night (Elvert et al. 1999). Torpor is usually associated with a pronounced decrease of body temperature. Even species that are known to display torpor in summer prefer to become torpid during cool hours and reduce body temperature below normothermic levels (Körtner and Geiser 2009; Turner et al. 2012; Liu and Karasov 2011). It remains questionable if torpor can be used without significant reduction of body temperature in a hot environment with ambient temperature close to or even above body temperature for most of the day. It has been shown that low torpor metabolism can be adjusted at moderately high body and ambient temperatures like in mouse lemurs and fat tailed lemurs on Madagascar, in dormice as well as in *A. russatus* (Merkt and Taylor 1994; Ortmann et al. 1997; Schmid and Speakman 2000; Elvert and Heldmaier 2005; Dausmann et al. 2009), but it has never been shown if torpor can occur in hot environments where no decrease of body temperature may be detectable in the torpid state.

In our study, we focused on metabolic rate of *A. russatus* during different temperatures and nutritional conditions. We exposed *A. russatus* to 50 % food restriction for three weeks at ambient temperatures of 23, 27, 32 and 35 °C, whereby the latter ambient temperature is close to body temperature preventing a decrease of body temperature during torpor. Body temperature and metabolic rate of each individual were recorded simultaneously for 48 through 120 h to determine resting metabolic rate (RMR), daily energy expenditure (DEE) and minimum metabolic rate. The measurements should allow a comparison if and how *A. russatus* adjust their body mass, RMR and DEE to food restriction in hot environments. The continuous measurement of metabolic rate should allow us to detect if metabolic depression occurs at high ambient temperature where no extensive hypothermia can be developed during torpor.

Materials and methods

Animals

Golden spiny mice (*A. russatus*) were bred and raised at the University of Marburg. Our breeding stock was originally established with animals obtained from Oranim Academic College of Education, Tivon, Israel and originated from the Judean desert. 31 adult male and female *A. russatus* were kept at 27 ± 1 °C in a light–dark cycle of LD 12:12 (lights on 6:30, lights off 18:30). Animals were housed individually in standard macrolon cages type III (56.5 cm × 34.5 cm × 19 cm) bedded with wood shavings and shelter. The animals were fed ad libitum with diet for breeding rodents (Altromin 1314, Langen, Germany 12.5 kJ/g) and had free access to water. Spiny mice were implanted

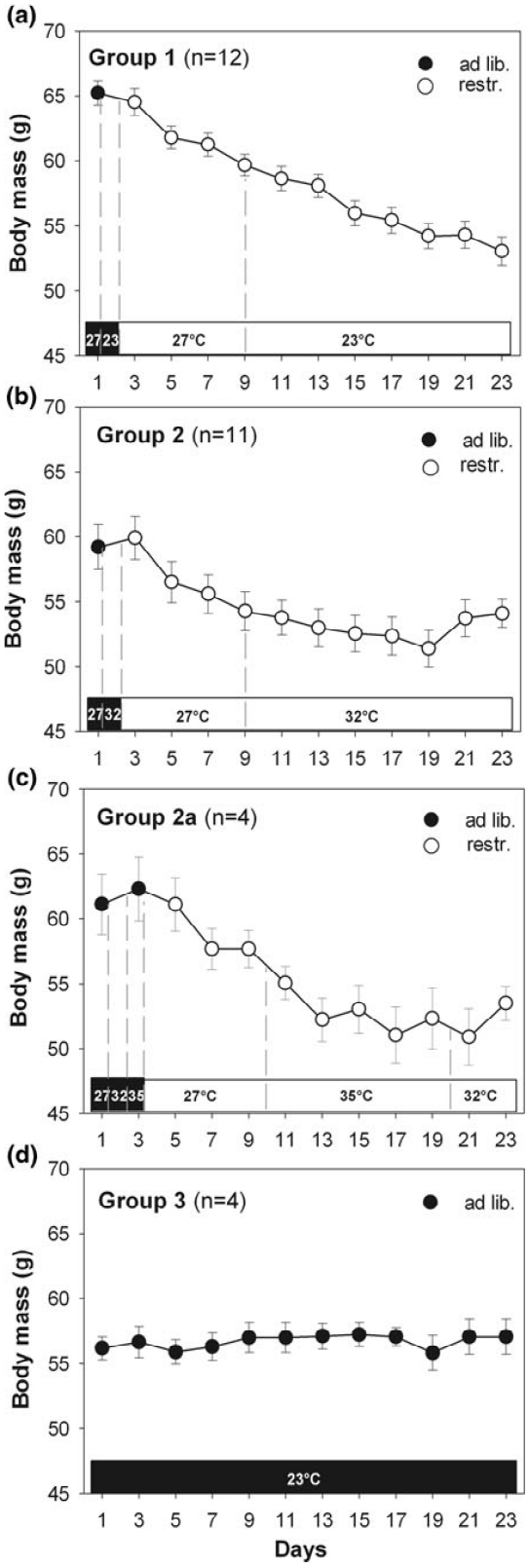

Fig. 1 Development of *A. russatus'* body mass during food restriction. Food restricted groups 1 and 2 were exposed to 27 °C for 1 week. Then ambient temperature was changed to 23 °C (group 1), 32 °C (group 2) or 35 °C (group 2a). A control group was maintained under ad libitum feeding at 23 °C. Days with food restriction are presented with *open symbols*, *closed symbols* for days with ad libitum feeding. Mean values ± SEM

intraperitoneally with temperature sensitive transmitters. During surgery, animals were anaesthetised with ketamine hydrochloride (66 mg kg^{-1}, Ketavet 10 %, Bela-Pharm GmbH + Co KG, Germany), xylazine hydrochloride (0.66 mg kg^{-1}, Rompun 2 %, Bayer Vital GmbH, Germany) and isoflurane (0.5–2 %; CP-Pharma GmbH, Germany). After surgery, they were kept for a recovery period of 10 days before the experiments started. Body weight of the animals was measured every second day. All handling procedures and food supply during food restriction were carried out 1–2 h before the onset of darkness. All experiments were performed in accordance with the German animal welfare act.

Experimental set up

Ad libitum food intake was recorded for three weeks in each individual spiny mouse. This value was then used for the calculation of a 50 % food reduction. Spiny mice were separated into three groups. Group 1 ($n = 12$) was exposed to ambient temperatures of 27 and 23 °C. Group 2 ($n = 15$) was exposed to temperatures of 27, 32 and 35 °C. Group 3 ($n = 4$) was kept under constant conditions, i.e. at an ambient temperature of 23 °C and the spiny mice were fed ad libitum throughout the entire period of observation (timeline of treatment and temperature exposures see Fig. 1). Prior to any food reduction, a 24-h record of body temperature and oxygen consumption was obtained at ambient temperatures of 27 and 23 °C (group 1) or 27 and 32 °C (group 2). Four spiny mice from group 2 were additionally measured at 35 °C (group 2a).

During the initial period of food reduction, all spiny mice were kept at 27 °C for 1 week. Body temperature and oxygen consumption were recorded for 4 days in each individual spiny mouse. Then spiny mice were transferred to ambient temperatures of 23 °C (group 1), 32 °C (group 2) or 35 °C (group 2a; 10 days 35 °C then 4 days 32 °C) for 2 weeks. The 24-h records of body temperature and oxygen consumption were continued at these different temperature levels.

Oxygen consumption and body temperature

Oxygen consumption (VO_2) and body temperature (T_b) were measured in a climate chamber (KPK 600, Feutron,

Germany) for 48, 96 or 120 h (only group 2a). The temperature of the climate chamber was adjusted to obtain different exposure temperatures of 23, 27, 32 or 35 °C inside the metabolic cuvettes. During these measurements, the spiny mice were kept in standard macrolon cages type II (25.5 cm × 15 cm × 17 cm) with wood shavings and shelter. The top of each cage was closed by a PVC sliding lid and air was pumped through the cages with a flow rate of 40 ± 0.5 L h^{-1}. The air was dried by an electric freeze trap (M and C Cooler, ECM, Ratingen, Germany) and the airflow was continuously monitored by electronic mass flow metres for each channel (FM 360, Tylan, München, Germany). O_2 and CO_2 content of the air were measured with a two-channel O_2 analyser (S3AII, Ametek, Sunnyvale, USA) and a two-channel CO_2 analyser (UNOR 6N, Maihak AG, Hamburg, Germany) with a resolution of 0.001 ΔVol % comparing the air entering and leaving the metabolic cuvettes (Heldmaier and Ruf 1992). A magnetic valve system allowed the simultaneous measurement of four animal cages and one empty cage for automated continuous zero readjustment, i.e. each mouse was measured every 5 min. VO_2 was calculated according to the equation: VO_2 [mL O_2 h^{-1}] = ΔVol% O_2 flow [L h^{-1}] × 10. Channel switching was controlled by a computer that also processed the analyser and flow metre signals (including automatic zero adjustment as well as volume corrections for gas analysis) and stored the results. T_b was measured using pre calibrated transmitters (Mini-Mitter, Model X, Sunriver, Oregon, USA, accuracy 0.1 °C). Mini-Mitter signals were detected by a radio receiver and recorded every 5 min simultaneously with measurements of metabolic rate.

Analysis of metabolic rates and torpor duration

The timing and duration of torpor bouts were determined by comparing three different methods, (1) a decrease in body temperature below a threshold 32 °C, (2) an energy based threshold of body temperature (Willis 2007) and (3) the duration of metabolic depression in torpor. The latter was based on an evaluation of the time course of metabolic rate instead of threshold metabolic rates. Beginning of torpor is usually marked by a rapid decrease of metabolic rate, followed by long periods of reduced metabolism and the end of torpor is characterised by a rapid return to the normometabolic level. The evaluation of torpor duration from metabolic rate occurred in two steps. First, an extended period of low metabolism was identified where metabolic rate remained for several hours below RMR. Beginning of torpor was then identified as the onset of this period of metabolic depression, which was often marked by a short peak metabolic rate. End of torpor was identified as the metabolic rate increase during arousal when it reached the level of normometabolic rate. The latter was sometimes accompanied by an overshoot of metabolic rate. The results and significance of the three different calculations are compared in discussion.

RMR and minimal metabolic rate were always average metabolic rates for 30 min. RMR was determined in a post-absorptive state during active phase (scotophase), when animals rested between activity bursts. Minimal metabolic rate was calculated during resting phase (mostly during the photophase 06:30–18:30), when animals were inactive (sleeping or torpid). Body temperatures were calculated as mean values for the same 30 min time window. DEE (J day^{-1}) was calculated from 24-h oxygen consumption (VO_2). Daily energy intake was roughly estimated by the consumed food energy per day (12.5 kJ g^{-1}). Q_{10} values for metabolic rate of torpid *A. russatus* at different body temperatures were calculated from $Q_{10} = (MR_1/MR_2)^{(10/Tb_1 - Tb_2)}$.

Statistical analysis

Mean values are presented ± standard error of mean (SEM). For comparison between two groups, Student's *t* test for paired or unpaired samples was used. When normal distribution of data could not be assumed, the groups were compared with the Mann–Whitney rank sum test. All calculations were performed using SigmaStat 3.5. The overall level of significance was set to $p < 0.05$.

Results

Body mass and effects of food restriction on daily energy expenditure

The initial body mass of *A. russatus* ranged between 50 and 72 g. During food restriction all spiny mice initially lost body mass. This was most obvious during the first week of food reduction at 27 °C ambient temperature (T_a) (Fig. 1). Mice which were then transferred to 23 °C decreased their body mass continuously till the end of the experiment (Fig. 1a), whilst mice transferred to high T_a of 32 or 35 °C lost body mass at a lower rate during the first few days and then maintained a stable body mass until the end of the observation period (Fig. 1b, c). This indicated that they had adjusted their energy balance to the reduced food supply. Mice fed ad libitum at 23 °C T_a did not change body mass over the entire period of observation.

During food restriction, *A. russatus* reduced their DEE at all ambient temperatures studied. It decreased from 45.3 to 33.0 kJ day^{-1} ($n = 12$) at a T_a of 23 °C. The lowered DEE was still greater than the daily energy intake

from restricted food supply (18.6 ± 1.6 kJ day^{-1}), indicating a negative energy balance which was in accordance with weight loss of these mice (Fig. 1a). Food restriction at 27 °C T_a reduced DEE from 30.2 ± 1.3 to 24.6 ± 1.9 kJ day^{-1} which was still greater than the energy they obtained from food intake (12.9 ± 0.9 kJ day^{-1}). However at 32 °C T_a, DEE was reduced from 23.9 ± 1.5 to 16.8 ± 1.2 kJ day^{-1} by food restriction, and under these conditions DEE approximately matched the amount of energy provided from feeding (14.2 ± 1.5 kJ day^{-1}).

Food restricted *A. russatus* had a lower body mass which could partially explain the lowered DEE. Therefore, we analyzed the relation between body mass and DEE at 27 °C T_a (Fig. 2). In ad libitum fed *A. russatus*, DEE significantly correlated with body mass (DEE = 0.601 BM$^{0.942}$; $n = 21$; $r^2 = 0.2508$, $p = 0.0207$). To compare food reduced and ad libitum fed mice, we calculated a single ANCOVA model with a feeding group factor and body weight as the covariate. The DEE of food reduced spiny mice was significantly lower than DEE of ad libitum fed mice (7 kJ lower DEE for a body weight of 59.5 g ($p < 0.001$)). The shift indicated that changes in DEE were not simply a consequence of changes in body mass and composition, e.g. a reduced body fat content, but required metabolic, thermoregulatory and behavioural adjustments for low energy expenditure.

Two individuals were not included in the comparison. In contrast to the other animals, they increased their DEE during food restriction and had a greater loss of body mass during the first week of food restriction (24 and 13 vs. 9 % in the other individuals). *A. russatus* can either reduce their energy expenses (resistant) or they become hyperactive in response to food restriction (non-resistant) (Gutman et al. 2007). The latter showed a high level of DEE as observed in the two individuals (Table 1, 27 °C restricted). At other ambient temperatures, we did not observe such a paradoxical response of DEE to food reduction.

Resting metabolic rate (RMR)

At 32 and 35 °C T_a, food restricted *A. russatus* had reduced RMRs (Table 1). 32 °C can be considered as the thermoneutral zone. The measurements were obtained in a post-absorptive state. Therefore, RMR at 32 °C represents basal metabolic rate (BMR). At 23 and 27 °C T_a, i.e. temperatures below thermoneutrality, no reduction of RMR was observed in food restricted *A. russatus*.

In order to compare RMR with DEE, we calculated daily RMR, i.e. the amount of energy requirements for *A. russatus* assuming that they were resting the entire day (Fig. 3). In *A. russatus* fed ad libitum, DEE always exceeded daily RMR by 20 % through 30 % indicating that

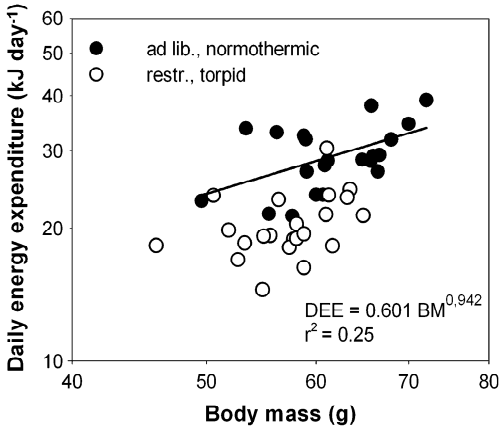

Fig. 2 Associations between body mass (BM) and daily energy expenditure (DEE) in *A. russatus* at 27 °C ambient temperature. The graph compares ad libitum fed *A. russatus* (ad lib., *closed symbols*, $n = 21$) and food restricted animals (restr., *open symbols*, $n = 22$). Non-resistant *A. russatus* ($n = 2$) were excluded from calculation. The correlation between BM and DEE was significant during ad libitum feeding ($p < 0.05$), but not during food restriction. The *regression line* and the corresponding equations illustrate the estimated linear relationship between BM and DEE of ad libitum fed *A. russatus*

beyond RMR extra energy was required for locomotor activity or other energetically costly processes. This was only observed in *A. russatus* fed ad libitum, whereas food reduced *A. russatus* had almost identical values for daily RMR and DEE. At first glance, it suggested that they were resting the entire day and developed no other energy requiring activities. However, the 24-h measurements showed bursts of activity, as can be seen from the ultradian patterns of elevated metabolic rate and body temperature in ad libitum fed as well as in food restricted mice (Fig. 4). The food reduced *A. russatus* were active beyond the level of RMR at certain times of the day, but these additional energy requirements must have been compensated by energy conserving measures at other times of the day, and this maintained DEE at the level of RMR.

24-hourly variations of metabolic rate and body temperature of A. russatus fed ad libitum

24-h records showed higher levels of metabolic rate and body temperature during the scotophase and lower levels during the photophase. This 24-h cycle was superimposed by ultradian fluctuations of metabolic rate and body temperature (Fig. 4, left diagrams). The nocturnal pattern of metabolic rate and body temperature was confirmed when mean values were calculated including all measurements during rest and ultradian activity bursts at 23 °C (Fig. 5a). High levels of metabolic rate were obtained during the beginning of the scotophase. Lowest values were reached

Table 1 Body mass, resting metabolic rate (RMR) during active phase and minimal metabolic rate (MR_{min}) during resting phase, corresponding body temperatures (T_b), daily energy expenditure (DEE) and daily energy intake (DEI) at different ambient temperatures (T_a) and feeding conditions

					Active phase		Resting phase			
T_a (°C)	Feeding condition	n	Torpor duration (min)	Body mass (g)	RMR (mL O_2 h^{-1})	T_b (°C)	MR_{min} (mL O_2 h^{-1})	T_b (°C)	DEE (kJ day^{-1})	DEI (kJ day^{-1})
23	Ad libitum[b]	12	–	62.9 ± 1.6	80.4 ± 7.0	34.7 ± 0.4	59.6 ± 2.3[A]	33.7 ± 0.2[A]	48.6 ± 2.8	40.9 ± 4.1
		7	300 ± 39	61.0 ± 1.6	69.8 ± 4.7	34.5 ± 0.3	27.4 ± 4.4[A]	28.7 ± 1.0[A]	36.9 ± 1.2	38.8 ± 6.1
	Restricted	11–12[a]	570 ± 65	57.7 ± 0.8	68.5 ± 3.3	34.9 ± 0.2	13.6 ± 1.7[A,B]	26.4 ± 0.6[A,B]	33.5 ± 2.8	18.6 ± 1.6
27	Ad libitum	23	–	62.0 ± 1.2	47.8 ± 2.2	34.8 ± 0.2	39.6 ± 1.0[A]	33.8 ± 0.1[A]	30.8 ± 1.5	36.5 ± 2.5
		4	340 ± 24	61.1 ± 2.9	47.7 ± 2.4	34.7 ± 0.2	23.6 ± 0.9[A]	31.1 ± 0.3[A]	26.7 ± 1.0	30.9 ± 3.3
	Restricted	21–22[a,c]	732 ± 35	57.4 ± 1.0	45.1 ± 1.7	35.0 ± 0.2	15.2 ± 0.6[A,B]	30.1 ± 0.1[A,B]	20.4 ± 0.7	13.0 ± 0.9
		2	487[e]	55.1	53.5	34.3	23.9	31.2	50.4	11.3
32	Ad libitum	10	–	57.3 ± 1.4	40.9 ± 2.9	35.9 ± 0.2	30.9 ± 1.8[A]	35.6 ± 0.1[A]	23.3 ± 1.5	35.1 ± 4.0
		1	421	70.0	61.2	37.1	28.0	35.3	30.09	42.5
	Restricted	9–11[a]	567 ± 51	52.9 ± 1.3	30.9 ± 2.2[B]	35.3 ± 0.4	19.1 ± 0.8[A,B]	34.6 ± 0.2[B]	16.8 ± 1.2	14.2 ± 1.5
35	Ad libitum	3	–	63 ± 2.0	47.9 ± 10.3	37.9 ± 0.5	40.4 ± 9.6	37.6 ± 0.5	31.2 ± 9.5	15.4 ± 3.3
		1	230	55.5	43.8	37.7	22.2	37.2	19.22	10
	Restricted	2–3[a,d]	489 ± 207	54.3 ± 1.8	25.2 ± 2.9	37.2 ± 0.1	18.9 ± 2.1	36.9 ± 0.1	13.1 ± 0.3	7.9 ± 0.4

Mean values ± SEM originates from groups 1–3

[A] Significant difference at $p < 0.05$ to active phase within same T_a and same feeding condition

[B] Significant difference at $p < 0.05$ to ad libitum feeding, no torpor within same T_a. Values at 35 °C T_a were not used for statistical evaluation, because of the low sample size

[a] From some individuals only metabolic rate could be obtained, because temperature sensitive transmitters failed during experiment. For this reason in groups sample size of body temperature is lower than sample size of metabolic rate

[b] This category includes *A. russatus* from group 1 and group 3

[c] Three *A. russatus* did not enter torpid state ($T_b < 32$ °C) at 27 °C ambient temperature

[d] One *A. russatus* did not enter torpid state (≤reference value during torpor at 27 °C) at 35 °C ambient temperature

[e] Non-resistant *A. russatus* that showed short torpor bouts and increased daily energy expenditure during food restriction

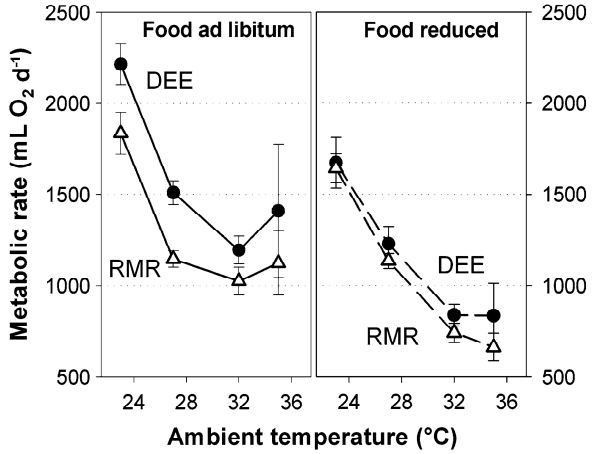

Fig. 3 Daily energy expenditure (DEE) and resting metabolic rate (RMR) at different ambient temperatures during ad libitum feeding and food restriction. Mean values ± SEM. Sample size was $n = 19$ (ad libitum) and $n = 12$ (restricted) at 23 °C, $n = 27$ at 27 °C, $n = 11$ at 32 °C and $n = 4$ at 35 °C ambient temperature

during the photophase at about 09:00. This coincides with 24-h variations of body temperature. Figure 5 includes all measurements of metabolic rate at rest and its ultradian activity peaks. Therefore, metabolic rates shown in this figure are higher than values presented in Table 1 which are based only on RMRs. The time course of metabolic rate and body temperature additionally showed that, despite of individual variations in the timing of ultradian bursts, the overall 24-h pattern was similar in all individuals.

Normothermic *A. russatus* fed ad libitum at a T_a of 23 °C decreased their RMR by 26 % during the diurnal resting phase. The decrease in metabolic rate was associated with a 1 °C lower body temperature (Table 1). Similar relative amplitudes of 24-h changes of metabolic rate were observed in ad libitum fed, normothermic *A. russatus* at 27 and 32 °C T_a, but absolute levels of metabolic rate were lower at 32 °C T_a. At 32 °C, body temperature of *A. russatus* decreased only by 0.3 °C during the 24-h resting phase. At 35 °C, we also observed lower levels of metabolic rate and body temperature during the diurnal resting phase in each individual *A. russatus*, but the number of observations was too small for a statistical evaluation (Table 1).

Daily torpor during ad libitum feeding

A. russatus showed torpor spontaneously when fed ad libitum (Fig. 5b). Torpor episodes were characterised by a major reduction of metabolic rate and body temperature. In most cases, torpor onset occurred prior to the beginning of the photophase. Minimum values of body temperature and metabolic rate were reached during early morning hours and torpor ended around noon. At 23 °C T_a (groups 1 and 3), spontaneous torpor was observed on 15 days in a total of 52 individual 24-h measurements of body temperature, and metabolic rate (29 %). The torpor episodes lasted for 300 ± 39 min ($n = 7$). Body temperature was lowered to 28.7 ± 1.0 °C and metabolic rate was reduced by 61 % as compared to normothermic values.

At 27 °C, the incidence of spontaneous torpor was less pronounced than at 23 °C (Fig. 6). Torpor occurred in four out of 27 individual 24-h measurements, i.e. 15 % of all observation periods. Torpor bout duration was 340 ± 24 min ($n = 4$). During torpor, body temperature decreased to 31.1 ± 0.3 °C and metabolic rate was reduced by 51 % (Table 1).

Daily torpor during food restriction

Food restriction lowered minimal metabolic rate during the resting phase of the 24-h cycle at 23 and 27 °C T_a (Fig. 4, right diagrams). This is largely due to torpor, i.e. 24 out of 27 mice displayed torpor during the first seven days of food restriction in 84 out of 125 measurements (67 %). Most food reduced *A. russatus* displayed torpor already on the second day of food reduction. Torpor duration increased from 439 ± 36 to 668 ± 39 min on day seven ($n = 23$, $p < 0.001$). The longest torpor bout observed at 27 °C T_a lasted for 869 min. Minimum metabolic rate during torpor was observed at the end of scotophase or just after lights on and was 66 % less than RMR in normothermic *A. russatus*. At the same time, body temperature was lowered to 30.2 ± 0.1 °C.

At 23 °C T_a, food reduced *A. russatus* displayed torpor almost every day. The amplitude of the 24-h pattern of metabolic rate and body temperature was on average more exaggerated than during ad libitum feeding (Fig. 5c). Torpor duration was 492 ± 65 min at the beginning of the 23 °C exposure and did not change significantly until the end of food restriction (412 ± 66 min). The longest torpor bout observed lasted for 852 min. During torpor, metabolic rate was lowered to 13.6 ± 1.7 mL O_2 h^{-1}, i.e. a reduction of 80 % as compared to normothermia. Body temperature decreased to 26.4 ± 0.6 °C.

Torpor was associated with a phase shift of the resting period and an increasing proportion of diurnal activity. This can be seen in individual records (Fig. 4) as well as in the mean values of metabolic rates at 23 °C T_a (Fig. 5). The median of metabolic rates was used as a threshold for separation of low and high metabolic rates. In ad libitum fed *A. russatus,* it revealed a period of low values lasting from 05:25 until 16:35, i.e. they were resting during daytime. In torpid *A. russatus* fed ad libitum, the period of low metabolic rate started much earlier and lasted from 02:45 to 13:55. In food restricted torpid *A. russatus,* this period of

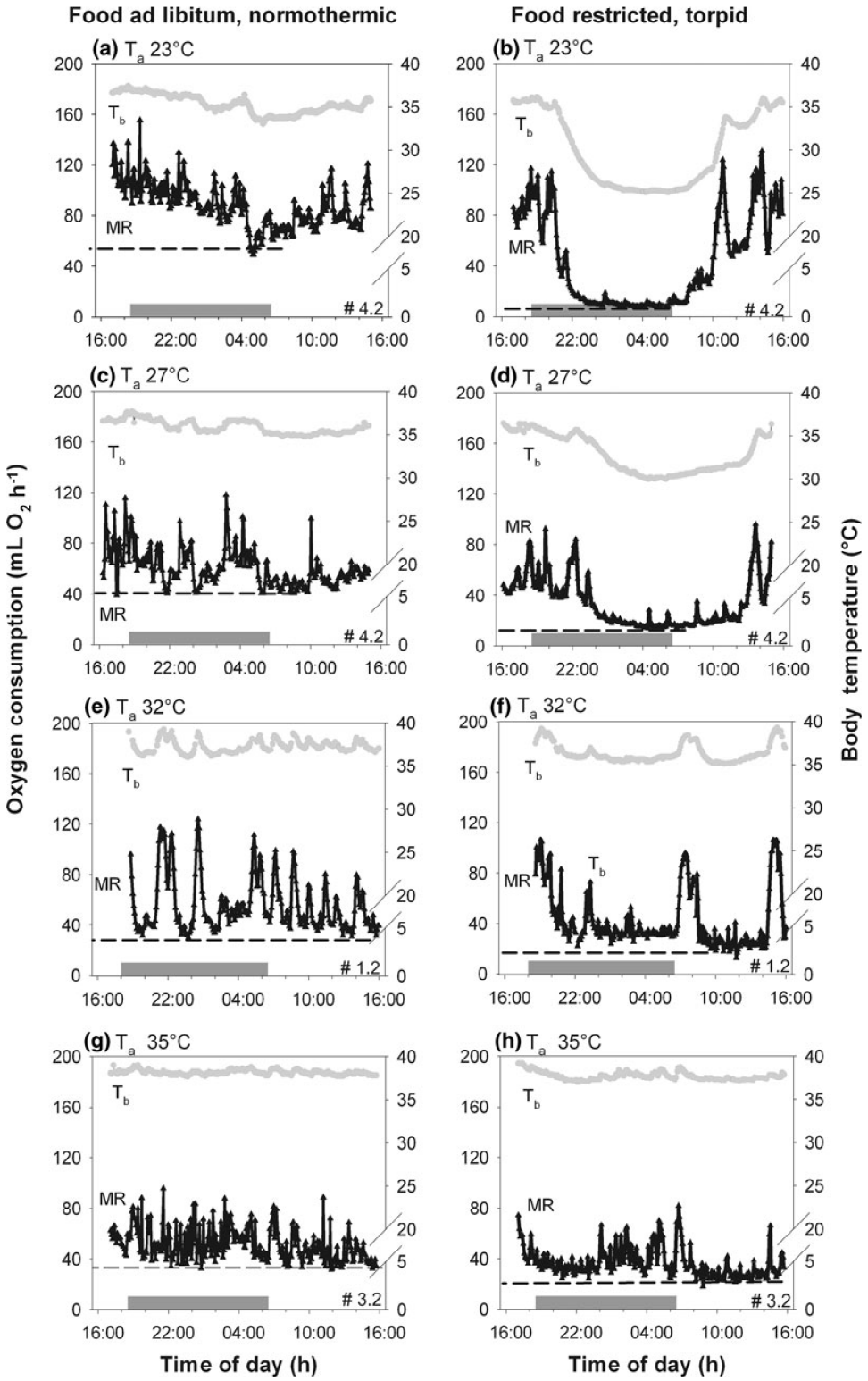

Fig. 4 24-h records of oxygen consumption and body temperature from *A. russatus* at different ambient temperatures (T_a). Pairs of normothermic and torpid state are presented for every ambient temperature. The *scattered black line* highlights the minimal metabolic rate of each animal at the different conditions. The *grey bar* on the time scale indicates the scotophase

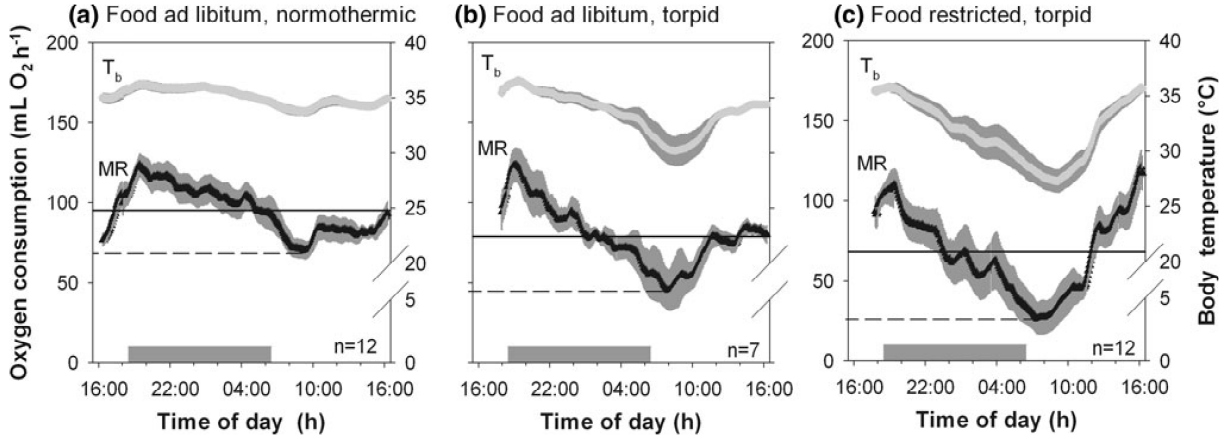

Fig. 5 Nycthemeral variation of mean oxygen consumption (MR) and body temperature (T_b) in ad libitum fed and food restricted *A. russatus* at 23 °C ambient temperature. The 50 % threshold for metabolic rate is indicated by the *solid black line*. The *dotted line* illustrates the minimal reached metabolic rate during the different conditions. The *grey bar* on the time scale indicates the scotophase. Mean values ± SEM

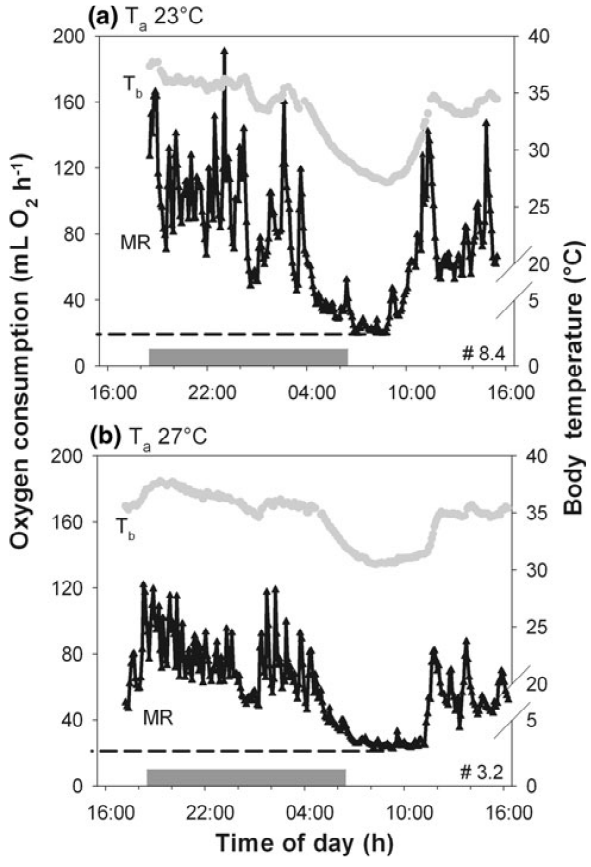

Fig. 6 Nycthemeral variation of oxygen consumption (MR) and body temperature (T_b) registration of *A. russatus* which displayed torpor during ad libitum feeding at 23 and 27 °C ambient temperature (T_a). The *scattered line* indicates the minimal metabolic. The *grey bar* on the time scale indicates the scotophase

low metabolic rate lasted from 23:40 to 11:55. Maximum metabolic rates were observed during the afternoon indicating that they were predominantly active during daytime.

At 27 °C, we observed two non-resistant individuals which did not reduce DEE in response to food reduction. Despite their high DEE, which was about twice the DEE of other food restricted *A. russatus*, they also showed daily torpor (Table 1, 27 °C restricted).

Daily torpor at high ambient temperatures

At high ambient temperatures (32 and 35 °C) *A. russatus* responded to food restriction by a reduction of RMR during their active phase as well as minimal metabolic rate during their resting phase (Table 1). The latter was largely due to an extensive use of daily torpor, which is, however, difficult to detect at these high ambient temperatures.

To identify torpor, we compared the metabolic rates of *A. russatus* at 32 and 35 °C T_a with their individual torpor metabolic rates at 27 °C T_a, where torpor can be easily identified (see examples in Figs. 4 and 6). Mean values and box plots were calculated for each individual to take into account the variability of metabolic rate during a stable torpor episode at 27 °C T_a. Minimum metabolic rate of food reduced *A. russatus* at 32 °C T_a reached the level of torpor metabolic rate at 27 °C, suggesting that they became torpid at 32 °C (Fig. 7). This was observed in 9 out of 11 *A. russatus*. Two mice did not enter torpor at 27 °C and we could not obtain a reference value for individual comparison with torpor at 32 °C. One *A. russatus* fed ad libitum became torpid at 32 °C and reached the same low metabolic rate as during food reduction (Fig. 7b), indicating that

torpor metabolic rates at 27 and 32 °C T_a were similar. In conclusion, this suggested that food restricted *A. russatus* at 32 °C T_a remained active during their circadian activity phase but most of them became torpid during their resting phase (38 out of 45 measurements, 84 %). Compared to RMR, minimum metabolic rate during torpor was reduced by 38 %.

A similar comparison was made for food reduced *A. russatus* at 35 °C (Fig. 8). During the active phase, they lowered their metabolic rate but it remained above the range of torpor metabolic rates, indicating that mice were active and normothermic. However, during the resting phase they lowered their metabolic rates approaching the torpor level, i.e. food reduced *A. russatus* at 35 °C T_a became torpid in 5 out of 19 measurements (26 %). The metabolic rate reduction at 35 °C T_a was 25 %.

Body temperature and thermal conductance at high ambient temperatures

At 32 °C T_a normothermic *A. russatus* had a body temperature (T_b) of 35.6 °C which decreased to 34.7 °C in the torpid state (Table 1). They sustained a $T_b - T_a$ gradient of 2.3 ± 0.16 °C (calculated from actual measurements of T_b and T_a) which was slightly less, but not fundamentally different from torpor at 27 °C T_a where T_b was lowered to 30.2 ± 0.1 °C, and the $T_b - T_a$ gradient was 2.9 ± 0.2 °C. At 35 °C T_a, the thermal situation was more complex because normothermic *A. russatus* elevated their T_b to 37.6 °C which decreased to 36.9 °C in the torpid state, resulting in a $T_b - T_a$ gradient of 2.0 °C (only three measurements 2.0, 2.6 and 1.3 °C). The behaviour of these mice clearly differed from their behaviour at lower

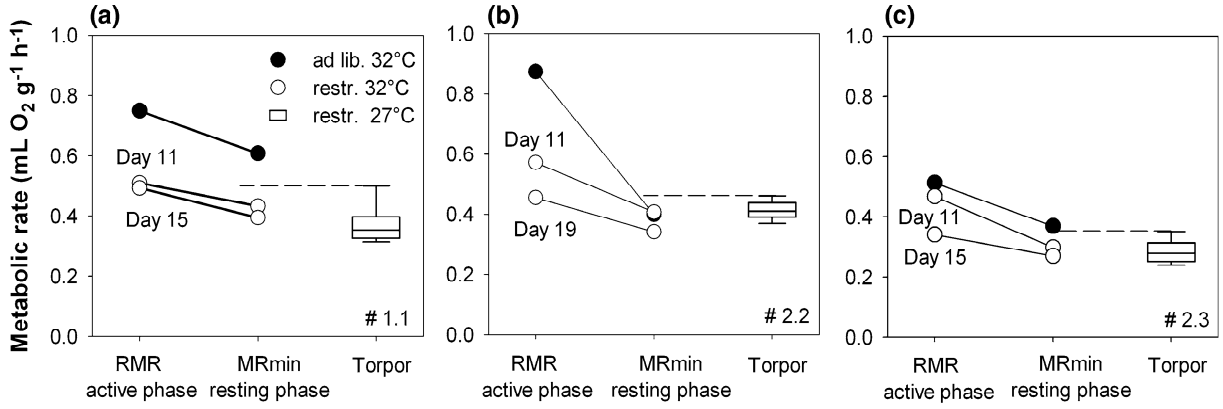

Fig. 7 Metabolic rates of three *A. russatus* during the 24-h cycle of rest and activity under ad libitum conditions (ad lib., *closed circles*) and different days of following food restriction (restr., *open circles*) at 32 °C ambient temperature. Metabolic rates are 30 min means of resting *A. russatus* in their nocturnal activity phase and during their diurnal resting phase. The *box plots* are metabolic rates from the same individuals measured during torpor at 27 °C ambient temperature

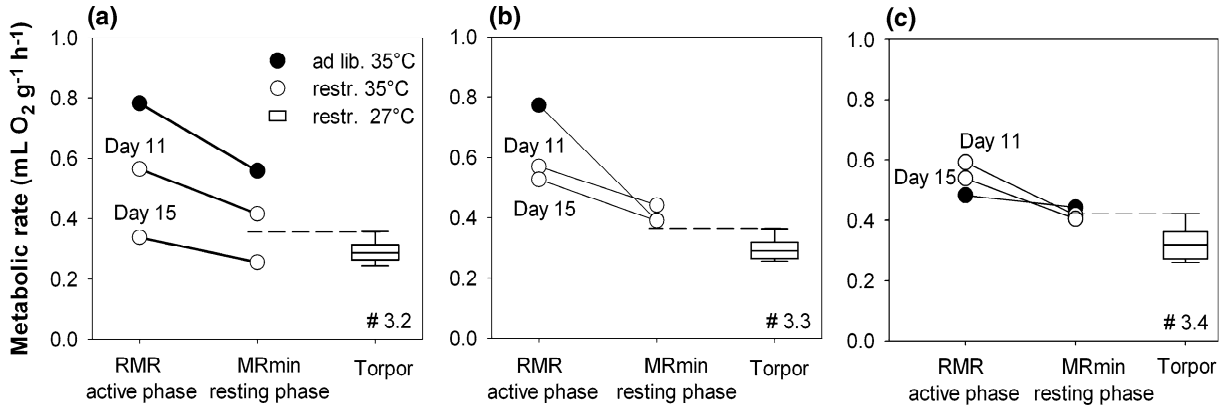

Fig. 8 Metabolic rates of three *A. russatus* during the 24-h cycle of rest and activity under ad libitum conditions (ad lib, *closed circles*) and different days of following food restriction (restr., *open circles*) at 35 °C ambient temperature. Metabolic rates are 30 min means of resting *A. russatus* in their nocturnal activity phase and during their diurnal resting phase. The *box plots* are metabolic rates from the same individuals measured during torpor at 27 °C ambient temperature

temperatures. At low T_a, *A. russatus* always had a hunched body posture when resting or torpid. At 35 °C T_a, *A. russatus* lay stretched out and frequently changed their position probably to facilitate conductive heat loss via their ventral body surface. The increasing efforts for heat loss at high T_a were obvious when comparing thermal conductance of torpid *A. russatus* which was 6.1 ± 1.1 mL O_2 $h^{-1}°C^{-1}$ at 27 °C T_a increased to 9.2 ± 1.0 mL O_2 $h^{-1}°C^{-1}$ at 32 °C T_a and even further to 13.0 ± 2.7 mL O_2 $h^{-1}°C^{-1}$ at 35 °C T_a.

Temperature relations of metabolic rate in torpid animals

Body temperature of torpid *A. russatus* changed with T_a and varied between 25 and 37 °C (Fig. 9). Individual values of torpid minimal metabolic rate varied between 7.9 and 28.2 mL O_2 h^{-1} indicating a relation between the level of metabolic rate and T_b during torpor. This relation could be described by an equation ($MR_{torp} = 4.0554e^{(0.0447Tb)}$) resulting in an apparent Q_{10} of 1.7. Active non-torpid *A. russatus* (food restricted) had a T_b of 35.3 ± 0.4 °C and a RMR of 30.9 ± 2.2 mL O_2 h^{-1} at thermoneutrality. This was well above the torpid level, which would be 19.6 mL O_2 h^{-1} at the same level of T_b, as predicted from the equation before, indicating a depression of metabolic rate by 36 % in the torpid state. The same was true for non-torpid, ad libitum fed *A. russatus* during resting phase (T_b of 35.6 ± 0.1 °C and a minimal metabolic rate of 30.9 ± 1.8 mL O_2 h^{-1}). If metabolic rate in torpor was compared with RMR of non-torpid, ad libitum fed *A. russatus* during active phase (40.9 ± 2.9 mL O_2 h^{-1}, T_b 35.9 ± 0.2 °C), the reduction of metabolic rate of torpid animals was even more exaggerated (20 mL O_2 h^{-1}), i.e. 51 %.

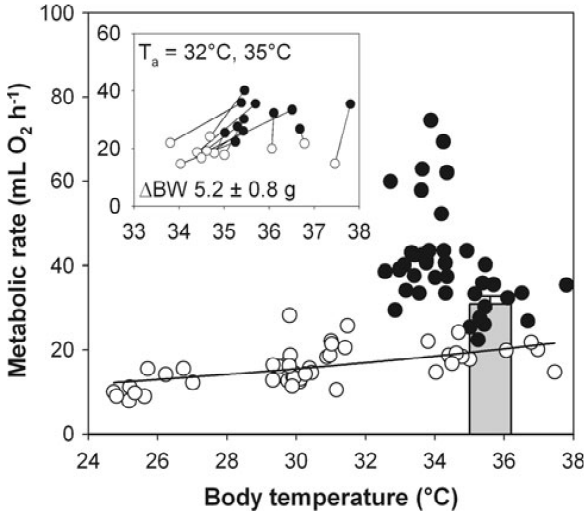

Fig. 9 Metabolic rate as a function of body temperature from *A. russatus* kept at an ambient temperature of 23, 27, 32 or 35 °C. Each *data point* represents minimal metabolic rate (30 min) and body temperature during a single torpor episode under food restriction (*open circles*) or at a normothermic day under ad libitum conditions (*closed circles*). The relation between torpid metabolic rate and related body temperature is $MR_{torp} = 4.0554\ e^{(0.0447\ Tb)}$ (48 data points). The *bar* shows minimal metabolic rate of resting, ad libitum fed *A. russatus* at 32 °C ambient temperature ($n = 11$ mean ± SEM) (= basal metabolic rate). The inset separates *A. russatus* kept at high ambient temperatures (≥32 °C) from the main graph. Normothermic and torpid values of the same individuals are connected. The body weight difference (ΔBW) is given as mean ± SEM

Discussion

Food restriction by 50 % caused a rapid initial loss of body mass. At T_a of 23 and 27 °C it continued for three weeks, but at ambient temperature of 32 and 35 °C *A. russatus* gradually approached a stable body mass within three weeks. This observation is in accordance with previous findings of Gutman et al. (2007) who described that starvation resistant *A. russatus* stabilized their body mass after 25 days of 50 % food restriction at 30 °C T_a. Merkt and Taylor (1994) reported a metabolic switch after two weeks of food restriction at a T_a of 31 °C where RMRs were reduced by 50 %. The mice in our experiment already reduced their minimal metabolic rate during the first days of food restriction at 27 °C and changed metabolic rate gradually during the further experiment depending on ambient temperature. The fast adjustment of metabolic rate could be due to a lower initial body weight of 65 g in the present study as compared to 85 g in Merkt and Taylor (1994).

The maintenance of a stable body mass indicates that *A. russatus* can adjust their energy requirements to a 50 % reduced food supply at thermoneutral or high ambient temperatures. At temperatures below thermoneutrality, they can tolerate shortage of food for several weeks, but they develop a negative energy balance and only partially compensate for the reduced food supply. This emphasises a unique property of *A. russatus* to cope with food shortage during the hot and dry season in their natural environment. It involves different kinds of metabolic adjustment.

Mammals living in arid environments are characterised by relatively low RMRs as compared to the metabolic rates of mammals from non-desert habitats. These reductions of BMR are considered as a classical example of genetic adaptation to hot and arid environments. Lower metabolic rates reduce evaporative water loss by respiration, and at the same time it reduces the endogenous thermal load which in addition reduces the need for evaporative cooling (McNab and Morrison 1963; McNab 1979; Haim and Izhaki 1993; Lovegrove 2003). The BMR of *A. russatus*

with a body mass of 57.3 g is 40 % less than expected for a small mammal of this size (40.9 mL O_2 h^{-1} as compared to 70.4 mL O_2 h^{-1} predicted from Lovegrove (2003)). The lower than predicted metabolic rate of *A. russatus* was described before in several studies (Shkolnik and Borut 1969; Haim and Borut 1981; Rubal et al. 1992, 1995). It underlines that, according to the criteria of metabolic depression, *A. russatus* can be considered as well adapted to hot and arid environments.

The low level of metabolic rate can further be reduced in response to food reduction. In our experiments, the response was based on two adjustments. The constitutively low RMR of *A. russatus* in its active phase was reduced by about 25 % compared to its resting phase at 32 °C. Reductions of metabolic rate in response to starvation were also observed in larger sized desert ungulates such as sand gazelles (*Gazella subgutturosa*) and Oryx (*Oryx leucoryx)* (Ostrowski et al. 2006a, b). In addition, *A. russatus* used daily torpor during its resting phase whereby metabolic rate was further lowered by 38 %. Torpor lasts only several hours per day and its actual contribution to the reduction of DEE in hot conditions will therefore be less than 30 %. Since DEE was found identical with RMR in food restricted *A. russatus,* it suggests that the extent of torpor is controlled in a manner that it balances the extra energy required for activity and other energetically costly behaviours. As a result the DEE of food restricted *A. russatus* remains at the level of BMR at 32 °C T_a. In our *A. russatus* measured at 32 and 35 °C T_a, the contribution of torpor to the reduction of DEE was probably less than 30 %. However, in these hot environments torpor has an additional benefit. It reduces the endogenous thermal load for *A. russatus* in the heat and thus helps to avoid the development of hyperthermia.

It is remarkable that torpor occurred even at high T_a of 32 or 35 °C, and this observation is in accordance with field studies that show a higher torpor occurrence in *A. russatus* during summer (Levy et al. 2011a). These temperatures are close to or even above the T_b of resting normothermic *A. russatus* when they were kept below thermoneutrality. At high T_a, *A. russatus* elevated their T_b from 34.9 °C (ad lib. at 27 °C) to 37.2 °C in resting normothermic individuals. This elevated T_b was then slightly lowered in torpor, but several *A. russatus* had even higher body temperatures during torpor than in the normothermic state. It allowed a direct comparison of individual metabolic rates in normothermia and torpor at the same level of T_b, which revealed a 36 % metabolic rate depression in torpor (30.9 mL O_2 h^{-1} in normothermia versus 19.6 mL O_2 h^{-1} in torpor at an identical T_b of 35.3 °C). This is in accordance with previous estimates of active depression metabolic rate in *Cercartetus nanus* (32 %), *Glis glis* (54 %) and *Cheirogaleus medius* (28 %) (Song et al. 1997; Heldmaier and Elvert 2004; Dausmann et al. 2009). The observed metabolic rate reduction supports earlier observations that torpor can occur in warm environments, but the present observations set a new record that torpor can even occur in the heat when normothermic T_b is elevated in response to heat exposure and remains above the normal level of T_b during torpor.

This indicates that T_b is no reliable indicator for the occurrence of torpor, especially in a warm or hot environment. The entry into torpor is usually assumed when body temperature falls below a threshold value of 32 or 30 °C. These arbitrary thresholds do not really mark the physiological onset and end of torpor, but are easy to apply as a descriptor for changes in torpor behaviour. However, they are only a suitable measures at low ambient temperatures (<28 °C) where obvious changes in body temperature below 32 °C are to be expected.

Willis (2007) suggested an improved procedure where threshold temperatures are calculated individually, taking into account energetic constraints like T_a and body mass. This, however, is also based on changes in body temperature. The measurement of metabolic rate is a more reliable indicator instead, because it measures entrance and arousal from torpor directly. According to Willis' procedure, threshold temperatures for *A. russatus* in our study are above 34 °C. Torpor entrance calculated according to Willis (2007) coincides with the onset of depression of metabolic rate. However, it did not always match metabolic arousal at the end of torpor. The rise of body temperature was lagging behind and passed its threshold level with a delay of up to several hours later than metabolic arousal. The animals became active and body temperature was only gradually approaching the threshold value with a delay of several hours. At 27 °C T_a, Willis' procedure calculated a torpor duration of 778 ± 75 min but according to metabolic beginning and end of torpor it lasted only 570 ± 65 min. A threshold temperature of 32 °C would produce a torpor duration of 582 ± 62 min which is similar to the metabolic torpor duration. However, the 32 °C body temperature threshold is limited to low ambient temperatures and cannot be applied for determination of torpor duration at higher ambient temperatures, where body temperature during torpor remains above 32 °C.

Ad libitum fed *A. russatus* were night active, as can be concluded from high metabolic rate, high body temperature and high frequency of ultradian bursts of metabolic activity at night. Food restriction not only reduced metabolic rate in starvation resistant *A. russatus*, but additionally shifted their nocturnal activity into daylight hours. One could suggest that the feeding schedule might have contributed to this shift of nocturnal activity into the day (Gutmann et al. 2007). However, in ad libitum fed *A. russatus* which became torpid spontaneously, we also observed an increase

in diurnal activity. This suggests that shifting the activity phase is not necessarily linked to the shortage of food, but may accompany the occurrence of torpor behaviour.

House mice also shift their nocturnal activity rhythm into daytime when they have to work for food. When the food reward is reduced, diurnal activity increase and the mice start to become torpid (Hut et al. 2011). In these experiments, food was provided continuously by automatic feeders in response to revolutions of the running wheel, which excludes a direct effect of external feeding schedules on the phasing of activity. When mice were kept in constant conditions with free running circadian rhythm, the decrease of food reward also phase advanced the activity phase without altering the circadian frequency. This suggests that the energy challenge per se causes a gradual shift towards diurnality and that this is based on mechanisms downstream of the circadian master clock, the suprachiasmatic nucleus (Hut et al. 2011).

There are increasing numbers of observations that small mammals that have a diurnal activity pattern in their natural habitat turn strictly nocturnal in the laboratory. *A. russatus* is an example for this (Elvert et al. 1999; Kronfeld-Schor et al. 2001b). Golden hamsters that are famous for their nocturnality in captivity are diurnal in nature (Gattermann et al. 2008). House mice kept in outdoor enclosures are also not exclusively nocturnal, but become predominantly or sometimes exclusively diurnal during winter months (Daan et al. 2011). The latter supports the view that energetic challenges influence the timing and extent of activity.

A. russatus is able to accumulate high amounts of abdominal white fat stores during times of food abundance. Utilising the endogenous energy stores, they can bridge periods of food and water shortage. For long-term starvation tolerance, the reductions of BMR, RMR and the reduction of minimal metabolic rate during torpor are the most important measures to reduce energy requirements in *A. russatus*. BMR is generally considered as a physiological constant characterising the minimum maintenance energy requirements of mammals. It scales with body mass in an allometric manner, but also correlates with life-history, foraging mode, ecological factors as well as phylogeny (Kleiber 1932; Elgar and Harvey 1987; White and Seymour 2003; Lovegrove 2003).

BMR includes metabolic activities of all organs. Most prominent are muscle, heart, kidney, intestine, liver and skin in small mammals, as predicted from distribution of blood flow (Thurlby and Trayhurn 1980; Puchalski et al. 1987; Heldmaier et al. 1989). Any change in the size and metabolic activity of these tissues may change BMR. During food reduction or starvation not only white adipose tissue but also other organs may be reduced. Food restricted mice have a lower wet weight of pancreas, liver, spleen, kidneys and heart, a slightly reduced wet weight of the intestine, and this is accompanied by an improved uptake of some nutrients per size unit of the intestine (Ferraris et al. 2001). A similar response was also observed in desert dwelling sand gazelles which reduced the weight of the heart liver and muscle by 20 through 40 % (wet and dry weight), whereas the intestine had a constant dry weight but its wet weight was reduced by 30 % (Ostrowski et al. 2006a). If *A. russatus* would show similar changes in the size of internal organs during food restriction this may have contributed to the observed reduction of BMR.

On the cellular level, BMR reflects mitochondrial respiration in the different tissues whereby 80 % of O_2 consumption is used for coupled respiration to supply ATP consuming process, and about 20 % may be used for uncoupled respiration, e.g. mitochondrial proton leaks (Buttgereit and Brand 1995; Rolfe and Brown 1997). A considerable part of ATP (20-30 %) is required for RNA and protein synthesis. It is not known which organs or metabolic pathways contribute to the reduction of metabolic rate in food restricted *A. russatus*. A likely candidate for reduction of BMR may be a decrease of enzyme activities and transport processes involved in the processing of food. Metabolic rate reduction in torpor may be associated with an inhibition of glycolysis, fuelling rerouted to lipid utilisation, as well as an inhibition of RNA and protein biosynthesis (Storey 1997; van Breukelen and Martin 2002; Berriel Diaz et al. 2004; Andrews 2007). Even without this knowledge we can conclude that minimum metabolic rate is not a physiological constant, but is the result of controlled regulation which allows mammals to cope with challenges of their energy balance. However, the physiological mechanisms controlling the level of BMR are still unknown.

Acknowledgments The authors would like to acknowledge the technical support of Mr. Gabor Szerencsi.

References

Andrews MT (2007) Advances in molecular biology of hibernation in mammals. BioEssays 29:431–440

Berriel Diaz M, Lange M, Heldmaier G, Klingenspor M (2004) Depression of transcription and translation during daily torpor in the Djungarian hamster (*Phodopus sungorus*). J Comp Physiol B 174:495–502

Buttgereit F, Brand MD (1995) A hierarchy of ATP-consuming processes in mammalian cells. Biochem J 312(Pt 1):163–167

Daan S, Spoelstra K, Albrecht U, Schmutz I, Daan M, Daan B, Rienks F, Poletaeva I, Dell'Omo G, Vyssotski A, Lipp H (2011) Lab mice in the field: unorthodox daily activity and effects of a dysfunctional circadian clock allele. J Biol Rhythms 26:118–129

Dausmann KH, Glos J, Heldmaier G (2009) Energetics of tropical hibernation. J Comp Physiol B 179:345–357

Ehrhardt N, Heldmaier G, Exner C (2005) Adaptive mechanisms during food restriction in *Acomys russatus*: the use of torpor for desert survival. J Comp Physiol B 175:193–200

Elgar MA, Harvey PH (1987) Basal metabolic rates in mammals: allometry, phylogeny and ecology. Funct Ecol 1:25–36

Elvert R, Heldmaier G (2005) Cardiorespiratory and metabolic reactions during entrance into torpor in dormice, *Glis glis*. J Exp Biol 208:1373–1383

Elvert R, Kronfeld N, Dayan T, Haim A, Zisapel N, Heldmaier G (1999) Telemetric field studies of body temperature and activity rhythms of *Acomys russatus* and *A. cahirinus* in the Judean Desert of Israel. Oecologia 119:484–492

Ferraris RP, Cao QX, Prabhakaram S (2001) Chronic but not acute energy restriction increases intestinal nutrient transport in mice. J Nutr 131(3):779–786

Fluxman S, Haim Λ (1993) Daily rhythms of body temperature in *Acomys russatus*: the response to chemical signals released by *Acomys cahirinus*. Chronobiol Int 10:159–164

Friedman D, Haim A, Zisapel N (1997) Temporal segregation in coexisting spiny mice (Genus *Acomys*): role of photoperiod and heterospecific odour. Physiol Behav 62:407–411

Gattermann R, Johnston RE, Yigit N, Fritzsche P, Larimer S, Ozkurt S, Neumann K, Song Z, Colak E, Johnston J, McPhee ME (2008) Golden hamsters are nocturnal in captivity but diurnal in nature. Biol Lett 4:253–255

Gutman R, Dayan T (2005) Temporal partitioning: an experiment with two species of spiny mice. Ecology 86:164–173

Gutman R, Choshniak I, Kronfeld-Schor N (2006) Defending body mass during food restriction in *Acomys russatus*: a desert rodent that does not store food. Am J Physiol Regul Integr Comp Physiol 290:881–891

Gutman R, Yosha D, Choshniak I, Kronfeld-Schor N (2007) Two strategies for coping with food shortage in desert golden spiny mice. Physiol Behav 90:95–102

Haim A, Borut A (1976) Thermoregulation and non-shivering thermogenesis as factors limiting distribution of the golden spiny mouse (*Acomys russatus*). Isr J Med Sci 12:896

Haim A, Borut A (1981) Heat production and dissipation in golden spiny mice, *Acomys russatus* from two extreme habitats. J Comp Physiol 142B:445–450

Haim A, Izhaki I (1993) The ecological significance of resting metabolic rate and non-shivering thermogenesis for rodents. J Therm Biol 18:71–81

Haim A, Rozenfeld FM (1993) Temporal segregation in coexisting *Acomys* species: the role of odour. Physiol Behav 54:1159–1161

Heldmaier G, Elvert R (2004) How to enter torpor: thermodynamic and physiological mechanisms of metabolic depression. In: Barnes BM, Carey HV (eds) Life in the cold: evolution, mechanisms, adaptation, and application, 27 Biological Papers of the University of Alaska, p 185–198

Heldmaier G, Ruf T (1992) Body temperature and metabolic rate during natural hypothermia in endotherms. J Comp Physiol B 162:696–706

Heldmaier G, Klaus S, Wiesinger H, Friedrichs U, Wenzel M (1989) Cold acclimation and thermogenesis. In: Malan A, Canguilhem B (eds) Living in the cold II. John Libbey Eurotext, Paris, pp 347–358

Hut RA, Pilorz V, Boerema AS, Strijkstra AM, Daan S (2011) Working for food shifts nocturnal mouse activity into the day. PLoS ONE 6:e17527

Kleiber M (1932) Body Size and Metabolism. Hilgardia 6:315–353

Körtner G, Geiser F (2009) The key to winter survival: daily torpor in a small arid-zone marsupial. Naturwissenschaften 96:525–530

Kronfeld-Schor N, Dayan T (1999) The dietary basis for temporal partitioning: food habits of coexisting *Acomys* species. Oecologia 121:123–128

Kronfeld-Schor N, Shargal E, Haim A, Dayan T, Zisapel N, Heldmaier G (2001a) Temporal partitioning among diurnally and nocturnally active desert spiny mice: energy and water turnover costs. J Therm Biol 26:139–142

Kronfeld-Schor N, Dayan T, Elvert R, Haim A, Zisapel N, Heldmaier G (2001b) On the use of the time axis for ecological separation: diel rhythms as an evolutionary constraint. Amer Nat 158:451–457

Levy O, Dayan T, Kronfeld-Schor N (2011a) Adaptive thermoregulation in golden spiny mice: the influence of season and food availability on body temperature. Physiol Biochem Zool 84:175–184

Levy O, Dayan T, Kronfeld-Schor N (2011b) Interspecific competition and torpor in golden spiny mice: two sides of the energy-acquisition coin. Integr Comp Biol 51:441–448

Levy O, Dayan T, Kronfeld-Schor N, Porter WP (2012) Biophysical modeling of the temporal niche: from first principles to the evolution of activity patterns. Am Nat 179:794–804

Liu JN, Karasov WH (2011) Hibernation in warm hibernacula by free-ranging Formosan leaf-nosed bats, *Hipposideros terasensis*, in subtropical Taiwan. J Comp Physiol B 181:125–135

Lovegrove BG (2003) The influence of climate on the basal metabolic rate of small mammals: a slow–fast metabolic continuum. J Comp Physiol B 173:87–112

McNab BK (1979) Climatic adaptation in the energetics of heteromyid rodents. CompBiochem Physiol A 62:813–820

McNab BK, Morrison P (1963) Body temperature and metabolism in subspecies of *Peromyscus* from arid and mesic environments. Ecol Monogr 33:63–82

Merkt JR, Taylor CR (1994) 'Metabolic switch' for desert survival. Proc Natl Acad Sci USA 91:12313–12316

Morhardt JE, Hudson JW (1966) Daily torpor induced in white-footed mice (*Peromyscus spp.*) by starvation. Nature 212:1046–1047

Mzilikazi N, Lovegrove BG (2004) Daily torpor in free-ranging rock elephant shrews, *Elephantulus myurus*: a year-long study. Physiol Biochem Zool 77:285–296

Oelkrug R, Heldmaier G, Meyer CW (2011) Torpor patterns, arousal rates, and temporal organization of torpor entry in wildtype and UCP1-ablated mice. J Comp Physiol B 181:137–145

Oelkrug R, Meyer CW, Heldmaier G, Mzilikazi N (2012) Seasonal changes in thermogenesis of a free-ranging afrotherian small mammal, the Western rock elephant shrew (*Elephantulus rupestris*). J Comp Physiol B 182:715–727

Ortmann S, Heldmaier G, Schmid J, Ganzhorn JU (1997) Spontaneous daily torpor in Malagasy mouse lemurs. Naturwissenschaften 84:28–32

Ostrowski S, Mesochina P, Williams JB (2006a) Physiological adjustments of sand gazelles (*Gazella subgutturosa*) to a boom-or-bust economy: standard fasting metabolic rate, total evaporative water loss, and changes in the sizes of organs during food and water restriction. Physiol Biochem Zool 79:810–819

Ostrowski S, Williams JB, Mésochina P, Sauerwein H (2006b) Physiological acclimation of a desert antelope, Arabian oryx (*Oryx leucoryx*), to long-term food and water restriction. J Comp Physiol B 176:191–201

Puchalski W, Böckler H, Heldmaier G, Langefeld M (1987) Organ blood flow and brown adipose tissue oxygen consumption during noradrenaline-induced non-shivering thermogenesis in the Djungarian hamster. J Exp Zool 242:263–271

Rolfe DF, Brown GC (1997) Cellular energy utilisation and molecular origin of standard metabolic rate in mammals. Physiol Rev 77:731–758

Rubal A, Choshniak I, Haim A (1992) Daily rhythms of metabolic rate and body temperature of two murids from extremely different habitats. Chronobiol Int 9:341–349

Rubal A, Haim A, Choshniak I (1995) Resting metabolic rates and daily energy intake in desert and non-desert murid rodents. Comp Biochem Physiol 112A:511–515

Ruf T, Heldmaier G (1992) The impact of daily torpor on energy requirements in the Djungarian hamster, *Phodopus sungorus*. Phys Zool 65:994–1010

Schmid J, Speakman JR (2000) Daily energy expenditure of the grey mouse lemur (*Microcebus murinus*): a small primate that uses torpor. J Comp Physiol B 170:633–641

Schmid J, Ruf T, Heldmaier G (2000) Metabolism and temperature regulation during daily torpor in the smallest primate, the pygmy mouse lemur (*Microcebus myoxinus*) in Madagascar. J Comp Physiol B 170:59–68

Shafrir E, Adler JH (1983) Enzymatic and metabolic responses to affluent diet of two diabetes-prone species of spiny mice: *Acomys cahirinus* and *A. russatus*. Int J Biochem 15:1439–1446

Shargal E, Kronfeld-Schor N, Dayan T (2000) Population biology and spatial relationships of coexisting spiny mice of the genus *Acomys*. Israel J Mammal 81:1046–1052

Shkolnik A (1971) Diurnal activity in a small desert rodent. Int J Biometeorol 15:115–120

Shkolnik A, Borut A (1969) Temperature and water relations in two species of spiny mice (*Acomys*). J Mammal 50:245–255

Song X, Kortner G, Geiser F (1997) Thermal relations of metabolic rate reduction in a hibernating marsupial. Am J Physiol 273:2097–2104

Storey KB (1997) Metabolic regulation in mammalian hibernation: enzyme and protein adaptations. Comp Biochem Physiol A 118:1115–1124

Thurlby PL, Trayhurn P (1980) Regional blood flow in genetically obese (ob/ob) mice. The importance of brown adipose tissue to the reduced energy expenditure on non-shivering thermogenesis. Pflugers Arch 385:193–201

Turner JM, Körtner G, Warnecke L, Geiser F (2012) Summer and winter torpor use by a free-ranging marsupial. Comp Biochem Physiol A 162:274–280

van Breukelen F, Martin SL (2002) Reversible depression of transcription during hibernation. J Comp Physiol B 172:355–361

White CR, Seymour RS (2003) Mammalian basal metabolic rate is proportional to body mass$^{2/3}$. Proc Natl Acad Sci USA 100:4046–4049

Willis CK (2007) An energy-based body temperature threshold between torpor and normothermia for small mammals. Physiol Biochem Zool 80:643–651

6.3 Grimpo and Kutschke et al. 2014

Metabolic depression during warm torpor in the Golden spiny mouse (*Acomys russatus*) does not affect mitochondrial respiration and hydrogen peroxide release

Comparative Biochemistry and Physiology, Part A 167 (2014) 7–14

Contents lists available at ScienceDirect

Comparative Biochemistry and Physiology, Part A

journal homepage: www.elsevier.com/locate/cbpa

Metabolic depression during warm torpor in the Golden spiny mouse (*Acomys russatus*) does not affect mitochondrial respiration and hydrogen peroxide release

Kirsten Grimpo [a,1], Maria Kutschke [b,1], Anja Kastl [a], Carola W. Meyer [b], Gerhard Heldmaier [a], Cornelia Exner [a], Martin Jastroch [b,*]

[a] Philipps-Universität Marburg, Faculty of Biology, Department of Animal Physiology, Karl-von-Frisch-Strasse 8, 35043 Marburg, Germany
[b] Institute for Diabetes and Obesity, Helmholtz-Zentrum München, German Research Center for Environmental Health (GmbH), Ingolstädter Landstr. 1, 85764 Neuherberg, Germany

ARTICLE INFO

Article history:
Received 8 July 2013
Received in revised form 3 September 2013
Accepted 3 September 2013
Available online 8 September 2013

Keywords:
Mitochondrial respiration
Daily torpor
Hypothermia
Hypometabolism
Acomys russatus

ABSTRACT

Small mammals actively decrease metabolism during daily torpor and hibernation to save energy. Recently, depression of mitochondrial substrate oxidation in isolated liver mitochondria was observed and associated to hypothermic/hypometabolic states in Djungarian hamsters, mice and hibernators. We aimed to clarify whether hypothermia or hypometabolism causes mitochondrial depression during torpor by studying the Golden spiny mouse (*Acomys russatus*), a desert rodent which performs daily torpor at high ambient temperatures of 32 °C. Notably, metabolic rate but not body temperature is significantly decreased under these conditions. In isolated liver, heart, skeletal muscle or kidney mitochondria we found no depression of respiration. Moderate cold exposure lowered torpor body temperature but had minor effects on minimal metabolic rate in torpor. Neither decreased body temperature nor metabolic rate impacted mitochondrial respiration. Measurements of mitochondrial proton leak kinetics and determination of P/O ratio revealed no differences in mitochondrial efficiency. Hydrogen peroxide release from mitochondria was not affected. We conclude that interspecies differences of mitochondrial depression during torpor do not support a general relationship between mitochondrial respiration, body temperature and metabolic rate. In Golden spiny mice, reduction of metabolic rate at mild temperatures is not triggered by depression of substrate oxidation as found in liver mitochondria from other cold-exposed rodents.

1. Introduction

Small mammals enter torpor to save energy as for example during periods of food shortage. Although this physiological phenomenon occurs in diverse members of at least eight mammalian orders (Geiser, 1998; Heldmaier et al., 2004; Melvin and Andrews, 2009), the molecular mechanisms underlining entry, maintenance and arousal from metabolic reduction are still unclear.

Torpor entrance is defined as a decrease in metabolic rate (measured as oxygen consumption of the whole animal) below resting values, usually followed by a reduction in body temperature up to 24 hours. As the oxygen consumption drops rapidly before body temperature, it is assumed that torpor entrance is triggered by a temperature independent down-regulation of oxygen consuming processes (Lyman and Chatfield, 1955; Heldmaier and Ruf, 1992; Buck and Barnes, 2000). Presumably coordinated by the central and autonomic nervous system, heart rate is slowed down reducing peripheral substrate and oxygen supply (Swoap and Gutilla, 2009; Braulke and Heldmaier, 2010; Jinka et al., 2011; Iliff and Swoap, 2012). Energetically expensive gene transcription and protein synthesis are decreased during torpor, contributing to reduced metabolic energy demand in the torpid state (Berriel Diaz et al., 2004). Mitochondria provide a major proportion of cellular energy by oxidative phosphorylation. Metabolites of glucose, fats and proteins are oxidized and electrons are donated to respiratory chain complexes. As electrons are transported along the respiratory chain, the energy is harvested to pump protons out of the matrix, thereby generating the proton motive force. The proton motive force drives the ATP synthase but protons also re-enter the matrix via leaks in the mitochondrial inner membrane, decreasing mitochondrial efficiency (Jastroch et al., 2010). Proton permeability besides capacity of substrate oxidation may adjust the energy budgets of animals in response to environmental and physiological challenge (Gnaiger et al., 2000; St-Pierre et al., 2000; Trzcionka et al., 2008; Jastroch, 2012).

Abbreviations: ADP, adenosine-diphosphate; ATP, adenosine-triphosphate; T_a, ambient temperature; T_b, body temperature; TPMP, triphenylmethylphosphonium; FCCP, carbonyl cyanide-p-trifluoromethoxyphenylhydrazone; MR, metabolic rate, measured as oxygen consumption; RCR, respiratory control ratio; RET, reverse electron transfer; ROS, reactive oxygen species.

* Corresponding author. Fax: +49 89 3187 3799.
E-mail address: martin.jastroch@helmholtz-muenchen.de (M. Jastroch).

[1] K.G. and M.K. equally contributed to this study.

1095-6433/$ – see front matter © 2013 Elsevier Inc. All rights reserved.
http://dx.doi.org/10.1016/j.cbpa.2013.09.002

Recent studies suggest that mitochondrial adjustments of energy transduction occur in the liver during fasting-induced torpor in mice and spontaneous torpor of the Djungarian hamster. In isolated liver mitochondria, mitochondrial succinate oxidation is reduced in torpid individuals at 37 °C assay temperature (Brown et al., 2007; Brown and Staples, 2010; Kutschke et al., 2013). Based on the reduction of respiration in liver at 37 °C but not 15 °C assay temperature, one study concluded that active depression of mitochondrial respiration plays an important role during torpor entrance (Brown et al., 2007). In isolated mitochondria of other tissues, however, there was no evidence for depression of respiration, questioning the significance of liver depression for whole metabolic rate (Kutschke et al., 2013). However, in liver mitochondria, there is a positive correlation between mitochondrial respiration and body temperature in hamsters and mice (Brown and Staples, 2010; Kutschke et al., 2013). Metabolic rate was not measured in these studies but the correlation between metabolic rate and body temperature in daily torpor of the Djungarian hamster is well-established (Heldmaier and Ruf, 1992), implicating that mitochondrial respiration also correlates with metabolic rate.

The question whether mitochondrial depression contributes to the active down-regulation of metabolic rate during torpor prompted us to further comparative studies using the Golden spiny mouse. The Golden spiny mouse (*Acomys russatus*) inhabits hot and dry environments where it enters torpor even in the summer when high ambient temperatures prevent a decrease in body temperature (Levy et al., 2011). In the laboratory, torpor can be induced by caloric restriction in thermoneutrality and moderate cold (Ehrhardt et al., 2005; Gutman et al., 2006; Grimpo et al., 2012). The amount of saved energy during the hypometabolic state is further promoted by hypothermia at low ambient temperatures as it reduces costs of thermoregulation. We showed that the Golden spiny mouse enters torpor in captivity in response to food restriction at 32 °C housing temperature (Grimpo et al., 2012). In this regime metabolic rate of the spiny mice is significantly reduced during the torpor bout (about 40%) along with minor reduction in body temperature, enabling us to investigate adjustments of mitochondrial bioenergetics during torpor excluding the effects of body temperature.

2. Materials and methods

2.1. Animals

Twenty-eight Golden spiny mice (*A. russatus*) of the breeding colony from Philipps-Universität Marburg were kept in a 12:12 light:dark cycle (lights on: 06:30 h, lights off: 18:30 h Central European Time). Spiny mice were housed individually in type III makrolon-cages (56.5 cm × 35.5 cm × 19 cm) bedded with wood shavings and shelter. Before the beginning of the experiments all spiny mice were kept at 27 ± 1 °C and were fed *ad libitum* with breeding rodent diet (Altromin 1314).

2.2. Food restriction experiments

Ad libitum food intake of spiny mice was recorded over 3 weeks to calculate 50% food reduction during the subsequent food restriction experiment. Food consumption and body weight of the animals were measured every second day. Twenty-four spiny mice were food restricted at an ambient temperature of 27 ± 1 °C, until they showed daily torpor. Then 12 individuals were transferred to thermoneutral temperature (32 ± 1 °C) and the other 12 individuals were transferred to moderate cold (23 ± 1 °C). In total, the period of food restriction lasted 3 weeks. Four mice were maintained under *ad libitum* conditions at 32 ± 1 °C for 2 weeks before sampling.

2.3. Measurement of oxygen consumption

The oxygen consumption of food restricted and *ad libitum* fed spiny mice was measured in a temperature controlled climate chamber (KPK 600, Feutron GmbH, Germany) at the respective ambient temperatures of 32 °C or 23 °C (±0.5 °C accuracy). Oxygen consumption was measured by indirect calorimetry using an open two channel respiratory system. The experimental setup to calculate metabolic rate from measured oxygen consumption was described previously (Heldmaier and Ruf, 1992; Grimpo et al., 2012). Oxygen consumption of each individual was detected every 5 min. During the measurements animals were kept individually in makrolon-cages type II (16 cm × 21 cm × 13 cm).

2.4. Measurement of body temperature (T_b)

Core body temperatures of spiny mice were measured with temperature sensitive transmitters intraperitoneally (Mini-Mitter, Model X, Sunriver, Oregon, USA, accuracy ±0.1 °C). Mini-Mitter signals were detected by a radio receiver and processed by a microcomputer system as reported previously (Ruf and Heldmaier, 1987). T_b of spiny mice was recorded simultaneously to oxygen consumption every 5 min.

2.5. Definition of torpor and tissue dissection

Torpor of warm acclimated (32 °C) spiny mice was defined by the reduction of their oxygen consumption (as body temperature at high ambient temperatures almost remained at normothermic values) and deep torpor was considered as stable plateau at low oxygen consumption levels (30% below resting level). Cold acclimated (23 °C) spiny mice were considered as torpid if body temperature dropped below 32 °C and oxygen consumption was maintained at a stable plateau. For tissue sampling all spiny mice were killed by cervical dislocation towards the end of the food restriction period, one torpid and one normometabolic (normothermic) spiny mouse in the morning for one set of measurements. As we did not want to disturb torpid animals, the sequence of sacrificing the experimental animals was torpid, and then the normometabolic (normothermic) individual.

2.6. Mitochondrial isolation

Tissues of a torpid and a normothermic spiny mouse were sampled pairwise to control for day-to-day variations of the mitochondrial isolation process. Mitochondria were isolated from tissue homogenates by differential centrifugation. Heart, liver, kidney and skeletal muscle were immediately dissected, weighed and transferred to ice-cold isolation buffer. All steps of mitochondrial isolation were performed on ice, ice-cold buffer or at 4 °C in the centrifuge to minimize proteolytic activity.

The heart muscle, liver and kidney were cut with scissors in STE buffer (250 mM sucrose, 5 mM Tris, 2 mM EGTA, pH 7.4 at 4 °C) and rinsed with buffer several times, to wash out blood.

Using a Dounce homogenizer, liver tissue was homogenized by 10 passes with a loose glass pestle and kidney tissue by 15 passes with a tight pestle. Differential centrifugation of liver and kidney was performed as described previously (Trzcionka et al., 2008).

The heart muscle was incubated in 5 mL STE buffer containing 14.8 U mL^{-1} protease (Subtilisin A, Type III, Sigma-Aldrich GmbH, Germany) for 2 min. Volume was filled up to 20 mL with STE buffer and the tissue was minced with a polytron (PT 3100; Kinematica AG, Switzerland), giving a 5 s burst at 1,800 rpm. The heart muscle homogenate was centrifuged for 10 min at 8,000 *g*. The pellet was resuspended in STE buffer and then centrifuged at 500 *g* for 10 min. The supernatant was centrifuged at 9,000 *g* for 10 min and the centrifugation was repeated with the resuspended pellet. The final pellet was carefully aspirated and the mitochondria were resuspended in a minimal volume of isolation buffer.

M. quadriceps, *M. tibialis* and *M. pectoralis* were removed and placed in CP1 buffer (100 mM KCl, 50 mM Tris-HCL, 2 mM EGTA, pH 7.4 at 4 °C). The muscle was cut in small pieces and cleared of blood. Tissue was transferred to 35 mL CP1 buffer containing 1 mM ATP, 5 mM MgCl, 0.5% (w/v) defatted BSA and 1.45 U mL^{-1} protease (Subtilisin A, Type III, Sigma-Aldrich GmbH, Germany) and incubated for 2.5 min. Then tissue was homogenized twice at 1,800 rpm for 2 × 3 s (Polytron, PT 3100). Suspension was incubated for 3 min and afterwards centrifuged at 500 *g* for 10 min in centrifuge tubes. The supernatant was filtered through two layers of cheesecloth and centrifuged at 9,000 *g* for 10 min. The pellet was resuspended in 30 mL CP1 buffer and the high spin cycle was repeated. The suspension of the resulting pellet was centrifuged at 6,000 *g* for 10 min. Then mitochondria were resuspended in 200 μL CP1 buffer.

Content of mitochondrial protein was determined by colorimetric analysis with the biuret assay (Gornall et al., 1949) using fatty acid-free bovine serum albumin as a standard.

2.7. Measurement of mitochondrial respiration

Oxygen consumption of mitochondria was measured using a Clark-type oxygen electrode (Rank Brothers Ltd., United Kingdom) maintained at 34 °C (reflecting the body temperature of torpid spiny mice acclimated to 32 °C ambient temperature) and calibrated with air-saturated KHE buffer (120 mM KCl, 5 mM KH_2PO_4, 3 mM HEPES, 1 mM EGTA, 0.3% (w/v) BSA, pH 7.2 at room temperature), which was assumed to contain 421 nmol O mL^{-1} (Reynafarje et al., 1985).

Mitochondria were diluted to 0.5 mg mitochondrial protein mL^{-1} in 2.5 mL (liver and kidney) and to 0.2 mg mitochondrial protein mL^{-1} in 0.5 mL (heart and skeletal muscle). Rotenone (4.8 μM) was added to inhibit complex I of the respiratory chain and mitochondrial respiration was started by adding 4 mM succinate (state 2). ADP was added to induce state 3 respiration (120 μM for: kidney and liver; 600 μM for heart and skeletal muscle). Then, 1 μg mL^{-1} oligomycin (blocking the ATP-synthase) was used to establish leak (state 4) respiration. In heart and skeletal muscle mitochondria oligomycin was added, when steady state 3 respiration occurred. To compare ADP turnover in liver and kidney mitochondria oligomycin was added after depletion of ADP, which was indicated by a decrease in the slope of the oxygen consumption. Finally, FCCP (carbonyl cyanide-p-trifluoromethoxyphenyl-hydrazone) was added incrementally to induce maximum substrate oxidation.

The respiratory control ratio (RCR) was calculated as the quotient of state 3 and state 4 respiration to ascertain the integrity of isolated mitochondria. All mitochondrial experiments were performed in duplicate.

To determine proton leak kinetics mitochondrial respiration rate and mitochondrial membrane potential were measured simultaneously using a clark type electrode and a TPMP (triphenylmethylphosphonium) sensitive electrode (Brand, 1995).

2.8. Hydrogen peroxide release from isolated mitochondria

Hydrogen peroxide release of heart, kidney and skeletal muscle was detected fluorometrically using the Amplex red assay according to Lambert et al. (2008). Mitochondria (0.175 mg mL^{-1}) were incubated in KHE buffer (120 mM KCl, 3 mM HEPES, 1 mM EGTA, 0.3% (w/v) BSA, pH 7.2 at room temperature) supplemented with 1 μg mL^{-1} oligomycin (inhibiting the ATP-synthase), 30 U mL^{-1} superoxide dismutase (converting superoxide to hydrogen peroxide), 50 μM Amplex red and 6 U mL^{-1} horseradish peroxidase (catalyzing the oxidation of amplex red with hydrogen peroxide to generate the fluorescent dye resorufin). The fluorescence signals were detected with a microplate reader (Fluostar Optima, BMG Labtech GmbH, Germany), maintained at 34 °C equal to the mitochondrial respiration measurements. Excitation/emission wavelengths were chosen at 550 nm/585 nm. Succinate was added after 7 min and the forerun was used to subtract basal fluorescence from succinate dependent fluorescence. The signal was calibrated using H_2O_2 standards ranging from 0.0 to 0.8 nmol. In parallel, each sample was measured in the presence of rotenone (2 μM) to calculate different sites of superoxide production.

2.9. Statistics

All data are expressed as mean ± standard error of mean (SEM) of non-transformed data. In each experimental group data were examined for absence of normal distribution using the Kolmogorov–Smirnov test. In most cases the normal distribution assumption was not rejected ($p > 0.05$), and Student's *t*-test or one-way analysis of variance (ANOVA) followed by Holm–Sidak post-hoc procedure was used to reveal significant group differences between group means, as indicated. The respiratory control ratio of kidney mitochondria (Fig. 2B) and the data for hydrogen peroxide release in kidney, heart muscle and skeletal muscle mitochondria (Fig. 7A, B, C, D) were Box–Cox transformed to improve normality (Osborne, 2010) and re-analyzed using ANOVA (if the assumption of normal distribution was met). The data displayed in Fig. 7B failed to meet the assumption of normality and were analyzed for group differences using non-parametric Mann–Whitney *U*-test. Statistical analyses were performed using SigmaStat 3.5. or IBM SPSS Statistics (22.0). The overall level of significance was set to $p \leq 0.05$.

3. Results

3.1. Body mass of spiny mice

Prior to food restriction, spiny mice had an average body mass of 62.9 ± 0.9 g ($n = 24$). During food restriction, the loss in body mass varied between single animals resulting in a significantly higher body mass of torpid spiny mice in the warm acclimated group at the time point of sampling (Table 1). There was no body mass difference between the torpid and normothermic spiny mice in the 23 °C acclimated group. The average body mass of the *ad libitum* fed cohort ($n = 4$) was 90.0 ± 2.9 g and therefore suitable as a control for feeding and body mass effects.

3.2. Torpor in food restricted spiny mice

After establishing torpor by food restriction at 27 °C, the spiny mice continued torpor behavior when transferred to 32 °C or 23 °C ambient temperature (T_a). Body temperature and metabolic rate (measured as oxygen consumption, MR) of spiny mice were recorded for several days prior to tissue sampling. Generally, torpor bouts started in the dark phase, and MR decreased to the lowest plateau in the morning hours (Fig. 1). The minimal observed MR in deep torpor was 17.6 ± 0.8 mL O_2 h^{-1} at 32 °C T_a, i.e. it was reduced by 37% compared to basal metabolic rate (28.0 ± 1.6 mL O_2 h^{-1}). At 23 °C T_a normometabolic rate of the spiny mice was elevated compared to thermoneutrality (68.46 ± 3.3 mL O_2 h^{-1}). In torpor, MR decreased to minimal values of 13.64 ± 1.7 mL O_2 h^{-1}, i.e. a reduction of 80%. The individual timing of torpor behavior was rather constant at both ambient temperatures. This ensured tissue sampling during the plateau phase of the torpor bout when oxygen consumption reached minimal values. Mean MR of torpid spiny mice at sampling time was significantly different from normothermic animals at 32 °C as well as 23 °C (Table 1). Mean T_b of torpid animals at sampling time was significantly different from normothermic animals at 23 °C T_a but not at 32 °C (Table 1).

3.3. Mitochondrial respiration of normothermic vs. torpid spiny mice

The respiration of isolated mitochondria revealed no differences between mitochondria from normothermic and torpid spiny mice acclimated to 32 °C, neither in liver, nor in kidney, heart and skeletal muscle (Fig. 2). Furthermore we found no major differences in mitochondrial respiration between food restricted and *ad libitum* fed spiny mice,

Table 1
Metabolic rate, body temperature, body mass and organ wet weights of normometabolic and torpid Golden spiny mice at time point of sampling. Spiny mice were acclimated to 32 °C or 23 °C ambient temperature for 2 weeks and received 50% of their individual food intake for a period of 3 weeks. Torpid animals were sacrificed during the torpor plateau, when metabolic rates were about 30% below basal metabolic values and animals acclimated to 23 °C dropped body temperature additionally below 32 °C. Mean values of torpid versus normometabolic groups were compared using Student's *t*-test (*p*-values indicated).

	32 °C acclimated			23 °C acclimated		
	Normometabolic	Torpid	*p*	Normometabolic	Torpid	*p*
Metabolic rate (mL O_2 h^{-1})	57.9 ± 11.0	20.0 ± 1.8	0.007	130.4 ± 11.6	21.2 ± 5.3	<0.001
Body temperature (°C)	35.9 ± 0.5	34.7 ± 0.3	0.061	35.7 ± 0.3	26.8 ± 0.6	<0.001
Body mass (g)	52.2 ± 1.1	55.2 ± 0.8	0.046	51.8 ± 2.0	54.3 ± 1.1	0.289
Organ wet mass (g)						
Liver	1.26 ± 0.06	1.28 ± 0.04	0.761	1.37 ± 0.06	1.50 ± 0.16	0.478
Kidney	0.32 ± 0.01	0.28 ± 0.01	0.050	0.35 ± 0.01	0.35 ± 0.01	0.951
Heart	0.14 ± 0.01	0.12 ± 0.00	0.341	0.15 ± 0.01	0.14 ± 0.00	0.228
Skeletal muscle	1.40 ± 0.11	1.33 ± 0.10	0.617	1.43 ± 0.04	1.41 ± 0.04	0.677

indicating that food restriction per se did not alter the rate of mitochondrial respiratory properties. Small differences in state 2 respiration were detected in isolated kidney mitochondria of food restricted and *ad libitum* fed spiny mice, but these differences vanished when oligomycin was added (state 4). Respiratory control ratios were significantly lower in kidney mitochondria of *ad libitum* fed spiny mice. In response to 23 °C acclimation, body temperatures of the torpid animals were significantly lower as compared to normothermic animals. Here, we found no depression of mitochondrial respiration during torpor. As a matter of fact, state 3 respiration was higher in kidney mitochondria, while state 3 and state 4 respiration was significantly higher in skeletal muscle mitochondria of torpid animals (Fig. 3).

3.4. Relation of state 3 respiration to metabolic rate

To examine whether respiration of isolated mitochondria correlates with other physiological parameters we plotted state 3 and state 4 respiration against metabolic rate and against body temperature of all food restricted spiny mice (Fig. 4). Furthermore, we tested for an association of state 3 respiration vs. liver wet weight and body mass (Fig. 5). We found no correlation, of neither metabolic rate nor body temperature, organ or body weight with mitochondrial respiration.

3.5. Mitochondrial efficiency of ATP synthesis and basal proton conductance

The P/O ratio corresponds to the amount of ATP produced by oxidative phosphorylation when one atom of oxygen is consumed by complex IV. An altered P/O ratio would suggest a change in mitochondrial efficiency of ATP synthesis that may be either caused by differences in proton leak, electron slip or a modified efficiency of ATP synthase. We measured P/O ratios of liver and kidney mitochondria from normometabolic and torpid spiny mice to identify any changes in the efficiency of ADP/ATP turnover (Fig. 6). We found no differences between normometabolic and torpid groups, neither in 32 °C nor in 23 °C acclimated spiny mice. We also measured the proton leak kinetics of liver mitochondria from normometabolic, torpid and *ad libitum* fed mice kept at 32 °C T_a (Fig. 6). While the proton conductance of *ad libitum* fed animals was slightly increased, we observed no differences between normometabolic and torpid mice.

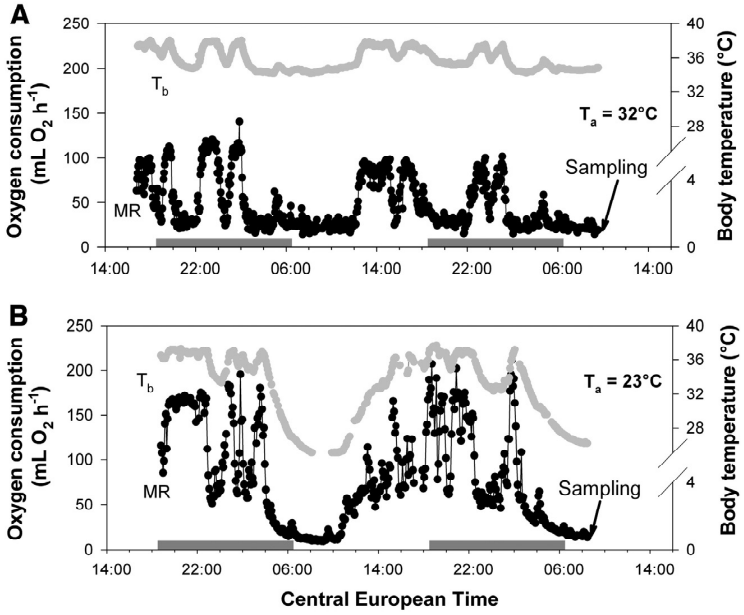

Fig. 1. Representative 48-hour registrations of oxygen consumption (MR) and body temperature (T_b) from Golden spiny mice. Spiny mice were kept at either 32 °C (A) or 23 °C (B) ambient temperature (T_a). The arrows indicate the time point of sacrifice in deep torpid state. Note that the animal kept at 23 °C displayed a lower body temperature during torpor as compared to the warm acclimated animal. The gray bars indicate the scotophase.

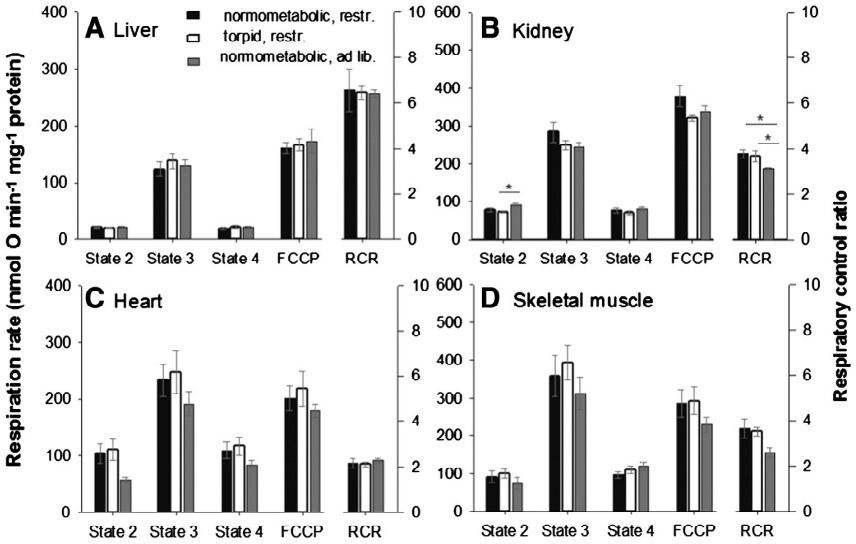

Fig. 2. Mitochondrial respiration of normometabolic and torpid spiny mice acclimated at 32 °C. Spiny mice were food restricted (restr.) or fed *ad libitum* (ad lib.). Mitochondria were isolated from liver (A), kidney (B), heart muscle (C) and skeletal muscle (D). All measurements were performed at 34 °C with succinate as substrate. The respiratory control ratio (RCR) was calculated as the quotient of state 3 and state 4 respiration. Bars indicate means ± SEM, food restricted groups with $n = 5$–6, *ad libitum* group with $n = 4$. Data for each measurement condition were analyzed using ANOVA, and asterisks (*) indicate $p \leq 0.05$ for significant post-hoc differences between animal groups.

3.6. Hydrogen peroxide release rates from energized mitochondria

Detection of hydrogen peroxide release is a semi-quantitative measure of superoxide production by the respiratory chain. By measuring the hydrogen peroxide release with and without rotenone we calculated superoxide production deriving from reverse electron transfer (RET), majorly mediated by the Q-site of complex I. The residual hydrogen peroxide in the presence of rotenone derives presumably from complex II and complex III. In skeletal muscle, heart, and kidney mitochondria energized with succinate, a great proportion of superoxide derived from RET (Fig. 7). After inhibiting complex I with rotenone, hydrogen peroxide release was reduced by about 70%. Between normothermic and torpid groups of both acclimation groups, there was no significant difference in hydrogen peroxide release rates. Superoxide derived

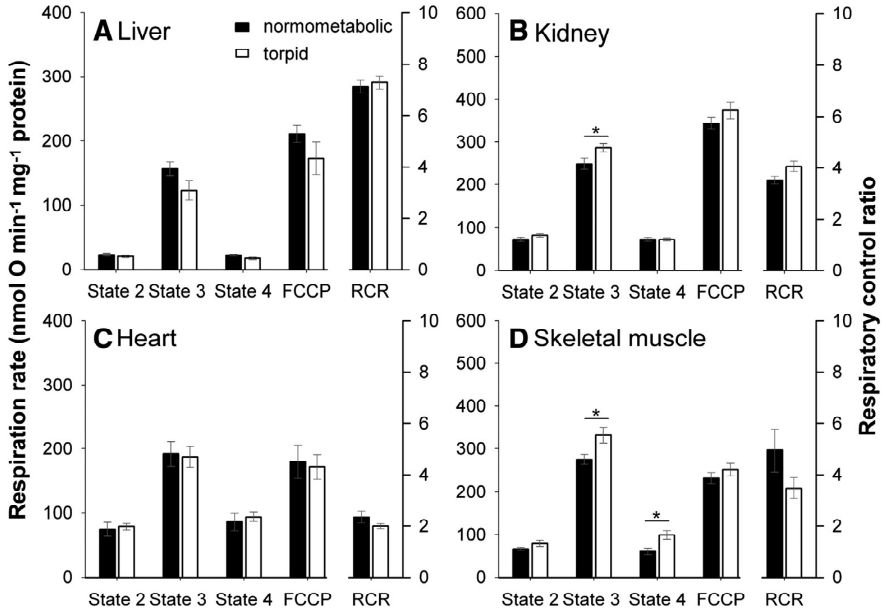

Fig. 3. Mitochondrial respiration of normothermic and torpid spiny mice acclimated at 23 °C. Mitochondria were isolated from liver (A), kidney (B), heart muscle (C) and skeletal muscle (D). The experimental procedure was performed identically to Fig. 2. The respiratory control ratio (RCR) was calculated as the quotient of state 3 and state 4 respiration. Values are means ± SEM, $n = 6$. For each respiratory condition normometabolic versus torpid group means were compared using Student's *t*-test. * indicates $p \leq 0.05$.

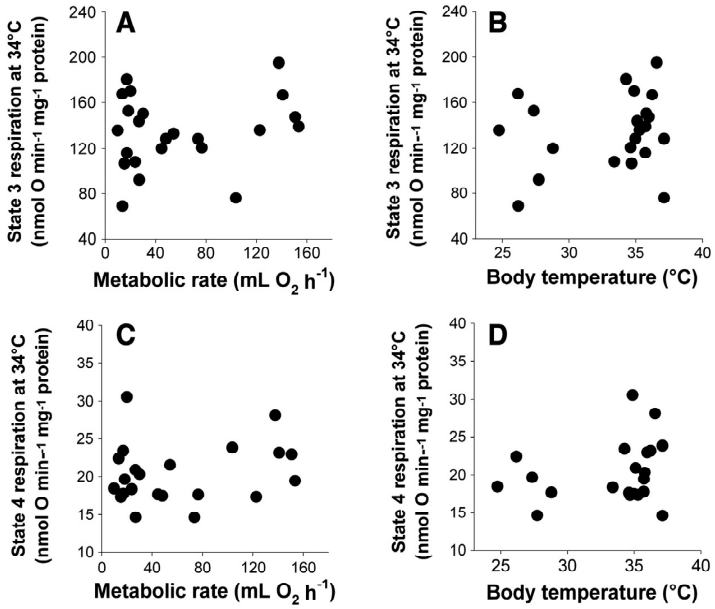

Fig. 4. Association between liver mitochondrial respiration and metabolic rate or body temperature from food restricted spiny mice. Animals of both acclimation temperatures (32 °C and 23 °C) were used for the graphs. There was no correlation between state 3 respiration (A) and state 4 (C) respiration with metabolic rate ($n = 23$). Metabolic rate was measured by indirect calorimetry and values of sampling time point were pooled in the graphs. There was also no correlation between state 3 respiration (B) and state 4 respiration (D) with body temperature at sampling point ($n = 22$). Symbols represent single animals.

from RET was slightly higher in skeletal muscle of 23 °C acclimated torpid as compared to normothermic animals, possibly resembling increased mitochondrial activity as found for respiration.

4. Discussion

Metabolic rate is actively decreased during the entry phase of daily torpor and subsequently maintained at a fraction of basal metabolic rate, before returning to normometabolic levels after arousal. While comparative physiologists agree that torpor entry must be initiated by the central nervous system, the peripheral molecular mechanisms underlying metabolic depression are unknown (reviewed by Drew et al., 2007). Conceptually, at the cellular level, metabolic rate may be decreased by substrate supply, energy production or energy consumption. Recently, data on isolated mitochondria demonstrated depression of mitochondrial respiration in liver of torpid mice and hamsters, suggesting that cellular energy production contributes to the reduction of metabolic rate during torpor (Brown et al., 2007; Brown and Staples, 2010; Kutschke et al., 2013). Notably, two studies showed a correlation between mitochondrial substrate oxidation and body temperature, the latter also implicating a correlation to metabolic rate (Brown and Staples, 2010; Kutschke et al., 2013).

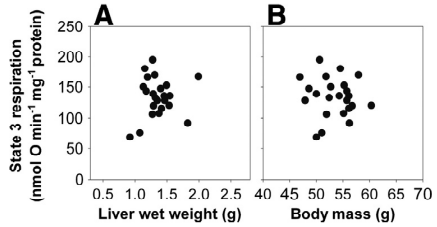

Fig. 5. Association between state 3 respiration of liver mitochondria and liver wet weight or body mass. Food restricted spiny mice ($n = 23$) were acclimated at 32 °C or 23 °C ambient temperature. There was no correlation between state 3 respiration and organ mass or body mass of spiny mice.

In this study, we studied the Golden spiny mouse intending to untangle the effects of temperature and metabolic rate reduction. We previously demonstrated that a hypometabolic torpor state in the spiny mouse is induced by food restriction, even at high ambient temperatures (32 °C) resulting in only minor reduction of body temperature (Grimpo et al., 2012). Despite significant reductions of basal metabolic rate during torpor, we found no evidence for mitochondrial depression in isolated liver mitochondria. Also, mitochondria from other metabolically active tissues such as skeletal muscle, kidneys and heart showed no reduction of mitochondrial substrate oxidation during torpor.

Reducing the ambient temperature to 23 °C resulted in significant decreases of body temperature in torpor, while the minimal metabolic rate was only slightly affected. Because spiny mice displayed higher normometabolic rates during cold exposure as compared to thermoneutrality, the amplitude between normometabolic and torpid metabolic rates was increased in spiny mice acclimated at 23 °C. However, none of the mitochondrial respiration states correlated with metabolic rate or body temperature. While constant exposure to 23 °C represents a marked cold stimulus (thermoneutral ambient temperature is about 32 °C) for Golden spiny mice which reached body temperatures as low as 25 °C during torpor, torpid hamsters of previous studies were exposed to 15 °C and experienced deeper torpor temperatures. From our observations, we speculate that liver mitochondria of the Djungarian hamster may require/exhibit special mitochondrial adjustments in response to deeper torpor temperatures.

The lack of mitochondrial depression in torpid spiny mice questions a general role for metabolic depression and hypometabolism in daily torpor. Additionally, we also found no mitochondrial effects of long-term food restriction, which highly increases disposition of torpor in the Golden spiny mouse.

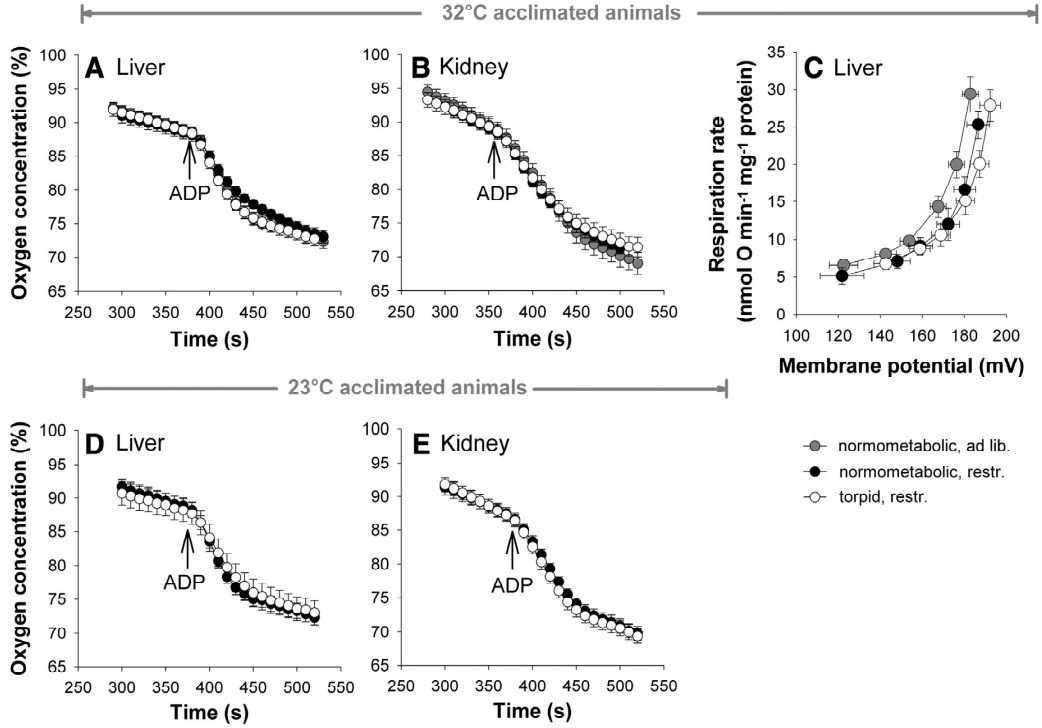

Fig. 6. Measurement of ATP/O ratios and proton leak kinetics of normometabolic and torpid spiny mice. Spiny mice were food restricted (restr.) or fed *ad libitum* (ad lib.). Acclimation temperature of spiny mice was 32 °C (A–C) or 23 °C (D–E). For ATP/O calculation (n = 5–6) mitochondria from liver (A, D) and kidney (B, E) were energized with 4 mM succinate at an assay temperature of 34 °C and mitochondrial respiration was measured. The arrows indicate addition of ADP to induce state 3 respiration. The amount of oxygen consumption to fully convert ADP into ATP gives the ATP/O ratio. The traces of normometabolic and torpid mitochondria overlap as they demonstrated identical ATP/O ratios. Proton leak kinetics of liver mitochondria from 32 °C acclimated spiny mice (C) (n = 4–5) were determined by simultaneous measurements of mitochondrial respiration rate and membrane potential using a clark type electrode and a TPMP sensitive electrode. Means ± SEM.

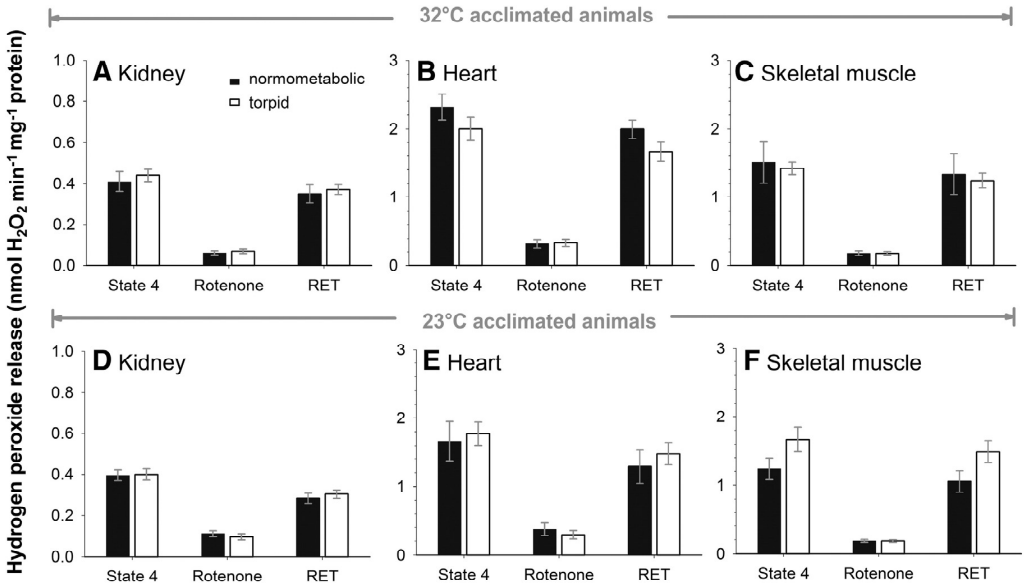

Fig. 7. Hydrogen peroxide release rate of isolated mitochondria from normothermic and torpid spiny mice acclimated to 32 °C (A–C) and 23 °C (D–F). Mitochondria were isolated from kidney (A, D), heart muscle (B, E) and skeletal muscle (C, F). Hydrogen peroxide production was measured in mitochondria respiring on succinate in state 4 (in the presence of oligomycin). Rotenone was added to inhibit complex I as it binds to the Q_I-site. The difference of values without and with rotenone served to estimate the hydrogen peroxide that derives from reverse electron transport (RET). The rotenone-insensitive proportion of hydrogen peroxide may be addressed to complex II and complex III sites. Values are means ± SEM. n = 4–6. Student's t-test and Mann-Whitney U-test (B) did not reveal significant differences in mean hydrogen peroxide release from mitochondria of the normometabolic versus the torpid group (all $p > 0.05$).

Since we found no difference in the capacity of mitochondrial substrate oxidation, we also analyzed spiny mouse mitochondria for differences in mitochondrial efficiency (Fig. 6), but found no differences in P/O ratios and proton leak kinetics.

Other studies reported an alteration in mitochondrial ROS (reactive oxygen species) production during daily torpor and hibernation (Okamoto et al., 2006; Brown and Staples, 2011; Brown et al., 2012). In this study, assessment of mitochondrial hydrogen peroxide release, using the Amplex red assay, revealed no differences between torpid and normometabolic Golden spiny mice. In our experiments, energization with succinate and administration of rotenone allowed us to distinguish hydrogen peroxide release rates of RET, which are primarily mediated by the Q site of complex I-ROS and residual ROS production, presumably generated at complex II and complex III (Orr et al., 2012; Quinlan et al., 2012a,b).

Taken together, depression of respiration in isolated mitochondria is not a general feature of daily torpor. Although we cannot exclude that some factors are lost during the mitochondrial isolation process, mitochondrial depression is maintained in mitochondria of the Djungarian hamster in our and other laboratories (Brown et al., 2007; Brown and Staples, 2010; Kutschke et al., 2013). Therefore, this mode of depression appears not to be required for hypometabolic states and torpor with shallow body temperature drops, but mitochondrial adjustments may be important in the liver at low body temperatures or in particular species. The processes that control reduced cellular energy production and consumption most likely have evolved on a higher systemic level controlling mitochondrial energy flux. It has to be considered that in torpid animals the respiration and blood flow are decreased, possibly affecting oxygen and substrate supply and that ATP consumption is reduced, also affected by cellular temperature.

For future directions, the exact molecular mechanisms of mitochondrial depression, as it is found in mice and hamsters, and factors controlling cellular energy flux, require further attention. As a mechanism of mitochondrial depression, a metabolite inhibition has been suggested, but this also does not fully account for intrinsic mitochondrial depression (Armstrong and Staples, 2010). Non-invasive sophisticated methods on whole animals appear promising, in particular applying novel magnetic resonance imaging (MRI) technology that allow measurements of mitochondrial energy transduction *in vivo* (Marcinek, 2004). However, we suggest that *A. russatus* is an excellent model organism to address molecular mechanisms of hypometabolism as temperature effects can be excluded by the experimental setup.

References

Armstrong, C., Staples, J.F., 2010. The role of succinate dehydrogenase and oxaloacetate in metabolic suppression during hibernation and arousal. J. Comp. Physiol. B. 180, 775–783.

Berriel Diaz, M., Lange, M., Heldmaier, G., Klingenspor, M., 2004. Depression of transcription and translation during daily torpor in the Djungarian hamster (*Phodopus sungorus*). J. Comp. Physiol. B. 174, 495–502.

Brand, M., 1995. Measurements of mitochondrial protonmotive force. In: Brown, G.C., Cooper, C.E. (Eds.), Bioenergetics: A Practical Approach. Oxford University Press, USA, pp. 39–62.

Braulke, L.J., Heldmaier, G., 2010. Torpor and ultradian rhythms require an intact signalling of the sympathetic nervous system. Cryobiology 60, 198–203.

Brown, J.C., Staples, J.F., 2010. Mitochondrial metabolism during fasting-induced daily torpor in mice. Biochim. Biophys. Acta 1797, 476–486.

Brown, J.C., Staples, J.F., 2011. Mitochondrial metabolic suppression in fasting and daily torpor: consequences for reactive oxygen species production. Physiol. Biochem. Zool. 84, 467–480.

Brown, J.C., Gerson, A.R., Staples, J.F., 2007. Mitochondrial metabolism during daily torpor in the dwarf Siberian hamster: role of active regulated changes and passive thermal effects. Am. J. Physiol. Regul. Integr. Comp. Physiol. 293, 1833–1845.

Brown, J.C., Chung, D.J., Belgrave, K.R., Staples, J.F., 2012. Mitochondrial metabolic suppression and reactive oxygen species production in liver and skeletal muscle of hibernating thirteen-lined ground squirrels. Am. J. Physiol. Regul. Integr. Comp. Physiol. 302, 15–28.

Buck, C.L., Barnes, B.M., 2000. Effects of ambient temperature on metabolic rate, respiratory quotient, and torpor in an arctic hibernator. Am. J. Physiol. Regul. Integr. Comp. Physiol. 279, 255–262.

Drew, K.L., Buck, C.L., Barnes, B.M., Christian, S.L., Rasley, B.T., Harris, M.B., 2007. Central nervous system regulation of mammalian hibernation: implications for metabolic suppression and ischemia tolerance. J. Neurochem. 102, 1713–1726.

Ehrhardt, N., Heldmaier, G., Exner, C., 2005. Adaptive mechanisms during food restriction in *Acomys russatus*: the use of torpor for desert survival. J. Comp. Physiol. B. 175, 193–200.

Geiser, F., 1998. Evolution of daily torpor and hibernation in birds and mammals: importance of body size. Clin. Exp. Pharmacol. Physiol. 25, 736–739.

Gnaiger, E., Mendez, G., Hand, S.C., 2000. High phosphorylation efficiency and depression of uncoupled respiration in mitochondria under hypoxia. Proc. Natl. Acad. Sci. U. S. A. 97, 11080–11085.

Gornall, A.G., Bardawill, C.J., David, M.M., 1949. Determination of serum proteins by means of the biuret reaction. J. Biol. Chem. 177, 751–766.

Grimpo, K., Legler, K., Heldmaier, G., Exner, C., 2012. That's hot: golden spiny mice display torpor even at high ambient temperatures. J. Comp. Physiol. B. 183, 567–581.

Gutman, R., Choshniak, I., Kronfeld-Schor, N., 2006. Defending body mass during food restriction in *Acomys russatus*: a desert rodent that does not store food. Am. J. Physiol. Regul. Integr. Comp. Physiol. 290, 881–891.

Heldmaier, G., Ruf, T., 1992. Body temperature and metabolic rate during natural hypothermia in endotherms. J. Comp. Physiol. B. 162, 696–706.

Heldmaier, G., Ortmann, S., Elvert, R., 2004. Natural hypometabolism during hibernation and daily torpor in mammals. Respir. Physiol. Neurobiol. 141, 317–329.

Iliff, B.W., Swoap, S.J., 2012. Central adenosine receptor signaling is necessary for daily torpor in mice. Am. J. Physiol. Regul. Integr. Comp. Physiol. 303, 477–484.

Jastroch, M., 2012. Adjustments of mitochondrial energy transduction in response to physiological and environmental challenge. In: Ruf, T., Bieber, C., Arnold, W., Millesi, E. (Eds.), Living in a Seasonal World: Thermoregulatory and Metabolic Adaptations. Springer, Berlin Heidelberg, pp. 387–398.

Jastroch, M., Divakaruni, A.S., Mookerjee, S., Treberg, J.R., Brand, M.D., 2010. Mitochondrial proton and electron leaks. Essays Biochem. 47, 53–67.

Jinka, T.R., Toien, O., Drew, K.L., 2011. Season primes the brain in an arctic hibernator to facilitate entrance into torpor mediated by adenosine A(1) receptors. J. Neurosci. 31, 10752–10758.

Kutschke, M., Grimpo, K., Kastl, A., Schneider, S., Heldmaier, G., Exner, C., Jastroch, M., 2013. Depression of mitochondrial respiration during daily torpor of the Djungarian hamster, *Phodopus sungorus*, is specific for liver and correlates with body temperature. Comp. Biochem. Physiol. A Mol. Integr. Physiol. 164, 584–589.

Lambert, A.J., Buckingham, J.A., Boysen, H.M., Brand, M.D., 2008. Diphenyleneiodonium acutely inhibits reactive oxygen species production by mitochondrial complex I during reverse, but not forward electron transport. Biochim. Biophys. Acta 1777, 397–403.

Levy, O., Dayan, T., Kronfeld-Schor, N., 2011. Adaptive thermoregulation in golden spiny mice: the influence of season and food availability on body temperature. Physiol. Biochem. Zool. 84, 175–184.

Lyman, C.P., Chatfield, P.O., 1955. Physiology of hibernation in mammals. Physiol. Rev. 35, 403–425.

Marcinek, D.J., 2004. Mitochondrial dysfunction measured in vivo. Acta Physiol. Scand. 182, 343–352.

Melvin, R.G., Andrews, M.T., 2009. Torpor induction in mammals: recent discoveries fueling new ideas. Trends Endocrinol. Metab. 20, 490–498.

Okamoto, I., Kayano, T., Hanaya, T., Arai, S., Ikeda, M., Kurimoto, M., 2006. Up-regulation of an extracellular superoxide dismutase-like activity in hibernating hamsters subjected to oxidative stress in mid- to late arousal from torpor. Comp. Biochem. Physiol. C Toxicol. Pharmacol. 144, 47–56.

Orr, A.L., Quinlan, C.L., Perevoshchikova, I.V., Brand, M.D., 2012. A refined analysis of superoxide production by mitochondrial sn-glycerol 3-phosphate dehydrogenase. J. Biol. Chem. 287, 42921–42935.

Osborne, J.W., 2010. Improving your data transformations: applying the Box–Cox transformation. Practical Assessment, Research & Evaluation. 15 1–9.

Quinlan, C.L., Orr, A.L., Perevoshchikova, I.V., Treberg, J.R., Ackrell, B.A., Brand, M.D., 2012a. Mitochondrial complex II can generate reactive oxygen species at high rates in both the forward and reverse reactions. J. Biol. Chem. 287, 27255–27264.

Quinlan, C.L., Treberg, J.R., Perevoshchikova, I.V., Orr, A.L., Brand, M.D., 2012b. Native rates of superoxide production from multiple sites in isolated mitochondria measured using endogenous reporters. Free Radic. Biol. Med. 53, 1807–1817.

Reynafarje, B., Costa, L.E., Lehninger, A.L., 1985. O_2 solubility in aqueous media determined by a kinetic method. Anal. Biochem. 145, 406–418.

Ruf, T., Heldmaier, G., 1987. Computerized body temperature telemetry in small animals: use of simple equipment and advanced noise suppression. Comput. Biol. Med. 17, 331–340.

St-Pierre, J., Brand, M.D., Boutilier, R.G., 2000. The effect of metabolic depression on proton leak rate in mitochondria from hibernating frogs. J. Exp. Biol. 203, 1469–1476.

Swoap, S.J., Gutilla, M.J., 2009. Cardiovascular changes during daily torpor in the laboratory mouse. Am. J. Physiol. Regul. Integr. Comp. Physiol. 297, 769–774.

Trzcionka, M., Withers, K.W., Klingenspor, M., Jastroch, M., 2008. The effects of fasting and cold exposure on metabolic rate and mitochondrial proton leak in liver and skeletal muscle of an amphibian, the cane toad *Bufo marinus*. J. Exp. Biol. 211, 1911–1918.

6.4 Kutschke and Grimpo et al. 2013

Depression of mitochondrial respiration during daily torpor of the Djungarian hamster, *Phodopus sungorus*, is specific for liver and correlates with body temperature

Comparative Biochemistry and Physiology, Part A 164 (2013) 584–589

Contents lists available at SciVerse ScienceDirect

Comparative Biochemistry and Physiology, Part A

journal homepage: www.elsevier.com/locate/cbpa

Depression of mitochondrial respiration during daily torpor of the Djungarian hamster, *Phodopus sungorus*, is specific for liver and correlates with body temperature

Maria Kutschke [a,1], Kirsten Grimpo [b,1], Anja Kastl [b], Sandra Schneider [c], Gerhard Heldmaier [b], Cornelia Exner [b], Martin Jastroch [a,*]

[a] Institute for Diabetes and Obesity, Helmholtz Centre Munich, Ingolstädter Landstr. 1, 85764 Neuherberg, Germany
[b] Philipps-Universität Marburg, Faculty of Biology, Department of Animal Physiology, Karl-von-Frisch-Strasse 8, 35043 Marburg, Germany
[c] Department of Genetics, University of Cambridge, Downing Street, Cambridge, Cambs CB2 3EH, United Kingdom

ARTICLE INFO

Article history:
Received 7 December 2012
Received in revised form 17 January 2013
Accepted 18 January 2013
Available online 1 February 2013

Keywords:
Mitochondrial respiration
Daily torpor
Hypothermia
Hypometabolism
Phodopus sungorus

ABSTRACT

Small mammals actively decrease metabolism during daily torpor and hibernation to save energy. Increasing evidence suggests depression of mitochondrial respiration during daily torpor of the Djungarian hamster but tissue-specificity and relation to torpor depth is unknown. We first confirmed a previous study by Brown and colleagues reporting on the depressed substrate oxidation in isolated liver mitochondria of the Djungarian hamster (*Phodopus sungorus*) during daily torpor. Next, we show that mitochondrial respiration is not depressed in kidneys, skeletal muscle and heart. In liver mitochondria, we found that state 3 and state 4 respirations correlate with body temperature, suggesting inhibition related to torpor depth and to metabolic rate. We conclude that molecular events leading to depression of mitochondrial respiration during daily torpor are specific to liver and linked to a decrease in body temperature. Different tissue-specificity of mitochondrial depression may assist to compare and identify the molecular nature of mitochondrial alterations during torpor.

1. Introduction

Small mammals enter hibernation or daily torpor to cope with prolonged periods of energy shortage. Although this physiological phenomenon occurs in diverse members of the majority of mammalian orders (Geiser, 1998; Heldmaier et al., 2004; Melvin and Andrews, 2009) and is studied extensively, the molecular mechanisms are still unclear.

Daily torpor is defined as a decrease in metabolic rate, usually measured indirectly as oxygen consumption, below normometabolic resting values followed by a reduction in body temperature for less than 24 h. It occurs spontaneously or can be induced by cold exposure and caloric restriction (Heldmaier and Ruf, 1992; Ehrhardt et al., 2005; Swoap et al., 2006; Oelkrug et al., 2011). A torpor bout can be separated into three stages; entrance, deep steady-state and arousal from torpor. During deep torpor, metabolic rate is decreased to a fraction of the basal metabolic rate, i.e. a reduction by about 30–60%.

Torpor entrance and maintenance are triggered by active downregulation of metabolism (Lyman and Chatfield, 1955; Heldmaier and Ruf, 1992; Buck and Barnes, 2000), but there is some controversy on the significance of passive thermic Q10-effects (Geiser, 1988; Guppy and Withers, 1999). Supporting evidence for an active downregulation is given by the inhibition of energetically expensive gene transcription and protein synthesis contributing to metabolic depression in hibernators and in daily heterotherms (Frerichs et al., 1998; van Breukelen and Martin, 2002; Berriel Diaz et al., 2004). Most crucial during the reduction of cellular processes is the coordinated maintenance of cellular homeostasis, which requires cellular energy. Mitochondria are central to the conversion of nutrient energy into cellular energy by oxidative phosphorylation, which consumes over 90% of the oxygen in normothermic mammals (Rolfe and Brown, 1997). Mitochondrial substrates are oxidized and their electrons are transported along the respiratory complexes before reducing oxygen to water. The potential energy of the electrons is used to pump protons out of the matrix, generating a proton motive force. This proton motive force drives the ATP-synthase that converts ADP into ATP. ATP synthesis is, however, not fully efficient, and proton motive force is also consumed by the proton leak and potentially by electron slip reactions in the respiratory complexes (Jastroch et al., 2010). The energy budgets of an animal can be adjusted by alterations in mitochondrial efficiency, as shown for many ectotherms, either by a decrease of substrate oxidation or by proton permeability (Gnaiger et al., 2000; St-Pierre et al., 2000; Trzcionka et al., 2008).

Whether active downregulation of mammalian metabolism is promoted by mitochondrial adjustments has been investigated in

Abbreviations: ADP, adenosine-diphosphate; ATP, adenosine-triphosphate; T_b, body temperature; FCCP, carbonyl cyanide-p-trifluoromethoxyphenylhydrazone; MR, metabolic rate; RCR, respiratory control ratio; TPMP+, Triphenylmethylphosphonium.

* Corresponding author. Tel.: +49 8931872105; fax: +49 89 3187 3799.
E-mail address: martin.jastroch@helmholtz-muenchen.de (M. Jastroch).

[1] Contributed equally to this study.

1095-6433/$ – see front matter © 2013 Elsevier Inc. All rights reserved.
http://dx.doi.org/10.1016/j.cbpa.2013.01.008

hibernating and daily torpid animals. A decrease in phosphorylating (state 3) respiration of liver mitochondria was observed in hibernating ground squirrels (Martin et al., 1999; Barger et al., 2003; Muleme et al., 2006). Arctic ground squirrels' liver, but not skeletal muscle mitochondria tended to a lower mitochondrial proton leak, and the depression of respiration was controlled by a downregulation of substrate oxidation (Barger et al., 2003). Various other studies report on similar and controversial observations depending on species and tissue, mitochondrial substrate and assay temperature (reviewed in Staples and Brown, 2008).

In liver mitochondria of the Djungarian hamster, which displays daily torpor spontaneously, state 3 respiration was reduced by about 30% in torpid individuals when compared to normothermic ones at 37 °C assay temperature (Brown et al., 2007). The authors concluded that active depression of mitochondrial respiration plays an important role during torpor entrance, because the difference to normothermic animals vanished at an assay temperature of 15 °C.

In this study, we first confirmed the findings of Brown and colleagues in isolated liver mitochondria of the Djungarian hamster and explored the adjustments of mitochondrial bioenergetics in other tissues. To exclude the effects of nutritional deprivation during torpor that may affect mitochondrial respiration, we also measured isolated mitochondria of liver and kidney from 18-h fasted hamsters.

2. Materials and methods

2.1. Animals

Thirty Djungarian hamsters (*Phodopus sungorus*) of an in-house breeding colony were kept under short day conditions of 8:16 h light: dark cycle as short day acclimated hamsters undergo torpor spontaneously. During the experiment, hamsters were housed individually in type II makrolon-cages (16 cm×21 cm×13 cm) with wood shavings and free access to water and food (ssniff V2144) at an ambient temperature of 15±1 °C. Twenty hamsters were kept for effects of torpor, while 10 hamsters were kept for 18 h fasting/ad libitum experiments investigating the effect of nutritional status.

2.2. Measurement of body temperature (T_b) in Djungarian hamsters

Core body temperatures of hamsters were measured with temperature sensitive transmitters intraperitoneally (Mini-Mitter, Model X, Sunriver, OR, USA, accuracy ±0.1 °C). Mini-Mitter signals were detected by a radio receiver and processed by a microcomputer system as reported previously (Ruf and Heldmaier, 1987). T_b of hamsters was obtained every 6 min. The body temperature of non-transplanted fasted hamsters was controlled by rectal probing upon sacrifice.

2.3. Definition of torpor and tissue dissection

Hamsters that were capable to enter torpor were body mass-matched, and body temperature was continuously monitored with the implanted temperature transmitters. All hamsters were sacrificed by decapitation. Torpid hamsters were decapitated after body temperature dropped below 32 °C for 1.5 to 3 h, similar to Brown et al. (2007) (Fig. 1). The body temperature was recorded, together with the body mass and organ masses (Table 1).

2.4. Mitochondrial isolation

The tissues of a torpid and a normothermic hamster were sampled pairwise to control for day-to-day variations of the mitochondrial isolation process. Mitochondria were isolated from tissue homogenates by differential centrifugation. Heart, liver, kidney and skeletal muscle were immediately dissected, weighed and transferred to ice-cold isolation buffer. All steps of mitochondrial isolation were performed on ice, ice-cold buffer or at 4 °C in the centrifuge to minimize proteolytic activity.

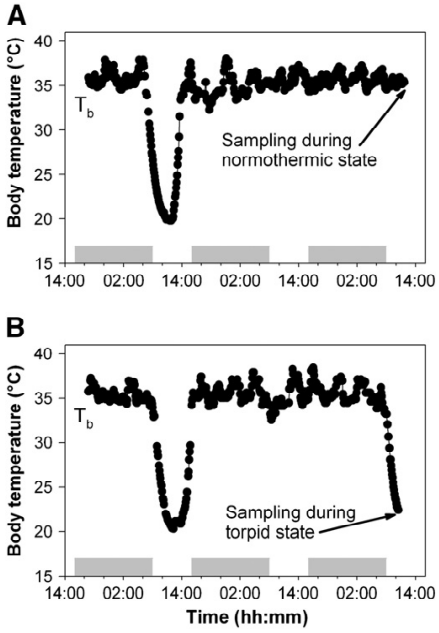

Fig. 1. Representative multiday measurements of body temperature (T_b) from Djungarian hamsters. The hamsters were kept at 15 °C ambient temperature and frequently entered torpor before sampling. The arrows indicate the time point of sacrifice during (A) normothermic state and (B) during entrance into torpid state. The gray bars indicate the scotophase.

The heart muscle, liver and kidney were cut with scissors in STE buffer (250 mM sucrose, 5 mM Tris, 2 mM EGTA, pH 7.4 at 4 °C) and rinsed with buffer several times, to wash out blood.

By using a Dounce homogenizer, liver tissue was homogenized by 10 passes with a loose glass pestle and kidney tissue by 15 passes with a tight pestle. Differential centrifugation of liver and kidney was performed as described previously (Trzcionka et al., 2008).

The heart muscle was incubated in 5 mL STE buffer containing 14.8 units mL^{-1} protease (Subtilisin A, Type III, Sigma-Aldrich GmbH, Germany) for 2 min. Volume was filled up to 20 mL with STE buffer and the tissue was minced with a polytron (PT 3100; Kinematica AG, Swiss), giving a 5 s burst at 1800 rpm. The heart muscle homogenate was centrifuged for 10 min at 8000 *g*. The pellet was resuspended in STE buffer and then centrifuged at 500 *g* for 10 min. The supernatant was centrifuged at 9000 *g* for 10 min and the centrifugation was

Table 1
Body temperature, body mass and organ masses of normothermic and torpid *Phodopus sungorus*.

Metabolic state	Normothermic (n=8)	Torpid (n=8)	Significance (p)
Body temperature (°C)	35.3±0.4	23.2±0.6	<0.001
Body mass (g)	28.2±1.4	25.8±1.0	n.s
Organ wet mass (mg)			
Liver	1.17±0.07	1.09±0.07	n.s
Kidney	0.37±0.04	0.37±0.07	n.s
Heart	0.21±0.01	0.19±0.01	n.s
Skeletal muscle	0.41±0.04	0.40±0.03	n.s

Hamsters were kept at 15 °C ambient temperature, acclimated to short photoperiod and fed *ad libitum*. Torpid hamsters were sacrificed 2 h after body temperature dropped below 32 °C. The normothermic hamsters were sacrificed 1 h later. Means±SEM.

repeated with the resuspended pellet. The final pellet was carefully aspirated and the mitochondria were resuspended in a minimal volume of isolation buffer.

Hindlimb and pectoralis muscles of the hamsters were removed and placed together in CP1 buffer (100 mM KCl, 50 mM Tris–HCl, 2 mM EGTA, pH 7.4 at 4 °C). The skeletal muscle was cut in small pieces and cleared of blood. The tissue was transferred to 25 mL CP1 buffer containing 1 mM ATP, 5 mM MgCl, 0.5% (w/v) defatted BSA and 1.45 units mL^{-1} protease (Subtilisin A, Type III, Sigma-Aldrich) and incubated for 2.5 min. Then tissue was homogenized at 1800 rpm for 5 s (Polytron, PT 3100). Suspension was incubated for 3 min and afterwards centrifuged at 500 *g* for 10 min in centrifuge tubes. The supernatant was filtered through two layers of cheesecloth and centrifuged at 9000 *g* for 10 min. The pellet was resuspended in 30 mL CP1 buffer and the high spin cycle was repeated. The suspension of the resulting pellet was centrifuged at 6000 *g* for 10 min. Then mitochondria were resuspended in a minimal volume of CP1 buffer.

Content of mitochondrial protein was determined by colorimetric analysis with a biuret assay (Gornall et al., 1949) by using fatty acid-free bovine serum albumin as a standard.

2.5. Measurement of mitochondrial respiration

Oxygen consumption of mitochondria was measured by using a Clark-type oxygen electrode (Rank Brothers Ltd., United Kingdom) maintained at 37 °C and calibrated with air-saturated KHE buffer (120 mM KCl, 5 mM KH_2PO_4, 3 mM HEPES, 1 mM EGTA, 0.3% (w/v) BSA, pH 7.2 at room temperature), which was assumed to contain 406 nmol O mL^{-1} (Reynafarje et al., 1985).

Mitochondria were diluted to 0.5 mg mitochondrial protein mL^{-1} in 2.5 mL (liver and kidney) and to 0.2 mg mitochondrial protein mL^{-1} in 0.5 mL (heart and skeletal muscle). Rotenone (4.8 μM) was added to inhibit complex I of the respiratory chain and mitochondrial respiration was started by adding 4 mM succinate (state 2). ADP (600 μM) was added to induce state 3 respiration. Then, 1 μg mL^{-1} oligomycin (blocking the ATP-synthase) was used to establish leak respiration (state 4). Oligomycin was added, when steady state 3 respiration occurred. Finally, FCCP (carbonyl cyanide-p-trifluoromethoxyphenylhydrazone) was added to induce maximum substrate oxidation.

The respiratory control ratio (RCR) was calculated as the quotient of state 3 and state 4 respirations to ascertain the integrity of isolated mitochondria. All mitochondrial experiments were performed in duplicate.

To determine proton leak kinetics mitochondrial respiration rate and mitochondrial membrane potential were measured simultaneously by using a Clark-type electrode and a TPMP+ sensitive electrode (Brand, 1995).

2.6. Statistics

All data are expressed as mean ± standard error of mean (SEM). For comparison between two groups Student's *t*-test for unpaired samples was used. When normal distribution of data could not be assumed the groups were compared with a Mann Whitney *U*-test. All calculations were performed by using SigmaStat 3.5. The overall level of significance was set to $p<0.05$.

3. Results

3.1. Physiological data of hamsters

All hamsters in this study exhibited torpor. The normothermic hamsters were sacrificed during normothermic periods (Fig. 1). Torpid hamsters were sacrificed 1.5–3 h after body temperature dropped below 32 °C. On average, the body temperature of torpid animals was about 12 °C lower than the normothermic body temperature (Table 1). Neither body mass nor organ masses of the normothermic and torpid hamsters differed significantly.

3.2. Mitochondrial respiration of normothermic vs. torpid hamsters

In liver mitochondria of torpid hamsters, we found significantly lower state 2 respiration, where succinate was added as a substrate for respiration (Fig. 2). State 3 respiration, induced by the addition of ADP allowing for the synthesis of ATP, and state 4 respiration, induced by the addition of oligomycin inhibiting ATP synthase, were also lower in the mitochondria of torpid animals. The FCCP respiration of the mitochondria was not different but showed a trend towards lower values ($p=0.111$; Fig. 2). In kidney, heart and skeletal muscle, the mitochondrial respiration was not different between the normothermic and torpid hamsters.

Then, we studied whether nutritional status has an effect on mitochondrial respiration, in particular in the liver. We show that an 18-h fasting period did not affect mitochondrial respiration in isolated liver and kidney mitochondria (Fig. 3).

In calculating the RCR (respiratory control ratio), it elucidated neither differences between the normothermic and torpid state in all tissues (Fig. 2) nor it appeared different in liver and kidney mitochondria of fasted hamsters (Fig. 3). RCR may be used as a rough estimate of mitochondrial efficiency (Jastroch, 2012). Relatively high and consistent values (>3 in soft tissues such as liver and kidneys; >2 in fibrous tissues such as heart and skeletal muscle) demonstrated the integrity of mitochondrial membranes during the isolation process.

3.3. Mitochondrial proton leak of normothermic vs. torpid hamsters

In measuring proton leak kinetics at 37 °C, we found no differences between liver mitochondria of the normothermic and torpid hamsters (Fig. 4A). To control for nutritional status, we also measured the mitochondria from 18-h fasted, normothermic hamsters but found no effects on the respiration states and proton leak kinetics (Fig. 4B).

3.4. Correlation of mitochondrial respiration with body temperature

Next, we correlated the mitochondrial data of individual hamsters with physiological parameters. We found that state 3 and state 4 respirations of liver mitochondria strongly correlated with T_b of the hamsters prior to tissue sampling (state 3 $p=0.0008$, state 4 = 0.0042, Fig. 5), but not with the organ mass or the body mass (Fig. 5).

4. Discussion

While daily torpor is a fascinating physiological trait of small mammals that underlines their extreme metabolic plasticity and scope, its molecular mechanisms are not understood. The understanding of these mechanisms is not only of academic interest, but would also be valuable for translational sciences, e.g., to avoid tissue damage in hypothermic surgery and organ preservation. The physiology of the torpid animals has evolved to cope with dramatic decreases in T_b, which would cause thermal stress and imbalance in energy homeostasis by a decrease of the metabolic rate (MR). In recent years, it has been established that the entry into daily torpor is an actively regulated rather than a passively regulated cooling process of the animal. Therefore, one would expect actively regulated cellular processes that are coordinated during the entry and maintenance of hypothermia and hypometabolism. The decrease in MR, usually measured as oxygen consumption by indirect calorimetry, also suggests that the terminal consumer of oxygen in the cell, the mitochondrion, is altered in the hypothermic/hypometabolic state. Some data on the regulation of respiration in hibernation and torpor have been controversially discussed in the past (reviewed in Staples and Brown, 2008).

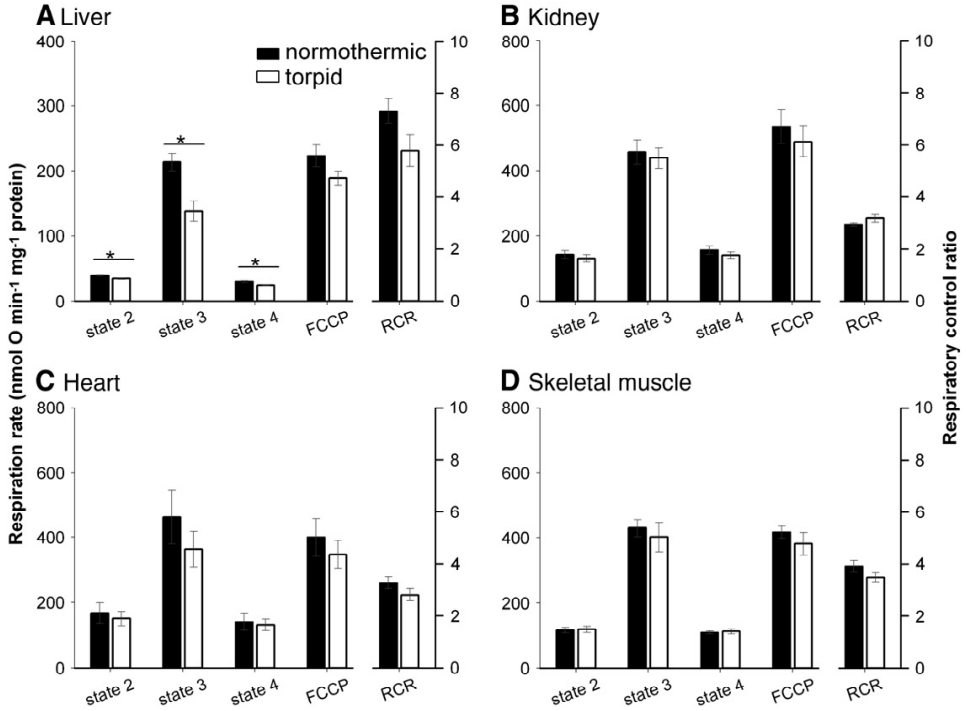

Fig. 2. Mitochondrial respiration of normothermic and torpid hamsters acclimated to 15 °C. Respiration of mitochondria from liver, kidney, heart muscle, and skeletal muscle was measured at 37 °C by using succinate as substrate (state 2). The addition of ADP shifted the mitochondria to state 3 respiration; the addition of oligomycin inhibited the ATP synthase; and the residual respiration represents consumption of proton motive force by the proton leak. The maximal substrate oxidation was measured by adding the uncoupler FCCP. The respiratory control ratio (RCR) was calculated as the quotient of state 3 and state 4 respirations. Means ± SEM, n = 8 except for heart mitochondria with n = 7.

Here we first confirmed the findings of a recent study by Brown and colleagues, who showed a reduction of the mitochondrial respiration in isolated liver mitochondria of torpid Djungarian hamsters (Fig. 2), supporting the active regulation of metabolism and mitochondrial adjustments during daily torpor (Brown et al., 2007). The authors suggested that mitochondrial depression is important during torpor entrance. The depression of the substrate oxidation was concluded from the results of the substrate oxidation kinetics, while in our study, we confirmed this by observing a significant reduction of all respiratory states and a trend towards lower maximal substrate oxidation. We emphasize, however, that the collection of our data further corroborates the findings by Brown and colleagues, as we also controlled all hamsters for the ability to perform torpor (Fig. 1) and excluded non-responders from the study. Furthermore, we weight-matched the normothermic and torpid hamsters (Table 1) to exclude body mass effects that may impact mitochondrial respiration in the liver (Polymeropoulos et al., 2012). To exclude the effects of nutritional deprivation that possibly affect mitochondria, we also measured the mitochondrial respiration of

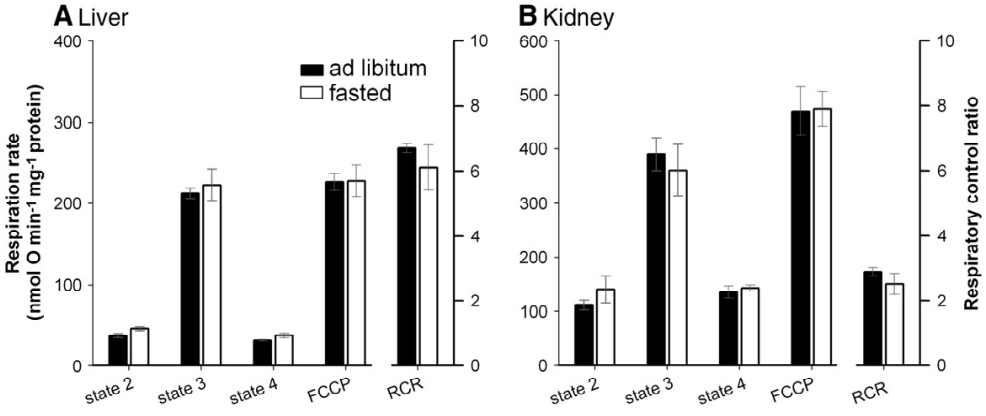

Fig. 3. Mitochondrial respiration of *ad libitum* fed and 18-h fasted hamsters acclimated at 15 °C. Mitochondria were isolated from liver and kidney. Mitochondrial respiration was measured at 37 °C with identical sequential additions as in Fig. 2. Body mass of hamsters from the *ad libitum* fed group (25.6 ± 1.6 g) did not differ significantly from fasted hamsters (24.0 ± 1.3 g). Means ± SEM, n = 5.

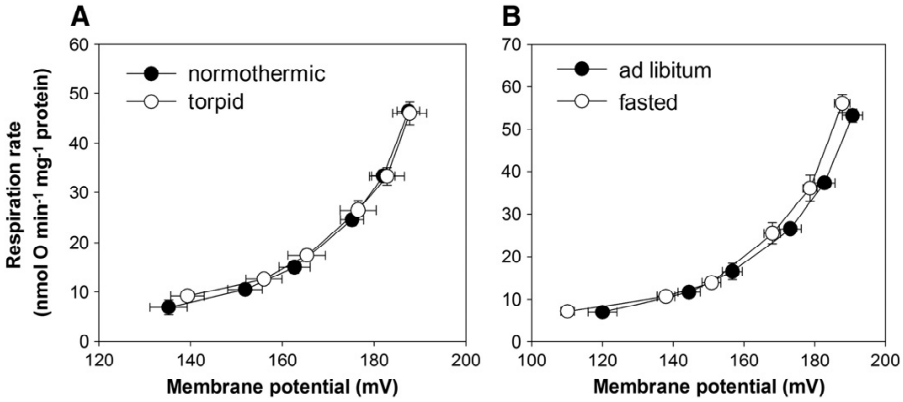

Fig. 4. Proton leak kinetics of normothermic vs torpid (A) and ad libitum vs fasted (B) hamsters acclimated at 15 °C. To determine proton leak kinetics, mitochondrial respiration rate and mitochondrial membrane potential were measured simultaneously by using a Clark type electrode and a TPMP+ sensitive electrode at an assay temperature of 37 °C. State 4 respiration and potential were step-wise inhibited by increasing the concentration of the competitive complex II inhibitor malonate. Means ± SEM, n = 5.

liver and kidney from 18-h fasted hamsters. Taken together the data of Brown and colleagues and our data, the depression of substrate oxidation in liver mitochondria during torpor of the Djungarian hamster appears to be a robust, reproducible phenomenon that is independent of nutritional status and may be related to either a decrease in metabolic rate or body temperature.

While it was concluded that the active mitochondrial depression in the liver could contribute significantly to the decrease of metabolism, we were curious to study the mitochondria in other metabolically active organs. We found that the respiration of isolated mitochondria from other metabolically active organs such as kidneys, heart or skeletal muscle was not reduced. The unique depression of the respiration in isolated liver mitochondria questions whether the reduction of substrate oxidation in one organ contributes significantly to the whole animal reduction of the metabolic rate. It rather appears that liver mitochondria possess a special physiological role during daily torpor that requires additional intrinsic regulation. This intrinsic depression, however, is sustained during the experimental isolation of liver mitochondria. We cannot exclude that other factors of regulation are lost during the isolation process. Further explanation for the reduced substrate oxidation in torpor may

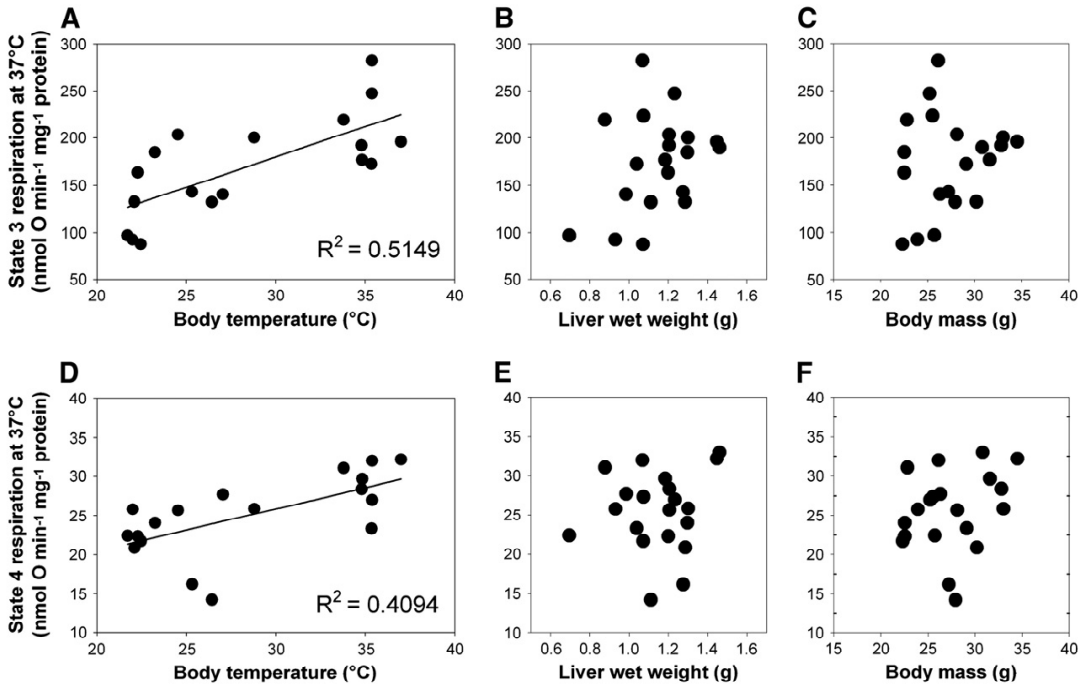

Fig. 5. Association of liver mitochondrial respiration and body temperature, liver wet mass and body mass of 15 °C-acclimated hamsters. There was a significant correlation between (A) state 3 respiration ($p<0.001$) and (D) state 4 respiration ($p<0.01$), measured at an assay temperature of 37 °C, with body temperature at timepoint of sampling. The regression line illustrates the estimated linear relationship between mitochondrial respiration and body temperature. No correlation was found between state 3 respiration with liver wet mass (B) or with body mass (C), and no correlation between state 4 respiration with liver wet mass (E) or with body mass (F). Symbols represent single animals (n = 18 for body temperature, n = 20 for liver mass and body mass).

be the mitochondrial damage during the entrance phase impacting substrate oxidation. This could be specific for the liver as the RCR data suggest that the highest proton motive force in liver mitochondria as compared to the other tissues. Damaging parameters, such as mitochondrial ROS production, increase with a higher proton motive force and may contribute to mitochondrial damage.

We demonstrate that both state 3 (ATP generating) and state 4 (proton leak) respirations correlate with T_b. Mitochondrial adjustments may be important for the liver at low body temperatures. Although we did not measure MR in the hamsters, the relation between MR and body temperature in daily torpor of the Djungarian hamster is well-established (Heldmaier and Ruf, 1992), implying that mitochondrial respiration also correlates strongly with MR. While temperature effects will dramatically decrease mitochondrial respiration during torpor, the initial phase of torpor entry may be promoted by the active reduction of the substrate oxidation in the liver. It is however surprising, that organs such as the heart, which is one of the first peripheral sites slowing down activity, display no depression in isolated mitochondria. Again, the experimental limitation of this study did not allow excluding the loss of depressing factors during the isolation process.

While the correlation of the respiration states and T_b was robust, the number of animals was unfortunately not sufficient to exclude the normothermic individuals from the analysis and re-analyze the respiration rates vs. torpor temperature per se, requiring larger animal cohorts for future investigations.

5. Conclusions

During torpor of the Djungarian hamster, the respiration of isolated mitochondria reflects tissue-specific regulation and in the liver it correlates with the body temperature. For future directions, the exact molecular mechanism of mitochondrial depression requires further attention. A metabolite inhibition has been suggested, but it has been shown that this also does not fully account for intrinsic mitochondrial depression (Armstrong and Staples, 2010). Whether there are cellular factors controlling the mitochondrial respiration that are lost during the mitochondrial isolation process, requires more sophisticated technologies, in particular applying novel MRI technology that allow measurements of mitochondrial energy transduction *in vivo* (Marcinek, 2004). In torpid animals, respiration and blood flow are decreased, possibly affecting oxygen and substrate supply, but that they also reduce the ATP consumption during torpor should be considered.

References

Armstrong, C., Staples, J.F., 2010. The role of succinate dehydrogenase and oxaloacetate in metabolic suppression during hibernation and arousal. J. Comp. Physiol. B. 180, 775–783.

Barger, J.L., Brand, M.D., Barnes, B.M., Boyer, B.B., 2003. Tissue-specific depression of mitochondrial proton leak and substrate oxidation in hibernating arctic ground squirrels. Am. J. Physiol. Regul. Integr. Comp. Physiol. 284, R1306–R1313.

Berriel Diaz, M., Lange, M., Heldmaier, G., Klingenspor, M., 2004. Depression of transcription and translation during daily torpor in the Djungarian hamster (*Phodopus sungorus*). J. Comp. Physiol. B. 174, 495–502.

Brand, M., 1995. Measurements of mitochondrial protonmotive force. In: Brown, G.C., Cooper, C.E. (Eds.), Bioenergetics: A Practical Approach. Oxford University Press, USA, pp. 39–62.

Brown, J.C.L., Gerson, A.R., Staples, J.F., 2007. Mitochondrial metabolism during daily torpor in the dwarf Siberian hamster: role of active regulated changes and passive thermal effects. Am. J. Physiol. Regul. Integr. Comp. Physiol. 293, R1833–R1845.

Buck, C.L., Barnes, B.M., 2000. Effects of ambient temperature on metabolic rate, respiratory quotient, and torpor in an arctic hibernator. Am. J. Physiol. Regul. Integr. Comp. Physiol. 279, R255–R262.

Ehrhardt, N., Heldmaier, G., Exner, C., 2005. Adaptive mechanisms during food restriction in *Acomys russatus*: the use of torpor for desert survival. J. Comp. Physiol. B. 175, 193–200.

Frerichs, K.U., Smith, C.B., Brenner, M., DeGracia, D.J., Krause, G.S., Marrone, L., Dever, T.E., Hallenbeck, J.M., 1998. Suppression of protein synthesis in brain during hibernation involves inhibition of protein initiation and elongation. Proc. Natl. Acad. Sci. U.S.A. 95, 14511–14516.

Geiser, F., 1988. Reduction of metabolism during hibernation and daily torpor in mammals and birds: temperature effect or physiological inhibition? J. Comp. Physiol. B. 158, 25–37.

Geiser, F., 1998. Evolution of daily torpor and hibernation in birds and mammals: importance of body size. Clin. Exp. Pharmacol. Physiol. 25, 736–739.

Gnaiger, E., Mendez, G., Hand, S.C., 2000. High phosphorylation efficiency and depression of uncoupled respiration in mitochondria under hypoxia. Proc. Natl. Acad. Sci. U.S.A. 97, 11080–11085.

Gornall, A.G., Bardawill, C.J., David, M.M., 1949. Determination of serum proteins by means of the biuret reaction. J. Biol. Chem. 177, 751–766.

Guppy, M., Withers, P., 1999. Metabolic depression in animals: physiological perspectives and biochemical generalizations. Biol. Rev. Camb. Philos. Soc. 74, 1–40.

Heldmaier, G., Ruf, T., 1992. Body temperature and metabolic rate during natural hypothermia in endotherms. J. Comp. Physiol. B. 162, 696–706.

Heldmaier, G., Ortmann, S., Elvert, R., 2004. Natural hypometabolism during hibernation and daily torpor in mammals. Respir. Physiol. Neurobiol. 141, 317–329.

Jastroch, M., 2012. Adjustments of mitochondrial energy transduction in response to physiological and environmental challenge. In: Ruf, T., Bieber, C., Arnold, W., Millesi, E. (Eds.), Living in a Seasonal World: Thermoregulatory and Metabolic Adaptations. Springer, Berlin Heidelberg, pp. 387–398.

Jastroch, M., Divakaruni, A.S., Mookerjee, S., Treberg, J.R., Brand, M.D., 2010. Mitochondrial proton and electron leaks. Essays Biochem. 47, 53–67.

Lyman, C.P., Chatfield, P.O., 1955. Physiology of hibernation in mammals. Physiol. Rev. 35, 403–425.

Marcinek, D.J., 2004. Mitochondrial dysfunction measured in vivo. Acta Physiol. Scand. 182, 343–352.

Martin, S.L., Maniero, G.D., Carey, C., Hand, S.C., 1999. Reversible depression of oxygen consumption in isolated liver mitochondria during hibernation. Physiol. Biochem. Zool. 72, 255–264.

Melvin, R.G., Andrews, M.T., 2009. Torpor induction in mammals: recent discoveries fueling new ideas. Trends Endocrinol. Metab. 20, 490–498.

Muleme, H.M., Walpole, A.C., Staples, J.F., 2006. Mitochondrial metabolism in hibernation: metabolic suppression, temperature effects, and substrate preferences. Physiol. Biochem. Zool. 79, 474–483.

Oelkrug, R., Heldmaier, G., Meyer, C.W., 2011. Torpor patterns, arousal rates, and temporal organization of torpor entry in wild type and UCP1-ablated mice. J. Comp. Physiol. B. 181, 137–145.

Polymeropoulos, E.T., Heldmaier, G., Frappell, P.B., McAllan, B.M., Withers, K.W., Klingenspor, M., White, C.R., Jastroch, M., 2012. Phylogenetic differences of mammalian basal metabolic rate are not explained by mitochondrial basal proton leak. Proc. Biol. Sci. 279, 185–193.

Reynafarje, B., Costa, L.E., Lehninger, A.L., 1985. O_2 solubility in aqueous media determined by a kinetic method. Anal. Biochem. 145, 406–418.

Rolfe, D.F., Brown, G.C., 1997. Cellular energy utilization and molecular origin of standard metabolic rate in mammals. Physiol. Rev. 77, 731–758.

Ruf, T., Heldmaier, G., 1987. Computerized body temperature telemetry in small animals: use of simple equipment and advanced noise suppression. Comput. Biol. Med. 17, 331–340.

Staples, J.F., Brown, J.C.L., 2008. Mitochondrial metabolism in hibernation and daily torpor: a review. J. Comp. Physiol. B. 178, 811–827.

St-Pierre, J., Brand, M.D., Boutilier, R.G., 2000. The effect of metabolic depression on proton leak rate in mitochondria from hibernating frogs. J. Exp. Biol. 203, 1469–1476.

Swoap, S.J., Gutilla, M.J., Liles, L.C., Smith, R.O., Weinshenker, D., 2006. The full expression of fasting-induced torpor requires beta 3-adrenergic receptor signaling. J. Neurosci. 26, 241–245.

Trzcionka, M., Withers, K.W., Klingenspor, M., Jastroch, M., 2008. The effects of fasting and cold exposure on metabolic rate and mitochondrial proton leak in liver and skeletal muscle of an amphibian, the cane toad *Bufo marinus*. J. Exp. Biol. 211, 1911–1918.

van Breukelen, F., Martin, S.L., 2002. Reversible depression of transcription during hibernation. J. Comp. Physiol. B. 172, 355–361.

6.5 Grimpo et al. in Vorbereitung

A new perspective for the investigation of torpid Djungarian hamsters (*Phodopus sungorus*) and photoperiod changes in adipose tissue composition using magnetic resonance

A new perspective for the investigation of torpid Djungarian hamsters (*Phodopus sungorus*) and photoperiodic changes in adipose tissue composition using magnetic resonance

Kirsten Grimpo[1], Maximilian N. Völker[2], Craig L. Frank [3], Johannes T. Heverhagen[4], Gerhard Heldmaier[1]

[1]Philipps-Universität Marburg, Faculty of Biology, Department of Animal Physiology, Karl-von-Frisch-Strasse 8, 35043 Marburg, Germany

[2]Philipps-Universität Marburg, Faculty of Medicine, Department of Diagnostic Radiology, Baldingstrasse, 35043 Marburg, Germany

[3]Fordham University, Louis Calder Center, Department of Biological Science, 53 Whippoorwill Road, Armonk, New York 10504

[4]Institute for Diagnostic, Interventional and Paediatric Radiology, University Hospital Inselspital, Bern, Switzerland

Address correspondence to:

Kirsten Grimpo, Philipps-Universität Marburg, Faculty of Biology, Department of Animal Physiology, Karl-von-Frisch-Straße 8, 35043 Marburg, Germany

Email: kirsten.grimpo@biologie.uni-marburg.de

Phone: 0049 6421 28 23832

Fax: 0049 6421 28 22052

Running head: The use of MRI for investigating *P. sungorus*

Introduction

Daily torpor and hibernation occur in a variety of mammals in response to seasonal variations in ambient temperature, food availability or photoperiod in order to reduce their daily energy expenditure (Geiser 2004; Heldmaier et al. 2004; Melvin and Andrews 2009). The Djungarian hamster (*Phodopus sungorus*) is strongly photoperiodic and displays daily torpor after several weeks of exposure to short photoperiod. Short-day acclimated *P. sungorus* enter torpor spontaneously for several hours during their resting period, even under thermoneutral conditions and *ad libitum* food availability (Heldmaier and Steinlechner 1981; Kirsch et al. 1991). A higher torpor disposition can be attained due to cold exposure and food restriction (Ruf et al. 1993). Torpid phases are characterized by a controlled reduction of oxygen consumption, respiration rate, heart rate and often by a decreased body temperature (Morhardt 1970; Mertens et al. 2008). Energetically expensive gene transcription and protein synthesis are decreased during torpor, enzyme activities are adjusted from glycolysis towards lipid metabolism and substrate oxidation of liver mitochondria declines, contributing to a reduced metabolic energy demand in the torpid state (Heldmaier et al. 1999; Carey et al. 2003; Berriel Diaz et al. 2004; Brown et al. 2007; Kutschke et al. 2013). Understanding the driving mechanisms of metabolic reduction during torpor and the processes to tolerate the ischemic and hypothermic state without harm attracts interest in academic science as well as in translational medicine (Maathuis et al. 2007; Aslami and Juffermans 2010). The number of torpor studies increased rapidly in the last years and the potential of new and innovative methods should applied as much as possible to satisfy animal welfare aspects in this research field (Jinka and Duffy 2013).

Whole-body imaging techniques have been developed and refined in the last decades to meet the purpose of investigating living animals in science (Koba et al. 2013). Today improvements in software and miniaturization of hardware allow the imaging of small animals. Imaging morphological structures or monitoring functional processes *in vivo* are carried out non-invasively, except for anesthesia to minimize motion artifacts. Therefore, modern imaging techniques have a high potential to complement or even replace *ex vivo* studies and satisfy the principle of 3R in animal research; replacement, reduction and refinement (Russell and Burch 1959). Especially the performance of serial studies using the same animals during different metabolic states (normometabolic, torpor entrance, torpor, torpor arousal) or at different treatments (temperature regimes, diets) can eliminate the need to sacrifice the animal and thereby can contribute to a reduction of the number of animals needed.

The magnetic resonance imaging (MRI) provides an excellent soft tissue contrast, e.g. to determine body fat distribution or to differentiate between brown and white adipose tissue (Hu et

al. 2010; Peng et al. 2013; Holstila et al. 2013; Müller et al. 2013). In contrast to computed tomography (CT) MRI runs without ionizing radiation and no radiotracers as used for positron emission tomography (PET) or single photon emission computed tomography (SPECT) are necessary.

The occurrence of daily torpor is not the only physiological adaption of *P. sungorus* to a short photoperiod. Winter acclimated *P. sungorus* have a reduced body weight and testis size, their fur lightens from brownish-grey to white and alterations in fat mass and gene expression in adipose tissue, e.g. a reduced expression of leptin mRNA, can be observed (Klingenspor et al. 1996a; Demas et al. 2002). Brown adipose tissue shows a higher thermogenic capacity in short-day acclimated hamsters in order to maintain body temperature at cold ambient temperatures and further to reheat a hypothermic body temperature back to normothermia during the arousal from torpor via non-shivering thermogenesis (Heldmaier et al. 1981; Heldmaier et al. 1982). In contrast, white adipose tissue serves mainly as energy storage but is also a provider of free fatty acids for heat production in brown adipose tissue, is reduced in short-day acclimated hamsters. Several studies indicate that fatty acid composition of brown and white adipose tissue alters with diet and even photoperiod and that there is some incidence for a relation between torpor behavior and composition of adipose tissue (Geiser and Heldmaier 1995; Geiser et al. 2013). Essential unsaturated fatty acids have been found to be beneficial for torpor disposition, length and depth (Geiser and Kenagy 1987; Frank 1992; Florant et al. 1993). The procedure to analyze the tissue composition in these studies was to sample tissues from sacrificed animals or to take biopsies from anaesthetized animals and to analyze the samples with gas chromatography.

We divided the present study into two parts for investigating *P. sungorus* with magnetic resonance imaging. The first part aimed to develop an experimental set-up that allows MRI simultaneously with measuring the metabolic state of hamsters via indirect calorimetry. Hamsters became torpid within the setup spontaneously and furthermore stayed torpid during the imaging without requiring anesthesia.

The second part of the study was completely independent of part one and investigated tissue composition of brown and white adipose tissue from long and short-day acclimated animals using MRI and magnetic resonance spectroscopy (MRS) in anesthetized hamsters. Afterwards the results of MRS were compared with *ex-vivo* gas-chromatographic analyses in order to evaluate the MRI-methods.

Material and Methods

Animals

Djungarian hamsters (*P. sungorus*) were housed individually in type II makrolon-cages (16 cm x 21 cm x 13 cm) with wood shavings and free access to water and food (ssniff V2144) at the Philipps-Universität Marburg.

For part one of the study, 13 *P. sungorus* were kept under short-day conditions of 8:16 light:dark cycle (lights on: 8:00 h, central European time (CET)) at an ambient temperature of 23 ± 1°C.

For part two of the study, 7 hamsters were kept under long day conditions of 16:8 light:dark cycle (lights on: 6:00 (CET)) at 23°C. 7 hamsters were kept under short-day conditions for 14 weeks at 23°C and further 8 individuals were first kept at short photoperiod at 23°C and then transferred to 5°C maintaining the short photoperiod.

Magnetic resonance imaging and spectroscopy

All imaging and spectroscopic experiments were performed with a 7 Tesla small animal MRI scanner equipped with a 290 mT/m gradient system (ClinScan, Bruker Biospin MRI GmbH, Ettlingen, Germany).

All gathered data were post processed and analyzed with the Syngo software (Siemens Healthcare, Erlangen, Germany).

Metabolic cage with integrated proton-coil for torpor experiments

In order to investigate torpid hamsters we developed a metabolic cage for simultaneous measurement of metabolic rate and magnetic resonance imaging (Fig. 1). The cylindrical cage with an inner volume of 385 cm^3 (7 cm in radius and 10 cm in height) was made of acrylic glass. A perforated seat was installed at the inferior third of the cylindrical cage to separate feces and urine from the animal. Glands on both sides of the cage allowed a continuously perfusion with air. The cage was equipped with an in-house built 8-leg low pass Birdcage coil tuned to the hydrogen Larmor frequency at 7 T (300.40 MHz). For noise protection the cage with the integrated coil was insulated with acoustic foam (Suppl. Fig. 1a-c).

Measurement of oxygen consumption during torpor experiment

To monitor oxygen consumption as an indicator for the metabolic state of the hamsters inside the imaging system, we established an experimental set-up for measuring indirect calorimetry (Fig 1). The calorimetry was installed outside of the faraday chamber of the magnetic resonance imaging system to avoid interferences between the systems.

Individual short-day acclimated hamsters were placed inside the metabolic cage with nesting material and a slice of cucumber just before lights off (about 3:30 pm CET). The cage was fixed in a large animal bed (Bruker Biospin MRI GmbH, Ettlingen, Germany) and located in the center of the magnetic bore.

The disposition of *P. sungorus* to undergo torpor is more pronounced at cold ambient temperatures (Ruf et al. 1993). Therefore an in-house made copper heat exchanger was used to cool the room air that was pumped (200l/h) into the metabolic cage. The air was dried with silica gel to minimize water condensation before entering the heat exchanger. The inner helix of the heat exchanger was perfused with 1°C cold antifreeze mixture using a water bath (F25-ED, Julabo GmbH, Seelbach, Germany). The tube between heat exchanger and metabolic cage was thermally insulated and the air entered the cage with a temperature of 13-15°C. Temperature of air exiting the cage was continuously measured with a thermocouple.

Oxygen consumption and carbon dioxide production were measured with an open respiratory system (previously described by Heldmaier and Ruf 1992). Air was sucked through the cage with a rate of 30 ± 0.5 l/h and dried by an electric freeze trap (M and C Cooler, ECM, Ratingen, Germany). The airflow was displayed with optic mass flow meters and was continuously monitored with an electronic mass flow meter (Bronkhorst High-Tech B.V., Ruurlo, Netherlands). O_2 and CO_2 content of the air were measured with a two-channel O_2 analyzer (Oxzilla II, Sable systems int., Las Vegas, USA) and a two-channel CO_2 analyzer (AO2000, ABB Automation GmbH, Frankfurt, Germany) with a resolution of 0.001 ΔVol % comparing the air entering and leaving the metabolic cage. The read out interval was set to 30 seconds. A magnetic valve system allowed the measurement of room air every hour (for a time span of 2.5 min) for automated continuous zero readjustment. Channel switching was controlled by a computer that processed the thermocouple-, analyzer- and the flow meter signals of the selected channel (including automatic zero adjustment and volume corrections for gas analysis) and also stored the results. VO_2 was calculated according to Haldane equation: $VO_2 = Flow_{in} \times FO_{2in} - Flow_{out} \times FO_{2out}$, where FO_{2in} *and* FO_{2out} are fractional concentrations of O_2 in fresh gas and mixed exhaust gas respectively.

Imaging of torpid hamsters

The imaging of non-anaesthetized hamsters was started when hamsters displayed deep torpor. Using the home-made receive/transmit coil around the metabolic cage different sequences were started to acquire T2 weighted images in sagittal, transversal and coronal view. Furthermore angiographic images were acquired and ^{1}H-spectroscopy was performed. The sequences used are described beneath the corresponding figure (Fig. 3).

Characterization of adipose tissue

Brown and white adipose tissues (BAT and WAT) of anaesthetized hamsters were examined using a quadrature mouse body coil with an inner diameter of 35 mm (Bruker) for transmission and reception. For image acquisition, anesthesia was induced in an induction chamber by inhalation of air containing 5% isoflurane (Baxter, Unterschleissheim, Germany). Hamsters were fixed in an animal bed where the anesthesia was maintained by continuous isoflurane inhalation (1.5–2.5%). Eye ointment was applied and the body temperature of the hamsters was stabilized with a heating unit during the measurements. Animal respiration rate and rectal body temperature were continuously monitored during the measurements (Small Animal Monitoring & Gating System, SAInstruments, Stony Brook, NY, USA).

The following sequences were used to characterize adipose tissue: T2-weighted turbo spin echo sequence (TR (repetition time): 1010 ms, TE (echo time): 52 ms, FoV: 30 x 30 mm^2, matrix: 192 x 192, slices: 16, slice thickness: 0.8 mm, voxel size: 0.156 x 0.156 x 0.8 mm^3, acquisition time: 111 s). For measuring the size of interscapular brown adipose tissue a T1-weighted turbo spin echo sequence was used (TR: 478 ms, TE: 7.7 ms, FoV: 35 x 35 mm^2, matrix size: 192 x 192, slices: 30-32, slice thickness 0.8 mm, voxel size 0.182 x 0.182 x 0.8 mm^3, acquisition time: 159 s). To determine relaxation times of adipose tissue the orientations of the MRI sequences were transversal in brown adipose tissue and sagittal in epididymal white adipose tissue. Relaxation times were acquired in duplicate. Sequences were performed with FoV: 30 x 30 mm^2, matrix: 128 x 128, slices: 5-7, slice thickness: 0.5 mm and voxel size: 0.547 x 0.273 x 0.5 mm^3. Longitudinal relaxation time (T1-time) was acquired using turbo inversion recovery (TIR) sequences with TR: 3,500 ms, TE: 14 ms and 10 different inversion times (TI: 31, 50, 100, 200, 300, 400, 500, 600, 800, 1,000 ms). The transversal relaxation time (T2-time) was acquired with a spin echo sequence with TR: 2,500 ms and 10 echo times (TE: 10-100 ms in 10 ms steps).

To investigate lipid composition a PRESS ^{1}H-spectroscopy without water suppression was used (TR 2,500 ms; TE 28 ms; flip angle 90°, voxel size 1.0 x 3.1 x 1.0 mm^3; 128 averages; acquisition time 335 seconds).

Determination of relaxation times

To calculate T1 relaxation time a three parametric inversion curve was modeled with a logarithmic relation $S(TI) = c(1-2e^{-TI/T1}) + e^{-TR/T1}$ using Sigma Plot 10. The TI value at the zero-crossing / ln 2 was count as T1 value (Graaf 2007).

T2 values were calculated using an exponential fit function in Sigma Plot 10, signal intensity at echo time TE, $S(TE) = c\,e^{-TE/T2}$. The logarithmized signal value was plotted against the ten measured echo times and the $slope^{-1}$ of the resulting linear equation was assumed as T2 relaxation time (Graaf 2007).

Volume and weight of interscapular brown adipose tissue

Volume of interscapular brown adipose tissue (cm^3) was calculated for every hamster individually on the basis of sagittal T1-weighted images. Interscapular brown adipose tissue was circled in each consecutive slice using a freehand ROI tool. The sum of all areas was calculated and multiplied by slice thickness (0.08 cm). Hamsters were sacrificed 2 days after the last imaging. Interscapular brown adipose tissue and epididymal white adipose tissue were dissected post mortem, balance weighted and immediately frozen in liquid nitrogen. The samples were stored at -80°C.

Gas chromatography of adipose tissue

Fatty acid composition of brown interscapular and white epidydimal adipose issue was analyzed using gas-liquid chromatography (Frank 1992). Free fatty acids of the adipose tissue samples were extracted as described previously (Folch et al. 1957) using chloroform/methanol (2:1) for tissue homogenization and filtration. Isolated lipids were transesterificated with 1.5 mL 1.0 N methanolic HCl which produces acid methyl ester (Christie 1982, 1993). The transesterification reaction was speeded up by incubating the samples at 80°C for 1 hour and stopped afterwards by adding 1 mL distilled water. Methyl esters were extracted thoroughly in three washing steps using all together 4.5 mL pentane as solvent that was dried over magnesium sulfate. An aliquot of this was directly injected into the gas chromatograph (Hewlett-Packard model 5890) with a J&W Scientific capillary column (model DB-23). When more than 100 mg lipid samples were transesterified the methyl ester stock was diluted with pentane (1:5). The oven temperature was 110°C for 3 min and was then increased to 160°C in 20/min steps. The oven temperature was held at 100°C for 3 min and was then increased from 160 to 210°C in 4°C/min increments. Temperature was held at 210°C for 1 min. The gas chromatograph identified fatty acids with 12-

22 carbon atoms. The data were recorded and quantified by a Hewlett-Packard model 3390A integrator.

Results

Imaging of torpid hamsters

10 of the 13 tested *P. sungorus* entered into torpor within the magnetic resonance imaging system. Only two hamsters became torpid when they were placed into the metabolic cage the first time. Usually the hamsters displayed torpor at the second or third stay within the cage. We observed 13 torpor events in 30 try outs and in 10 of the 13 cases hamsters stayed torpid during the MRI scanning procedure (Fig. 2). All in all, one out of three tries was successful. During torpor *P. sungorus* decreased metabolic rate from resting values of 42.16 ± 2.74 mLO_2/h to minimal metabolic rates of 9.19 ± 1.33 mLO_2/h. The scanning was started when the hamsters had reached a deep torpor plateau. The torpid metabolic rate did not change during the scan (12.31 ± 1.57 mLO_2/h) when compared to values before the scan (12.80 ± 1.406 mLO_2/h).

The hamsters moved repeatedly in the cage, even during torpor. Therefore it was necessary to check the position of the hamsters with short localizer sequences frequently. Morphological images as well as proton spectroscopy could be obtained in torpid hamsters (Fig. 3). The posture of a torpid hamster was completely different from that of an anaesthetized individual. Torpid hamsters were curled up in a hunchback posture; with the result that brown adipose tissue was located in direct vicinity to the heart. Visceral organs (liver, intestine, stomach and kidney) were agglomerated close together (Fig. 3b). T2 weighted close up images of the head were performed, where relevant structures of the brain such as the cerebellum, the hypothalamus and the ventricle could be detected (Fig. 3c). The detection of spectroscopic data and angiographic images was more challenging as these sequences last longer than ordinary T2 weighted images and were susceptible against motion artifacts (Fig. 3 d, e). It was possible to perform H^+-spectroscopy in brown adipose tissue of the torpid hamster. The water and the lipid-fraction and even some smaller peaks (i.e. CH=CH) were resolved in this spectrum. With angiographic sequences big vessels could be visualized. For further studies, technical advancements are required in order to increase the signal-to-noise ratio and spatial resolution. An improved setup would be highly valuable for the detection of functional processes during torpor (i.e. changes in lipid composition of adipose tissue or perfusion of specific organs). All together some further developments are required to improve the MRI measurement in torpid animals for the future.

Body weights and organ weights of long-day and short-day acclimated hamsters

Long-day acclimated hamsters had a brownish-grey fur and a significantly higher body mass than short-day acclimated hamsters. They changed their fur color to a light gray or white (Suppl. Fig. 2). Both short-day groups (acclimated to 23°C or 5°C ambient temperature) had the same lightish fur color, but the hamsters acclimated to 5°C were about 5 g heavier (Tab. 1). Besides body mass, the epididymal white adipose tissue depot was greater in cold acclimated short-day hamsters, indicating a beginning recrudescence of short-day adaption. This was confirmed as cold acclimated hamsters had the same substernal and interscapular brown adipose tissue mass as compared to long-day hamsters. The interscapular BAT volumes obtained from T1 weighted images were compared with wet weight of interscapular BAT from the 22 hamsters of the three acclimation groups (data not shown). A significant correlation between volume and wet weight was obtained ($p=0.005$, $r^2= 0.347$), but MRI data overestimated balance weights twice to thrice depending on acclimation group.

Relaxation times of adipose tissue

Longitudinal relaxation times (T1 time) were not different between white and interscapular brown adipose tissue, but the transversal relaxation time (T2 time) of white adipose tissue was significantly higher at all acclimation states (Fig. 4). In T1 weighted images the signal of white adipose tissue appeared hyperintense compared to brown adipose tissue in short-day acclimated *P. sungorus*, indicating higher lipid content in white adipocytes (Fig. 5). No differences in T2 time were observed between the two investigated brown adipose tissue depots within the same acclimation state, but T1 time was lower in the substernal compared to the interscapular brown adipose tissue depot during short-day at 23°C (Tab. 1).

The signal in T1 weighted images was hypointense following short-day acclimation and during cold acclimation especially in brown adipose tissue, indicating a thermogenic activation of brown adipose tissue. T1 time of brown adipose tissue was higher following short-day acclimation and T2 time was lower respectively. Relaxation times of white adipose tissue did not differ between acclimation states.

Fatty acid composition of adipose tissue determined by Proton-spectroscopy

The mean fatty acid chain length (according to Zancanaro et al. 1994) did not differ between brown and white adipose tissue or between acclimation states (Fig. 6 a).

Mean chain length of fatty acids lay between 20 and 26 carbon atoms. Several calculations according to saturation of adipose tissue (Fig. 6 b-d) indicated a higher unsaturation of white adipose tissue compared to brown adipose tissue. Mean unsaturation of fatty acids was 1.39 ± 0.16 and 1.47 ± 0.13 in brown adipose tissue and 1.51 ± 0.16 and 1.71 ± 0.42 in white adipose tissue for long and short-day conditions respectively. Mean polyunsaturation of fatty acids in white adipose tissue of short-day acclimated hamsters was significantly higher (0.46 ± 0.03) than in brown adipose tissue (0.35 ± 0.03) and higher than in white adipose tissue following long day conditions (0.33 ± 0.04). For a further, CH_3 peak independent variable, we calculated the ratio between the CH_2 and the CH=CH peak. The ratio was significantly lower in white adipose tissue than in brown adipose tissue at both acclimation states, indicating a higher level of double bounds per CH_2 in white adipose tissue.

Fatty acid composition of adipose tissue determined by gas chromatography

Seven different fatty acids were detected in adipose tissue of short- and longday acclimated hamsters with gas chromatography (Tab 3, 4). The concentration of palmitoleic acids (16:1) was higher while the concentration of linoleic acids (18:2) was lower in long photoperiod in brown as well as in white adipose tissue. Furthermore, the sum of polyunsaturated fatty acids (PUFA) was lower during long compared to short photoperiod. Sums of saturated (SFA) and unsaturated (UFA) fatty acids did not differ significantly between long and short photoperiod. Stearic acid (18:0) was absent in the most white adipose tissue samples but it was present in brown adipose tissue with a higher concentration in the long-day conditions. In white adipose tissue but not in brown adipose tissue the amount of palmitic acid (16:0) was significantly higher at 23°C ambient temperature than at 5°C, resulting in a lower sum of SFA in white fat of cold acclimated hamsters.

The comparison between brown and white adipose tissue with paired t-test showed significantly less palmitoleic acids and more stearic acids in brown fat at all acclimation states. This caused a significant higher sum of UFA in white adipose tissue while SFA were higher in brown adipose tissue.

In addition, hamsters in long photoperiod and hamsters in short photoperiod acclimated to 5°C ambient temperature had higher palmitic acid concentrations in their brown adipose tissue and

higher linoleic acid concentrations in white adipose tissue, resulting in a higher amount of PUFA in white adipose tissue.

To validate the spectroscopic data we calculated the same parameters for chromatographic data as shown in Fig. 7.

The variability of the group data acquired with gas chromatography was far smaller than that of spectroscopic data. The mean chain length did not differ between brown and white adipose tissue or between acclimation states as it was observed in spectroscopic data but the chain length calculated from chromatography was only about 17 carbons (Fig. 7 a). The mean unsaturation calculated from chromatography was also much lower than that calculated from proton spectroscopy. However, a higher unsaturation of fatty acids and a higher amount of unsaturated fatty acids in white adipose tissue could be confirmed statistically in chromatographic data where only a tendency could be assumed from proton spectroscopy. An increased polyunsaturation of fatty acids following short-day acclimation was observed in white and brown adipose tissue. The mean unsaturation is equivalent to the so called double bond index that was described in previous studies (Richardson et al. 1961; Frank 1992). It is the sum of the weight percentages of each fatty acid in the sample multiplied by the number of double bonds contained in each molecule divided by the total amount of fatty acids measured in the sample. The mean polyunsaturation was calculated respectively considering only the polyunsaturated fatty acid in each sample.

Parameters for lipid composition acquired from *in vivo* proton spectroscopy were plotted against the data acquired from *ex vivo* gas chromatography. Therefore data from brown and white adipose tissue from animals acclimated to short and long photoperiods were pooled in one plot. Assosiations of the data were calculated for mean chain length, mean unsaturation and mean polyunsaturation and we found significant correlations ($p < 0.05$) for all three parameters (Fig. 8).

Discussion

To do

References

Aslami H, Juffermans NP (2010) *Induction of a hypometabolic state during critical illness - a new concept in the ICU?* Neth J Med 68:190–198.

Berriel Diaz M, Lange M, Heldmaier G, Klingenspor M (2004) *Depression of transcription and translation during daily torpor in the Djungarian hamster (Phodopus sungorus).* J Comp Physiol B 174:495–502.

Brown JCL, Gerson AR, Staples JF (2007) *Mitochondrial metabolism during daily torpor in the dwarf Siberian hamster : role of active regulated changes and passive thermal effects*. Am J Physiol Regul Integr Comp Physiol 293:1833–1845.

Carey H V, Andrews MT, Martin SL (2003) *Mammalian hibernation: cellular and molecular responses to depressed metabolism and low temperature*. Physiol Rev 83:1153–1181.

Demas GE, Bowers RR, Bartness TJ, et al. (2002) *Photoperiodic regulation of gene expression in brown and white adipose tissue of Siberian hamsters (Phodopus sungorus)* . Am J Physiol Regul Integr Comp Physiol 282:114–121.

Florant GL, Hester L, Ameenuddin S, Rintoul DA (1993) *The effect of a low essential fatty acid diet on hibernation in marmots.* Am J Physiol 264:747–753.

Frank CL (1992) *The Influence of Dietary Fatty Acids on Hibernation by Golden-Mantled Ground Squirrels (Spermophilus lateralis).* Physiol Zool 65:906–920.

Geiser F (2004) *Metabolic rate and body temperature reduction during hibernation and daily torpor*. Annu Rev Physiol 66:239–274.

Geiser F, Heldmaier G (1995) *The impact of dietary fats, photoperiod, temperature and season on morphological variables, torpor patterns, and brown adipose tissue fatty acid composition of hamsters, Phodopus sungorus*. J Comp Physiol B 165:406–415.

Geiser F, Kenagy GJ (1987) *Polyunsaturated lipid diet lengthens torpor and reduces body temperature in a hibernator.* Am J Physiol 252:897–901.

Geiser F, Klingenspor M, McAllan BM (2013) *A Functional Nexus between Photoperiod Acclimation, Torpor Expression and Somatic Fatty Acid Composition in a Heterothermic Mammal*. PLoS One 8:e63803.

Graaf RA De (2007) *In Vivo NMR Spectroscopy: Principles and Techniques – 2nd Edition*. John Wiley & Sons, West Sussex, pp 1–592.

Heldmaier G, Klingenspor M, Werneyer M, et al. (1999) *Metabolic adjustments during daily torpor in the Djungarian hamster.* Am J Physiol 276:896–906.

Heldmaier G, Ortmann S, Elvert R (2004) *Natural hypometabolism during hibernation and daily torpor in mammals.* Respir Physiol Neurobiol 141:317–329.

Heldmaier G, Ruf T (1992) *Body temperature and metabolic rate during natural hypothermia in endotherms*. J Comp Physiol B 162:696–706.

Heldmaier G, Steinlechner S (1981) *Seasonal pattern and energetics of short daily torpor in the Djungarian hamster, Phodopus sungorus*. Oecologia 48:265–270.

Heldmaier G, Steinlechner S, Rafael J, Latteier B (1982) *Photoperiod and ambient temperature as environmental cues for seasonal thermogenic adaptation in the Djungarian hamster, Phodopus sungorus.* Int J Biometeorol 26:339–345.

Heldmaier G, Steinlechner S, Rafael J, Vsiansky P (1981) *Photoperiodic Control and Effects of Melatonin on Nonshivering Thermogenesis and Brown Adipose Tissue.* Science 212:917–919.

Holstila M, Virtanen K a, Grönroos TJ, et al. (2013) *Measurement of brown adipose tissue mass using a novel dual-echo magnetic resonance Imaging Approach: A validation study*. Metabolism 62:1189–1198.

Hu HH, Smith DL, Nayak KS, et al. (2010) *Identification of brown adipose tissue in mice with fat-water IDEAL-MRI.* J Magn Reson imaging 31:1195–1202.

Jinka TR, Duffy LK (2013) *Ethical considerations in hibernation research*. Lab Anim (NY) 42:248–252.

Kirsch R, Ouarour A, Pevet P (1991) *Daily torpor in the Djungarian hamster (Phodopus sungorus): photoperiodic regulation, characteristics and circadian organization*. J Comp Physiol A 168:121–128.

Klingenspor M, Dickopp A, Heldmaier G, Klaus S (1996) *Short photoperiod reduces leptin gene expression in white and brown adipose tissue of Djungarian hamsters*. FEBS Lett 399:290–294.

Koba W, Jelicks LA, Fine EJ (2013) *MicroPET / SPECT / CT Imaging of Small Animal Models of Disease.* Am J Pathol 182:319–324.

Kutschke M, Grimpo K, Kastl A, et al. (2013) *Depression of mitochondrial respiration during daily torpor of the Djungarian hamster, Phodopus sungorus, is specific for liver and correlates with body temperature*. Comp Biochem Physiol A 164:584–589.

Maathuis M-HJ, Leuvenink HGD, Ploeg RJ (2007) *Perspectives in organ preservation*. Transplantation 83:1289–1298.

Melvin RG, Andrews MT (2009) *Torpor induction in mammals: recent discoveries fueling new ideas.* Trends Endocrinol Metab 20:490–498.

Mertens A, Stiedl O, Steinlechner S, Meyer M (2008) *Cardiac dynamics during daily torpor in the Djungarian hamster (Phodopus sungorus).* Am J Physiol Regul Integr Comp Physiol 294:639–650.

Morhardt JE (1970) *Heart rates, breathing rates and the effects of atropine and acetylcholine on white-footed mice (Peromyscus sp.) during daily torpor*. Comp Biochem Physiol 33:441–457.

Müller H-P, Niessen HG, Kaulisch T, et al. (2013) *MRI allows for longitudinal quantitative analysis of body fat composition in rats: An analysis of sibutramine-associated changes at the group level.* Magn Reson Imaging 31:1150–1155.

Peng X-G, Ju S, Fang F, et al. (2013) *Comparison of brown and white adipose tissue fat fractions in ob, seipin, and Fsp27 gene knockout mice by chemical shift-selective imaging and $^{(1)}$H-MR spectroscopy.* Am J Physiol Endocrinol Metab 304:160–167.

Richardson T, Tappel AL, Gruger EH (1961) *Essential fatty acids in mitochondria*. Arch Biochem Biophys 94:1–6.

Ruf T, Stieglitz A, Steinlechner S, et al. (1993) *Cold exposure and food restriction facilitate physiological responses to short photoperiod in Djungarian hamsters (Phodopus sungorus).* J Exp Zool 267:104–112.

Russell WMS, Burch RL (1959) *The principles of humane experimental technique*., Reprinted, Methuen and Co, London 1-238.

Zancanaro C, Nano R, Marchioro C, et al. (1994) *Magnetic resonance spectroscopy investigations of brown adipose tissue and isolated brown adipocytes*. J Lipid Res 35:2191–2199.

Table 1 *Body weight and adipose tissue weights of long-day and short-day acclimated P. sungorus.* Hamsters were sacrificed after magnetic resonance imaging was finished and bilateral depots of substernal brown adipose tissue (sBAT), interscapular brown adipose tissue (iBAT) and epididymal white adipose tissue (eWAT) were dissected and balance weighted.

Photoperiod	Ambient temperature	n	Body mass (g)	sBAT weight (mg)	iBAT weight (mg)	eWAT weight (mg)
Long-day	23°C	7	36.51 ± 1.3	146.29 ± 6.4	131.29 ± 10.4	712.71 ± 61.5
Short-day	23°C	7	23.19 ± 0.7	96.86 ± 7.8	96.14 ± 8.3	199.00 ± 29.3
Short-day	5°C	8	28.13 ± 0.7	158.88 ± 6.9	146.13 ± 12.7	382.86 ± 44.5

Table 2 *Longitudinal (T1) and transversal (T2) relaxation of brown and white adipose tissue in P. sungorus acquired with magnetic resonance imaging.* Hamsters were acclimated at different photoperiods and ambient temperatures. Relaxations times were determined in duplicate for substernal (sBAT) and interscapular brown adipose tissue (iBAT) and epididymal white adipose tissue (eWAT).

Photoperiod	Ambient temperature	n	sBAT T1 (ms)	iBAT T1 (ms)	eWAT T1 (ms)	sBAT T2 (ms)	iBAT T2 (ms)	eWAT T2 (ms)
Long-day	23°C	7	418 ± 13	459 ± 9	444 ± 37	119 ± 8	110 ± 3	142 ± 4
Short-day	23°C	7	426 ± 6	508 ± 12	484 ± 17	94 ± 5	87 ± 7	122 ± 8
Short-day	5°C	8	446 ± 13	489 ± 13	469 ± 17	72 ± 4	75 ± 6	123 ± 6

Table 3 *Fatty acid contents (%) of interscapular brown adipose tissue from P. sungorus determined with gas chromatography.* Hamsters were acclimated to long photoperiod (LP, n=7) or short photoperiod (SP) acclimated to 23°C (n=7) or to 5°C (n=8) ambient temperature. Significant differences between acclimation states are indicated with the same letter, $p < 0.05$.

Fatty acid	LP 23°C	SP 23°C	SP 5°C
14:0	4.09 ± 0.74	3.45 ± 0.85	1.48 ± 0.61
16:0	38.20 ± 1.77	34.87 ± 1.73	33.08 ± 0.99
16:1	11.13 ± 0.91[a,b]	6.79 ± 0.49[a]	7.55 ± 0.75[b]
18:0	5.96 ± 0.61[a,b]	9.34 ± 0.47[a]	8.94 ± 0.71[b]
18:1	25.39 ± 1.63	24.30 ± 1.34	27.76 ± 1.01
18:2	15.17 ± 1.71[a,b]	20.83 ± 1.31[a]	20.93 ± 0.62[b]
18:3	0.00	0.40 ± 0.26	0.3 ± 0.20
total	99.93 ± 0.02	99.98 ± 0.02	100.04 ± 0.03
SFA	48.24 ± 1.98	47.67 ± 2.14	43.49 ± 1.12
UFA	51.69 ± 1.98	52.31 ± 2.13	56.55 ± 1.13
PUFA	15.17 ± 1.17[a,b]	21.23 ± 1.42[a]	21.23 ± 0.67[b]

Table 4 *Fatty acid contents (%) of epididymal white adipose tissue from P. sungorus determined with gas chromatography.* Hamsters were acclimated to long photoperiod (LP, n=7) or short photoperiod (SP) acclimated to 23°C (n=7) or to 5°C (n=8) ambient temperature. Significant differences between acclimation states are indicated with the same letter, $p < 0.05$.

Fatty acid	LP 23°C	SP 23°C	SP 5°C
14:0	2.59 ± 1.07	1.81 ± 0.88	1.95 ± 0.43
16:0	32.21 ± 1.45	34.17 ± 1.13[c]	28.49 ± 1.28[c]
16:1	19.01 ± 0.45[a,b]	11.30 ± 1.17	13.46 ± 0.82
18:0	0.00	1.07 ± 0.52	0.24 ± 0.24
18:1	25.80 ± 1.21	26.97 ± 1.33	30.25 ± 1.87
18:2	20.40 ± 0.85[a,b]	23.87 ± 1.01[a]	25.25 ± 0.77[b]
18:3	0.00	0.86 ± 0.41	0.39 ± 0.26
total	100.01 ± 0.01	100.06 ± 0.04	100.02 ± 0.02
SFA	34.80 ± 1.62	37.06 ± 1.96[c]	30.67 ± 1.36[c]
UFA	65.21 ± 1.63	63.00 ± 1.96[c]	69.35 ± 1.37[c]
PUFA	20.40 ± 0.85[a,b]	24.73 ± 1.14[a]	25.64 ± 0.99[b]

Figure 1

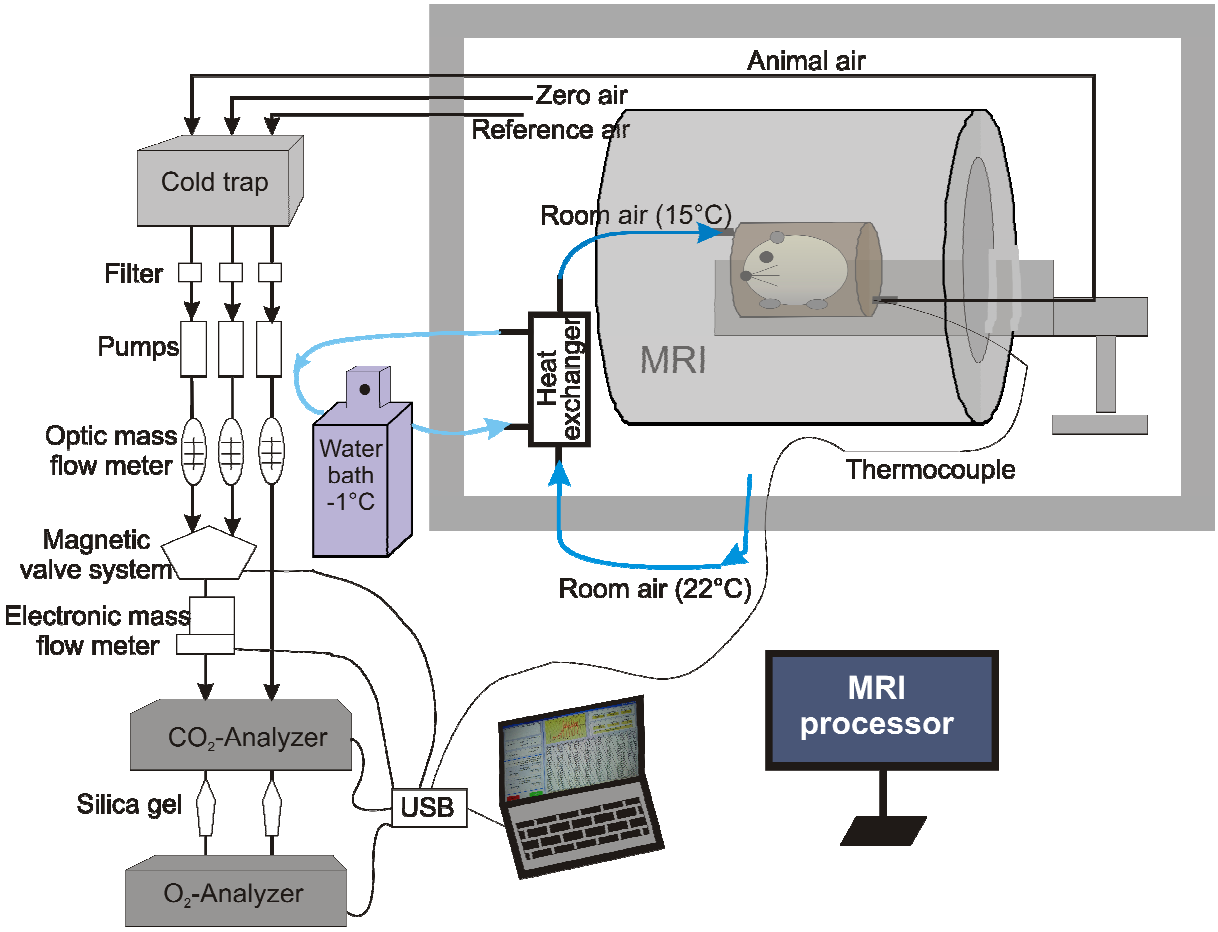

Figure 1 *MRI setup with integrated indirect calorimetry.* Room air was cooled with a heat exchanger before entering the metabolic cage. The air that exits the metabolic cage was analyzed with an O_2 and CO_2 analyzer using room air as reference gas.

Figure 2

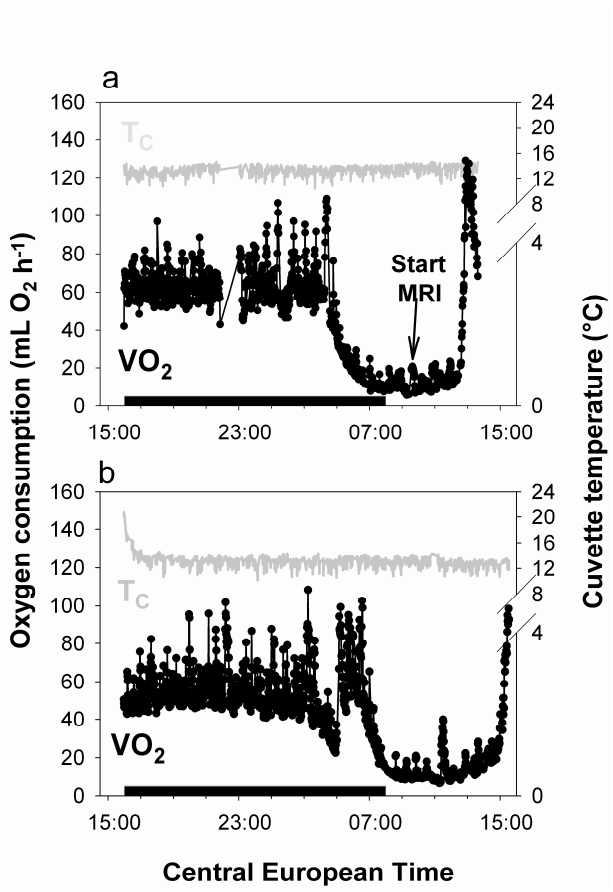

Figure 2 *Oxygen consumption (VO_2) and cuvette temperature (T_c) of P. sungorus in the magnetic resonance imaging setup.* Hamsters started torpor at the end of scotophase (indicated as black bar) and continued torpor irrespective of the MRI measurements (a). No differences compared to a torpor bout without MRI measurement were obvious (b).

Figure 3

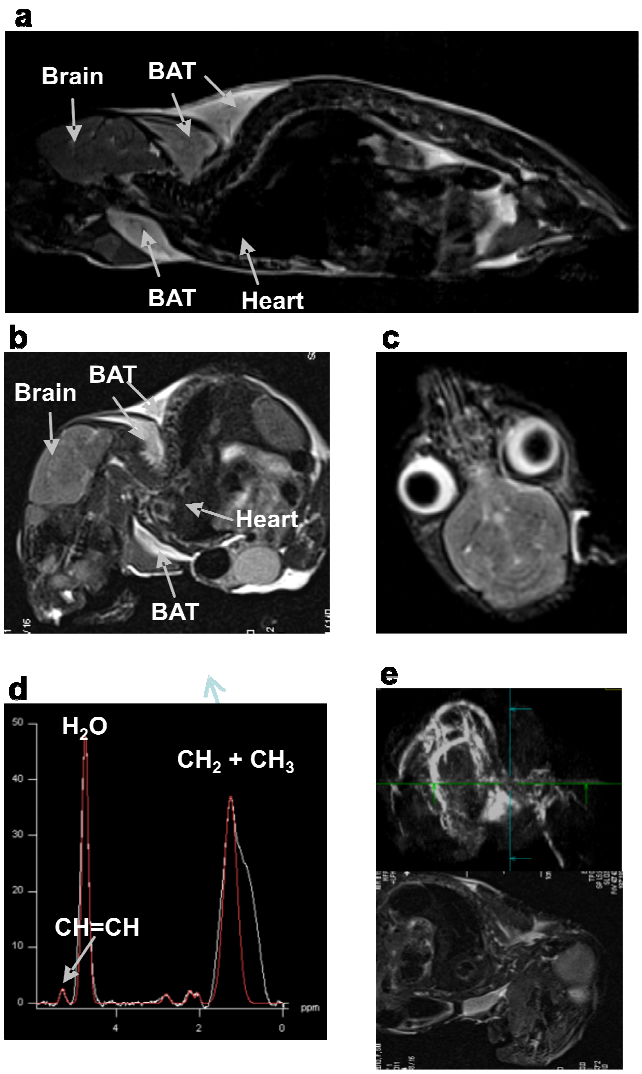

Figure 3 *Images and H^+-Spectroscopy acquired from P. sungorus inside the metabolic cage with integrated body coil.* The coil was tested with an anaesthetized hamster (**a**) and then used for imaging torpid hamsters without anesthesia (**b-e**). Br: Brain, iBAT: interscapular brown adipose tissue, dc: dorsocervical brown adipose tissue, ss: substernal brown adipose tissue, H: Heart, L: Liver, K: Kidney, B: Bladder, O: Olfactory bulb, Ht: Hypothalamus, C: Cerebellum, arrow: Ventricle. Sequences were as follow:

(**a**) T2-weighted turbo spin echo sequence of a normothermic hamster in sagittal view (TR: 2000 ms, TE: 45 ms, matrix size: 448 x 448, slices: 10, slice thickness 0.7 mm, voxel size 0.238 x 0.238 x 0.7 mm^3, acquisition time: 210 s). (**b** 12_1_4) T2-weighted turbo spin echo sequence of a torpid hamster in sagittal view (TR: 1420 ms, TE 55 ms, FoV: 48 x 48 mm^2, matrix: 192 x 192, slices: 24, slice thickness: 0.8 mm, voxel size: 0.250 x 0.250 x 0.8 mm^3, acquisition time: 156 s). (**c**) T2-weighted turbo spin echo sequence of the hamsters´ brain in axial view (TR (repetition

time): 1010 ms, TE (echo time): 50 ms, FoV: 50 x 50 mm^2, matrix: 192 x 192, slices: 16, slice thickness: 0.8 mm, voxel size: 0.260 x 0.260 x 0.8 mm^3, acquisition time: 111 s). **(d)** PRESS ^{1}H-spectroscopy without water suppression of brown adipose tissue (TR 2,500 ms; TE 28 ms; flip angle 90°, voxel size 3.8 x 3.1 x 2.6 mm^3; 128 averages; acquisition time 335 seconds). **(e)** Time of flight sequence for whole body angiography (TR: 21 ms, TE 4.68 ms, FoV: 50 x 50 mm^2, matrix: 256 x 256, slices: 80, slice thickness: 0.5 mm, voxel size: 0.195 x 0.195 x 0.5 mm^3, acquisition time: 568 s). Localization of hamster during time of flight sequence (TR: 23 ms, TE 4 ms, FoV: 60 x 60 mm^2, matrix: 256 x 256, slices: 1, slice thickness: 1.0 mm, voxel size: 0.234 x 0.234 x 1.0 mm^3, acquisition time: 19 s).

Figure 4

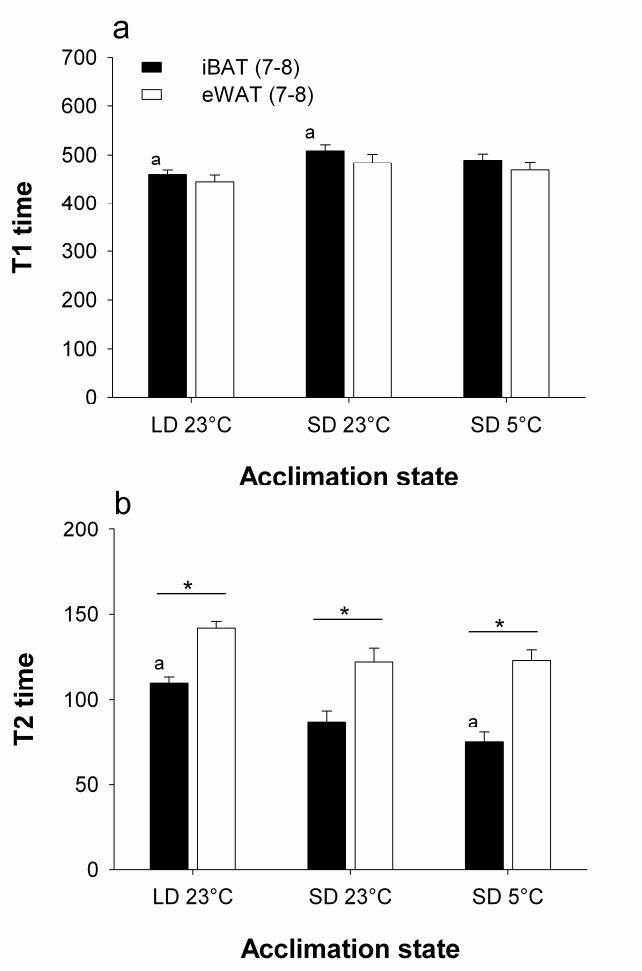

Figure 4: *Longitudinal (T1) and transversal (T2) relaxation times of interscapular brown (iBAT) and epididymal white (eWAT) adipose tissue from P. sungorus.* Hamsters were acclimated to

long photoperiod (LP) or to short photoperiod (SP). Significant differences between acclimation states are indicated with the same letter and between tissues with *, p< 0.05.

Figure 5

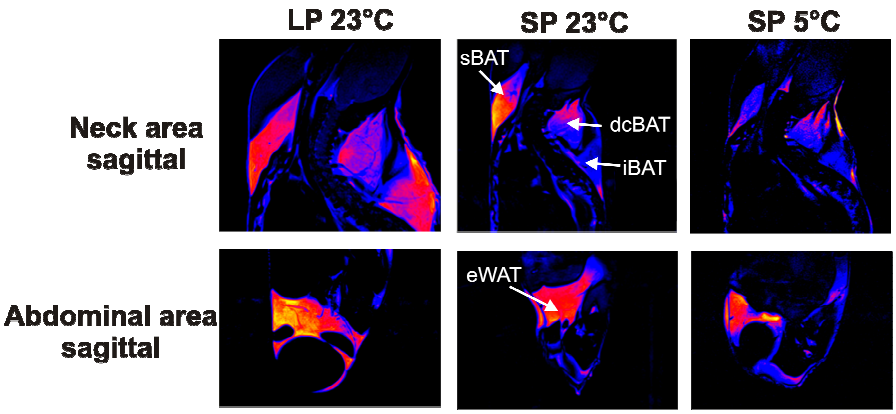

Figure 5 *T1 weighted images in pseudo color from the neck area and the abdominal area of P. sungorus acclimated to different photoperiods and ambient temperatures.* The neck area shows interscapular brown adipose tissue (iBAT), substernal (sBAT) and dorsocervical (dcBAT) brown adipose tissue. The abdominal area was visualizes the epididymal white adipose tissue (eWAT) depot. Images are acquired in sagittal orientation.

Figure 6

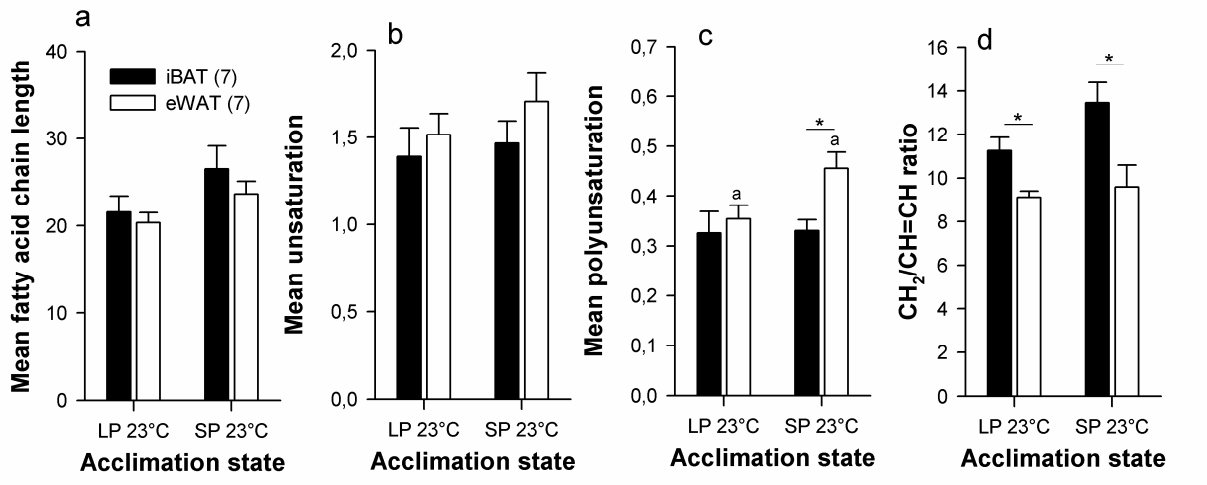

Figure 6 *Fatty acid composition of interscapular brown (iBAT) and epididymal white (eWAT) adipose tissue from anaesthetized P. sungorus determined with magnet resonance $^{+}$H-spectroscopy.* Hamsters were acclimated to long photoperiod (LP) or to short photoperiod (SP). Significant differences between acclimation states are indicated with the same letter and between tissues with *, $p < 0.05$.

Figure 7

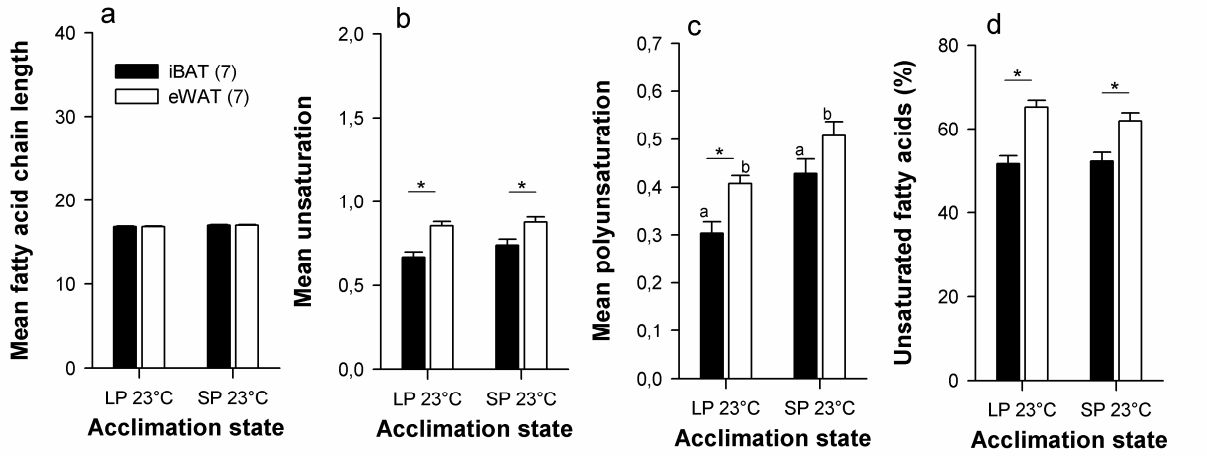

Figure 7 *Fatty acid composition of interscapular brown (iBAT) and epididymal white (eWAT) adipose tissue dissected from Djungarian hamsters.* Tissues were analyzed with gas chromatography. Sacrificed hamsters were acclimated to long photoperiod (LP) or to short photoperiod (SP). Significant differences between acclimation states are indicated with the same letter and between tissues with *, $p < 0.05$.

Figure 8

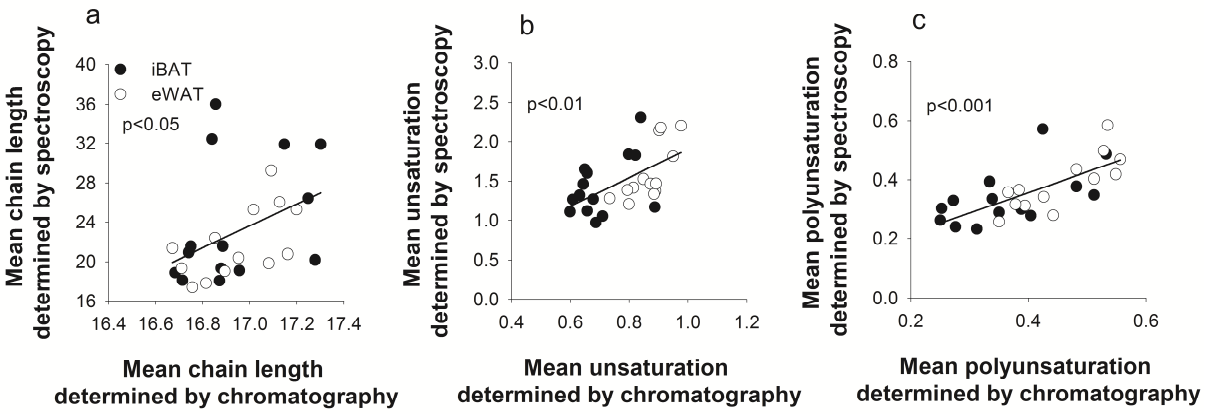

Figure 8 *Correlation between parameters of fatty acid composition from P. sungorus determined with $^{+}$H-spectroscopy and gas chromatography.* $^{+}$H-spectroscopy was acquired in interscapular brown (iBAT) and epididymal white (eWAT) adipose tissue of living, anaesthetized hamsters. Hamsters were sacrificed and adipose tissues were dissected and analyzed with gas chromatography. Data of hamsters kept at long and short photoperiod at 23°C ambient temperature were pooled here. The regression line illustrates the estimated relationship between both methods.

Supplemental figure 1

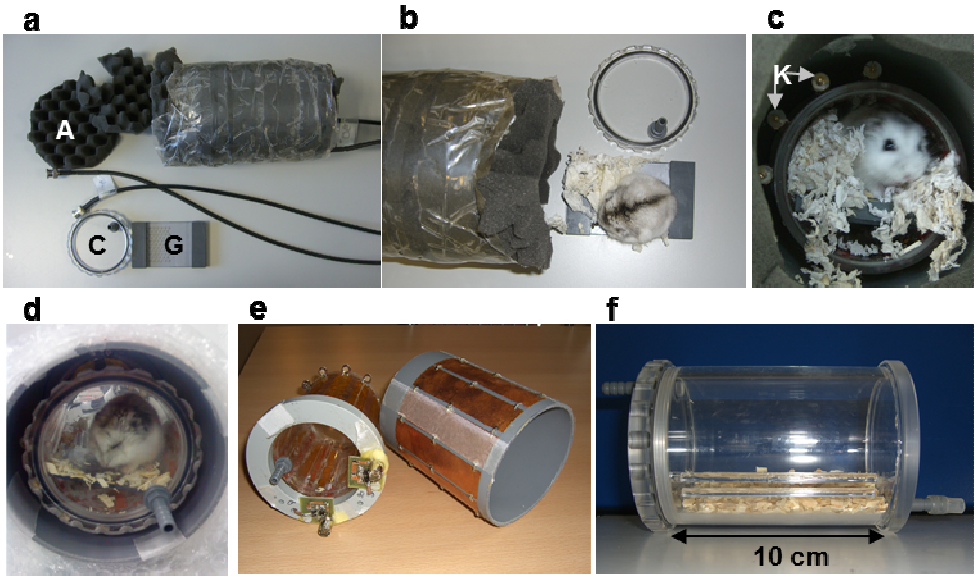

Supplemental figure 1

Metabolic cage with integrated body coil for magnetic resonance imaging of torpid hamsters. **a-c** The device was covered all over with acoustic foam for noise protection (A). A screw cup allowed opening and closing of the metabolic cuvette. A grid (G) served the hamsters as plain seat. **b-d** Nesting material of their home cages facilitated the hamsters to feel save inside the metabolic cuvette and they performed daily torpor spontaneously. **c** Capacitors and trimmers (K) allowed the tuning and the matching of the volume coil to the proton resonance frequency at 7 Tesla (300.40 MHz). **d,e** Conductors of the so-called 12-leg high pass Birdcage coil, were directly attached to the cylindrical cuvette. The coil was 9 cm long, circular polarized and shielded. 13 pico farad capacitors were used. **f** Acrylic glass was used to manufacture the basic frame and air was pumped through the integrated glands on both sides of the cuvette.

Supplemental figure 2

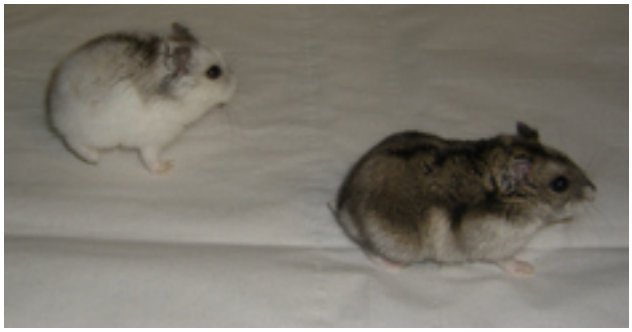

Supplemental figure 2

Seasonal dimorphism of Phodopus sungorus. Hamster in winter coat acclimated to short photoperiod (left) and hamster with summer fur acclimated to long photoperiod (right).

6.6 Grimpo et al. 2014

Brown adipose tissue dynamics in wild-type and UCP1-knockout mice: *in vivo* insights with magnetic resonance

Brown adipose tissue dynamics in wild-type and UCP1-knockout mice: in vivo insights with magnetic resonance[S]

Kirsten Grimpo,[1,*] Maximilian N. Völker,[†] Eva N. Heppe,[*] Steve Braun,[†] Johannes T. Heverhagen,[§] and Gerhard Heldmaier[*]

Faculty of Biology, Department of Animal Physiology,[*] and Faculty of Medicine, Department of Diagnostic Radiology,[†] Philipps-Universität Marburg, 35043 Marburg, Germany; and Institute for Diagnostic, Interventional, and Paediatric Radiology,[§] University Hospital Inselspital, Bern, Switzerland

Abstract **We used noninvasive magnetic resonance imaging (MRI) and magnetic resonance spectroscopy to compare interscapular brown adipose tissue (iBAT) of wild-type (WT) and uncoupling protein 1 (UCP1)-knockout mice lacking UCP1-mediated nonshivering thermogenesis (NST). Mice were sequentially acclimated to an ambient temperature of 30°C, 18°C, and 5°C. We detected a remodeling of iBAT and a decrease in its lipid content in all mice during cold exposure. Ratios of energy-rich phosphates (ATP/ADP, phosphocreatine/ATP) in iBAT were maintained stable during noradrenergic stimulation of thermogenesis in cold- and warm-adapted mice and no difference between the genotypes was observed. As free fatty acids (FFAs) serve as fuel for thermogenesis and activate UCP1 for uncoupling of oxidative phosphorylation, brown adipose tissue is considered to be a main acceptor and consumer of FFAs. We measured a major loss of FFAs from iBAT during noradrenergic stimulation of thermogenesis. This mobilization of FFAs was observed in iBAT of WT mice as well as in mice lacking UCP1. The high turnover and the release of FFAs from iBAT suggests an enhancement of lipid metabolism, which in itself contributes to the sympathetically activated NST and which is independent from uncoupled respiration mediated by UCP1.[F] Our study demonstrates that MRI, besides its potential for visualizing and quantification of fat tissue, is a valuable tool for monitoring functional in vivo processes like lipid and phosphate metabolism during NST.**—Grimpo, K., M. N. Völker, E. N. Heppe, S. Braun, J. T. Heverhagen, and G. Heldmaier. **Brown adipose tissue dynamics in wild-type and UCP1-knockout mice: in vivo insights with magnetic resonance.** ***J. Lipid Res.*** **2014.** 55: **398–409.**

Supplementary key words lipid metabolism • nonshivering thermogenesis • phosphorus spectroscopy • proton spectroscopy • ultra-high field • uncoupling protein 1

Brown adipose tissue (BAT) is a thermogenically active organ and its thermoregulatory function is crucial for body temperature maintenance of small eutherian mammals and newborns during periods of cold exposure. BAT thermogenesis is activated by the release of noradrenaline (NA) from sympathetic innervation. Uncoupling protein 1 (UCP1) in the inner mitochondrial membrane of the brown adipocytes uncouples the respiratory chain from ATP synthesis and thus energy is dissipated as heat (1–3). Prolonged cold exposure or a short photoperiod induces the recruitment of BAT (4–6). Brown adipocytes of cold-adapted mice, contain small and multilocular lipid vacuoles, which are rich in cytoplasm and have a high content of mitochondrial protein (7–9). This provides an enhanced thermogenic capacity during cold exposure, and BAT can be considered as the major site of adaptive nonshivering thermogenesis (NST) in rodents and other small mammals (4, 10–12).

The breakdown of lipids via lipoprotein lipase plays an important role during UCP1-mediated heat production (13). Free fatty acids (FFAs) directly activate UCP1 and feed the respiratory chain, i.e., FFAs are the major substrate for NST (14, 15). Therefore active BAT is considered as a main consumer of lipids and FFAs and its contribution to plasma clearance of administered triglycerides has been shown previously (16, 17). On the other hand a release of fatty acids during thermogenesis from BAT has been assumed, indicating a substrate supply to other tissues (18, 19). Sympathetic activation by cold exposure or injections of NA not only activate BAT but also stimulate sympathetic receptors in general, leading to an increase in heart rate, blood flow, and metabolic responses in other tissues. The contribution of these UCP1-independent processes to total NST remain unclear (20, 21).

This work was supported by the German Federal Ministry of Education and Research (BMBF, grant 0314100).

Manuscript received 1 August 2013 and in revised form 6 December 2013.

Published, JLR Papers in Press, December 16, 2013
DOI 10.1194/jlr.M042895

Abbreviations: BAT, brown adipose tissue; iBAT, interscapular brown adipose tissue; MRS, magnetic resonance spectroscopy; NA, noradrenaline; NST, nonshivering thermogenesis; PCr, phosphocreatine; TE, echo time; TR, repetition time; UCP1, uncoupling protein 1.

[1] To whom correspondence should be addressed.
e-mail: grimpok@biologie.uni-marburg.de

[S] The online version of this article (available at http://www.jlr.org) contains supplementary data in the form of three figures and two videos.

UCP1-knockout (KO) mice are well-suited for investigation of UCP1-independent thermogenesis as mitochondria of these mice are lacking the thermogenic potential of UCP1. Their brown adipocytes contain lager lipid vacuoles similar to white adipocytes (22). UCP1-KO mice raised at thermoneutrality cannot maintain their body temperature upon immediate exposure to 4°C, as one would expect from the lack of UCP1. Nevertheless, a stepwise reduction of ambient temperature improves their thermogenic capacity and they develop a presentable cold tolerance during cold adaption (23). For this reason it has been suggested that UCP1-deleted mice use alternative mechanisms of adaptive thermogenesis, such as an enhanced capacity for shivering thermogenesis or brown adipocyte-like cells in white adipose tissue with higher oxidative capacity (24–26).

We compared the role of BAT during NST in wild-type (WT) and UCP1-KO mice with the help of magnetic resonance imaging (MRI) and magnetic resonance spectroscopy (MRS). The higher water content and the abundance of iron-rich mitochondria in brown adipocytes allow differentiation between brown and white adipose tissue in vivo (27–29), and thermogenically active layers can be distinguished from thermogenically inactive BAT layers (30–32). Therefore, we acclimatized WT and UCP1-KO mice to warm or cold ambient temperatures. To analyze the metabolic activity of interscapular brown adipose tissue (iBAT) of anesthetized mice in vivo, we imaged its phenotype and measured changes in lipid composition and phosphate levels during NA-induced NST. Further, the metabolic rate of conscious mice was obtained after stimulation with NA using indirect calorimetry. These methods allowed us to differentiate the role of BAT in WT and UCP1-KO mice and to confirm the use of noninvasive MRI for investigation of functional in vivo processes.

MATERIAL AND METHODS

Mice and acclimation protocol

WT mice and UCP1-deleted littermates (genetic background C57Bl/6J) were derived from heterozygous breeding pairs in our colony at Philipps-Universität Marburg. The breeding colony was kept at 27°C ambient temperature. In the founder animals (originally provided by L. Kozak, Pennington Medical Research Centre, Baton Rouge, LA), the UCP1 gene had been inactivated by homologous recombination (33). Genotypes were identified using a PCR-based strategy (23) prior to the first measurements. Only male $UCP1^{+/+}$ (WT) and $UCP1^{-/-}$ (KO) mice were included in the experiments. The presence or absence of UCP1 protein in BAT of mice was verified post mortem by enhanced chemiluminescence (ECL) Western blot assay (34). The membranes were probed with a rabbit anti-UCP1 polyclonal antibody (1:30,000 dilution, 3046, Chemicon) followed by a goat anti-rabbit-IgG peroxidase-conjugated secondary antibody (1:10,000 dilution, Dako). The chemiluminescent signal was detected on X-ray film (Super RX, Fuji) using an ECL Plus Western blotting detection system (SRX-101A, Konika Minolta).

Throughout the experiments mice were housed individually in macrolon type II cages bedded with wood shavings and nesting material. Mice were fed ad libitum with standard chow diet (Ssniff 1534, Soest, Germany), had free access to water, and were kept at a 12:12 h light:dark cycle. To investigate mice adapted to different ambient temperatures, they were sequentially acclimated to ambient temperatures of 30°C, 18°C, and 5°C. Mice at an age of 3–6 months were transferred to 30°C for 3 weeks, afterwards acclimated to 18°C for 3 weeks, and finally to 5°C for a further 2 weeks. Even though UCP1-KO mice are cold sensitive, they can tolerate an ambient temperature of 5°C when using this stepwise acclimation protocol (24). Thermogenic properties were measured (metabolic rate, MRI, and MRS) at the end of each acclimation period. The experiments were performed in accordance with the German animal welfare act.

MRI and MRS

All MRI and MRS experiments were performed with a 7 Tesla small animal MRI scanner equipped with a 290 mT/m gradient system (ClinScan, Bruker Biospin MRI GmbH, Ettlingen, Germany). Mice were anesthetized with an intraperitoneal injection of pentobarbital sodium at a dose of 75 mg/kg body weight (Narcoren, Merial GmbH, Hallbergmoos, Germany). A subcutaneous access was administered to facilitate a NA injection (1 mg NA/kg body weight) through a polyethylene tube system during magnetic resonance measurements without relocating the mice.

During the measurements, the body temperature of the mice was stabilized with a heating unit. Respiration rate and rectal body temperature were continuously monitored (small animal monitoring and gating system, SAInstruments, Stony Brook, NY).

BAT composition and changes in lipid content of 31 mice [WT (n = 16), UCP1-KO (n = 15)] were examined using a quadrature mouse birdcage coil with an inner diameter of 35 mm (Bruker). To localize the iBAT depot and to differentiate it from other tissues, two imaging sequences were optimized in contrast parameters as follows (**Fig. 1A, B**): a T2-weighted turbo spin echo sequence [repetition time (TR), 1,010 ms; echo time (TE), 52 ms; FoV, 30 × 30 mm^2; matrix, 192 × 192; slices, 16; slice thickness, 0.8 mm; voxel size, 0.156 × 0.156 × 0.8 mm^3; acquisition time, 111 s] and a T1-weighted turbo spin echo sequence (TR, 478 ms; TE, 7.8 ms; matrix size, 256 × 256; slices, 16; slice thickness, 0.8 mm; voxel size, 0.117 × 0.117 × 0.8 mm^3; acquisition time, 94 s). Spectroscopic data were acquired with a point resolved spectroscopy sequence without water suppression (PRESS ^{1}H-spectroscopy; TR, 2,500 ms; TE, 28 ms; flip angle, 90°; voxel size, 1.0 × 3.1 × 1.0 mm^3; 128 averages; acquisition time, 335 s). The measurement volume was set within the iBAT depot (Fig. 1 C inset). For each individual mouse five spectra were acquired, one spectrum before subcutaneous NA injection and four consecutive spectra with an overall time span of 22 min (after injection).

Twelve mice [WT (n = 5), UCP1-KO (n= 7)] were subjected to ^{31}P-spectroscopic examination for energy-rich phosphates. For these measurements, a custom transmit/receive surface coil (16 × 16 mm in diameter) that was tuned to phosphorus Larmor frequency at 7 T (121.62 MHz) was built in-house (supplementary Fig. I). The coil was mounted on a curved tube section (20 × 40 mm) to ensure an optimal placement on the mouse's neck. The phosphorus spectroscopy was acquired using a free induction decay sequence (TR, 450 ms; 1,024 averages; flip angle, 50°; acquisition time, 461 s), i.e., an unlocalized sequence, which presupposes a precise coil localization on the interscapular region to obtain specific data of the BAT. The correct placement of the ^{31}P-coil on the interscapular region (the coil was marked with an adalat capsule, see Fig. 1 D inset) and the localization of the target volume for spectroscopy were controlled with sagittal, coronal, and transversal ^{1}H-imaging sequences via the integrated body coil insert of the tomograph. Adjustments of the MRI scanner were controlled manually and optimized in a 9.0 × 3.0 ×

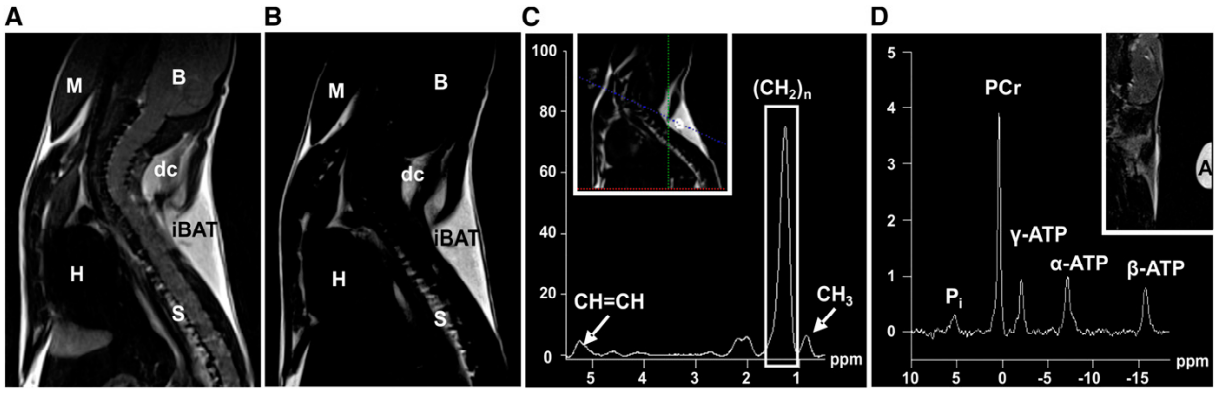

Fig. 1. Representative MRI and MRS acquired from the neck area of WT mice acclimated to 18°C ambient temperature. Overview of the neck area using a T2-weighted imaging sequence (A) and a T1-weighted sequence with water suppression (B). B, brain; M, muscle; H, heart; S, spinal cord; dc, dorsocervical brown fat depot; iBAT, interscapular brown fat depot. C: Single voxel ^{1}H-spectrum from selected region within iBAT (see inset) with eight peaks. The integral value of the $(CH_2)_n$ peak at 1.3 ppm was used as indicator for the lipid content. (A), (B), and (C) were acquired from the same individual. D: ^{31}P-spectrum from the neck area with the five major peaks. P_i, inorganic phosphates; A, adalat capsule marks the center of the surface coil.

9.0 mm^3 volume of the neck, including the interscapular and dorsocervical BAT depot, using advanced shimming options of the device. We acquired four spectra of each individual mouse, one before subcutaneous NA injection and three consecutive spectra with an overall time span of 23 min (after injection).

All MRI data were post processed and analyzed with the Syngo software (Siemens Healthcare, Erlangen, Germany).

Analysis of iBAT volume and composition

The volume of the iBAT (cm^3) was calculated for each mouse individually on the basis of sagittal T1-weighted images. The interscapular depot is the biggest of several BAT depots in mice and appears in sagittal slices as a triangular structure in the shoulder region (Fig. 1A, B). To determine the volume of the iBAT, the area of the fat depot was manually drawn on each slice. The sum of all areas was calculated and multiplied by slice thickness (0.08 cm).

The lipid content of BAT was calculated from ^{1}H-spectroscopy. Spectroscopic data were post processed as follows: Gaussian-filter with 256 ms width, zero filling to 2,048 points, Fourier transformation, phasing, frequency shift [$(CH_2)_n$ signal was set to 1.3 ppm], baseline correction, frequency shift [$(CH_2)_n$ signal set to 1.3 ppm], curve fitting. This protocol was adapted for the ^{1}H-spectrum of each mouse before NA injection and was then used with little adjustments in baseline correction, second frequency shift, and curve fitting for the spectra acquired after injection. The n-methylene peak $(CH_2)_n$ at 1.3 ppm integral value was used as an indicator of lipid content (Fig. 1C). Further, the integral values of the CH_3 peak at 0.9 ppm and of the CH=CH peak at 5.3 ppm were determined. The $(CH_2)_n$/CH=CH peak ratio and the CH=CH/(2/3CH_3) peak ratio that represents the mean unsaturation of lipids [according to (35)] were calculated from each spectrum before and 16.5 min after NA injection to get more information about unsaturated fatty acids during thermogenesis. Representative in vivo spectra of white fat have been shown previously (36, 37).

In vivo measurement of lipid content

In order to calculate the absolute lipid content in milligrams from the $(CH_2)_n$ peak integral value of the ^{1}H-spectra, we calibrated our assay with suspensions of oil and water using the same protocol as described for the in vivo measurements. The oil phantoms (extra virgin olive oil, Brändle, Empfingen, Germany) contained 20, 40, 60, and 80% oil by volume. The mixture was homogenized by ultrasonic disruption (Sonifier B-12, Branson Sonic Power Company, Danbury, CT). The correlation between the known percentage of lipid in the suspension and the $(CH_2)_n$ peak from proton spectroscopy was evaluated and, as a result, a conversion factor of 0.000286 was received that could be used to convert the peak integral values into milligrams of lipid.

In vivo measurement of energy-rich phosphate levels by phosphorus spectroscopy

Spectroscopic data were post processed with the following protocol: Gaussian-filter with 50 ms width, zero filling to 1,024 points, Fourier transformation, frequency shift [phosphocreatine (PCr) signal was set to 0 ppm], phase correction, baseline correction, frequency shift (PCr signal set to 0 ppm), curve fitting. The post processing protocol was adapted for the ^{31}P-spectrum of each mouse before NA injection and was then applied to the spectra acquired after injection.

Peak integrals were measured for inorganic phosphate, PCr, and α-, β-, and γ-ATP (Fig. 1D). For the purpose of detecting changes in ATP levels, we nominated the PCr/β-ATP ratio as an indicator for the PCr/ATP ratio and the β-ATP/α-ATP ratio as an indicator for ATP/ADP ratio.

BAT wet weight

Fourteen mice acclimated at 5°C ambient temperature (six WT mice and eight UCP1-KO mice) were euthanized after the magnetic resonance measurement. The iBAT depot was dissected and immediately weighed (Kern PB, Kern and Sohn GmbH, Germany). A correlation was calculated between iBAT wet weight and the volume of iBAT as estimated via MRI.

Measurement of oxygen consumption

The metabolic response to NA of mice acclimated to 30°C, 18°C, and 5°C was measured using an open circuit respirometry system with a short response time. Oxygen consumption and carbon dioxide production were measured as it has been described previously (38). Single mice were transferred to 1.8 l cages without food and water and were then placed in a temperature controlled climate chamber at 26°C (KPK 600, Feutron, Germany). A temperature of 26°C, which is just below thermoneutrality, was

chosen to prevent the development of hyperthermia in response to NA injections. Mice were habituated to the calorimetric system for 60–210 min and their resting oxygen consumption was measured. Then the mice were briefly removed from the system for subcutaneous injection of 1 mg NA per kilogram body weight. Air was pumped through the cages with a flow rate of 35 ± 0.5 l/h, dried by an electric freeze trap (M and C Cooler, ECM, Ratingen, Germany) and the airflow was continuously monitored for each channel by an electronic mass flow meter (FM 360, Tylan, München, Germany). O_2 and CO_2 content of the air were measured with a two-channel O_2 analyzer (S3AII, Ametek, Sunnyvale, CA) and a two-channel CO_2 analyzer (UNOR 6N, Maihak AG, Hamburg, Germany) with a resolution of 0.001 Δvol% comparing the air entering and leaving the metabolic cuvettes. The readout interval was set to 20 s and the air of an empty cage was measured before and after the NA test and was used for zero readjustment afterwards. The resting metabolic rate of mice was calculated from the lowest mean of 12 consecutive O_2 readings, i.e., a 4 min interval. Resting metabolic rate was subtracted from the oxygen consumption after NA injection to acquire the nonshivering thermogenic capacity. This is a standard procedure for the measurement of NST capacity in nonanesthetized mammals and we used it to facilitate comparison of UCP1-KO mice and WT mice as well as comparison with previous studies.

Statistical analysis

Mean values ± standard error of mean (SEM) are presented. For comparison between the two genotypes a Student's *t*-test for each acclimation temperature was used. When normal distribution of data could not be assumed, the groups were compared with the Mann-Whitney rank sum test. Changes in lipid content and phosphometabolites after NA injection were analyzed by two-way repeated-measures ANOVA followed by a Holm-Sidak comparison test (factors genotype and time point). The acclimation groups (30°C, 18°C, and 5°C) included independent as well as connected measurements where the same mice were measured following acclimation to different temperatures. Therefore, we used the data of each temperature acclimation step for descriptive statistics but analyzed only connected measurements with paired *t*-test statistics. All calculations were performed using SigmaStat 3.5. The overall level of significance was set to $P \leq 0.05$.

RESULTS

Heterogeneity of BAT

The iBAT changed its structure during cold acclimation (**Fig. 2**). T1-weighted images revealed that the relatively hyperintense areas of iBAT in warm-acclimated mice, indicating a shorter T1-time due to a higher lipid content, were replaced by hypointense areas, indicating a longer T1-time due to greater water and mitochondria content in cold-acclimated mice (Fig. 2A, B). Using proton spectroscopy, we found a significantly higher lipid content in iBAT of warm-acclimated mice. The lipid content of 30°C-acclimated mice was about three times higher than during cold acclimation at 5°C (**Table 1**). At all acclimation temperatures WT and UCP1-KO mice had the same lipid content in the tissue section used for lipid spectroscopy, i.e., in the core area of iBAT (Fig. 2C). Angiography of the neck area revealed a high vascularization and displayed the arterial vessels of the bilateral interscapular lobes and the Sulzer's vein (supplementary Video I).

Heterogeneity within iBAT was pronounced in WT mice (Fig. 2A) and in UCP1-KO mice (Fig. 2B) acclimated at 18°C. The medial core of iBAT contained more cytoplasm and mitochondria, as indicated by the hypointense signal, whereas the dorsal periphery showed a hyperintense signal. The medial core volume of iBAT was not different in WT compared with UCP1-KO mice at 18°C and 30°C. But it was larger in 5°C-acclimated WT mice than in KO mice ($P = 0.002$). The volume of the whole iBAT did not differ between the genotypes (Fig. 2D).

The iBAT volumes of mice acclimated to 5°C obtained from MRI were compared with their iBAT wet weights. The data indicated a linear relation: y = 1.07 (± 0.4) x + 17.0 (± 40.6) (supplementary Fig. II).

Lipid loss during NA-induced thermogenesis

We monitored the lipid content of iBAT during NA-induced thermogenesis with consecutive proton spectroscopy. The lipid content in iBAT decreased after NA application in WT mice and in UCP1-KO mice at all acclimation temperatures (**Fig. 3**). This response was faster in WT than in UCP1-KO mice, i.e., the lipid content in WT mice was lowered significantly within 5.5 min after NA injection, while a significant loss of lipids in UCP1-KO mice could first be detected after 11 min. Because cold-acclimated WT and KO mice had lower initial lipid contents, their relative loss of lipids was more pronounced than in warm-acclimated mice (Fig. 3A). The absolute amount of lipid loss was greater in WT mice than in UCP1-KO mice, but it was not affected by the acclimation status of mice (Fig. 3B). It ranged between 9 and 12 mg in WT mice and between 5 and 8 mg in UCP1-KO mice 16.5 min after NA injection (Table 1).

In order to investigate whether fatty acid composition changed during NST we calculated the mean unsaturation (CH=CH/(2/3CH_3) and the $(CH_2)_n$/CH=CH ratio of iBAT. The ratios did not differ between the genotypes. Mean unsaturation (30°C: WT = 1.3 ± 0.2, KO = 1.9 ± 0.2; 5°C: WT = 3.2 ± 0.6, KO = 2.5 ± 0.2) and the $(CH_2)_n$/CH=CH ratio (30°C: WT = 11.6 ± 1.6, KO = 9.4 ± 0.7; 5°C: WT = 10.4 ± 0.7, KO = 9.6 ± 0.8) of iBAT were maintained during the first 16.5 min of NA-induced NST.

Thermogenic response to NA

The injection of NA caused a rapid increase of metabolic rate in WT and UCP1-KO mice, reaching a maximum at about 17 min (**Fig. 4A**). Cold acclimation enhanced the maximal metabolic rate after NA stimulation in WT mice as well as in UCP1-KO mice (Fig. 4B). The increase in maximal thermogenic response following cold acclimation was accompanied by an increase of resting metabolic rate, which was not significantly different between genotypes (Fig. 4C). But the NA-induced capacity for NST (difference between maximum metabolic rate after NA and resting metabolic rate) was about 4-fold greater in cold-acclimated than in warm-acclimated WT mice. UCP1-KO mice also showed an increase of nonshivering thermogenic capacity following cold acclimation (**Table 2**).

The nature of this response to NA was further analyzed by simultaneous recordings of metabolic rate, heart

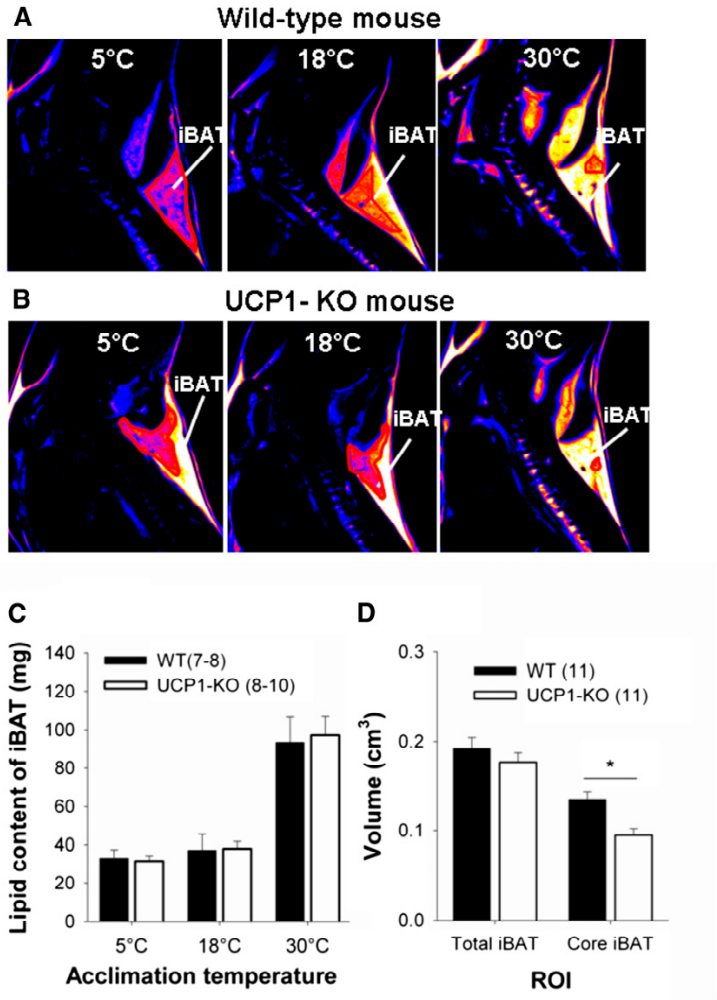

Fig. 2. Differences in BAT signal and volume of WT and UCP1- KO mice depending on acclimation temperature and genotype. Representative T1-weighted MR images acquired from a WT mouse (A) and a UCP1-KO mouse (B) sequentially acclimated to 30°C, 18°C, and 5°C. The biggest brown fat depot in the neck area is the iBAT. Images are shown in sagittal view and presented in pseudocolor "hot metal" where bright color encodes for hyperintense signal. C: Lipid content in iBAT of WT and UCP1-KO mice sequentially acclimated to 30°C, 18°C, and 5°C. The $(CH_2)_n$ peak of the proton-spectroscopy was used to calculate the lipid content. D: iBAT volume of WT and UCP1-KO mice acclimated to 5°C. The volume of the total iBAT depot as well as the volume of the darker core region of the iBAT depot [see red line in (A, B)] were calculated. Therefore, the respective areas from each slice were summed up and multiplied by the slice thickness. The core area of the iBAT of WT mice was significantly bigger compared with UCP1-KO mice ($P = 0.002$).

rate, ventilation rate, and the respiratory quotient in anesthetized mice (supplementary Fig. III). UCP1-KO mice responded to NA by a rapid increase in heart rate, which was identical to the response in WT mice. They also raised their metabolic rate and ventilation rate and showed a slight decrease of the respiratory quotient. These responses were less pronounced than in WT mice.

TABLE 1. Lipid content and lipid loss of BAT during 16.5 min NA-induced thermogenesis

Acclimation Temperature	Genotype	n	Lipid Content of iBAT before NA (mg)[a]	Lipid Content of iBAT 16.5 min after NA (mg)[a]	Lipid Loss of iBAT (mg/16.5 min)	Estimated Lipid Loss of Total BAT (mg/16.5 min)[b]
30°C	WT	8	97.19 ± 13.0	82.04 ± 11.8	11.37 ± 2.5	28.42 ± 6.3
	UCP1-KO	8	93.41 ± 9.6	88.92 ± 8.7	8.28 ± 2.3	20.69 ± 5.8
18°C	WT	7	37.18 ± 8.3	25.46 ± 6.0	11.72 ± 3.1	29.29 ± 7.8
	UCP1-KO	10	38.02 ± 3.8	32.28 ± 2.4	5.74 ± 1.9	14.35 ± 4.7
5°C	WT	8	32.89 ± 4.6	23.63 ± 3.4	9.26 ± 1.6	23.15 ± 4.1
	UCP1-KO	10	31.37 ± 2.8	26.02 ± 2.2	5.35 ± 1.8*	13.38 ± 4.37*

Calculations are based on proton spectroscopy of the iBAT depot. UCP1-KO and WT mice were sequentially acclimated to ambient temperatures of 30°C, 18°C, and 5°C. Values are means ± SEM. Statistically significant differences between the genotypes at each acclimation temperature ($P \leq 0.05$) are indicated with *.

[a]Calculation of lipid content from proton spectroscopy: lipid (mg) = I × V × A/B. I, integral of $(CH_2)_n$ peak from lipid spectrum; V, iBAT volume regarding MRI; A = 0.000286, conversion factor calculated from oil phantoms with lipid spectroscopy; B = 0.0031 ml, volume of interest in single voxel proton-spectroscopy.

[b]Lipid consumption of total BAT = (lipid content of iBAT before NA − lipid content of iBAT after NA) × 100/40. We estimated that the iBAT accounts for 40% of total BAT. According to Heldmaier (7) iBAT of albino mice makes up 50% of total BAT (without the perirenal depot). According to Thurlby and Trayhurn (21) iBAT of "Aston" mice makes up 34% of total BAT (without periaortic sites). According to own observations iBAT of C57/Bl6 mice represents 52% of total BAT (without perirenal and subventral depots).

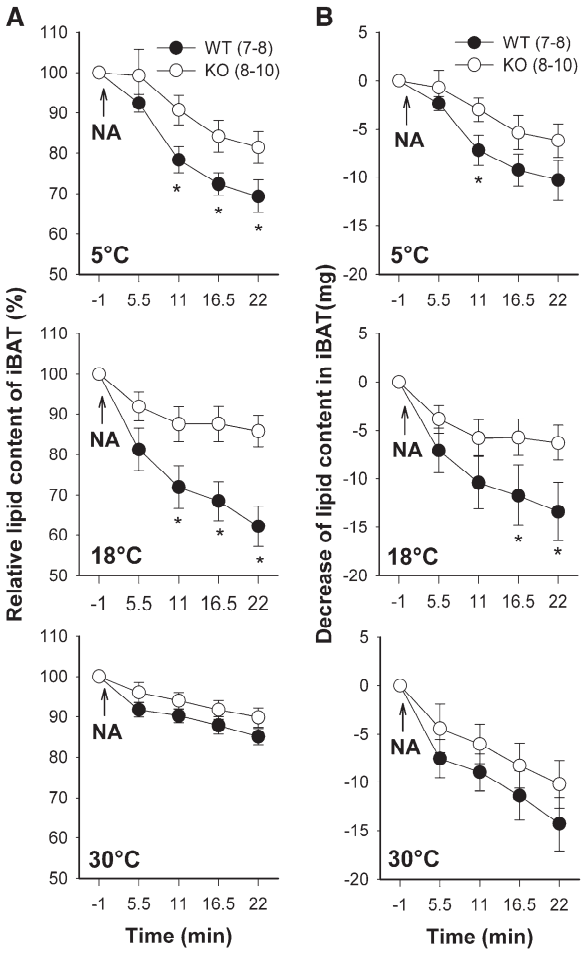

Fig. 3. Reduction of lipid content in the iBAT depot of WT and UCP1-KO mice during NA-stimulated NST. Mice were sequentially acclimated to 30°C, 18°C, and 5°C ambient temperature. NA was administered at time point zero and lipid content was monitored over a time span of 22 min after NA injection with consecutive proton spectroscopy using the $(CH_2)_n$ peak as indicator. Lipid content before administration of NA was set to 100% (A). Integral values of the $(CH_2)_n$ peak were converted into milligrams of lipid (B). A statistically significant difference between the genotypes at the same time point ($P \leq 0.05$) is indicated with *. Values are means ± SEM

In vivo lipid oxidation during NA-induced thermogenesis

Thermogenesis in BAT is fueled by lipids. We evaluated whether the loss of lipid from iBAT was in accordance with the amount of lipid actually oxidized during thermogenesis. The increase of oxygen consumption during 16.5 min of NA-induced thermogenesis was used to calculate the amount of lipids oxidized during this period for each individual mouse (2.01 ml O_2 per milligram lipid) (Fig. 4D). WT mice required more lipids to fuel NST than UCP1-KO mice at all acclimation temperatures, as can be expected from the greater metabolic response of WT mice (Fig. 4E, **Table 3**).

However, if these values were compared with the actual depletion of lipids in BAT measured with ^{1}H-spectroscopy, it revealed that all mice lost more lipids from BAT than actually required for the thermogenic activity of this tissue (**Fig. 5**). BAT thermogenesis of 5°C-acclimated WT mice, for example, combusted 7.37 mg of lipids during the measurement period of 16.5 min (Table 3), but they actually lost 23.15 mg from BAT during this time (Table 1). In warm-acclimated mice this discrepancy was even greater, they combusted 2.55 mg but lost 28.42 mg of lipids. This discrepancy was also observed in UCP1-KO mice, indicating that lipid loss is not functionally linked to uncoupled respiration of BAT mitochondria. The lipid loss of total BAT was reduced in 5°C-acclimated UCP1-KO as compared with WT mice ($P = 0.046$).

In vivo ATP levels in BAT during NA-induced thermogenesis

UCP1 uncouples oxidative phosphorylation from the respiratory chain, suggesting that ATP levels in brown adipocytes are changing during NST. Therefore, we analyzed the levels of energy-rich phosphates in BAT in vivo during NA-induced thermogenesis with phosphorus MRS. During thermogenesis the levels of all phosphates were maintained constant. Neither the PCr/ATP ratio (**Fig. 6A**) nor the ATP/ADP ratio (Fig. 6B) showed any response. The phosphate ratios of UCP1-KO mice, which cannot uncouple ATP synthesis from the respiratory chain, were identical with the phosphate ratios measured in WT mice. We pooled the data of WT and UCP1-KO mice before NA injection and found a significantly lower ($P = 0.035$) PCr/ATP ratio in cold-acclimated mice (3.16 ± 0.27) than following 30°C acclimation (4.02 ± 0.27). The ATP/ADP ratio showed a trend ($P = 0.062$) to higher values in cold-acclimated mice. Both results indicated an increased ATP level in the iBAT of cold-acclimated mice.

DISCUSSION

Structural changes of BAT during cold acclimation

The iBAT depot of mice did not present a uniform structure in our T1-weighted images, but it separated into a hypointense core and a relatively hyperintense dorsal periphery. This suggests a core area where brown adipocytes contain more cytoplasm and mitochondria, and thus the potential for a greater metabolic activity. In contrast, the brown adipocytes in the peripheral area are rich in lipids and contain less cytoplasm and mitochondria. An internal differentiation of BAT was not visible with CT imaging (39), while different layers of interscapular brown fat were described before in rats and mice using MRI (30, 32). Activation of BAT with adrenaline confirmed a higher metabolic activity in the core region of this organ (40). In mice, metabolically active BAT has been detected recently with T2-weighted MRI, as a signal loss of about 20% occurred due to decreased blood oxygenation in the tissue (41).

During cold adaptation, the hypointense core area of the interscapular lobe expanded toward the periphery. In 5°C-acclimated WT mice the entire interscapular lobe

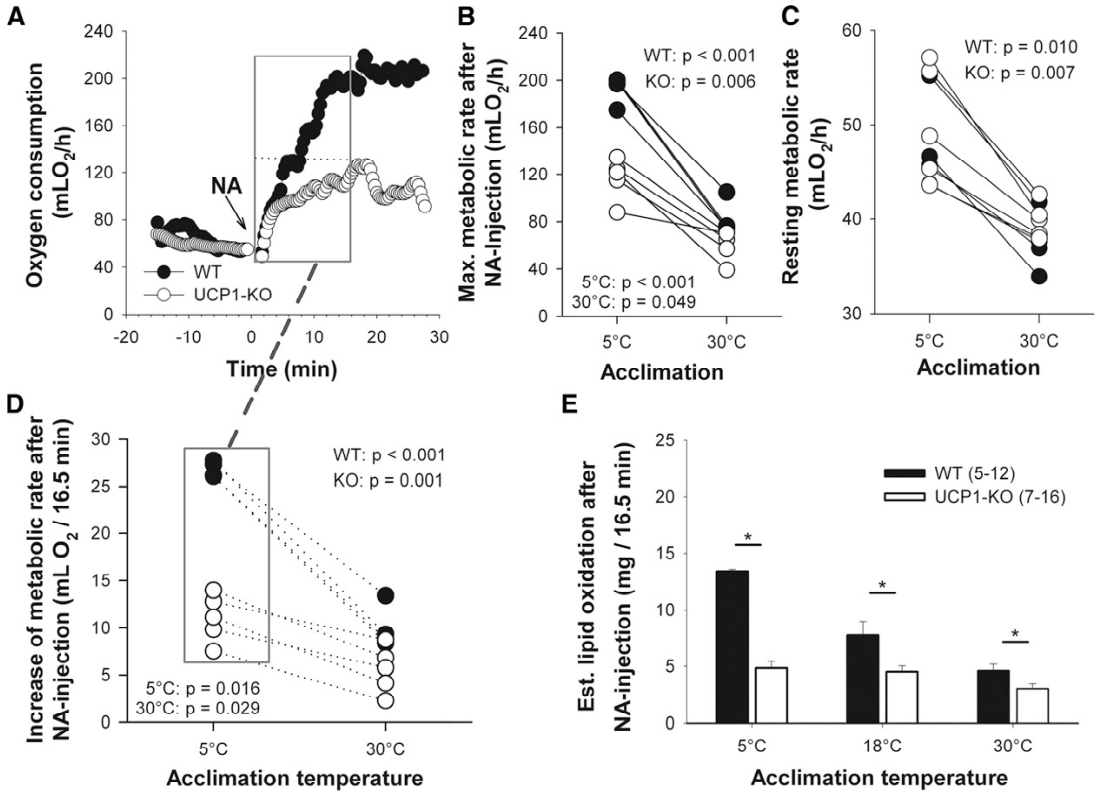

Fig. 4. Metabolic responses of mice to NA measured by indirect calorimetry. Representative oxygen consumption of a WT and a UCP1-KO mouse acclimated to 5°C ambient temperature (A). NA was injected at time point zero. Maximum (Max.) metabolic rate reached after NA injection (B) and resting metabolic rate (C) of the same individuals (WT mice, n = 4; UCP1-KO mice, n = 5) following 30°C and 5°C acclimation. The number of animals is lower than in Tables 2 and 3 because only connected measurements were included in the graph (corresponding values are connected by lines). The increase of metabolic rate during 16.5 min of NA-induced thermogenesis (D) (see gray box in A) was used to calculate the amount of oxidized lipids during this time span (E). For calculation of lipid oxidation, it was assumed that solely palmitate was metabolized. Values are means ± SEM. A statistically significant difference between the genotypes at each acclimation temperature ($P \leq 0.05$) is indicated with *.

became hypointense, i.e., all adipocytes were converted into the metabolically active form with a reduced lipid content, indicating a higher metabolic and thermogenic capacity. Cold-acclimated UCP1-KO mice also showed a core area with reduced lipid content in their iBAT, but only a part of the tissue lobe converted into the metabolically active form. Cold adaptive changes of BAT largely depend upon the activity of its sympathetic innervation (42, 43), as has been demonstrated in studies about denervation of BAT (44–47). The present findings show that the reorganization of BAT during cold acclimation toward an improvement of its thermogenic capacity occurs in the absence of UCP1, although a slightly reduced intensity was observed as compared with WT mice. This suggests a feedback of UCP1 or uncoupled mitochondrial respiration on the full deployment of BAT thermogenic capacity.

TABLE 2. Resting metabolic rate, maximal metabolic rate after NA, and capacity of NST

Acclimation Temperature	Genotype	n	Resting Metabolic Rate[a]	Maximal Metabolic Rate after NA[a]	NST Capacity after NA[a]
30°C	WT	5	36.65 ± 1.6	75.97 ± 8.9	39.32 ± 7.5
	UCP1-KO	7	41.17 ± 1.3	61.07 ± 4.7	19.90 ± 4.2*
18°C	WT	12	46.23 ± 0.9	175.21 ± 3.6	128.98 ± 3.8
	UCP1-KO	16	46.01 ± 0.9	96.48 ± 2.9*	50.47 ± 2.8*
5°C	WT	5	47.21 ± 2.1	200.77 ± 9.4	153.56 ± 10.1
	UCP1-KO	7	47.52 ± 2.5	107.46 ± 8.3*	59.94 ± 7.0*

NST capacity is the difference between resting metabolic rate and maximum metabolic rate after NA injection. UCP1-KO and WT mice were sequentially acclimated to ambient temperatures of 30°C, 18°C, and 5°C. Values are means ± SEM. Statistically significant differences between the genotypes at each acclimation temperature ($P \leq 0.05$) are indicated with *.

[a]Values are in milliliters of O_2 per hour.

TABLE 3. Increase of metabolic rate and the estimated lipid oxidation of mice during 16.5 min NA-induced thermogenesis

Acclimation Temperature	Genotype	n	Increase of Metabolic Rate[a,b]	Estimated Lipid Oxidation of Whole Body[a,c]	Estimated Lipid Oxidation of Total BAT[a,d]
30°C	WT	5	9.31 ± 1.1	4.63 ± 0.6	2.55 ± 0.3
	UCP1-KO	7	6.12 ± 0.9*	3.04 ± 0.4*	1.67 ± 0.2*
18°C	WT	12	23.34 ± 0.9	11.60 ± 0.5	6.38 ± 0.3
	UCP1-KO	16	10.30 ± 0.6*	5.12 ± 0.3*	2.82 ± 0.15*
5°C	WT	5	26.98 ± 0.4	13.41 ± 0.2	7.37 ± 0.1
	UCP1-KO	7	9.76 ± 1.2*	4.85 ± 0.6*	2.67 ± 0.3*

Lipid oxidation is calculated from original measurements of oxygen consumption measured via indirect calorimetry. UCP1-KO and WT mice were sequentially acclimated to ambient temperatures of 30°C, 18°C, and 5°C. Values are means ± SEM. Statistically significant differences between the genotypes at each acclimation temperature ($P \leq 0.05$) are indicated with *.

[a]Values are in milliliters of O_2 per 16.5 min.

[b]Increase of metabolic rate (milliliters of O_2/16.5 min) = amount of consumed oxygen after NA injection in 16.5 min − resting metabolic rate.

[c]Lipid oxidation whole body = metabolic rate (milliliters of O_2)/A × B. A = 515.2 l O_2/mol palmitate, necessary amount of oxygen for oxidation of 1 mol palmitate; B = 256 g/mol, molar weight of palmitate.

[d]Lipid oxidation of total BAT = lipid oxidation whole body × 0.55, estimating that BAT contributes 55% of NST [Thurlby and Trayhurn (21)].

BAT ATP levels during thermogenesis

BAT mitochondria have a relatively low capacity for ATP synthesis as compared with their respiratory potential [for review see (48)]. During thermogenesis mitochondrial respiration is uncoupled from ATP synthesis, including the risk that ATP levels in the cells are coming under pressure. Therefore, we analyzed the phosphate levels during NA-induced thermogenesis in vivo by MRS. Cold-acclimated mice had slightly lower PCr/ATP ratios and slightly higher ATP/ADP ratios, but these ratios did not change during sympathetic activation of thermogenesis, neither in WT nor in UCP1-KO mice. The constant ATP/ADP ratio suggests that ATP is still generated at a sufficient rate to cover the cellular needs for enzyme activation and biosynthesis. Maintenance of ATP levels during thermogenesis should be especially demanding for WT mice, whereas UCP1-KO mice should face no problems with ATP supply. The stable ATP levels in WT mice indicate that either oxidative phosphorylation is not completely prevented during NST or that other sources of ATP may compensate for mitochondrial deficits of ATP production, e.g., glycolysis (49). BAT utilizes glucose at high rates and may consume up to 12.5% of the entire glucose consumption in mice, although it amounts to only about 1% of total body mass (50). Glucose may be used for synthesis of fatty acids as well as for a glycolytic breakdown to pyruvate, lactate, and acetyl-CoA. During thermogenic stimulation rats released lactate and pyruvate from BAT accounting for 33% of the glucose uptake (51). This suggests an enhancement of glycolysis which could be a potential source of ATP. Cold acclimation also increases the activity of key enzymes for glycolysis, indicating that an increase in the capacity for uncoupled respiration is accompanied by an enhancement of glycolysis (52).

BAT lipid metabolism during thermogenesis

During NA-induced NST the lipid content of BAT decreased by about 30% within 16.5 min. A loss of lipids can be expected because β-adrenergic thermogenesis in BAT is largely fueled by lipids [for review see (3)]. However, the absolute amount of lipids decreased from BAT was much greater than could have been consumed during thermogenesis, e.g., cold-acclimated WT mice lost three times the amount of lipids that were required for thermogenesis in brown fat, as calculated from oxygen consumption during the same period of time. In warm-acclimated mice this discrepancy was even greater, i.e., 11 times more lipids were lost from BAT than actually consumed. For the direct comparison of lipid loss acquired from MRS and lipid oxidation acquired from indirect calorimetry, we assumed that iBAT represents 40% of total BAT (see footnotes of Table 1). So, the projected results of lipid loss and lipid oxidation are estimates. However, these are minimum estimates because lipid loss was measured in anesthetized mice during 16.5 min with MRS, whereas the metabolic rate for NST was measured for 16.5 min in nonanesthetized mice. Anesthesia reduces resting metabolic rate prior to NA as well as the maximal metabolic response to NA. The combination of both effects may reduce peak metabolic rates by up to 50% (11, 53) suggesting that lipid turnover is also reduced during MRS in anesthetized mice as compared with nonanesthetized mice. Considering the fact that NA-induced thermogenesis also increases glucose uptake and utilization in BAT, we suggest that the lipid oxidation is lower as assumed and lipid loss may be even greater than 11 times as compared with metabolic rate (51, 54).

An exaggerated mobilization and export of fatty acids from adipocytes was also observed in vitro following noradrenergic stimulation (18, 55, 56). The in vitro observations suggest that the export of fatty acids is a native property of brown adipocyte metabolism. In vivo studies measuring plasma levels and arteriovenous concentration differences revealed a release of glycerol and fatty acids from BAT during cold exposure, as well as β-adrenergic stimulation in mice (57, 58), rats (51, 59), and in humans (60). In Djungarian hamsters the plasma level of fatty acids was almost doubled during NA-induced thermogenesis,

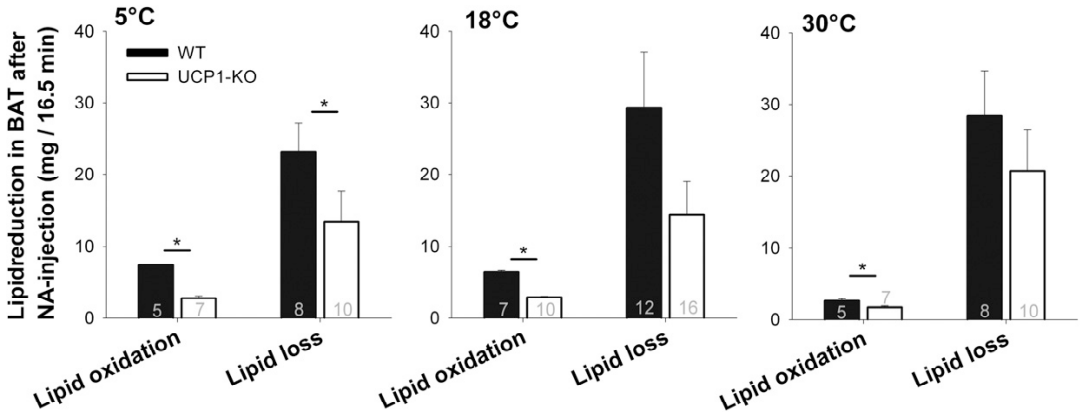

Fig. 5. Change in lipid levels through lipid oxidation and lipid loss in total BAT during 16.5 min NA-induced thermogenesis. WT and UCP1-KO mice were sequentially acclimated to 30°C, 18°C, and 5°C. Lipid loss and lipid oxidation were calculated over a time period of 16.5 min. Sample sizes are shown inside bars. Values are means ± SEM. Statistically significant differences in lipid loss or lipid oxidation comparing WT and UCP1-KO mice at each acclimation temperature ($P \leq 0.05$) are indicated with *.

as well as during cold exposure, and the release of fatty acids could be inhibited by blockade of adrenergic β-receptors (19).

Cold exposure and β-adrenergic stimulation of thermogenesis not only mobilize fatty acids in BAT, but also stimulate the uptake of fatty acids as was demonstrated in mice and humans (60, 61). Lipoprotein lipase is anchored to the periphery of brown adipocytes and liberates fatty acids from circulating lipoproteins, thus allowing the import of fatty acids. The activity of this enzyme is rapidly increased during cold exposure (13, 62, 63). This demonstrates that β-adrenergic stimulation of BAT simultaneously increases lipolysis and the oxidation of fatty acids as well as the uptake and the export of fatty acids, i.e., the turnover of lipids is exaggerated well beyond its need for fueling BAT metabolism. This response of BAT supports the view that its sympathetic activation induces heat production via UCP1 and additionally enhances triglyceride clearance (61). The mechanism of fatty acid action on UCP1 activation and on proton conductance of the mitochondrial membrane is still not clear. Current hypotheses prefer a direct action on UCP1 and suggest a flip-flop model or that fatty acids act as a cofactor on UCP1 (64, 65). No matter which mechanism might be in operation, the high turnover of lipids and fatty acids provides a high intracellular level of long chain fatty acids, thus facilitating the thermogenic uncoupling of brown fat mitochondria.

Physiological role of brown fat

BAT is considered to be the main contributor to NST in small mammals, but the magnitude of its contribution and the involvement of other tissues are still unclear. Blood flow studies with radioactively labeled microspheres estimate that about 60% of the thermogenic response is due to brown fat metabolic activity in rats, mice, and hamsters (21, 66, 20). In turn this indicates that other tissues contribute to total NST. Surgical removal of BAT or tying the Sulzer vein caused rather complex results. In one report rats did not reduce their capacity for NST immediately following removal of the interscapular lobe of brown fat (67), whereas other studies reported a reduction of the thermogenic capacity by about 16% (68, 69). In a more detailed study with stepwise partial removal of BAT from several lobes in Djungarian hamsters, it was estimated that in warm-acclimated hamsters 50% of NST can be ascribed to the respiratory capacity of BAT and this percentage increases to 85% following cold adaptation (70), indicating that 50% and 15% of heat is generated by other tissues, respectively.

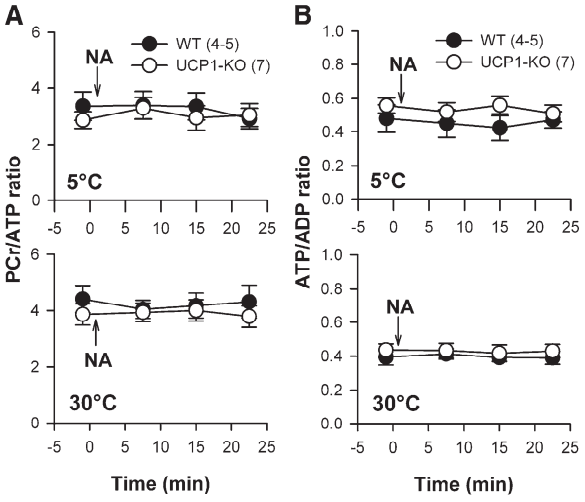

Fig. 6. PCr/ATP ratio (A) and ATP/ADP ratio (B) during NA-induced thermogenesis in WT and UCP1-KO mice acclimated to 30°C and 5°C ambient temperature. ^{31}P-spectroscopy was performed before and three times after NA stimulation in the neck region of mice. The β-ATP peak from the phosphate spectrum represents mainly ATP and was therefore used as ATP index. The α-ATP peak contains signal from ATP and ADP molecules. Therefore, the β-ATP/α-ATP peak ratio reflects the ATP/ADP ratio. Values are means ± SEM.

UCP1-KO mice can tolerate long term exposure to 4°C after a stepwise reduction of ambient temperature (23, 26, 71). In the present study, we showed a thermogenic response to NA which was enhanced following cold acclimation, indicating an adaptive increase of NST despite the lack of UCP1 in brown adipocytes. In accordance with our results, a thermogenic response to NA in UCP1-KO and UCP1-dta mice has been described previously (23, 72). In contrast, Golozoubova et al. (24), Nedergaard et al. (71), and Cannon and Nedergaard (73) did not observe an increase in the noradrenergic thermogenic response in these mice following cold acclimation at 18°C and therefore define "adaptive NST" as strictly limited to UCP1-mediated uncoupling of oxidative phosphorylation in brown adipocytes. They explain the increased cold tolerance of UCP1-KO mice by an adaptive improvement of shivering thermogenesis (24, 71, 73). However, cold-adapted UCP1-KO mice did not show any changes in gene expression, mitochondrial DNA, or respiratory capacity of isolated muscle tissue, which could support an increased contribution of skeletal muscle tissue to thermogenesis (23, 26, 72). During NA-induced thermogenesis, blood flow in skeletal muscle remained constant or even decreased, which contradicts a significant contribution to NST (20, 21, 66). Blood flow through the ventricular muscle tissue increased during NST and this response was enhanced following cold acclimation (20). In the current study, we observed a prominent increase of heart rate in WT and UCP1-KO mice (supplementary Fig. III), supporting the view that enhanced cardiovascular activity contributes to the UCP1-independent nonshivering thermogenic response.

More and more evidence is accumulating that heat dissipation from BAT is supported by white adipose tissue in order to maintain body temperature. During cold exposure, white adipose tissue of UCP1-KO mice shows changes in gene expression, enzyme activities, and cytochrome c oxidase activity as well as an increase of mRNA levels, suggesting that white adipose tissue may contribute to the adaptive improvement of NST (23, 26). In WT mice, UCP1-expressing beige adipocytes with an enhanced respiratory capacity can be recruited within white adipose tissue depots and may be involved in the global lipid clearance during NST (26, 74–76). Cold acclimation stimulates the recruitment of these cells and this response may be enhanced by a paucity of BAT cells (77).

Thermogenesis itself requires cooperation of brown and white adipose tissue. The noradrenergic stimulation of brown adipocytes causes lipolysis and reesterification simultaneously and a large portion of liberated fatty acids are exported into the bloodstream raising the plasma level of FFAs. The high rate of lipid mobilization in UCP1-KO mice in our study suggests that lipid cycling is not functionally linked to the presence of UCP1. In birds, which entirely lack UCP1, an activation of white adipocytes was observed when mesenchymal stem cells were treated with PPARγ, a coactivator which is specific for the differentiation of brown adipocytes. This indicates that the potential for activation of white adipose tissue is a physiological property separate from the evolutionary presence of UCP1 (78). Recently it has been demonstrated that the respiratory capacity of white adipose tissue, and potentially also of BAT, may be enhanced by the presence of n-3 polyunsaturated fatty acids in the absence of UCP1 (79, 80). This increased turnover of n-3 polyunsaturated fatty acids could not be corroborated in our study, as the saturation index of BAT lipids did not change during NST.

The cycling of lipolysis and reesterification of lipids can also be enhanced by β-adrenergic stimulation in isolated white adipocytes [see (81, 82) for review]. During prolonged cold exposure, BAT requires a continuous supply of fatty acids to fuel thermogenesis and these can only be provided by the much larger depots of white adipose tissue. In summary, this suggests a tight functional link of brown and white adipose tissue thermogenesis and cold acclimation.

The simultaneous activation of lipolysis and reesterification suggests a futile cycling of lipid metabolism (83) and consumes 8 mol of ATP per release and reesterification of three molecules of fatty acids (80). This could even generate heat in white adipose tissue, provided there is a sufficient supply of ATP. The apparently unnecessary large capacity for lipolysis and lipid cycling in BAT suggests that the tissue is also a major effector of triglyceride clearance (61). Neither the excitation of lipid cycling nor the adaptive modification of brown or white adipocytes for mitochondrial proliferation and multilocular lipid storage requires UCP1, as we found in our study in accordance with (26, 80). This suggests that the mechanism of lipid clearance could be considered as a separate physiological function of BAT, in addition to its role in thermogenesis. The recent discovery of brown and beige adipose tissue in humans (76, 84, 85) may further elucidate this view. The amount of BAT in humans in relation to the body mass is quite small, and thus it may generate only small amounts of heat. However, recent evidence indicates that brown adipose mass and activity in humans is highly variable and can change in response to the nutritional state, ambient temperature, photoperiod, etc., and a positive contribution of thermogenically activated brown fat on energy expenditure may have been underestimated in the past [for review see (86)]. Lipid cycling induced in BAT during thermogenesis exceeds the fuel needs for thermogenesis by far. Its potential effect on lipid clearance may dominate over its thermogenic role, thus explaining and promising a beneficial effect of human BAT on the prevention of atherosclerosis, cardiovascular diseases, and obesity (16, 75).

The authors would like to thank M. Kutschke, N. Linklater, and R. Oelkrug for their helpful comments on the manuscript and J. Donges for the technical support.

REFERENCES

1. Hull, D. 1966. The structure and function of brown adipose tissue. *Br. Med. Bull.* **22:** 92–96.
2. Heldmaier, G., H. Böckler, A. Buchberger, G. R. Lynch, W. Puchalski, S. Steinlechner, and H. Wiesinger. 1985. Seasonal acclimation and thermogenesis. *In* Circulation, Respiration, and

Metabolism. R. Gilles, editor. Springer-Verlag, Berlin, Heidelberg. 490–501.
3. Cannon, B., and J. A. N. Nedergaard. 2004. Brown adipose tissue: function and physiological significance. *Physiol. Rev.* **84:** 277–359.
4. Heldmaier, G., S. Steinlechner, J. Rafael, and P. Vsiansky. 1981. Photoperiodic control and effects of melatonin on nonshivering thermogenesis and brown adipose tissue. *Science.* **212:** 917–919.
5. Bukowiecki, L., A. J. Collet, N. Follea, G. Guay, and L. Jahjah. 1982. Brown adipose tissue hyperplasia: a fundamental mechanism of adaptation to cold and hyperphagia. *Am. J. Physiol.* **242:** E353–E359.
6. Golozoubova, V., H. Gullberg, A. Matthias, B. Cannon, B. Vennström, and J. Nedergaard. 2004. Depressed thermogenesis but competent brown adipose tissue recruitment in mice devoid of all hormone-binding thyroid hormone receptors. *Mol. Endocrinol.* **18:** 384–401.
7. Heldmaier, G. 1974. Temperature adaptation and brown adipose tissue in hairless and albino mice. *J. Comp. Physiol.* **92:** 281–292.
8. Ashwell, M., G. Jennings, D. Richard, D. M. Stirling, and P. Trayhurn. 1983. Effect of acclimation temperature on the concentration of the mitochondrial "uncoupling" protein measured by radioimmunoassay in mouse brown adipose tissue. *FEBS Lett.* **161:** 108–112.
9. Lowell, B. B., and B. M. Spiegelman. 2000. Towards a molecular understanding of adaptive thermogenesis. *Nature.* **404:** 652–660.
10. Smith, R. E., and J. C. Roberts. 1964. Thermogenesis of brown adipose tissue in cold-acclimated rats. *Am. J. Physiol.* **206:** 143–148.
11. Heldmaier, G. 1971. Zitterfreie Wärmebildung und Körpergröße bei Säugetieren. *Z. Vgl. Physiol.* **73:** 222–248.
12. Foster, D. O., and M. L. Frydman. 1979. Tissue distribution of cold-induced thermogenesis in conscious warm- or cold-acclimated rats reevaluated from changes in tissue blood flow: the dominant role of brown adipose tissue in the replacement of shivering by nonshivering thermogenesis. *Can. J. Physiol. Pharmacol.* **57:** 257–270.
13. Carneheim, C., J. Nedergaard, and B. Cannon. 1984. Beta-adrenergic stimulation of lipoprotein lipase in rat brown adipose tissue during acclimation to cold. *Am. J. Physiol.* **246:** E327–E333.
14. Portet, R., M. C. Laury, R. Bertin, C. Senault, M. T. Hluszko, L. Chevillard, and J. Le Blanc. 1974. Hormonal stimulation of substrate utilization in brown adipose tissue of cold acclimated rats. *Proc. Soc. Exp. Biol. Med.* **147:** 807–812.
15. LaFrance, L., G. Lagacé, and D. Routhier. 1980. Free fatty acid turnover and oxygen consumption. Effects of noradrenaline in nonfasted and nonanesthetized cold-adapted rats. *Can. J. Physiol. Pharmacol.* **58:** 797–804.
16. Bartelt, A., M. Merkel, and J. Heeren. 2012. A new, powerful player in lipoprotein metabolism: brown adipose tissue. *J. Mol. Med.* **90:** 887–893.
17. Hagberg, C. E., A. Falkevall, X. Wang, E. Larsson, J. Huusko, I. Nilsson, L. A. van Meeteren, E. Samen, L. Lu, M. Vanwildemeersch, et al. 2010. Vascular endothelial growth factor B controls endothelial fatty acid uptake. *Nature.* **464:** 917–921.
18. Nedergaard, J., and O. Lindberg. 1979. Norepinephrine-stimulated fatty-acid release and oxygen consumption in isolated hamster brown- fat cells. Influence of buffers, albumin, insulin and mitochondrial inhibitors. *Eur. J. Biochem.* **95:** 139–145.
19. Heldmaier, G., and K. Seidl. 1985. Plasma free fatty acid levels during cold-induced and noradrenaline-induced nonshivering thermogenesis in the Djungarian hamster. *J. Comp. Physiol. B.* **155:** 679–684.
20. Puchalski, W., H. Böckler, G. Heldmaier, and M. Langefeld. 1987. Organ blood flow and brown adipose tissue oxygen consumption during noradrenaline-induced nonshivering thermogenesis in the Djungarian hamster. *J. Exp. Zool.* **242:** 263–271.
21. Thurlby, P. L., and P. Trayhurn. 1980. Regional blood flow in genetically obese (ob/ob) mice. The importance of brown adipose tissue to the reduced energy expenditure on non-shivering thermogenesis. *Pflugers Arch.* **385:** 193–201.
22. Inokuma, K., Y. Okamatsu-Ogura, A. Omachi, Y. Matsushita, K. Kimura, H. Yamashita, and M. Saito. 2006. Indispensable role of mitochondrial UCP1 for antiobesity effect of beta3-adrenergic stimulation. *Am. J. Physiol. Endocrinol. Metab.* **290:** E1014–E1021.
23. Meyer, C. W., M. Willershäuser, M. Jastroch, B. C. Rourke, T. Fromme, R. Oelkrug, G. Heldmaier, and M. Klingenspor. 2010. Adaptive thermogenesis and thermal conductance in wild-type and UCP1-KO mice. *Am. J. Physiol. Regul. Integr. Comp. Physiol.* **299:** R1396–R1406.
24. Golozoubova, V., E. Hohtola, A. Matthias, A. Jacobsson, B. Cannon, and J. Nedergaard. 2001. Only UCP1 can mediate adaptive nonshivering thermogenesis in the cold. *FASEB J.* **15:** 2048–2050.
25. Granneman, J. G., M. Burnazi, Z. Zhu, and L. A. Schwamb. 2003. White adipose tissue contributes to UCP1-independent thermogenesis. *Am. J. Physiol. Endocrinol. Metab.* **285:** E1230–E1236.
26. Ukropec, J., R. P. Anunciado, Y. Ravussin, M. W. Hulver, and L. P. Kozak. 2006. UCP1-independent thermogenesis in white adipose tissue of cold-acclimated Ucp1-/- mice. *J. Biol. Chem.* **281:** 31894–31908.
27. Hu, H. H., D. L. Smith, K. S. Nayak, M. I. Goran, and T. R. Nagy. 2010. Identification of brown adipose tissue in mice with fat-water IDEAL-MRI. *J. Magn. Reson. Imaging.* **31:** 1195–1202.
28. Peng, X-G., S. Ju, F. Fang, Y. Wang, K. Fang, X. Cui, G. Liu, P. Li, H. Mao, and G-J. Teng. 2013. Comparison of brown and white adipose tissue fat fractions in ob, seipin, and Fsp27 gene knockout mice by chemical shift-selective imaging and (1)H-MR spectroscopy. *Am. J. Physiol. Endocrinol. Metab.* **304:** E160–E167.
29. Holstila, M., K. A. Virtanen, T. J. Grönroos, J. Laine, V. Lepomäki, J. Saunavaara, I. Lisinen, M. Komu, J. C. Hannukainen, P. Nuutila, et al. 2013. Measurement of brown adipose tissue mass using a novel dual-echo magnetic resonance imaging approach: a validation study. *Metabolism.* **62:** 1189–1198.
30. Lunati, E., P. Marzola, E. Nicolato, M. Fedrigo, M. Villa, and A. Sbarbati. 1999. In vivo quantitative lipidic map of brown adipose tissue by chemical shift imaging at 4.7 Tesla. *J. Lipid Res.* **40:** 1395–1400.
31. Hu, H. H., C. D. G. Hines, D. L. Smith, and S. B. Reeder. 2012. Variations in T(2)* and fat content of murine brown and white adipose tissues by chemical-shift MRI. *Magn. Reson. Imaging.* **30:** 323–329.
32. Smith, D. L., Y. Yang, H. H. Hu, G. Zhai, and T. R. Nagy. 2013. Measurement of interscapular brown adipose tissue of mice in differentially housed temperatures by chemical-shift-encoded water-fat MRI. *J. Magn. Reson. Imaging.* **38:** 1425–1433.
33. Enerbäck, S., A. Jacobsson, E. M. Simpson, C. Guerra, H. Yamashita, M. E. Harper, and L. P. Kozak. 1997. Mice lacking mitochondrial uncoupling protein are cold-sensitive but not obese. *Nature.* **387:** 90–94.
34. Klingenspor, M., C. Ebbinghaus, G. Hiilshorst, S. Stiihr, F. Spiegelhalter, K. Haas, and G. Heldmaier. 1996. Multiple regulatory steps are involved in the control of lipoprotein lipase activity in brown adipose tissue. *J. Lipid Res.* **37:** 1685–1695.
35. Zancanaro, C., R. Nano, C. Marchioro, A. Sbarbati, A. Boicelli, and F. Osculati. 1994. Magnetic resonance spectroscopy investigations of brown adipose tissue and isolated brown adipocytes. *J. Lipid Res.* **35:** 2191–2199.
36. Calderan, L., P. Marzola, E. Nicolato, P. F. Fabene, C. Milanese, P. Bernardi, A. Giordano, S. Cinti, and A. Sbarbati. 2006. In vivo phenotyping of the ob/ob mouse by magnetic resonance imaging and 1H-magnetic resonance spectroscopy. *Obesity (Silver Spring).* **14:** 405–414.
37. Strobel, K., J. van den Hoff, and J. Pietzsch. 2008. Localized proton magnetic resonance spectroscopy of lipids in adipose tissue at high spatial resolution in mice in vivo. *J. Lipid Res.* **49:** 473–480.
38. Heldmaier, G., and T. Ruf. 1992. Body temperature and metabolic rate during natural hypothermia in endotherms. *J. Comp. Physiol. B.* **162:** 696–706.
39. Lubura, M., D. Hesse, N. Neumann, S. Scherneck, P. Wiedmer, and A. Schürmann. 2012. Non-invasive quantification of white and brown adipose tissues and liver fat content by computed tomography in mice. *PLoS ONE.* **7:** e37026.
40. Sbarbati, A., I. Cavallini, P. Marzola, E. Nicolato, and F. Osculati. 2006. Contrast-enhanced MRI of brown adipose tissue after pharmacological stimulation. *Magn. Reson. Med.* **55:** 715–718.
41. Khanna, A., and R. T. Branca. 2012. Detecting brown adipose tissue activity with BOLD MRI in mice. *Magn. Reson. Med.* **68:** 1285–1290.
42. Girardier, L., and J. Seydoux. 1986. Neural control of brown adipose tissue. *In* Brown Adipose Tissue. P. Trayhurn and D. G. Nicholls, editors. Edward Arnold Ltd., London. 122–151.
43. Park, I. R., and J. Himms-Hagen. 1988. Neural influences on trophic changes in brown adipose tissue during cold acclimation. *Am. J. Physiol.* **255:** R874–R881.
44. Foster, D. O., F. Depocas, and C. Zaror-Behrens. 1982. Unilaterality of the sympathetic innervation of each pad of rat interscapular brown adipose tissue. *Can. J. Physiol. Pharmacol.* **60:** 107–113.

45. Hamilton, J. M., T. J. Bartness, and G. N. Wade. 1989. Effects of norepinephrine and denervation on brown adipose tissue in Syrian hamsters. *Am. J. Physiol.* **257:** R396–R404.
46. Meywirth, A., U. Redlin, S. Steinlechner, G. Heldmaier, and R. J. Reiter. 1991. Role of the sympathetic innervation in the cold-induced activation of 5′-deiodinase in brown adipose tissue of the Djungarian hamster. *Can. J. Physiol. Pharmacol.* **69:** 1896–1900.
47. Klingenspor, M., A. Meywirth, S. Stöhr, and G. Heldmaier. 1994. Effect of unilateral surgical denervation of brown adipose tissue on uncoupling protein mRNA level and cytochrome-c-oxidase activity in the Djungarian hamster. *J. Comp. Physiol. B.* **163:** 664–670.
48. Nicholls, D. G., and R. M. Locke. 1984. Thermogenic mechanisms in brown fat. *Physiol. Rev.* **64:** 1–64.
49. Himms-Hagen, J. 1990. Brown adipose tissue thermogenesis: interdisciplinary studies. *FASEB J.* **4:** 2890–2898.
50. Young, P., M. A. Cawthorne, and S. A. Smith. 1985. Brown adipose tissue is a major site of glucose utilisation in C57Bl/6 ob/ob mice treated with a thermogenic beta-adrenoceptor agonist. *Biochem. Biophys. Res. Commun.* **130:** 241–248.
51. Ma, S. W. Y., and D. O. Foster. 1986. Uptake of glucose and release of fatty acids and glycerol by rat brown adipose tissue in vivo. *Can. J. Physiol. Pharmacol.* **64:** 609–614.
52. Heldmaier, G., S. Klaus, H. Wiesinger, U. Friedrichs, and M. Wenzel. 1989. Cold acclimation and thermogenesis. *In* Living in the Cold II. A. Malan and B. Canguilhem, editors. Colloque INSERM/John Libby Eurotext Ltd., London. 347–358.
53. Wunder, B. A., and R. D. Gettinger. 1996. Effects of body mass and temperature on nonshivering thermogenic response of small mammals. *In* Adaptations to the Cold. Tenth International Hibernation Symposium. F. Geiser, A. J. Hulbert, and S. C. Nicol, editors. University of New England Press, Armidale, Australia. 131–139.
54. Cooney, G. J., I. D. Caterson, and E. A. Newsholme. 1985. The effect of insulin and noradrenaline on the uptake of 2-[1-14C]deoxyglucose in vivo by brown adipose tissue and other glucose-utilising tissues of the mouse. *FEBS Lett.* **188:** 257–261.
55. Rabi, T., Y. Cassuto, and A. Gutman. 1977. Lipolysis in brown adipose tissue of cold- and heat-acclimated hamsters. *J. Appl. Physiol.* **43:** 1007–1011.
56. Kuusela, P., J. Nedergaard, and B. Cannon. 1986. Beta-adrenergic stimulation of fatty acid release from brown fat cells differentiated in monolayer culture. *Life Sci.* **38:** 589–599.
57. Brooks, B. J., J. R. Arch, and E. A. Newsholme. 1983. Effect of some hormones on the rate of the triacylglycerol/fatty-acid substrate cycle in adipose tissue of the mouse in vivo. *Biosci. Rep.* **3:** 263–267.
58. Inokuma, K., Y. Ogura-Okamatsu, C. Toda, K. Kimura, H. Yamashita, and M. Saito. 2005. Uncoupling protein 1 is necessary for norepinephrine-induced glucose utilization in brown adipose tissue. *Diabetes.* **54:** 1385–1391.
59. Laury, M. C., M. F. Chapey, and R. Portet. 1987. Involvement of the sympathetic nervous system in lipolytic activity in brown adipose tissue of cold acclimated rats. *Comp. Biochem. Physiol. A.* **87:** 197–203.
60. Ouellet, V., S. M. Labbé, D. P. Blondin, S. Phoenix, B. Guérin, F. Haman, E. E. Turcotte, D. Richard, and A. C. Carpentier. 2012. Brown adipose tissue oxidative metabolism contributes to energy expenditure during acute cold exposure in humans. *J. Clin. Invest.* **122:** 545–552.
61. Bartelt, A., O. T. Bruns, R. Reimer, H. Hohenberg, H. Ittrich, K. Peldschus, M. G. Kaul, U. I. Tromsdorf, H. Weller, C. Waurisch, et al. 2011. Brown adipose tissue activity controls triglyceride clearance. *Nat. Med.* **17:** 200–205.
62. Klingenspor, M., S. Klaus, H. Wiesinger, and G. Heldmaier. 1989. Short photoperiod and cold activate brown fat lipoprotein lipase in the Djungarian hamster. *Am. J. Physiol.* **257:** R1123–R1127.
63. Uchida, K., T. Shiuchi, H. Inada, Y. Minokoshi, and M. Tominaga. 2010. Metabolic adaptation of mice in a cool environment. *Pflugers Arch.* **459:** 765–774.
64. Azzu, V., and M. D. Brand. 2010. The on-off switches of the mitochondrial uncoupling proteins. *Trends Biochem. Sci.* **35:** 298–307.
65. Fedorenko, A., P. V. Lishko, and Y. Kirichok. 2012. Mechanism of fatty-acid-dependent UCP1 uncoupling in brown fat mitochondria. *Cell.* **151:** 400–413.
66. Foster, D. O., and M. L. Frydman. 1978. Nonshivering thermogenesis in the rat. II. Measurements of blood flow with microspheres point to brown adipose tissue as the dominant site of the calorigenesis induced by noradrenaline. *Can. J. Physiol. Pharmacol.* **56:** 110–122.
67. Himms-Hagen, J. 1974. Interscapular location of brown adipose tissue: role in noradrenaline-induced calorigenesis in cold-acclimated rats. *Can. J. Physiol. Pharmacol.* **52:** 225–229.
68. Laury, M. C., and R. Portet. 1974. Effects of the partial removal of the brown fat and of theophylline on the calorigenic response to noradrenaline in the rat adapted to cold. *Rev. Can. Biol.* **33:** 15–25.
69. Foster, D. O., and M. L. Frydman. 1978. Brown adipose tissue: the dominant site of nonshivering thermogenesis in the rat. *Experientia Suppl.* **32:** 147–151.
70. Heldmaier, G., and A. Buchberger. 1985. Sources of heat during nonshivering thermogenesis in Djungarian hamsters: a dominant role of brown adipose tissue during cold adaptation. *J. Comp. Physiol. B.* **156:** 237–245.
71. Nedergaard, J., V. Golozoubova, A. Matthias, I. Shabalina, K. Ohba, K. Ohlson, A. Jacobsson, and B. Cannon. 2001. Life without UCP1 : mitochondrial, cellular and organismal characteristics of the UCP1-ablated mice UCP1. *Biochem. Soc. Trans.* **29:** 756–763.
72. Mineo, P. M., E. A. Cassell, M. E. Roberts, and P. J. Schaeffer. 2012. Chronic cold acclimation increases thermogenic capacity, non-shivering thermogenesis and muscle citrate synthase activity in both wild-type and brown adipose tissue deficient mice. *Comp. Biochem. Physiol. A Mol. Integr. Physiol.* **161:** 395–400.
73. Cannon, B., and J. Nedergaard. 2011. Nonshivering thermogenesis and its adequate measurement in metabolic studies. *J. Exp. Biol.* **214:** 242–253.
74. Petrovic, N., T. B. Walden, I. G. Shabalina, J. A. Timmons, B. Cannon, and J. Nedergaard. 2010. Chronic peroxisome proliferator-activated receptor gamma (PPARgamma) activation of epididymally derived white adipocyte cultures reveals a population of thermogenically competent, UCP1-containing adipocytes molecularly distinct from classic brown adipocytes. *J. Biol. Chem.* **285:** 7153–7164.
75. Vosselman, M. J., W. D. van Marken Lichtenbelt, and P. Schrauwen. 2013. Energy dissipation in brown adipose tissue: from mice to men. *Mol. Cell. Endocrinol.* **379:** 43–50.
76. Lidell, M. E., M. J. Betz, O. D. Leinhard, M. Heglind, L. Elander, M. Slawik, T. Mussack, D. Nilsson, T. Romu, P. Nuutila, et al. 2013. Evidence for two types of brown adipose tissue in humans. *Nat. Med.* **19:** 631–634.
77. Schulz, T. J., P. Huang, T. L. Huang, R. Xue, L. E. McDougall, K. L. Townsend, A. M. Cypess, Y. Mishina, E. Gussoni, and Y-H. Tseng. 2013. Brown-fat paucity due to impaired BMP signalling induces compensatory browning of white fat. *Nature.* **495:** 379–383.
78. Mezentseva, N. V, J. S. Kumaratilake, and S. A. Newman. 2008. The brown adipocyte differentiation pathway in birds: an evolutionary road not taken. *BMC Biol.* **6:** 17.
79. Flachs, P., R. Rühl, M. Hensler, P. Janovska, P. Zouhar, V. Kus, Z. Macek Jilkova, E. Papp, O. Kuda, M. Svobodova, et al. 2011. Synergistic induction of lipid catabolism and anti-inflammatory lipids in white fat of dietary obese mice in response to calorie restriction and n-3 fatty acids. *Diabetologia.* **54:** 2626–2638.
80. Flachs, P., M. Rossmeisl, O. Kuda, and J. Kopecky. 2013. Stimulation of mitochondrial oxidative capacity in white fat independent of UCP1: a key to lean phenotype. *Biochim. Biophys. Acta.* **1831:** 986–1003.
81. Garofalo, M. A., I. C. Kettelhut, J. E. Roselino, and R. H. Migliorini. 1996. Effect of acute cold exposure on norepinephrine turnover rates in rat white adipose tissue. *J. Auton. Nerv. Syst.* **60:** 206–208.
82. Lafontan, M., and D. Langin. 2009. Lipolysis and lipid mobilization in human adipose tissue. *Prog. Lipid Res.* **48:** 275–297.
83. Newsholme, E. A., and B. Crabtree. 1976. Substrate cycles in metabolic regulation and in heat generation. *Biochem. Soc. Symp.* **1976:** 61–109.
84. Nedergaard, J., T. Bengtsson, and B. Cannon. 2007. Unexpected evidence for active brown adipose tissue in adult humans. *Am. J. Physiol. Endocrinol. Metab.* **293:** E444–E452.
85. Wu, J., P. Boström, L. M. Sparks, L. Ye, J. H. Choi, A-H. Giang, M. Khandekar, K. A. Virtanen, P. Nuutila, G. Schaart, et al. 2012. Beige adipocytes are a distinct type of thermogenic fat cell in mouse and human. *Cell.* **150:** 366–376.
86. Enerbäck, S. 2010. Human brown adipose tissue. *Cell Metab.* **11:** 248–252.

Supplemental Figure I

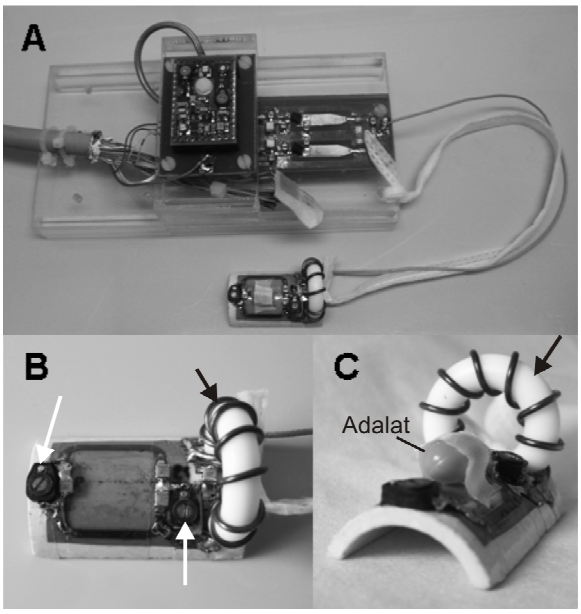

Supplemental Figure I *Transmit/receive surface loop coil for ^{31}P-spectroscopy in brown adipose tissue of mice*.

The loop coil is connected to a preamp board via a flexible coaxial cable to allow variable positioning of the coil. The board consists of a Tx/Rx- switch and a preamplifier in the receive line. **(A)**.

The coil has a rectangular shape (16 x 16 mm) and was mounted on a bisected glass reinforced plastic pipe to ensure an optimal placement on the mice's necks **(B, C)**. The coil was matched and tuned to phosphorus resonance frequency at 7 Tesla (121.62 MHz) using the capacitors and trimmers (see white arrows). The toroidal cable trap is marked with the black arrow. Correct coil position was controlled via proton imaging of the adalat capsule in the centre of the coil using the integrated body coil of the scanner.

Supplemental Figure II

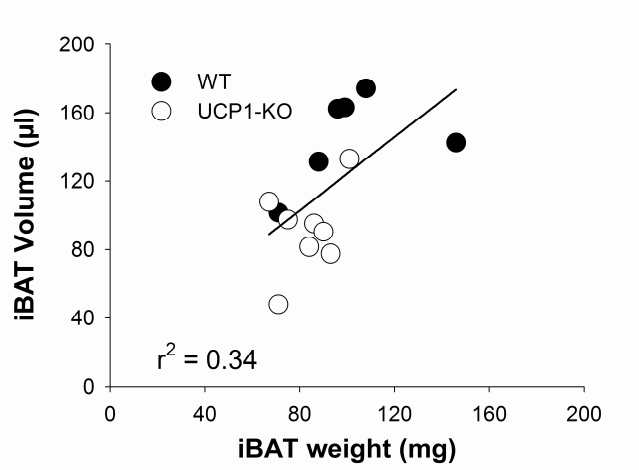

Supplemental Figure II *Association between iBAT wet weight and iBAT volume* of *UCP1-KO and WT mice acclimated to 5°C ambient temperature.* Two days after the MRI measurements mice were sacrificed and the dissected interscapular BAT was weighed by scale. The volume of the iBAT depot was acquired from T1 weighted images. Therefore the respective area from each slice were summed up and multiplied by the slice thickness. There was a significant correlation between iBAT volume and the tissue weight (p=0.03).

Supplemental Figure III

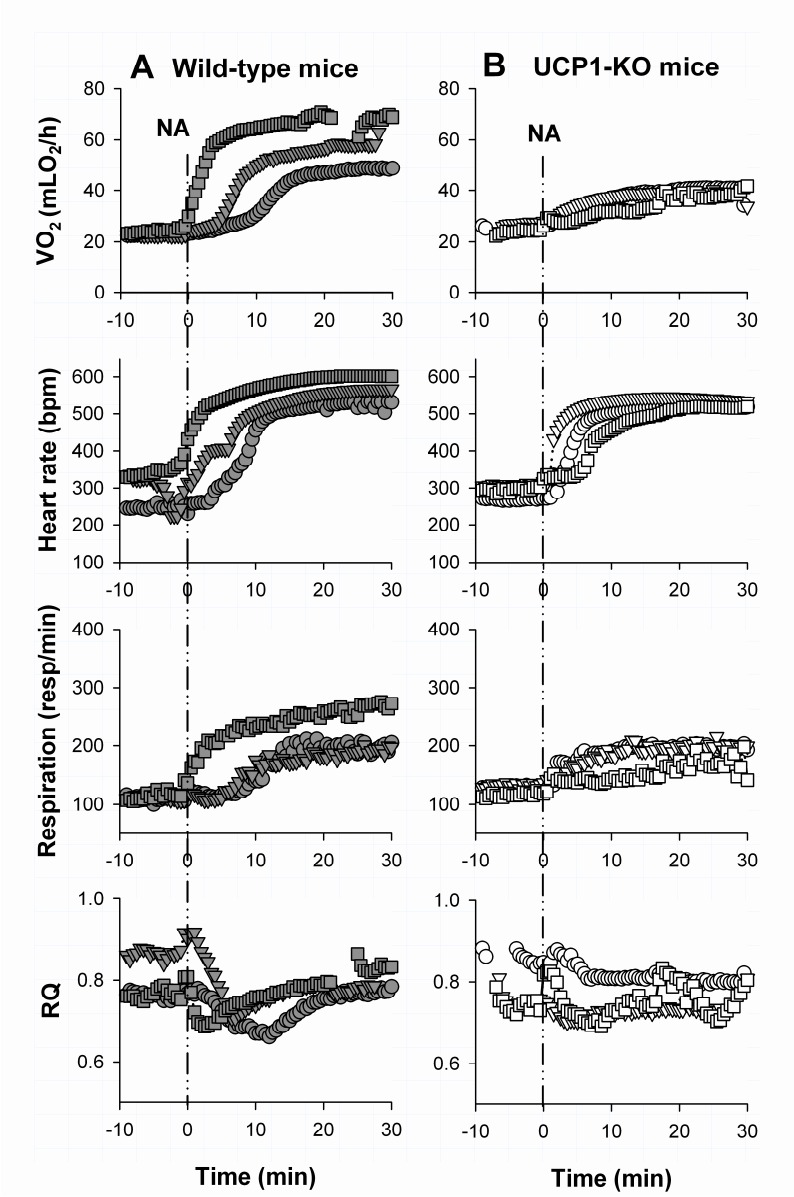

Supplemental Figure III *Response of oxygen consumption (VO_2), heart rate, respiration rate and respiratory quotient (RQ) to noradrenaline injection (NA).* All physiological parameters were monitored from three individual WT mice (column A) and from three individual UCP1-KO mice (column B). Noradrenaline was administered at time point zero. The mice were anesthetized with pentobarbital sodium intraperitoneally at a dose of 75 mg/kg body weight (Narcoren, Merial GmbH, Hallbergmoos, Germany). Single mice were placed in a mouse bed (Bruker Biospin MRI GmbH, Ettlingen, Germany). Oxygen consumption and carbon dioxide production were measured with an open respiratory system (previously described by Heldmaier and Ruf 1992). Therefore, mice were enclosed with a 6.0 l freezer bag. Air was sucked through the bag with a flow rate of 35 ± 0.5 l/h, dried by an electric freeze trap (M and C Cooler, ECM,

Ratingen, Germany) and the airflow was continuously monitored by an electronic mass flow meter (Bronkhorst High-Tech B.V., Ruurlo, Netherlands). O_2 and CO_2 content of the air were measured with a two-channel O_2 analyzer (Oxzilla II, Sable systems int., Las Vegas, USA) and a two-channel CO_2 analyzer (AO2000, ABB Automation GmbH, Frankfurt, Germany) with a resolution of 0.001 ΔVol % comparing the air entering and leaving the bag. The read out interval was set to 20 s and the room air was used for automatic zero readjustment before noradrenaline application. VO_2 was calculated according to Haldane equation: $VO_2 = Flow_{in} \times FO_{2in} - Flow_{out} \times FO_{2out}$, where FO_{2in} *and* FO_{2out} are fractional concentrations of O_2 in fresh gas and mixed exhaust gas respectively. NA (1 mg/kg body weight) was administered by a subcutaneous access through a polyethylene tube system during the measurement. The body temperature of mice was stabilized with a heating unit. Animal respiration rate and ECG were recorded continuously with an animal monitoring system (SAInstruments, Stony Brook, NY, USA).

7 Veröffentlichte Konferenzbeiträge

7th International Conference on Behaviour, Physiology and Genetics of Wildlife, Berlin 2009

That`s hot: golden spiny mice display torpor even at high ambient temperatures

GRIMPO KIRSTEN, HELDMAIER GERHARD, EXNER CORNELIA

Department of Animal Physiology, University of Marburg, GERMANY;
grimpo@students.uni-marburg.de

Daily torpor is a state of metabolic depression followed by a decrease of body temperature (T_b). This strategy of saving energy is often observed in small mammals during cold seasons. Golden spiny mice (*Acomys russatus*) live in rocky deserts, where they are exposed to seasonal fluctuations in ambient temperature (T_a) and food availability. It is already known that spiny mice are able to become torpid at 27°C under food restriction. We investigated if spiny mice may become torpid at T_a of 32°C or if heat load does inhibit torpor. Furthermore, we examined if cold alone is sufficient to induce torpor in these mice.
Oxygen consumption and T_b were monitored in animals kept at 18°C and 23°C T_a under ad libitum conditions as well as in animals kept at 23°C, 27°C and 32°C under 50 % food restriction. Respiration rate of isolated mitochondria from torpid and normothermic, food restricted spiny mice were compared.
At ambient temperatures of 23°C and 27°C food restricted spiny mice reduced minimal metabolic rate to 30 % and 50 % of ad libitum conditions and T_b clear below 32°C. Even in the heat the animals reduced their MR_{min} by 30 %, although T_b remained at 34.3 ± 0.2°C. We also detected torpor under ad libitum conditions *in single* individuals kept at 23°C. Mitochondrial measurements from several tissues showed no difference between normothermic and torpid mice.
The data indicate that hypometabolism during torpor is an active process, which seems not to be inhibited by a high T_b and does not depend on suppression of mitochondrial respiration. The use of torpor enables the golden spiny mouse to save energy in deserts and desert like habitats.

Leibniz-Institut für Zoo- und Wildtierforschung
IM FORSCHUNGSVERBUND BERLIN E.V.

196 Physiology Posters

P PH.20 - EN

On the role of mitochondrial metabolism during torpor in the golden spiny mouse (*Acomys russatus*) at high ambient temperature

Kirsten Grimpo, Maria Kutschke, Anja Kastl, Gerhard Heldmaier, Martin Jastroch, Cornelia Exner
Department of Animal Physiology, Philipps-Universität Marburg

In periods of food shortage small mammals have to cope with difficulties maintaining their high metabolic rate (MR). In such harsh times daily torpor and hibernation are common strategies to save energy. Recently, a depression of mitochondrial respiration during torpor had been demonstrated in the Djungarian hamster and a relation to the torpor entrance phase had been suggested. In this study, we investigated torpor behaviour and mitochondrial adjustments of the golden spiny mouse (*Acomys russatus*). To induce torpor the ad libitum food intake was reduced to 50% over a period of 3 weeks. MR and body temperature (T_b) of the animals were monitored at an ambient temperature (T_a) of 32°C. We demonstrated that even at this T_a animals were able to enter torpor. They decreased MR to 30% of euthermic values during a torpor bout, although T_b was kept at 34°C. We compared the bioenergetics of isolated mitochondria from torpid, alarm aroused, and ad libitum fed groups. We found no effect on mitochondrial superoxide production of several tissues and in contrast to previous studies, no difference in mitochondrial respiration states. Furthermore, torpor did not alter the basal proton leak measured in the liver. These data suggest that active depression of MR at high T_a does not depend on suppression of mitochondrial respiration, but rather seems to be a consequence of systemic regulation. Therefore, regarding previous suggestions on the importance of mitochondrial depression during torpor entrance may be questionable.

Poster PH.17

Visualizing morphological and functional changes in brown adipose tissue of cold acclimated mice

Kirsten Grimpo[1], Eva-Nina Heppe[1], Maximilian Völker[2], Gerhard Heldmaier[1]

[1] Tierphysiologie, Philipps-Universität Marburg — [2] Strahlendiagnostik, Philipps-Universität Marburg

Cold exposed small mammals are able to produce heat by non-shivering thermogenesis (NST) in their brown adipose tissue (BAT). Noradrenalin initiates the release of free fatty acids (FFA) by lipolysis for β-oxidation and activates the uncoupling protein 1 (UCP1) in the mitochondria. UCP1 uncouples ATP-synthesis from the respiratory chain and thus energy of the mitochondrial proton motive force is dissipated as heat. This means that mice without UCP1 cannot produce NST in their BAT. In our study, we investigated morphological and functional differences between BAT of UCP1-kockout (KO) and wild type mice (WT) using magnetic resonance (MR) Imaging and MR Spectroscopy. We scanned KO (n=7) and WT (n=9) mice acclimated to 18°C and 5°C ambient temperature and after 3 weeks deacclimatization at 30°C. We first measured the volume and physical parameters (T1 and T2 times) of the BAT and then determined the $(CH_2)_n$ -peak by spectroscopy as an indicator for lipid content. The morphology of the interscapular BAT depot looked similar in shape and size of both mouse genotypes. However, cold acclimated mice offered changes in volume and T2 time compared to warm animals. When NST was stimulated by injection of noradrenalin the mice decreased their lipid content. This response was more pronounced in WT mice and at cold ambient temperature, indicating an enhanced lipolysis in thermogenically active BAT.

P.28

Bildgebende Untersuchungen an nicht-anästhesierten, torpiden Zwerghamstern (*Phodopus sungorus*) mit Magnetresonanztomographie

K. Grimpo[1], M. Völker[2], J. T. Heverhagen[2], G. Heldmaier[1]

[1]*Philipps-Universität Marburg Tierphysiologie, Karl-von-Frisch-Str. 8, 35043 Marburg, Germany*
[2]*Philipps-Universität Marburg Kilink für Strahlendiagnostik, Baldingstr., 35043 Marburg, Germany*

Content

EINFÜHRUNG: Magnetresonanztomographie (MRT) ermöglicht eine differenzierte Darstellung von Weichteilgeweben und funktionelle Messungen *in vivo*. Da jede Bewegung das Messergebnis beeinträchtigt, werden die Versuchstiere für MRT Messungen in der Regel narkotisiert und fixiert. Eine Narkotisierung der Tiere ist jedoch nicht immer uneingeschränkt möglich. Wir interessieren uns für die aktive Stoffwechselabsenkung wie sie beim Dsungarischen Zwerghamster spontan während des täglichen Torpors auftritt. Bis heute ist dieses physiologische Phänomen nicht in Gänze verstanden. Unser Ziel ist es. neue Einblicke in die Abläufe und Steuermechanismen des täglichen Torpors zu erhalten ohne die natürlichen Vorgänge durch Narkose zu beeinflussen. Wir haben einen Messaufbau entwickelt, der gleichzeitig MRT-Bildgebung und stoffwechselphysiologische Untersuchungen am nicht anästhesierten torpiden Zwerghamster zulässt.

METHODEN: 12 Dsungarische Zwerghamster wurden an den Kurztag akklimatisiert (LD 8:16, 23°C Umgebungstemperatur), um spontanes Torporverhalten zu induzieren. Die Hamster wurden in den eigens angefertigten Stoffwechselkäfig mit Schalldämmung und integrierter H^+-Hochfrequenzspule eingesetzt und im 7 Tesla Magnetresonanztomographen platziert. Mit Hilfe indirekter Kalorimetrie wurde die Stoffwechselrate der frei beweglichen Tiere verfolgt. Im tiefen Torpor wurden morphologische Messungen an den Hamstern durchgeführt.

RESULTATE: Acht der 12 Hamster wurden im MRT-Aufbau spontan torpid. An zehn von insgesamt 27 Versuchtagen wurde Torpor beobachtet. Achtmal konnten MRT-Aufnahmen durchgeführt werden, ohne dass die Hamster aus ihrem torpiden Zustand erwachten. Trotz fortwährender Messungen behielten die Hamster minimale Stoffwechselraten von 10,5 ± 5,2 mLO_2/h und wachten nach mehren Stunden selbständig aus dem hypometabolen Zustand auf. Mit fett- und wassergewichtete Schnittaufnahmen (Schichtdicke von 0,8 mm) wurden die torpiden Hamster bildgebend dargestellt.

SCHLUSSFOLGERUNG: *Phodopus* zeigt in der neu entwickelte Messvorrichtung im Magnetresonanztomographen spontanes Torporverhalten. Es war erstmalig möglich, frei bewegliche, torpide Hamster ohne Narkose mittels MRT nicht-invasiv bildgebend darzustellen. Durch eine Weiterentwicklung der Hardware sollen zudem zukünftig spektroskopische Untersuchungen in vivo ermöglicht werden, die zu einem besseren Verständnis der metabolischen Regulation im Torpor beitragen.

GV-SOLAS
Gesellschaft für Versuchstierkunde

10. Kirsten Grimpo[1], E.N. Heppe, Völker, M., J.T. Heverhagen, and G. Heldmaier
Visualizing the response of brown adipose tissue to noradrenaline induced thermogenesis by magnetic resonance

(1) Department of Animal Physiology; Philipps-Universität Marburg; Germany;
grimpo@students.uni-marburg.de

Brown adipose tissue (BAT) enables small mammals to defend their body temperature during cold exposure and to arouse from hypothermic states like torpor. During noradrenaline-stimulated nonshivering thermogenesis (NST) lipids are mobilized and free fatty acids (FFA) activate the uncoupling protein 1 (UCP1) in the BAT mitochondria. UCP1 uncouples ATP-synthesis from the respiratory chain and thus energy of the mitochondrial proton motive force is dissipated as heat. This process is responsible for 30%-70% of total NST. The other sources of NST are still unclear. In our study, we measured the volume and biochemical responses of BAT in mice during noradrenaline-induced NST in vivo with a 7 T magnetic resonance tomograph. Mice were acclimated to thermoneutrality (30° C) and afterwards cold exposed to 18° C and 5° C ambient temperature. The dark core of interscapular BAT increased during cold acclimation and was bigger in wildtype mice than in UCP1-knockout mice having no thermogenically active BAT. When NST was stimulated by injection of noradrenaline the decrease of lipid content within the BAT exceeded the amount of lipid oxidation required for NST in BAT, as derived from measurements of oxygen consumption. Lipid oxidation as well as the decrease of BAT lipid content was more pronounced in wildtype mice than in UCP1-knockout mice. Thus lipolysis is enhanced in the presence of UCP1 in thermogenically active BAT. The ATP/ADP ratio remains constant during NST in the neck area of both genotypes. The results indicate that FFA are not only combusted in BAT but also exported from BAT after stimulation of NST. During heat generation levels of energy-rich phosphates are still maintained in the relating tissues. The role of the export of FFA from BAT during thermogenesis is presently not known. Target tissues that consume the released FFA may play an important role in BAT-independent NST.

8 Anhang

Die beiliegende CD beinhaltet ergänzendes Bild- und Videomaterial zu den MRT/MRS Ergebnissen. Zur vereinfachten Darstellung sind diese in einer PowerPoint Präsentation zusammengefasst.

9 Lebenslauf

Der Lebenslauf enthält persönliche Inhalte und wurde deshalb entfernt.

Der Lebenslauf enthält persönliche Inhalte und wurde deshalb entfernt.

Der Lebenslauf enthält persönliche Inhalte und wurde deshalb entfernt.

Der Lebenslauf enthält persönliche Inhalte und wurde deshalb entfernt.

10 Danksagung

Die Danksagung enthält persönliche Inhalte und wurde deshalb entfernt.

Die Danksagung enthält persönliche Inhalte und wurde deshalb entfernt.

11 Erklärung

Hiermit versichere ich, dass ich meine Dissertation

“Regulationsmechanismen während des Torpors und der zitterfreien Thermogenese: Neue Einblicke und der Einsatz von Magnetresonanztomographie“

selbstständig, ohne unerlaubte Hilfe angefertigt und mich keiner anderen als der von mir ausdrücklich bezeichneten Quellen und Hilfen bedient habe.
Die Dissertation wurde in der jetzigen oder in einer ähnlichen Form noch bei keiner anderen Hochschule eingereicht und hat noch keinen sonstigen Prüfungszwecken gedient.

Marburg, den _____

(Kirsten Grimpo)